ERUPTION DYNAMICS AND HYDROLOGICAL IMPLICATIONS OF BASALTIC VOLCANIC CENTRES AT LAKE TAUPO

A thesis
submitted in partial fulfilment
of the requirements for the degree
of

Master of Science in Earth Sciences

at

The University of Waikato

by

MAREE ANNETTE MATHESON

THE UNIVERSITY OF
WAIKATO
Te Whare Wānanga o Waikato

The University of Waikato

2010

Abstract

The Taupo Volcanic Centre (TVC) is a major rhyolite centre within the Taupo Volcanic Zone, yet a small volume of the centre is comprised of monogenetic basalt volcanoes. Four TVC basalts that lie north of Lake Taupo have been examined in this study: the tuff deposits of Acacia Bay, Kaiapo and Kinloch, and the scoria cone complex of Punatekahi. Inferred ages of the basalts range from ~ 200 ky (Acacia Bay tuff) to < 9.5 ky (Kinloch tuff). The particular aim of this study is to determine the volcanological and hydrological controls responsible for the nature of the basaltic deposits through: field description; data on grain size, vesicularity, componentry and clast morphology (including SEM); petrography; and XRF geochemistry of six representative samples.

The basalts share a similar mineralogy (plagioclase > olivine, augite) and geochemistry (low-K volcanic arc magmas), but can be clearly distinguished by their physical characteristics. The Punatekahi basalt deposit is comprised of thick beds of scoria lapilli, and welded agglutinate, formed by magmatic strombolian and hawaiian eruptions. The Acacia Bay, Kaiapo and Kinloch deposits are all tuff deposits that have a significant base surge component resulting from phreatomagmatic surtseyan and taalian eruptions. The Punatekahi scoria deposit has higher vesicularity values and lower lithic abundance than the other three basalt centres, reflecting the difference between magmatic and phreatomagmatic eruption mechanisms, respectively.

All of the four basalt deposits are located in areas that have at one time been covered by Lake Taupo (or its ancestor Lake Huka), and the phreatomagmatic deposits of Acacia Bay, Kaiapo and Kinloch all have evidence of partial subaqueous deposition, suggesting that a lake was present at those sites at the time of eruption. Explosive interaction of magma with groundwater occurred during all of the four eruptions. For the eruptions at Acacia Bay, Kaiapo and Punatekahi, Rangatira Ignimbrite is inferred as a likely aquifer source, and either the rhyolite dome or a fault is posited as the water source for the Kinloch basalt eruption.

The Kinloch tuff deposit is younger than the other TVC deposits by at least ~ 100 ky. The presence of this much younger basalt volcano indicates that, despite the dominance of rhyolitic eruptions, basalt volcanism has an ongoing presence in the TVC, and a future basalt eruption, with unique hazards, are a real possibility.

Acknowledgments

The foundation for this thesis topic was laid by Michael Rosenberg with his curiosity into the young basaltic tuff west of Kinloch township. His help during the initial stages of this project was indispensable.

Many thanks go to my supervisors Dr. Adrian Pittari and Assoc. Prof. Roger Briggs, who got me started, provided valuable insight into what I was looking at, and always willingly gave of their time to answer questions. The understanding of the need for flexibility in my schedule was much appreciated.

A lot of gratitude goes to Alex Robertson (Kaiapo) and Graham Seay (Punatekahi), who were both very obliging in allowing me access to field sites, and Graham Seay also shared his knowledge of the scoria cone. Additional thanks goes to everyone at the quarry for being warm and welcoming and giving me rides to and from the entrance to the quarry, and to random truckies who took pity on me and gave me a lift between the quarry and various points near town.

A big thank-you goes to my previous lecturer, Dr. Richard Smith, for very kindly sending me a copy of his BSc (Hons) thesis, and offering his support and advice.

The following technical staff at university were invaluable with help both in the field and in the laboratory: Steve Cooke, Craig Hosking, Chris McKinnon, Annette Rodgers, Helen Turner, Ganqing Xu. Renat Radosinsky patiently showed me how to make thin sections, powder samples and kindly provided a solution to my unworkable workstation.

The University of Waikato Masters Scholarship was a lifesaver, without which the struggle between work and study would have been even greater.

A sincere thank-you goes to my family and friends for their help and support. All of the kindness and wisdom I have received from fellow students, especially Bashirah, Fiona and Tehnuka is much appreciated.

Table of Contents

Chapter Seven – Punatekahi

Chapter Eight – Geochemistry

Chapter Nine – Discussion

List of Figures

Chapter One – Introduction

Chapter Two – Geological and Hydrological Setting of the Taupo Volcanic Centre (TVC)

Chapter Four – Acacia Bay

Chapter Five – Kaiapo

Chapter Six – Kinloch

Chapter Seven – Punatekahi

Chapter Eight – Geochemistry

Chapter Nine – Discussion

List of Tables

Chapter Nine – Discussion

1 Introduction

1.1 Introduction

The interaction between hydrological and geological sciences, and the importance of each to the other, has long been recognised, most notably in terms of aquifer characteristics to determine groundwater yields and susceptibility to pollution, and for geothermal exploration and exploitation (e.g. Glover and Stewart 1996). In some ways, though, a most obvious relationship between water and volcanoes has been ignored: although the role of water has been acknowledged for phreatomagmatic eruptions, there has been little attempt to make use of 'wet' deposits to gain any information as to the hydrology of the area that contributed to the nature of the eruption in question; rather, volcanic deposits have typically been investigated to learn more about volcanic processes and the origin of magmas. The focus of this thesis is to determine the feasibility of looking at volcanic deposits using currently known methods in order to get a first approximate

understanding of past hydrologic conditions. Four basaltic volcanic deposits within the Taupo Volcanic Centre (one of the volcanic centres within the Taupo Volcanic Zone, New Zealand), which have been previously studied to varying degrees, have been reviewed in an attempt to assess the hydrological conditions during time of eruption. This thesis describes the stratigraphy, grain size characteristics, clast vesicularity, componentry, clast morphology, petrography and some geochemistry of the volcanic deposits at Acacia Bay, Kaiapo, Kinloch and Punatekahi.

1.2 Objectives

The main objectives and motivation for this thesis are:-

- to determine the physical volcanological processes responsible for the four deposits, particularly Kinloch, which has not been previously studied;
- using known methodology for establishing external water involvement, determine the hydrology of eruptions;
- using known hydrological and geological information for the area, and physical volcanic deposit information, better constrain previous hydrological environments, including the source and nature of aquifers.

1.3 Field Sites

For this study, the field area comprises four basalt eruption centres within a 66 km^2 area north of present-day Lake Taupo, situated within the Taupo Volcanic Centre (TVC): Acacia Bay, Kaiapo, Kinloch, and Punatekahi (**Figure 1.1**).

Acacia Bay

The Acacia Bay basalts consist of remnants of a tuff ring: a small, northern outcrop (referred to here as Acacia Bay North) and a larger, southern exposure (Acacia Bay South). The deposits lie along the current shoreline just north and south of the Acacia Bay jetty, ~ 4 km southwest of Taupo township.

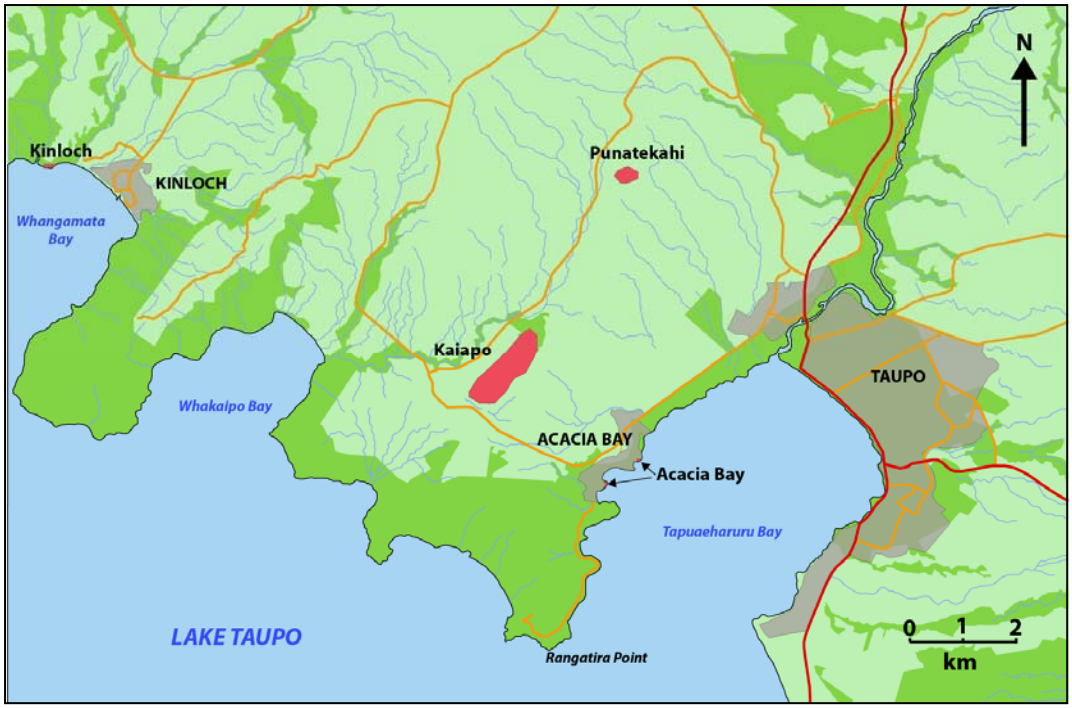

Figure 1.1: Location map of the four basalt deposits (in red) examined in this study. (Modified from Topo50 map BG36 1:50 000 - Taupo.)

Kaiapo (T-Trig)

Kaiapo refers to the construct that underlies T-Trig, a 635 m-high hill. From a previous study (Smith 1990), it has been ascertained that the deposit represents nearly half of an old tuff cone. Unlike the other phreatomagmatic deposits, the Kaiapo deposit is very thick and extends laterally almost continuously for nearly 2 km. Its exposure is fault-dependent, as outcrops are only found to the east of Tukairangi Road, which also marks the boundary of the Kaiapo Fault (Brown 1990). T-Trig is situated ~ 6 km to the west of Taupo.

Kinloch

The Kinloch tuff deposit is exposed in a cliff beside Lake Taupo. Unlike the other deposits, the base of the Kinloch basalt is found several metres above ground-level, with a clear stratigraphy underneath. The deposit is situated along the northern shoreline in Whangamata Bay, between Otaketake Stream and Okaia Stream, just west of the Whangamata Fault and 1 km west of Kinloch town.

Punatekahi

Punatekahi is the sole site in this study derived from 'dry' magmatic eruptions. The site holds two scoria cones: a large northwest cone, the top of which holds Punatekahi Trig, and a smaller, largely eroded remnant of a cone to the southeast. These cones are sited within a quarry ~ 4 km to the northeast of T-Trig, and ~ 5 km northwest of Taupo.

1.4 Previous Work

The TVC basalts, their relation to rhyolite magma genesis, and possible hydrological setting have all been studied to varying degrees, providing valuable background information and the platform for this thesis.

The first recorded detailed work on basalts in the Taupo region was by Grange (1937), who established the presence and extent of basalt west of the town. Most notably, Grange (1937) mapped the locations of outcrops of what he called K-Trig Basalt, which included Punatekahi, K-Trig, Kaiapo, and Acacia Bay. The inference from his mapping all of these deposits as being K-Trig is that they all originated from the same eruption or vent, although some of these are now treated as products from related, but isolated, events (e.g. Wilson and Smith 1985; Brown *et al.* 1994). Grange (1937) was also the first to undertake geochemical analyses of basalts in the area. He classified K-Trig as an auvergnose (an old CIPW classification) and noted that it was very similar in composition to Tarawera basalt of 1886 (from Okataina Volcanic Centre in the north) (Grange 1937).

For several decades following Grange (1937), the focus in the Taupo region shifted to geothermal production (e.g. Grindley 1965; Marshall 1970; Henley and Ellis 1983; Glover and Stewart 1996). In 1968, Stipp provided the first numerical ages of TVC basalts, with a K-Ar age of ~ 140 ka for Punatekahi (Brown 1990). This age is still regarded as valid, and is partly responsible for the inference that most of the basalts are late Pleistocene in age (Houghton *et al.* 1987; Brown *et al.* 1994). A few years later, Cole (1973) studied the TVZ basalts in relation to rhyolite, and classified the TVZ basalts as high-alumina basalts, or HABs (Cole 1973; Hiess *et al.* 2007). Cole (1973) looked at the K-Trig basalts at Punatekahi and K-Trig, as well as several from the Okataina and Maroa volcanic centres. He discovered that the HABs from all three volcanic centres were very similar in

terms of petrography and geochemistry, and that they were all aligned NNE, corresponding to local fault structures (Cole 1973). This lead to the stipulation that the HABs within TVZ all originated from a shared source (below the inferred ~ 30 km-thick crust, from peridotite or similar). Cole's (1973) model involved basalt magma heating overlying greywacke to form rhyolite, rising up into voids from erupted rhyolite, and eventually reaching the surface via faults. Reid (1983), who also associated rhyolite with basalt eruptions, investigated the possibility of rhyolite having been formed through fractional crystallisation of basalt. Reid (1983) concluded that geochemical differences were too great to support basalt being genetically related to the rhyolite, and also cited the proposed vast volume of basalt that would be required to produce the rhyolite, and the lack of geophysical support for this (Reid 1983). There was some thought that the original source may have been the Mesozoic greywackes that are prominent in the North Island outside of the TVZ but have not been found in large volumes within the TVC (Cole 1981; Reid 1983; Graham *et al.* 1995; Charlier *et al.* 2005). Cole (1981) proposed that the negative Eu anomaly found in both rhyolite eruptives and crustal sediments would suggest partial crustal melting, although the heat source required to produce ~ 12,000 km^3 of rhyolite was problematic.

It wasn't until the 1980s that a more physical approach to the TVC basalts was presented. Wilson and Smith (1985) analysed the Acacia Bay basalt. They studied deposits to the east and south-east of Acacia Bay township, north of the main outcrop examined in this study. As well as correcting Grindley's (1960) identification of the basalt as Huka Formation, Wilson and Smith (1985) determined that the deposits represented an old tuff ring, which was caused by eruption through lake sediments, probably east of the remnants. Geochemically, they were found to represent a different magma from that of the K-Trig basalts, making concurrent eruption with the K-Trig basalts unlikely. An age of 100-200 ka was inferred from the stratigraphy and preservation of the outcrops (Wilson and Smith 1985).

Brown (1990) and Smith (1990) (and Brown *et al.* 1994) did complementary work on TVC basalts: Brown (1990) on the scoria complex at Punatekahi and the scoria and tuff at K-Trig; Smith (1990) on the Kaiapo tuff ring and Mine Bay. Brown (1990) discovered the presence of two geochemically distinct lavas at Punatekahi, and inferred the presence of two vents. A migration of activity within the main

cone was also considered. Brown found no evidence for involvement of external water during formation of Punatekahi, but inferred an initial phreatomagmatic phase from the observation of a change from phreatomagmatic to strombolian activity at K-Trig. At K-Trig, a lake water source was deduced from the existence of diatomite and lacustrine sediment both below and above the deposit. A change to strombolian activity was deemed to have occurred following movement to a relatively dry part of the cone (Brown 1990; Brown *et al.* 1994). Smith's (1990) detailed work at Kaiapo established the involvement of both surface and ground water during the construction of a tuff ring, which involved at least six eruption phases. It was found that roughly half of the deposit, which lies along the Kaiapo Fault, had been removed due to consequent fault movement and erosion. Due to the presence of pumice and ignimbrite lithics in the deposit, the Waiora Formation was postulated as the likely aquifer for interaction with groundwater (Smith, 1990). The supposition that the K-Trig deposits represent geologically concurrent eruptions lead Brown *et al.* (1994) to propose that, at ~ 140 ka, the northern extent of proto-Lake Taupo was situated at some point between Punatekahi and K-Trig.

Despite the earlier work by Reid (1983) on basalt with regard to rhyolite, the role of basalts in a rhyolite-dominated centre continued to be debated. Strengthening the case against basalt being a parent to rhyolite, Hochstein *et al.* (1993) argued that more surface evidence might be expected of the more than 100,000 km^3 of basalt that would be required to produce the rhyolite that has been extruded throughout TVZ. Other theories, such as assimilation of greywacke into a basic magma prior to evolution via fractional crystallisation, or partial melting of a different source have also been presented (Graham *et al.* 1995; Price *et al.* 2005), but the role of basalt within the TVC and TVZ as a whole is still unknown. Wilson *et al.* (1995) have found that all TVZ basalts are younger than the Whakamaru eruption (~ 330 ka) and are of very small volume, suggesting that having surface expression is anomalous.

Recently, the basalt at Kinloch was discovered. Preliminary field work has been undertaken by M. D. Rosenberg and a lone geochemical analysis has been done (M. D. Rosenberg pers. comm. 2008), but no detailed physical description of the deposit has been completed. Work on the possibly related Marotiri and Ben Lomond basalts to the north of Kinloch includes the brief physical description by Houghton *et al.* (1987) that shows Ben Lomond to have both magmatic and

phreatomagmatic eruptions, and the petrography and geochemistry by Cole (1973) and Gamble *et al.* (1990, 1993).

1.5 Literature Review on Magma:Water Interaction

The focus of this study on hydrology of eruptions necessitates the understanding of current methods for determining the involvement of water during an eruption from the characteristics of the resulting deposits. This literature review outlines the importance of water in basaltic eruptions and how it affects eruption style, along with current methods for assessing qualitative and quantitative active water involvement in phreatomagmatic eruptions.

1.5.1 Role of External Water in Basaltic Eruptions

Basaltic volcanic landforms are the most common volcanic landforms on earth. They consist of shield volcanoes, scoria cones, tuff rings, tuff cones and maars (Sheridan and Wohletz 1983; Grunewald *et al.* 2007; Valentine and Gregg 2008). Through observations of volcanic eruptions (e.g. Thorarinsson 1964; Moore *et al.* 1966) it has become apparent that the most significant difference between volcano type is the presence of external water (Lorenz 1987). This has led to research into the role of water in volcanic eruptions.

Nomenclature of explosive eruptions involving water has been debated over the years, with phreatomagmatic *sensu stricto* relating to groundwater interaction with magma (Sheridan and Wohletz 1983; White 1996), but often being extended to include all situations where magma interacts explosively with external water (e.g. Fisher and Schmincke 1984; Lorenz 1987; Starostin *et al.* 2005). This *sensu lato* definition of phreatomagmatism likely comes from both the difficulty to ascertain the source of water for old deposits (Fisher and Schminke 1984), and possibly to distinguish from other types of hydrovolcanism (Sheridan and Wohletz 1983). Phreatomagmatic eruptions occur in a variety of environments and with numerous water sources, such as in the sea, under glaciers, in lakes and on land (Sheridan and Wohletz 1983; Fisher and Schmincke 1984; Starostin *et al.* 2005). Despite this variety, phreatomagmatic craters all appear to be sited in topographically low

areas, reflecting the greater probability of large volumes of groundwater and surface water in such settings (Abrams and Siebe 1994). Water's explosive impact on eruptions is achieved through rapid heating and expansion of the water (Wohletz 1986). According to White (1996), there are only two known ways by which boiling water can produce explosive eruptions: confinement and disruption; and fuel-coolant interaction (FCI). In the 1970s (e.g. Bradley and Witte 1972), observed similarities between explosive basaltic eruptions and industrial explosions involving hot melt led to the use of FCI to explain the complex processes involved in hydrovolcanic eruptions (Mastin *et al.* 2009), more correctly termed molten fuel-coolant interaction (MFCI) (Wohletz and Zimanowski 2000). FCIs occur when a fuel (e.g. magma) comes into contact with a coolant (e.g. water) that has a boiling point lower than the temperature of the fuel (Wohletz 1983; White 1996). The ensuing mixing, transfer of heat and vaporisation (and expansion) of the coolant causes fragmentation of the fuel (Wohletz 1983; White 1996; Wohletz and Zimanowski 2000) (**Figure 1.2**). The critical component in causing an explosive eruption is breakdown of the insulating vapour film that develops in the initial stage of magma-water interaction (Wohletz 1986; White 1996; Wohletz and Zimanowski 2000). This can be achieved either by superheating or thermal detonation (Wohletz 1986).

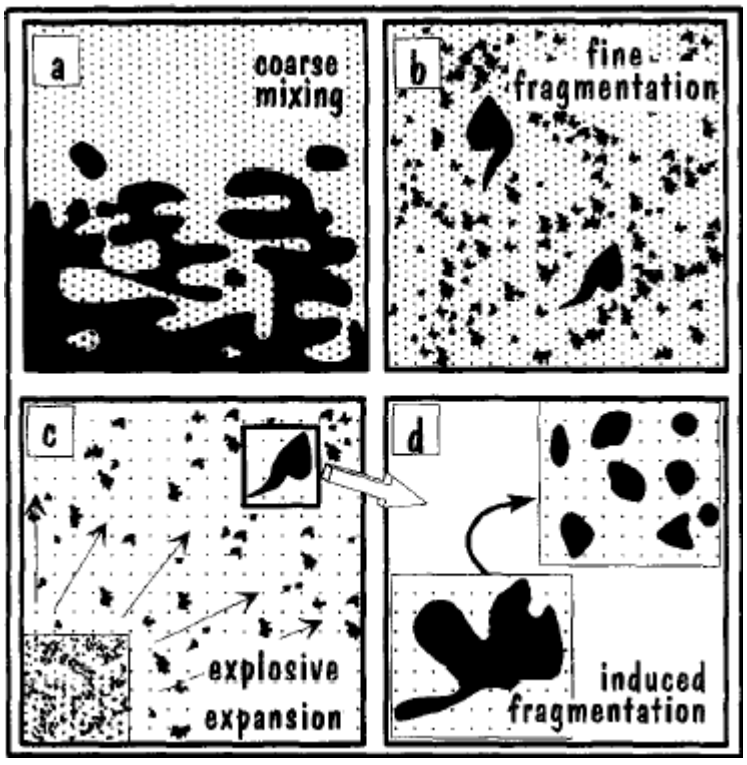

Figure 1.2 (previous page) Four-stage fragmentation by fuel-coolant interaction: a) coarse mixing of magma with coolant; b) fine fragmentation of the magma, along with superheating of the coolant; c) explosive fragmentation through rapid expansion of the coolant as it vaporises; d) 'induced' fragmentation of the magma through shear movement. (From White 1996.)

Magma interaction with external water does not always lead to explosive eruption, as is the case with submarine and subterranean pillow lavas (Kokelaar 1986; Befus *et al.* 2009). Kokelaar (1986) highlighted the importance of pressure in limiting explosivity, correlating this to a water depth (**Figure 1.3**). Kokelaar was careful, however, to note that there are many factors that contribute to explosivity, or containment of it, with a difference between volatile fragmentation depth (VFD) and magma fragmentation depth (Kokelaar 1986). Mastin *et al.* (2004) looked at turbulence of mixing in causing fragmentation, and suggested that for optimum mixing and fragmentation, a depth no greater than that of the vent diameter would be required.

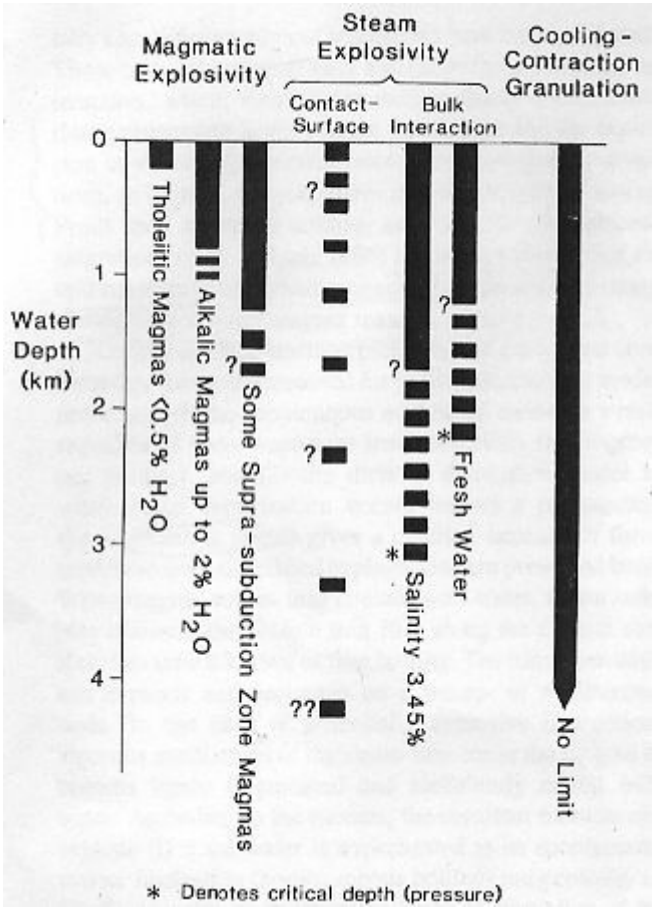

Figure 1.3 Diagram showing critical water depths for explosive interaction (Kokelaar 1986).

A key consequence of subsequent research using FCI as a framework was the mass water:magma ratio. The seminal paper by Sheridan and Wohletz (1981)

cemented the importance of the relative amounts of water and magma in explosive eruptions by linking them to volcanic eruption phases and products. Sheridan and Wohletz stated that mass water:magma ratios between 0.3 and 1.0 were required for most efficient fragmentation, after which, a dampening down of explosivity would occur. This figure was later revised to between 0.1 and 0.3 (Sheridan and Wohletz 1983; Wohletz 1983). These water:magma ratios were later linked with landforms (Wohletz and McQueen 1984) and styles of volcanic activity (Wohletz 1983; Frazzetta *et al.* 1983; Kokelaar 1986) (**Figure 1.4**).

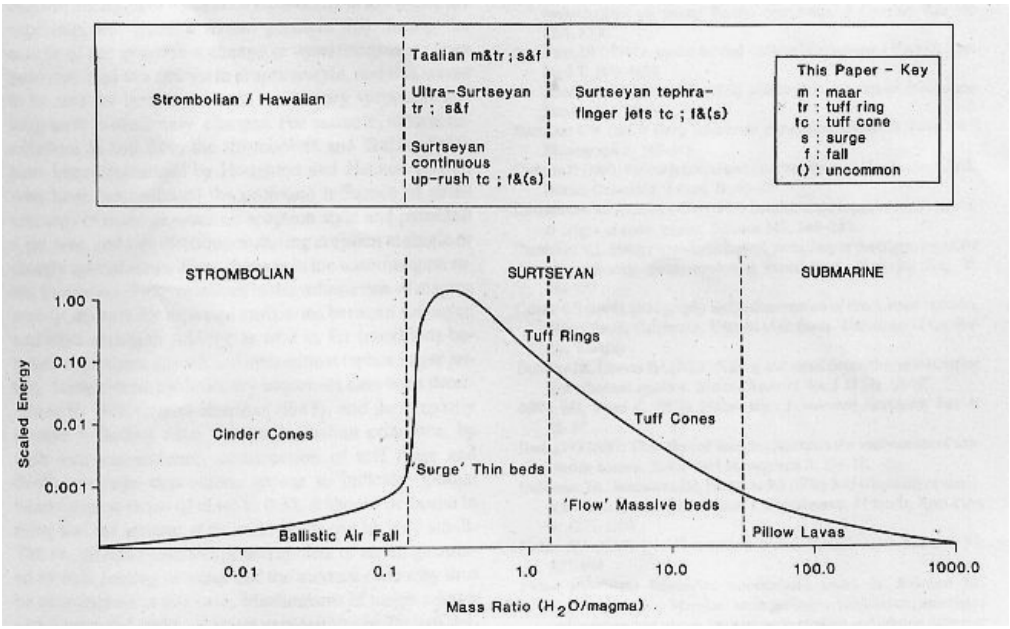

Figure 1.4 Eruption style and landform associations with magma:water ratios (Kokelaar 1986).

More recently, Sohn (1996), who looked at two tuff rings and two tuff cones on Cheju Island in Korea, argued that the entrenched relationship between water:magma ratio and resulting volcanic deposit did not always hold (**Figure 1.5**). He came to this conclusion following the observation of features in each type of deposit that seemed contrary to what the apparent environment of deposition (i.e. the water source and volume) would have suggested (Sohn, 1996). The inference was that it is the 'amount of *interactive water*' (cf. available water) and depositional processes that are most important in determining the morphology of a deposit, and that these are controlled by numerous other factors, such as magma flux ratio, aquifer characteristics (e.g. lithology) and country rock strength (Sohn, 1996).

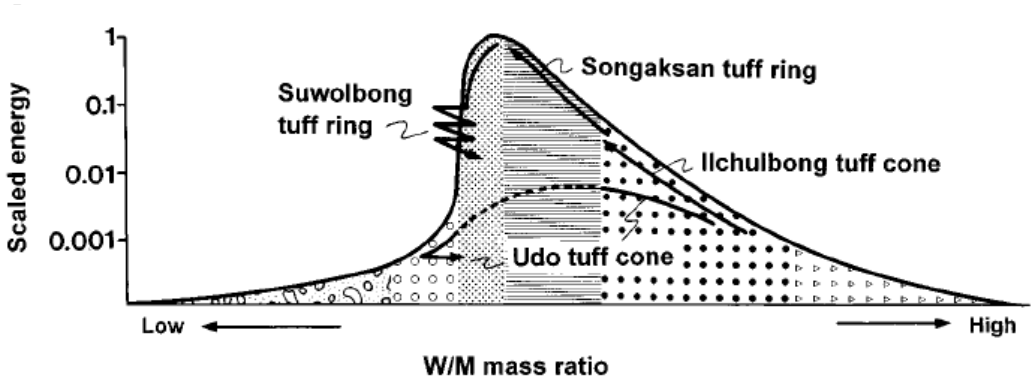

Figure 1.5 Inferred magma:water ratios for Cheju Island volcanoes (Sohn 1996). Note difference with that in Figure 1.4.

Sohn (1996) also suggested that there are both wet and dry versions of tuff rings and cones as a result of the interaction between the aforementioned 'direct controls'. Sohn (1996) made a valid (if not obvious) point in stipulating that the relative amounts of water and magma that interact in a given eruption (or phase during eruption) are based on things like the storage and permeability of an aquifer and the rate of magma ascent and replacement; less valid perhaps is the intention to separate depositional processes from magma:water ratios, especially given the fact that the tuff rings had more in common with each other than the cone deposits.

Similarly, White (1996) noted that FCI models tend to oversimplify the mechanisms involved in hydrovolcanic eruptions. He focussed on the problems with the application of mass water:magma ratios, in particular the assumption that the coolant was pure water. (This may not be entirely true – see Wohletz 1983, 1986). White (1996) cited two main situations when impure coolants would be expected: phreatomagmatic eruptions *sensu stricto* (involving groundwater), and after the initial explosion, when erupted clasts could be incorporated back into the eruption mixture (recycled clasts). In addition, the inclusion of sediment and/or recycled clasts in the coolant mixture would affect viscosity, density, thermal conductivity and heat capacity of the coolant, changing the length and degree of mixing between fuel and coolant. It is possible that the mechanisms that supply sediment to the coolant or magma supply and the effects of the sediment, along with magma supply rates, are a stronger control on resulting phreatomagmatic landforms than simply the relative quantities of available water and magma (White 1996).

1.5.2 Qualifying External Water Involvement

There are several key features of basaltic volcanic landforms that point to involvement of water. Some features are diagnostic, but due to the complexity of volcanic eruptions, the deduction of external water involvement during an eruption is only valid with the presence of several indicators. A principal feature of tuff cones and tuff rings is the presence of base surges (Sheridan and Wohletz 1983; Cas and Wright 1987, Sohn and Chough 1989). Base surge deposits are thin beds (usually less than 10 cm thick) of tuff that are often capped by a preserved ash-fall unit (Fisher and Schmincke 1984; Sohn and Chough 1989). A base surge indicates significant water:magma interaction, but can be either of a 'dry' or 'wet' nature, depending on the temperature of the water within the surge (<100 º C and >100 º C respectively; Sheridan and Wohletz 1981; Pardo *et al.* 2009). 'Wet' base surges show structures such as cross-bedding, flame structures, bomb sags, and vesiculated tuff, and tend to thin more rapidly than their drier counterparts (Fisher and Schmincke 1984; Pardo *et al.* 2009). The types of bedforms produced by base surges (planar, sandwave, massive) have also been associated with grain size and sorting (**Figure 1.6**; Wohletz 1983). By inference, this can lead to an assessment of relative wetness of surge.

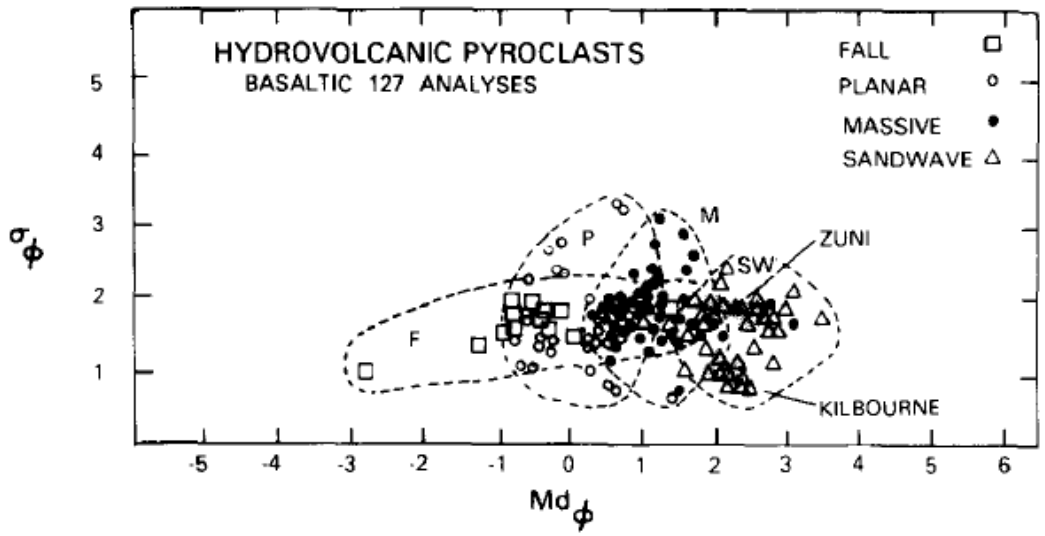

Figure 1.6 Plot illustrating fields of phreatomagmatic fall and base surge deposit types with regard to median grain size and sorting (Wohletz 1983).

One of the fundamental proxies for inferring magma interaction with external water is the pairing of grain size and sorting within a deposit. Phreatomagmatic

deposits are typically finer grained than their magmatic counterparts, and tend to be more poorly sorted (Walker and Croasdale 1971). There is, however, a degree of overlap between eruption styles and deposits, as the median diameter vs. sorting plot of Houghton and Gonnermann (2008) demonstrates (**Figure 1.7**).

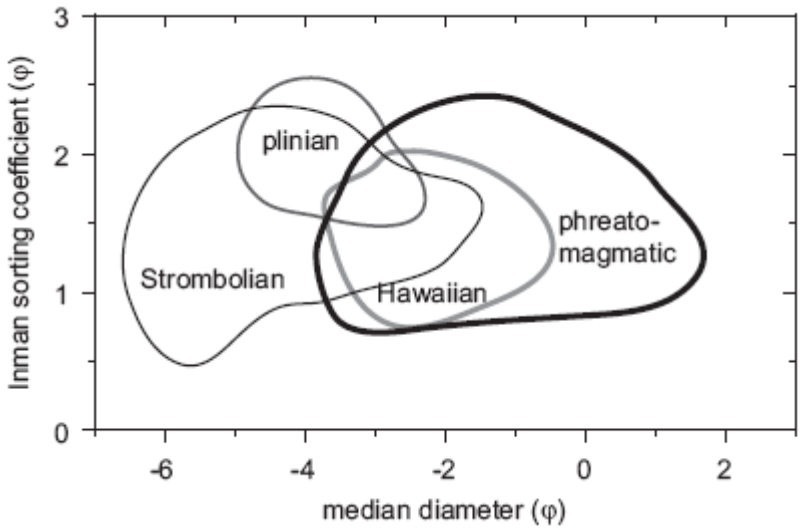

Figure 1.7 Median diameter vs. sorting plot with eruption style fields (Houghton and Gonnermann 2008).

Furthermore, grain size data are highly dependent on distance from the vent (Walker and Croasdale 1971; Chough and Sohn 1990; Riedel *et al.* 2003; Carey *et al.* 2007; Houghton and Gonnermann 2008), and it has been noted that such data are most accurate for younger deposits (Houghton and Wilson 1989), although the proxy is still helpful. Consequent experimental studies support the grain size observations: Wohletz (1986) attributed spikes of material < 1 mm in size to phreatomagmatic activity, and Zimanowski *et al.* (1991) found sizes of 20-500 μm from the main phase of explosions involving water. Grain size might also be a clue as to water source. Grunewald *et al.* (2007) noted that more saline water results in coarser-grained and fewer interactive clasts than fresh water, due to the greater energy required for reactions between water molecules and chloride ions. The morphology of juvenile grains also gives an indication of water involvement. Wohletz (1983) identified five morphology types under SEM (**Figure 1.8**), attributing types 3 ('moss-like and convoluted') and 4 ('spherical or drop-like') unequivocally to phreatomagmatic eruptions. A study of Vesuvian deposits (Cioni *et al.* 1992), however, found that type 4 morphologies only occurred in

deposits resulting from magmatic phases involving very fluid magma, suggesting that morphology is not a clear indication of magma:water interaction.

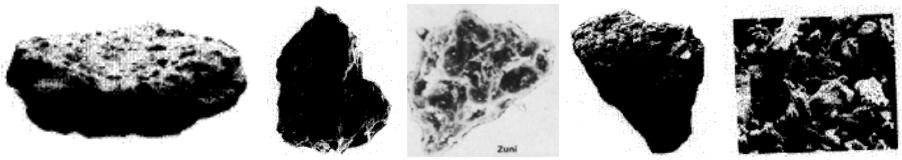

Figure 1.8 The five pyroclast morphology types (in order 1-5) of Wohletz (1983).

Barberi *et al.* (1989) used lithic proportions to distinguish between wet and dry eruption deposits. Their work on Vesuvius led to the conclusion that phreatomagmatic eruptions (*sensu stricto*) produce deposits with high lithic amounts (compared with dry magmatic eruptions with close to, or 100%, juveniles). Lithics were then used to deduce fragmentation depth level(s) and aquifer source. Barberi *et al.* (1989) also suggested that increase in gas pressures within the conduit could hinder further interaction of water with magma (rather than fluxes of material). They also established the use of lithics to identify probable fragmentation depth, aiding both knowledge of magmatic processes and hydrological information (aquifer vs. aquiclude) (e.g. Auer *et al.* 2007; Di Traglia *et al.* 2009). A high abundance of lithics is often interpreted as signifying a groundwater source, given that fragmentation will more likely be sub-surface (e.g. Allen *et al.* 1996; Németh and White 2003; Carey *et al.* 2007; Di Traglia *et al.* 2009); this is backed up by White's (1996) observation that lower lithics are more likely with interaction with relatively clear water and a higher water content. Carey *et al.* (2007) pointed out with the 1886 Tarawera eruption that a high lithics content, especially if of one type, can simply indicate passive entrainment of weak country rock. There is a distinct lack of using such information to gain further insight into aquifer characteristics, such as storativity and transmissivity, however. Changes in eruption style from phreatomagmatic to magmatic (or vice versa) are deemed to be either a magmatic effect (change in ascent rate) (Houghton *et al.* 1999; Martin and Németh 2006; Di Traglia *et al.* 2009), or due to a lack of water supply/being cut off from the supply (following Walker and Croasdale 1971), with no attempt at exploring this further.

A significant indicator of external water involvement in eruptions is clast vesicularity. Building on previous observations, Houghton and Wilson (1989) wrote a seminal paper providing both a method and numerical data to help determine the presence of external water and eruption processes. For 'dry'

eruptions, the arithmetic mean of vesicularity of 70-80 % is to be expected for a sample of juvenile lapilli; for 'wet' eruptions, this value could be as low as 4 %. The difference in vesicularity is thought to result from water chilling the magma prior to peak vesiculation. A greater range of vesicularity values will also result from water-magma interaction due to the fact that magma is usually heterogeneous and vesiculation will be at different stages in different parts of the magma (Houghton and Wilson 1989). This general pattern can, however, be affected by several factors: magma ascent rate, bubble ascent rate, magma viscosity, magma discharge rate, and timing of magma-water interaction. It is possible for rapidly degassing basaltic magma to have magmatic vesiculation values as low as 50 % (Houghton and Wilson 1989).

The appearance of glass is a sign of water involvement during an eruption. The rapid quenching of basaltic magma leads to the formation of tachylite, a dark brown-black opaque Fe/Ti-oxide-rich glass, or sideromelane, a lighter, transparent variety (Walker and Croasdale 1971; Fisher and Schmincke 1984; Stroncik and Schmincke 2002; Befus *et al.* 2009). The lighter, relatively microlite-free sideromelane reflects a much more rapid quenching and, hence, an abundance of external water (Fisher and Schmincke 1984). In aqueous environments, sideromelane can alter to palagonite, a distinct yellow-brown amorphous substance (Cas and Wright 1987; Stroncik and Schmincke 2002; Zanon *et al.* 2009). The identification of palagonite in volcanic deposits is therefore important, not only for determining the existence of sideromelane, but it may also reflect a high water content in the host base surge (Cas and Wright 1987). Quench textures in juvenile crystals, such as swallow-tailed plagioclase laths and skeletal olivine, can also point to water involvement (Shelley 1993).

The most recent method employed in determining external water involvement in eruptions is geochemistry. Slejko *et al.* (2004) identified a slight Sr enrichment along with OH differences in phreatomagmatic glass relative to purely magmatic eruptions.

1.5.3 Quantifying External Water Involvement

Despite the evidence that water:magma interaction plays an important role in determining eruption style, and the establishment of deposit characteristics, there

is still no satisfactory way to establish the actual ratio of water to magma. The first and still most commonly used attempt at applying a numerical value to the external water input is that devised by Wohletz and Sheridan (1981), Sheridan and Wohletz (1983), Wohletz (1983) and Wohletz (1986). Although their values, obtained through experiments using thermite and water, are valid, there is no accurate way to gain a water:magma ratio without replicating fully thee eruption conditions, given the vast array of factors that contribute to the resulting deposit (e.g. Sohn 1996). To confuse matters, Zimanowski *et al.* (1991) found that water:magma ratios from 1:6 to 1: 25 can produce explosive eruptions. The result is that researchers who are not interested in detail in the hydrology of eruptions can either give rough estimates of water:magma ratio from figures such as Kokelaar (1986), or just refer to relatively high or low water:magma ratios (e.g. Carey *et al.* 2007).

Fisher and Schmincke (1984) related soft sedimentary deformation structures in base surges to water contents of 15-20 %, which could aid calculation of external water input, although the source of this water might not be directly related to eruption processes. This water content would imply an overabundance of water relative to that necessary for optimum fragmentation, which is not always reflected in grain size (Cas and Wright 1987).

One criticism of the experiments by Sheridan and Wohletz (1981) and Zimanowski *et al.* (1991) is the use of bi-distilled water as a coolant. An impure coolant will have a clear impact on the mass water/magma ratio, a quantity that is hard to figure out even for experimental conditions, given that not all of the water and/or magma will interact with the other (White 1996) (although one could argue that mass volumes are more important for palaeogeographical reconstruction). White (1996) made the important distinction between a mixing coolant:magma ratio and a mass water:magma ratio, with the coolant:magma ratio controlling the water:magma ratio. In order to get the supposed 'optimum' water:magma ratio of 0.33 (near the figure of Wohletz 1986), 3 g of water per cm^3 would be required; if an impure coolant is used, then the mixing ratio would have to increase depending on the amount of sediment, but if the ratio refers to the relative amounts of coolant and magma, then the mass ratio has to be lower (White 1996). One method for overcoming this problem would be to calculate the amount of passively entrained

and interactive particles and then input that into a simple equation, such as follows:

Interaction mass ratio = M_w/M_m

Where M_w = proportion of interactive particles in a bed

$M_m = M_c - M_{c.\ solids}$

Where M_c = total coolant = $M_{c.\ solids}$/ inferred water content of tephra

$M_{c.\ solids}$ = (non-interactive particles or 1-M_w) (White 1996).

The main limitation with this is the ability to accurately estimate the amount of interactive versus non-interactive particles (White 1996); another problem is the assumption of water content of the tephra.

A rare example of estimating water volumes from volcanic deposits was presented by Jurado-Chichay and Walker (2001). In this paper, Plinian rhyolitic deposits were assessed. The total volume of each bed was calculated using Pyle's (1989) method, and then water was calculated as a fraction of that volume. Assumptions used in calculating the water volume were that 50% of the bulk volume of each water-affected deposit, and that the mixing volume water:magma ratio was 1. Actual equations were not included, but they worked out for one unit with a volume of 15.5 km^3, a water volume of 64 $x10^6$ m^3 was involved, the same size as that of a nearby lake (Jurado-Chichay and Walker 2001). An important note about this study was that the calculation of the volume of water involved was simply that needed to flush ash out of an eruption plume. Explosive interaction with magma was inferred for some of the units, but the volume of interactive water was not quantified (Jurado-Chichay and Walker 2001). This paper highlights the fact that, despite having excellent field data, assumptions were still prevalent in arriving at water volumes, and were only seemingly validated using known hydrology of the area, which may not have been an accurate reflection of hydrology at the time of eruption.

1.5.4 Summary

Field observation of volcanic eruptions has revealed that the most obvious distinction between the various basaltic volcanic landforms is the existence of external water. Laboratory experiments and analogy led to the attribution of this difference to fuel-coolant interaction, whereby water causes a chain-reaction

explosive fragmentation of magma. Over the last few decades, significant progress has been made in correlating deposits' physical characteristics with the involvement of external water, so that this can be determined with a high degree of certainty. Unfortunately, the quantification of relative and numerical volumes of magma and water continues to be plagued by the number of confounding variables that exist in a given dynamic eruption system. This limits the application of deposits to paleogeographical reconstruction or furthering hydrological knowledge. The difficulties inherent in discriminating between underlying processes are such that they may never be solved to enable accurate estimation of external water involvement.

2 *Geological and Hydrological Setting of the Taupo Volcanic Centre (TVC)*

2.1 Introduction

The geological setting and hydrological setting are both pivotal to the occurrence and nature of the basalt deposits that exist within the Taupo Volcanic Centre (TVC). This chapter describes the setting of the four basalts examined in this study, illustrating the close relationship between geology and hydrology in the area.

2.2 Geological Setting

The monogenetic basaltic volcanoes of this study lie within the Taupo Volcanic Centre (TVC), which is one of the most productive rhyolitic centres in the world, with an average eruption rate of 6.5 km^3 of magma per thousand years since c. 65

ka (Wilson 1993). The TVC is one of more than eight volcanic centres within the Taupo Volcanic Zone (TVZ) (Hiess *et al.* 2007), which is an area of back arc crustal extension in the North Island of New Zealand (Rowland and Sibson 2001). The tectonic situation of the TVZ is complex, in that it is the continental continuation of both a) the Tonga-Kermadec Trench, a 3000 km-long zone that marks where the Pacific Plate subducts under the Indo-Australian Plate, and b) rifting that originates in the Havre Trough (**Figure 2.1**) (Rowland and Sibson 2001).

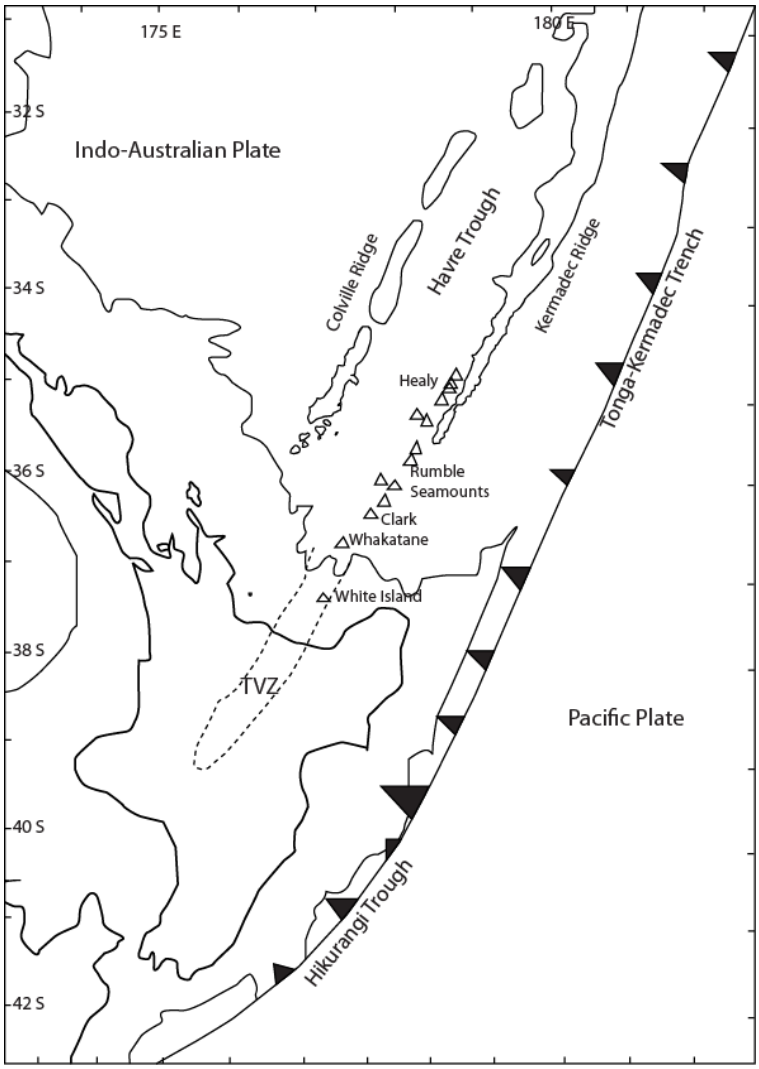

Figure 2.1 Map showing tectonic setting of the Taupo Volcanic Zone (TVZ). Modified from Gamble *et al.* (1990); Price *et al.* (2005).

Subduction began near the beginning of the Miocene (~ 23 Ma), but rifting did not commence until nearly 1 Ma (Wilson *et al.* 1995). The continental crust below the TVZ is estimated to be 15 km thick, significantly thinner than typical continental crust (> 30 km; Wilson *et al.* 1995; Smith *et al.* 2007), and

accommodates a magmatically-derived heat flow of up to 800 MW m^{-2} (Wilson *et al.* 1995; Rowland and Sibson 2001; Smith *et al.* 2007).
As a result of its active tectonic setting and thin 'sub-continental' crust (R. M. Briggs pers. comm. 2009), the TVZ is known for its seismic, volcanic and geothermal activity.

Andesitic volcanism began in the TVZ c. 2 Ma, with dacite, rhyolite and basalt eruptions occurring from c. 1.6 Ma (Wilson *et al.* 1995; Hiess *et al.* 2007). Since that time, approximately 15,000 to 20,000 km^3 of magma has been erupted. The composition of magma has dominantly been rhyolite (95 %), with minor andesite and dacite, and rare basalt (comprising 0.1 %) (Cole 1981; Graham *et al.* 1995; Houghton *et al.* 1995; Wilson *et al.* 1995). Wilson *et al.* (1995) note that all basalts have an age post-dating the Whakamaru eruption (~ 320 ka), possibly reflecting their susceptibility to burial or erosion, instead of an absence of basaltic volcanism prior to the Whakamaru eruption. The distribution of surface outcrops has lead to the generalisation that andesite and dacite occur together, whereas rhyolite and high-alumina basalt (HAB) co-occur, often as assemblages within individual calderas (Cole 1981; Graham *et al.* 1995). The rhyolite-basalt dichotomy has given rise to theories of genetic relationships (such as evolution of basic magma or basalt inducing melting of a crustal source – e.g. Hochstein *et al.* 1993; Graham *et al.* 1995; Smith *et al.* 2005; Hiess *et al.* 2007), although the link between faults and the location of basalt eruptions indicates that faulting may be a key factor in basalt eruptions (Gamble *et al.* 1990; Hiess *et al.* 2007).

Possibly as a result of an easterly migration of the axis of rifting (Wilson *et al.* 1995), the geological record suggests that volcanic activity at the TVC began ~ 320 ka, coinciding with the abatement of activity at Whakamaru caldera (Sutton *et al.* 1995). Little is known about eruptive activity over the next ~ 255 ky, although the large volumes of sub-surface andesite and andesite xenoliths within ignimbrites suggest that andesitic volcanism was important (Browne *et al.* 1992; Cole *et al.* 1998); at least two ignimbrites were also produced, and several HAB eruptions (including three of the four studied in this thesis) occurred (Brown *et al.* 1994; Cole *et al.* 1998). There has been recent debate as to whether or not these basalts belong to TVC or Whakamaru, given their age and location outside of

Taupo caldera (Rowland and Sibson 2001; Hiess *et al.* 2007); however, most geologists associate the HABs with TVC (e.g. Cole 1981; Brown *et al.* 1994; Hiess *et al.* 2007), and this is the stance taken here. From ~ 65 ka, as marked by Rotoehu Ash, several pyroclastic eruptions and accompanying rhyolite dome-building episodes are preserved in the rock record, but it is in the last 26.5 ky that Taupo has been most frequently and most explosively active: the 26.5 ka Oruanui eruption, which erupted an estimated 530 km^3 of magma, was followed by at least 28 more (rhyolite) eruptions, including the 232 A.D. plinian eruption (Wilson 1993; Sutton *et al.* 1995).

The TVC, like the rest of TVZ, is also known for its seismic and geothermal activity. There are many faults in the area; most strike north-north-east, parallel to the axis of subduction (Brown *et al.* 1994; Wilson *et al.* 1995; Hiess *et al.* 2007), and a number of them, including the Horomatangi Fault and the Northern Bays Fault, appear to be related to calderas (Wilson 1993). All of the faults are situated within the Taupo Fault Belt, an extensional area ~ 15 km wide comprised of normal faults that have been active during the last 10 ky (some are still active; Cole 1981; Villamor and Berryman 2001; de Ronde *et al.* 2002),which has more recently been termed the Raumoko Rift System by Rowland and Sibson (2001). Most of the estimated 8 ± 4 mm of rifting that takes place each year in the TVZ is accommodated by the Raumoko Rift (Rowland and Sibson 2001). As a result of the ongoing seismic activity, there are several horst and graben features in the area, forming a sharply defined set of bays, including Whakaipo and Whangamata (Brown 1990 Brown *et al.* 1994; Rowland and Sibson 2001; de Ronde *et al.* 2002). This has important implications for the surface distribution of geological units: along the Kaiapo Fault, for example, both the Huka Falls Formation and the Kaiapo Basalt are found directly east of the fault, but there is no trace to the west (**Figure 2.2**) (Brown 1990; Wilson 1993; Brown *et al.* 1994). Earthquakes in the area tend to occur in swarms at shallow depths, suggesting that they are the result of magma movement within the crust (Smith *et al.* 2007). Wilson (1993) also raised the possibility that earthquakes and faulting on a long timescale is related to supply of magma bodies.

The geothermal activity in the Taupo area is well known, with the majority of the area north of the town being exploited for commercial use (e.g. Wairakei,

Broadlands-Ohaaki, Mokai) (Browne *et al.* 1992). The volcanic centre to which the geothermal systems belong can be debated, given the rather arbitrary nature of the Taupo and Maroa caldera boundaries, but there is additional geothermal activity around and within the lake margins, such as Spa, Waitahanui, Western Bay, and Horomatangi (Sutton *et al.* 1995; de Ronde *et al.* 2002). Little work has been done to establish the age of currently active geothermal systems, although the the average TVZ geothermal system is stable for at least 200 ky (Bibby *et al.* 1995). Given their volcanic setting, it is logically assumed that these geothermal systems are magmatically driven, rather than being sedimentary (Kühn, 2004). For Western Bay, cooling Oruanui magma has been postulated as that system's heat source, whereas Horomatangi system is actually associated with the Taupo 232 A.D. eruption vent, and therefore believed to be younger than 1.8 ka (de Ronde *et al.* 2002).

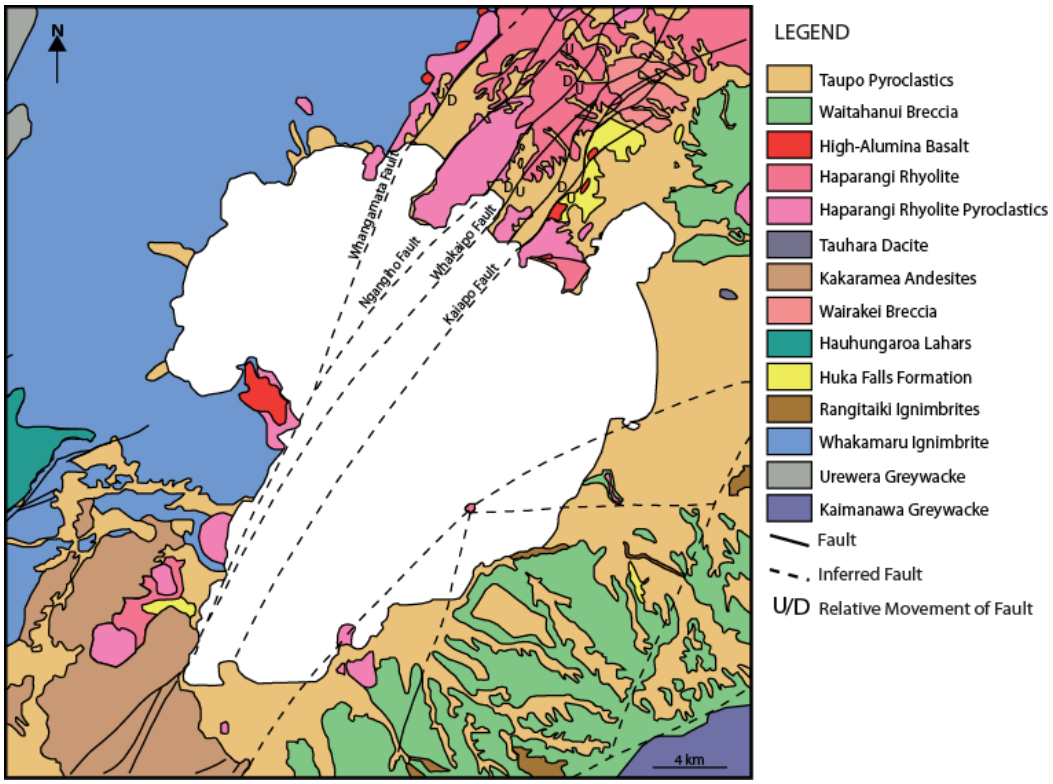

Figure 2.2 Geological map of the Taupo region (modified from Grindley 1960; Brown *et al.* 1994; Hadfield *et al.* 2001).

The complex 320,000-year volcanic and tectonic history of the Taupo area has buried or eroded most of the earlier rock record of the TVC (Wilson *et al.* 1995). One consequence is that the Mesozoic basement greywacke that underlies the

majority of the North Island is not exposed at the surface (Wilson *et al.* 1995). The discovery of greywacke at 1-3 km depth at Rotokawa and Ohaaki indicates that the sediment comprising the greywacke basement was at least deposited there initially (Browne *et al.* 1992; Wilson *et al.* 1995; Wood *et al.* 2001). The nature of this greywacke and its connection with magma genesis in the area is still being debated, however (Hochstein *et al.* 1993; Graham *et al.* 1995; Wilson *et al.* 1995; Wood *et al.* 2001; Charlier *et al.* 2005).

2.3 Hydrological Setting

Lake Taupo is the result of several volcanic eruptions and consequent structural collapse (Manville and Wilson 2004) and is New Zealand's largest lake, with an area of 623 km^2 and a maximum depth of 185 m (Nelson and Lister 1995). The sheer size of the lake renders it to be of great hydrological significance in the region. Many streams flow into the lake, and outflow is to the Waikato River. Equally important is the groundwater resource, which tends to flow toward the lake (Hadfield 1995, 2007; Morgenstern 2007). The hydrological systems in the Taupo region appear to be more affected by volcanism than by climate (Clement and Fuller 2007), and this is illustrated by the change in the configuration of the lake, and the development and nature of the groundwater systems.

2.3.1 Lake Taupo

Lake Taupo formed following the c. 26.5 ka Oruanui eruption, when water in-filled the resulting caldera (in addition to other depressions) (Manville and Wilson 2003). Establishing the presence and/or configuration of any lakes prior to Oruanui is more problematic, due to the lack of remaining geological evidence, partly due to the Oruanui eruption itself (Cole *et al.* 1998; Manville and Wilson 2004). The presence of the Huka Falls Formation has, however, provided some indication of pre-Oruanui surface hydrology: lacustrine sediments in the area (the Huka Formation) represent a former lake, referred to as Lake Huka by Manville and Wilson (2004). The location of this lake was the Taupo-Reporoa Basin and, with the age of the Huka Falls Formation being estimated at between ~ 300 ka and 27 ka (Henley and Stewart 1983; Manville *et al.* 2007), it is likely that this lake

was a stable topographical feature for the majority of the late Pleistocene (Manville and Wilson 2004). In fact, the widespread nature of lacustrine sediments throughout TVZ indicates that large lakes have existed for most of the time since volcanic activity began (Manville *et al.* 2007).

The exact nature of any lakes in the intervening time cannot be known for certain, although work by Brown *et al.* (1994) on the K-Trig basalts suggests that there was a lake that covered the southern part of that area, up to 4 km north of the modern lake. There is also evidence that, at some point (maybe a few thousand years) preceding the Oruanui eruption, Lake Huka was divided into two lakes: a northern one in the Wairakei area, and a southern one presently covered by the eastern part of Lake Taupo (Manville and Wilson 2004). The presence of Oruanui fall tephra overlying fluvial sands also points to the possibility of a wide, shallow river connecting the two lakes (Manville and Wilson 2004).

Since the Oruanui eruption, there are indications that the lake level (and size) has changed continually. The Oruanui eruption, when ~ 530 km^3 of magma was erupted, had a significant impact on the prevailing landscape. The Oruanui ignimbrite destroyed the previous lake, blocked water flow between Taupo and Reporoa, and created an elevated rim (Manville and Wilson 2004). Infilling of the lake occurred during the Last Glacial Maximum (LGM), when conditions were most likely cooler, drier and windier, so inflow rates from streams (once re-established) could have been 30% lower than today's 70-110 m^3 s^{-1}. Nevertheless, it is estimated that refilling to the new elevation of 500 m a.s.l. (140 m above the present level) would have taken less than 200 years (Manville and Wilson 2004). The ensuing overflow of the lake created an outlet at Waihora, ~ 20 km west of the present-day outlet. Accompanying erosion lead to a 10-20 m drop in water level to 480 m a.s.l., where the lake level stabilised until ~ 22.5 ka, when a catastrophic breakout occurred, with the water level dropping by up to 80 m, releasing about 60 km^3 of water downstream (Manville *et al.* 2007). The newer level of nearly 405 m a.s.l. was held up by the Huka Falls Formation, until consequent downcutting by the Waikato River lowered the level of the lake to its present level by 12 ka (Manville *et al.* 2007).

Apart from a possible further flood at 3.5 ka following the Waimihia eruption, the lake remained semi-stable until the 232 A.D. Taupo eruption, which palaeo-lake levels suggest brought about another raising of the lake level and subsequent flooding; this time the rise was to 34 m above current level and ~ 20 km^3 of water was released (Manville and Wilson 2003; Manville *et al.* 2007). Since that time, the lake is presumed to have had a stable configuration. **Figure 2.3** illustrates the inferred changes in major surface hydrology over the last ~ 220 ky.

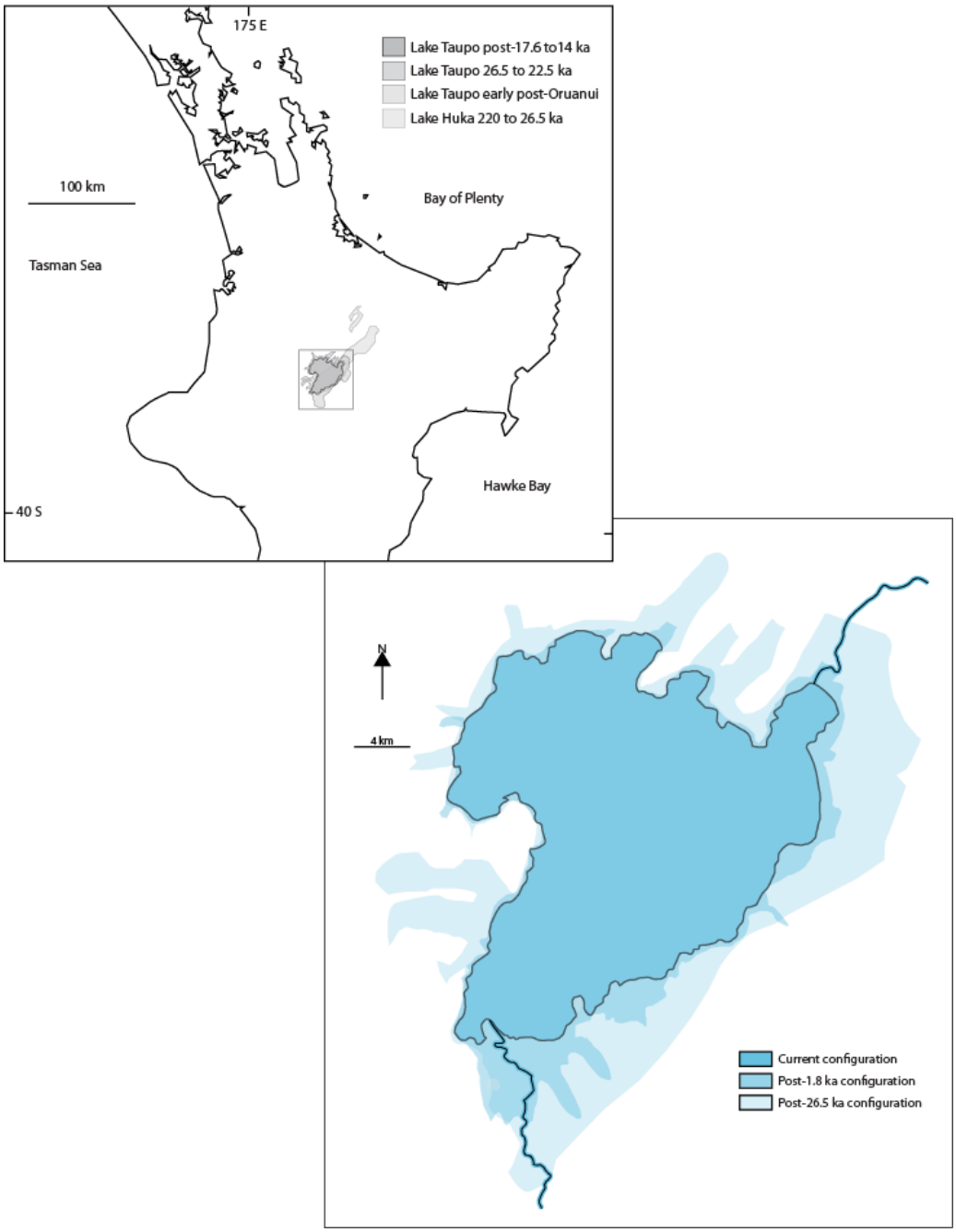

Figure 2.3 Configurations of Lake Taupo over last ~220 ky (adapted from Manville and Wilson 2003, 2004).

2.3.2 Groundwater and Geohydrology

The immediate area surrounding Lake Taupo is an important groundwater resource, with ~ 5 % of groundwater flow going directly to the lake and constituting up to 90 % of stream baseflow into the lake (Hadfield *et al.* 2001; Vant and Smith 2004). This resource's importance has grown with increased awareness of pollution via non-point sources into the lake. Recent findings indicate that currently, in the northern and western parts of the catchment at least, the hydrology is 'very complex', in large part due to changes in geology, with up to 80 % of flow being piston flow (Morgenstern 2007). Establishing the sub-surface hydrological history of an area is difficult, and this is particularly so for the TVC, where geological forces such as earthquakes and volcanic eruptions have continually changed the landscape (e.g. Wilson 1993). Local geothermal activity adds further difficulty in assessing hydrogeology: Oruanui pyroclastic flow deposits, for example, become cemented in areas of hot water movement (Manville and Wilson, 2004). The change in lake configuration and climatic conditions over time would also have a strong bearing on the nature of the groundwater system.

The hydrology of Taupo is strongly constrained by its geology. The majority of the area surrounding the lake is comprised of rhyolitic ignimbrite, including the Whakamaru, Oruanui and, to a lesser extent, Taupo ignimbrites (Hadfield *et al.* 2001). The existence of older ignimbrites has been inferred from analysis of lithic clasts within phreatomagmatic deposits (e.g. Smith, 1990) and other, younger ignimbrites (Cole *et al.* 1998), along with rare surface ignimbrite exposures (Sutton *et al.* 1995; Cole *et al.* 1998). However, neither the hydrological characteristics nor a clear correlation between these ignimbrites has been established (Cole *et al.* 1998). A similar case exists for the andesites and dacites in the area (e.g. Graham and Worthington 1988; Browne *et al.* 1992; Graham *et al.* 1995; Brown *et al.* 1998).

There is a marked difference in hydrology between the northern and western parts of the Taupo catchment due to a difference in the dominant ignimbrites found there, as summarised in **Table 2.1**.

Table 2.1 Difference in hydrology due to ignimbrite units for Taupo catchment. Note that the dominant ignimbrite is underlined. (Vant and Smith 2004; Morgenstern 2007)

Area of Catchment	Ignimbrite	Nature of Dominant Ignimbrite	Dominant Flow	Stream Example
North	Taupo <u>Oruanui</u> Whakamaru	Non-welded	Lake bed seepage	Whangamata: 110 L s^{-1}, 3 L s^{-1} km^{-2}, 110 mm yr^{-1}
West	Oruanui <u>Whakamaru</u>	Welded	Quick, near-surface runoff	Waihora: 1900 L s^{-1}, 29 L s^{-1} km^{-2}, 900 mm yr^{-1}

The difference in stream flow reflects, in part, the wetter climate of the west, but also points to differences in permeability, and implies that the Oruanui ignimbrite makes a better aquifer than the Whakamaru ignimbrite (Vant and Smith 2004; Morgenstern 2007). Indeed, according to Henley and Stewart (1983), most domestic wells draw from the Oruanui ignimbrite. There are, however, three other known aquifers: the Taupo pumice that overlies the Oruanui ignimbrite; the Huka J pumice breccias within the Huka Falls Formation; and the Waiora Formation, which is the principal reservoir at Wairakei. Although currently the main aquifer at Kinloch, the 20 m-thick Taupo pumice aquifer is too young to be considered here further (Dabell *et al.* 2006). The other two aquifers, the Huka Falls Formation and the Waiora Formation, are both rather generic units that comprise part of the Huka Group (Henley and Stewart, 1983; Brown *et al.* 1994). Within the field area, surface exposure of the Huka Falls Formation, the uppermost unit of Huka Group, is found east of the Kaiapo Fault; west of the fault, it disappears, but is presumed to occur at depth (**Figure 2.2**). This assumption is tentative, however, given the thinning of the unit to the west, along with its dominantly lacustrine depositional environment (Grindley 1965). Although nomenclature and definition of the Huka Group has changed over time (e.g. Martin 1961), the Huka Falls Formation is defined as a largely impermeable unit comprised of volcaniclastic (including basalt) and diatomaceous mudstones and sandstones (Grindley 1965; Glover and Stewart 1996).

Work by Environment Waikato (Hadfield *et al.* 2001; Vant and Smith 2004; Hadfield 2007) has established a simplified geological division for the northern and western catchments, based on observed and tested hydrological characteristics

(**Table 2.2**). Older pyroclastic units are understood to underlie the Whakamaru ignimbrite at depth (Reporoa Group; Gravley *et al.*2006), but are deemed to have similar aquifer potential as the Whakamaru ignimbrite (Hadfield *et al.* 2001).

Table 2.2 Geohydrological units of northern Taupo catchment (Hadfield *et al.* 2001; Hadfield 2007).

Geohydrological unit	Estimated Age (ka)	Intrinsic Permeability	Fracture-Induced Permeability	Hydraulic Conductivity (m d^{-1})
Rhyolite domes	3-320	low	high	n/a
Oruanui Ignimbrite	26.5	high	low	0.03-13.9
Rhyolite pyroclastics†	26.5-150	high	low	0.008-17.3
Basalt lava/pyroclastics	100-300	tuff, lava - low scoria - v. high	tuff, lava - high	n/a
Huka Falls Formation	100-200*	low	low	n/a
Rhyolite pyroclastics	150-320	low	high in welded zones	0.008-17.3
Whakamaru Ignimbrite	320-340	low	variable (0.2-1/m)	0.007-2.02

† Note that 'rhyolite' pyroclastics' were treated as one unit for hydraulic conductivity testing.

*** Age taken from Brown et al. (1994).**

The dominance of fault permeability is expected, given both the nature of most of the materials, and the tectonic nature of the region. Rowland and Sibson (2001) propose that fault 'accommodation zones' are responsible for increasing local permeability; such fault zones can increase permeability of volcanic rocks by up to 10 orders of magnitude (Forster and Smith 1989). The importance of faults is highlighted by Hadfield's (2007) flow path simulation map, which shows large movement along the Whangamata Fault, and the recent discovery of fracture-dependent permeability of up to 120 m d^{-1} in the Whakaroa Rhyolite near Kinloch (Hadfield 2007).

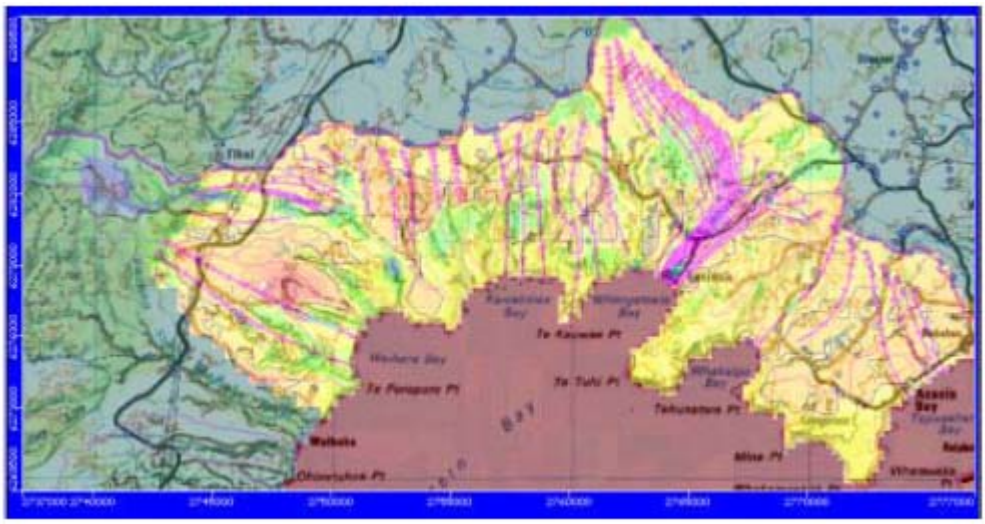

Figure 2.4: Flow simulation path for northern Lake Taupo catchment (from Hadfield 2007). Note concentration of flow that enters the lake by Kinloch (along Whangamata Fault).

3 *Methodology*

A number of methods were employed in obtaining of data for analysis. The various methods are presently described in approximate order of appearance in subsequent chapters.

3.1 Field methods

At each field site, stratigraphic logging of representative vertical sections was undertaken, and where possible, GPS coordinates were obtained for these sites. Changes in stratigraphy were recorded at the mm-cm scale for phreatomagmatic deposits, and on a cm-dm scale for the magmatic deposits, reflecting the nature of the respective deposits. Characteristics noted were: bed thickness, colour, sorting, grading, average grain size (mm), range of grain sizes (fine ash to bomb/block), morphology and componentry of five largest grains (in mm), induration, description of componentry, any sedimentary or deformation structures, and

geometry of bedding. Where bedding was clear or faults were present, dips and strikes were obtained using a Silva compass. At the quarry (Punatekahi), some dips were obtained by sighting, so are apparent dips. Logging was for the most part restricted to parts of the deposit that were directly accessible (within reach from ground level or by use of a ladder), but sight logging was completed for the upper half of the main outcrop at Kinloch, and one log at Kaiapo (site KC) was completed using scales from photographs. Accompanying field sketches were drawn, but were only used as reference and have not been included here.

3.2 Sampling

Sampling of material was primarily undertaken from representative layers from vertical logged sections, with a small amount of sampling at other points of interest at field sites, but at which logging was not done in detail. The locations of these and the other samples are given in **Appendix A**. Sampling was also restricted to levels which could be easily accessed and to material that could be extracted from the site and without altering the nature of the sample. The former restriction was most notable at Kinloch, for which the majority of the section could not be accessed, and the latter was a limiting factor at Kaiapo. At all sites, sample size was also an important consideration, given that the majority of samples had to be carried by hand or in a pack during transportation between the field site and the laboratory. The samples listed in **Appendix A** have their full University of Waikato sample number (from W20100001 toW201000107). For brevity, these samples are referred to as W1 to W107 in the text.

3.3 Grain Size Analysis

Grain size analysis was undertaken for all unconsolidated and friable samples by dry sieving. For dry sieving, the sample was oven-dried at ~ 45 °C for at least 24 hours, usually a week or more, depending on the nature of the sample. Manual shaking of the sample in a sieve stack (containing sieves for -4 to 4 Φ) for one minute was then done, before each fraction was weighed and retained. All weight and cumulative percentages were worked out using the post-sieving weight. Calculating the error from sieving was complicated by instrument error, at times

giving a total post-sieving weight greater than before sieving; the error from this source was not able to be accurately assessed, but in one case (sample W4) the post-weight was 22 % more than the pre-sieve weight. Where a loss of sample was found to have occurred during sieving, the average loss was 0.2 %, with a maximum of 0.5 %. The maximum sample loss was 4.5 g.

The raw data from each sample were then entered into an Excel spreadsheet (care of R. T. Smith and A. Pittari), which calculated cumulative percentage, modes, percentiles, median diameter and graphic standard deviation; the last two being Inman's (1952) statistics used to plot size versus sorting, following Walker (1971).

3.4 Vesicularity

Vesicularity was tested for as many loose (unconsolidated) units as possible. Testing involved the use of two methods:-

- ballast
- pycnometer.

The ballast method, which enables calculation of vesicularity and extent of magma:water interaction, was deemed the primary method; the pycnometer, which indirectly measures connectedness of vesicles and aids insight into eruption processes, provided complementary data.

The first method, described by Houghton and Wilson (1989), consisted of weighing 10 -4Φ juvenile clasts from each sample in air, moulding Parafilm to the clasts and re-weighing each under water, using a ballast if needed. The weight measurements (*W*) from this were used to calculate the density (or specific gravity, *SG*) of the clasts using the following equation (modified from Houghton and Wilson (1989):

$$SG = \frac{W_{air\ clast}}{W_{air\ clast} + W_{water\ sheet} - (W_{water\ clast+sheet+sinker} - W_{water\ sinker})}$$

The weight of each 5 cm^2 Parafilm square was assumed to weigh -0.03 g in water. In order to calculate actual vesicularity (*V*) using the density values obtained, the following equation was used:

$$V = \frac{100\ (DRE\ density - clast\ density)}{DRE\ density}$$

Instead of using a standard basalt dense rock equivalent (DRE) density value, a DRE density value was obtained for each site (with three from Punatekahi). For this, a powdered sample was placed into the MegaPycnometer 1000 and its density was measured (**Appendix C**). The pycnometer was calibrated prior to use (**Appendix C**) and resulting DRE values are given in **Table 3.1**.

Table 3.1 Dense Rock Equivalent (DRE) density values used for ballast vesicularity.

Sample Site	DRE (g/cm^3)
Acacia Bay	2.9092
Kaiapo	2.9592
Kinloch	2.9572
Punatekahi A	3.0173
Punatekahi A North	3.0218
Punatekahi B	3.2829

The pycnometer method involved cutting two clasts from each available sample into cubes, re-drying them in the oven (at ~ 45 °C) for more than 12 hours, weighing them, and then putting the cubes (one at a time) into the MegaPycnometer 1000 for volume and density measurement/analysis. The pycnometer was calibrated before each session to ensure accuracy. Vesicularity (connected porosity) was then calculated using the same equation as that of the ballast method. The cubes used in the pycnometer were also measured for density and vesicularity using simple volume: weight measurements. Volume of the cubes was measured using digital callipers (accuracy to 10^{-2} mm). Possibly due to the combination of the small size and the vesicular nature of the samples put into the pycnometer, results obtained from the pycnometer were in error, so have not been included in the thesis.

3.5 Componentry and Clast Morphology

For Punatekahi, componentry was undertaken for all fractions of sieved samples large enough to be analysed using a binocular microscope (2 Φ and coarser). For each fraction, a split was taken; the number of grains counted decreased with increase in grain size, so that at least 300 grains were counted for the 2 Φ fraction, and at least 25 grains were counted for the -4 Φ fraction (unless there were not enough grains in the fraction). The phreatomagmatic samples were invariably coated by secondary material (usually ash), making discrimination between components near-impossible for coarser fractions, becoming clearest for the 1 Φ and 2 Φ fractions. For analysis, the 1 Φ fraction was taken as representative, as clasts could more easily be identified, and the lower crystal content was a truer reflection of crystal content for the sample as a whole (as crystal content decreases with an increase in grain size). 200 grains were counted for each sample. To be consistent, componentry values for all sites were based solely on the 1 Φ values. Each fraction was divided up into three component types: juvenile basalt, juvenile crystals and lithics. Notes on colour, vesicularity and morphology were taken and, where possible, the different lithics and crystals were identified, aided by petrographic analysis. Scanning Electron Microscope (SEM) images were also taken on The University of Waikato's Hitachi Field Emission Scanning Electron Microscope for 10 selected samples, to get representative complementary morphology information on juvenile material from the four sites, and of powders from coatings of several clasts were analysed using Waikato University's X-Ray Diffractometer (XRD).

3.6 Petrography

Thin sections were produced from selected representative samples. The initial process in the making of thin sections differed for consolidated and for unconsolidated material. For consolidated samples, sample blocks were cut, and surface impregnation was done if required, before the blocks were mounted, grinded, and the cover slip adhered. For loose material, a representative sample of unsieved material was oven-dried, then further heated on a hot plate before

impregnation using araldite, after which, the samples could be treated like normal blocks.

Point counting was done on representative thin sections which were of good enough quality to enable accurate point counting. For basaltic samples, twelve categories were used for analysis (**Table 3.2**).

Table 3.2 Categories used for point counting of juvenile samples.

Category	Description
1	Plagioclase
2	Olivine
3	Augite
4	Groundmass
5	Vesicles
6	Sideromelane
7	Scoria
8	Xenocrysts
9	Ignimbrite
10	Rhyolite (not glass)
11	Pumice
12	Other (including glass)

For basaltic rock samples (lava, agglutinate, scoria), the boundary between groundmass and phenocrysts could be rather arbitrary, depending on the nature of the sample in question. Distinguishing between juvenile phenocrysts and xenocrysts was most difficult for plagioclase. Given the tendency for plagioclase to be strongly resorbed and contain oscillatory zoning or polysynthetic twinning in the non-basaltic samples, these were the main criteria used to categorise plagioclase as being a xenocryst, although it is accepted that this would not always be reliable. Large tabular or anhedral plagioclase crystals were also treated as being foreign in origin, although most of these also exhibited oscillatory zoning. The 'other' category consisted of sedimentary rocks, intrusive rocks, volcanic glass and unidentifiable material. Efforts were made to keep the latter type to a minimum, but at times were unavoidable, particularly for material which had been altered.

Silicic samples were given substitute categories depending on the nature of the rock. Such categories included quartz, hornblende, orthopyroxene, spherulites, glass (shards), and opaques (Fe-Ti oxides).

300 counts per slide was the goal count, but for several samples this was exceeded, with a maximum of 332 counts. Modal analyses are given in **Appendix E**.

3.7 Geochemical Analysis

X-Ray Fluorescence (XRF) major and trace element geochemical analysis was carried out on samples that were relatively fresh, had negligible vesicularity, and were of sufficient size to ensure enough powder was obtained for analysis. Analysis was constrained to basaltic material, except for a rhyolite sample of particular interest from Kinloch. Due to the ubiquity of fine-grained, vesicular, and weathered material, only five basalt samples were able to be analysed, and none from Acacia Bay met the criteria. For major element analysis, fused discs were made. For basalt samples, the flux and sample mixture was step-heated from 700 ºC, to 800 ºC to 1040 ºC at 15-minute intervals. The rhyolite sample was step-heated from 645 ºC, to 720 ºC, to 780 ºC to 825 ºC, to 1000 ºC at 15-minute intervals. Ammonium iodide was added to each sample before being poured.

To determine Loss on Ignition (LOI), for each sample an empty crucible was weighed, tared and then filled with 1-2 g of sample. The crucibles were then put in a furnace at 1000 °C for 60 minutes, left to cool, then re-weighed. The difference in weight (LOI) was converted to wt. %. The process was repeated for sample W74, which indicated a method error of 60 %. The results are given in **Table 3.4**.

Table 3.3 Calculation of Loss on Ignition (LOI) for major elements. W74* was second run used to calculate error in method.

Sample	Crucible (g)	Pre-heat sample (g)	Total weight (g)	Post weight (g)	Post sample (g)	Difference (pre-post) (g)	LOI (%)
W23	11.3368	1.9943	13.3311	13.3287	1.9919	0.0024	0.12
W60	11.405	1.9958	13.4008	13.4021	1.9971	-0.0013	-0.07
W74	12.918	1.9941	14.9121	14.9192	2.0012	-0.0071	-0.35
W74*	26.3944	1.9969	28.3913	28.3955	2.0011	-0.0042	-0.21
W87	13.127	1.9934	15.1204	15.1211	1.9941	-0.0007	-0.04
W93	12.6934	1.9985	14.6919	14.6957	2.0023	-0.0038	-0.19
W64	13.0762	1.9975	15.0737	15.0363	1.9601	0.0374	1.91

For trace element data, pellets were made. This involved mixing about 5 g of sample with a few drops of PVA before pressing.

4 Acacia Bay

4.1 Site and Facies Description

Phreatomagmatic tuff exposed along the modern Lake Taupo shoreline near Acacia Bay is interpreted as the remnants of a tuff ring. Vegetation cover and deep erosion have caused piecemeal outcrop exposure along ~ 1 km of the shoreline, although there is sufficient to demonstrate considerable lateral and vertical variation within the deposits. Two localities were selected for detailed study: a composite exposure south of the Acacia Bay (North) jetty (referred to as the 'Acacia Bay South' outcrop), and an outcrop situated to the north-east, at the shoreline of a smaller bay at Te Rimupotaka Point ('Acacia Bay North') (**Figure 4.1**). While it is possible that the northern outcrop was examined by Wilson and Smith (1985) and included in their Outlying Tuff facies, Acacia Bay South was not included and lies several hundred metres south of Wilson and Smith's (1985) field area.

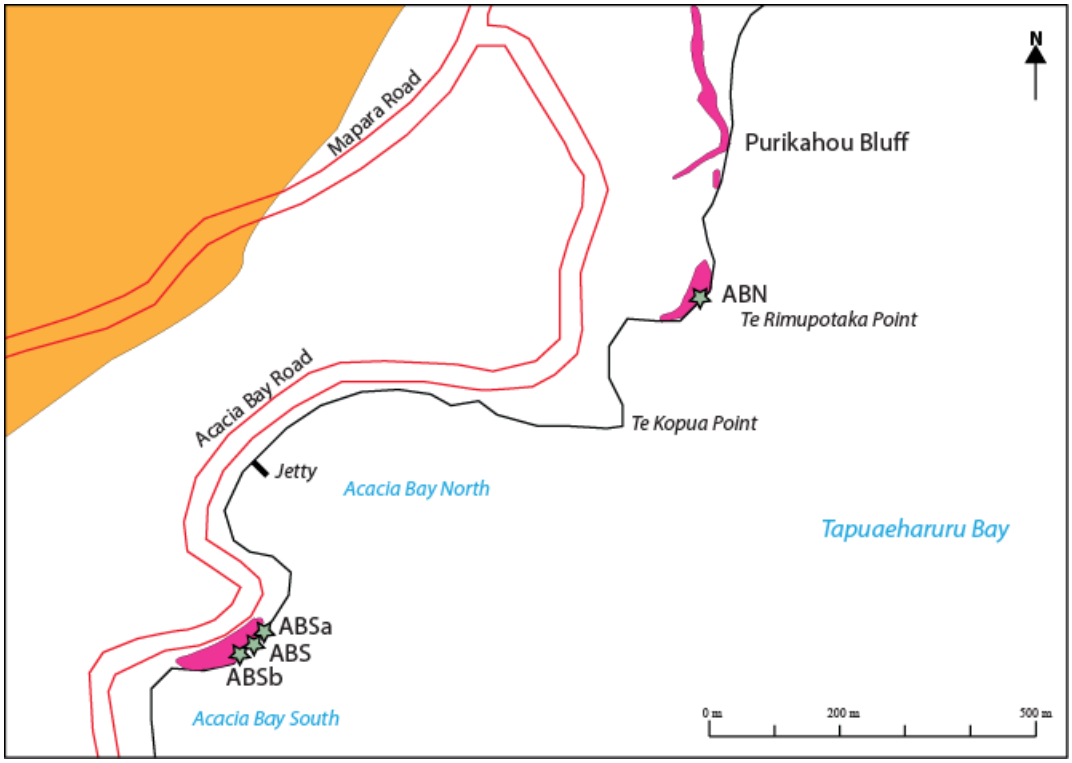

Figure 4.1 Map of Acacia Bay volcanics. Orange is rhyolite, pink is basalt. Stars mark field sites. Modified from NZMS260 Series U18 (1:50 000) Sheet U18.

4.1.1 Acacia Bay South

The deposit south of the Acacia Bay jetty is a ~ 20-m semi-continuous outcrop along the Acacia Bay walking track, and reaches a maximum thickness of 4 m. The exposure was logged at three sites (ABS, ABSa, ABSb) along the track (**Figures 4.2**, **4.3**, **4.4**) to examine apparent small-scale lateral variation. Given the proximity of the three logged sections, correlation of many features was expected; however, this was complicated by the poor exposure and the undulating nature of the track. An unconformity occurs just north of the southernmost section, where darker ash onlaps lighter grey, unconsolidated, sediment (**Figure 4.5**), otherwise there are no visible upper or lower contacts to constrain lithostratigraphic units, although it is possible that the deposit overlies the Huka Formation (following Hadfield *et al.* 2001; Manville and Reeves 2006).

A few metres above the ABS sites is an outcrop of rhyolitic ash (**Figure 4.6**). Correlation of it with known tephras was not determined, but it does constrain the height of the (preserved) subaerial outcrop to a maximum of ~ 10 m.

Acacia Bay South (Main Outcrop)

(GPS No.) E2773324 N6272577

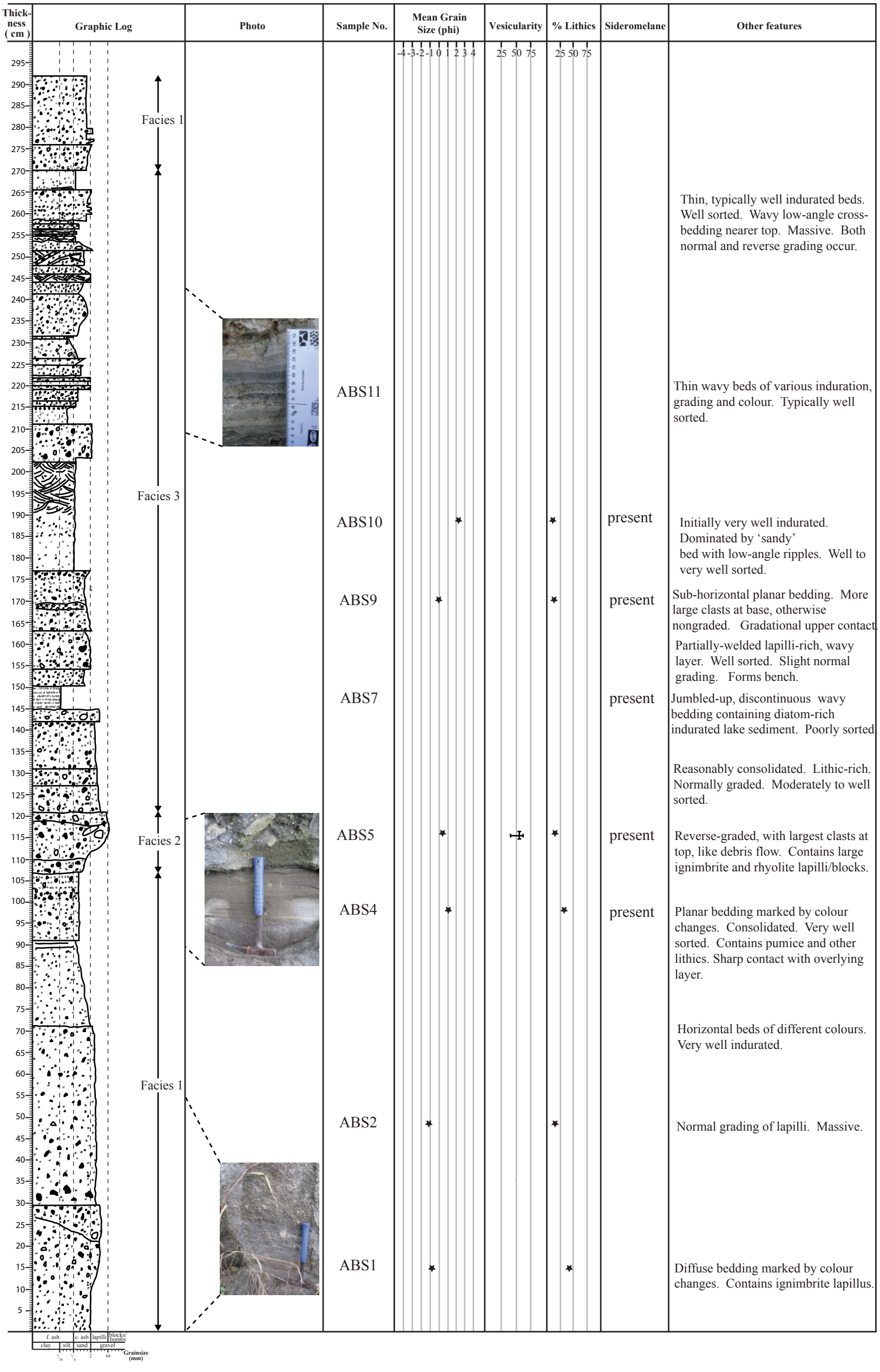

Figure 4.2 Stratigraphic log and data for Acacia Bay South (main outcrop).

Figure 4.3 Stratigraphic log and data for Acacia Bay South A.

Acacia Bay South A

(GPS No.) E2773335 N6272594

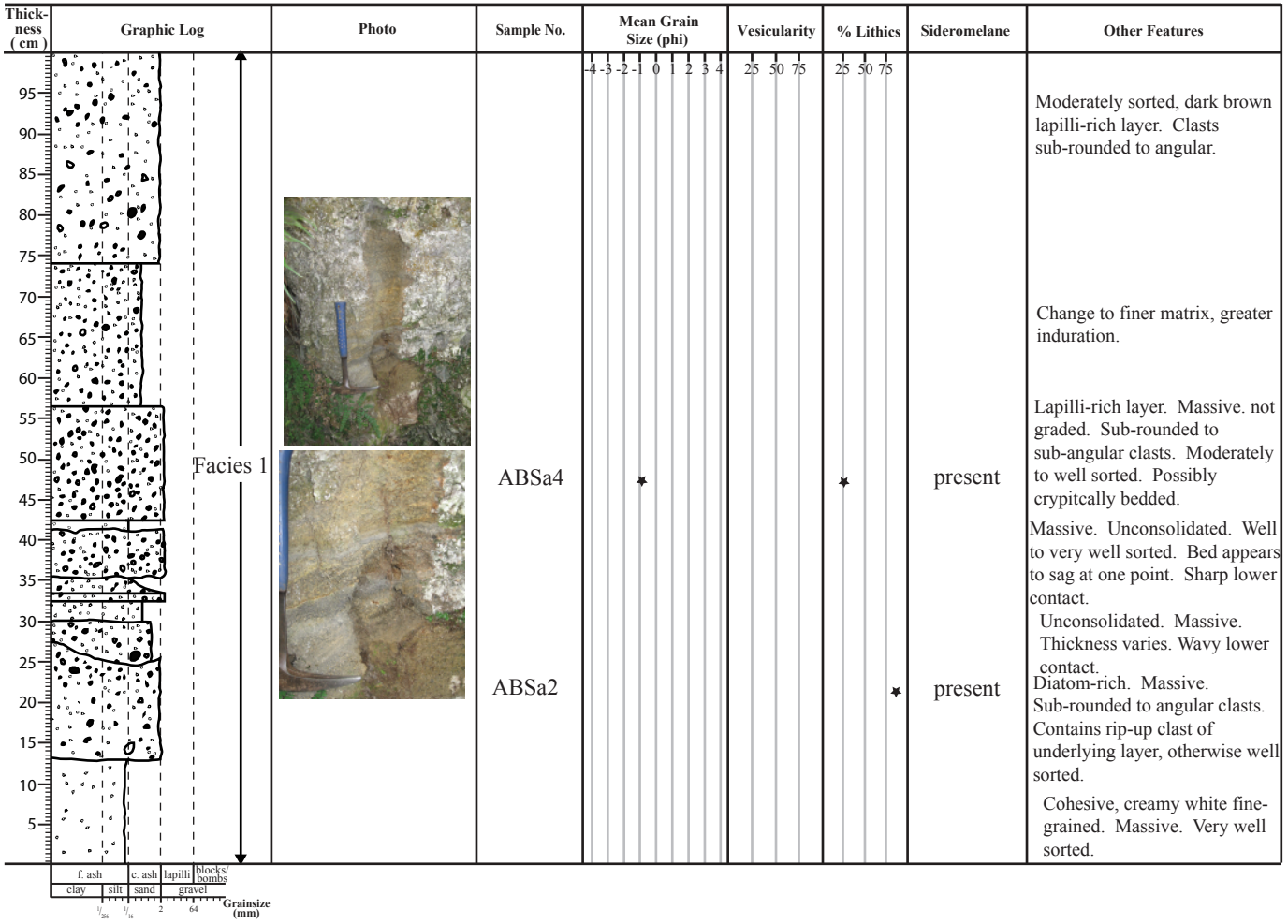

Acacia Bay South B

(GPS No.) E2773304 N6272566

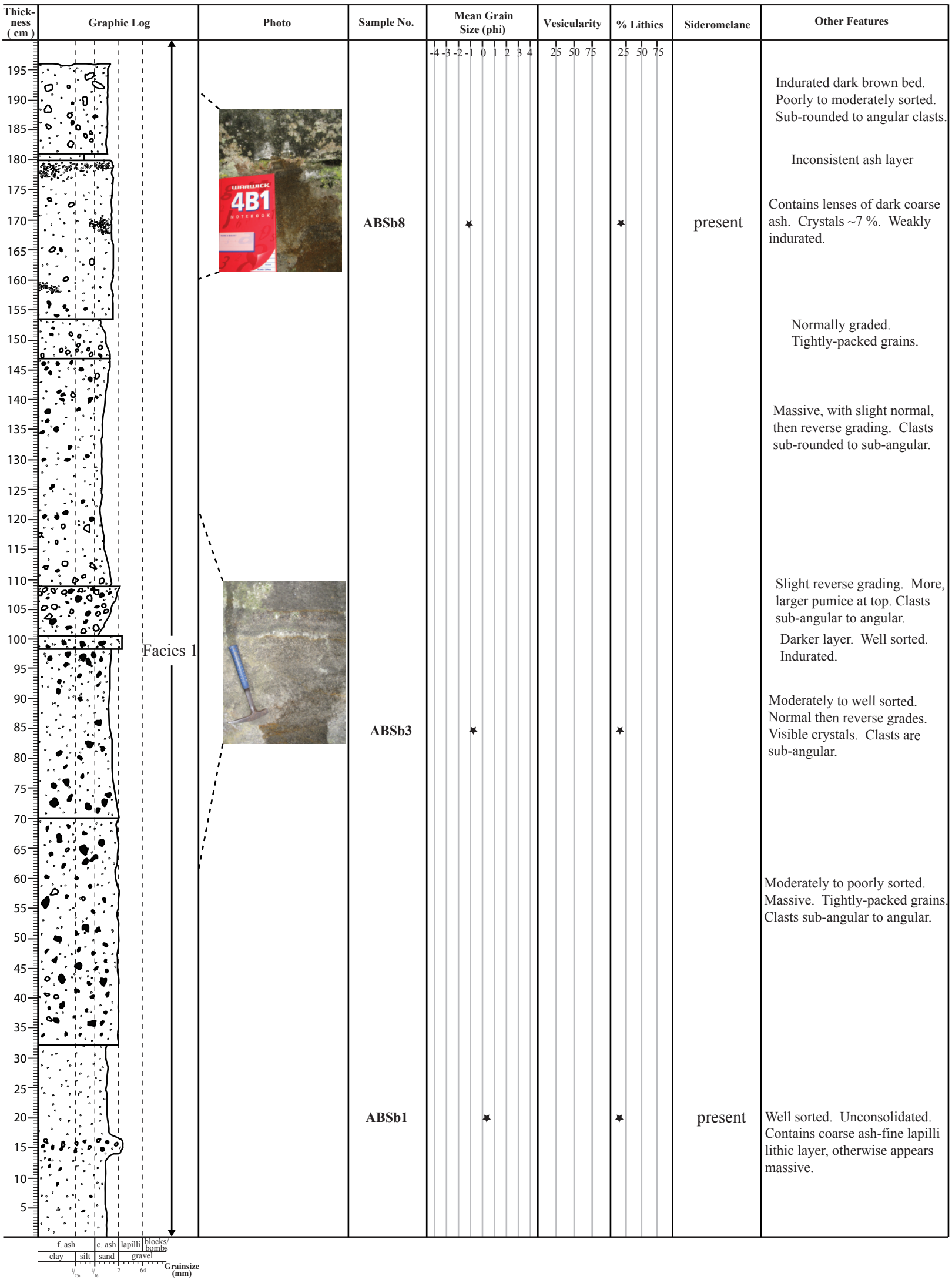

Figure 4.4 Stratigraphic log and data for Acacia Bay South B.

Figure 4.5 Onlap of Acacia Bay tephra onto lighter grey sediment at ABSb. Hammer is 30 cm long.

The best exposure of the tuff is halfway along the outcrop, where there is a transition from grey and brown massive coarse ash layers, to a mix of variously hued thin beds, and back to massivecoarse ash and lapilli beds. Taking into account the wavy nature of the beds, there is a shallow dip (2 °) to the south. Three main facies have been distinguished, as follows **(Figure 4.7**; numbers correlate with facies labels on stratigraphic logs):-

1) Coarse ash facies

   This facies is dominated by normally graded, moderately to well sorted, dark grey layers, several dm thick, within which are obvious bands of browner and lighter colours, reflecting variations in composition. The most noticeable lithic type is pumice, the larger clasts of which tend to form concentration clusters. Other lithics are less conspicuous and problematic to identify, due to the ash/secondary mineral coating, but appear to represent several rock types including rhyolite and ignimbrite. Light brown ignimbrite 30 mm across was the largest clast found. Both lithic and juvenile components are commonly sub-angular to angular. Although the layers are generally coherent, induration is variable, with a tendency towards greater induration with height.

Figure 4.6 Rhyolite tephra along Acacia Bay Road, inland of Acacia Bay South. Notebook is 17 cm long.

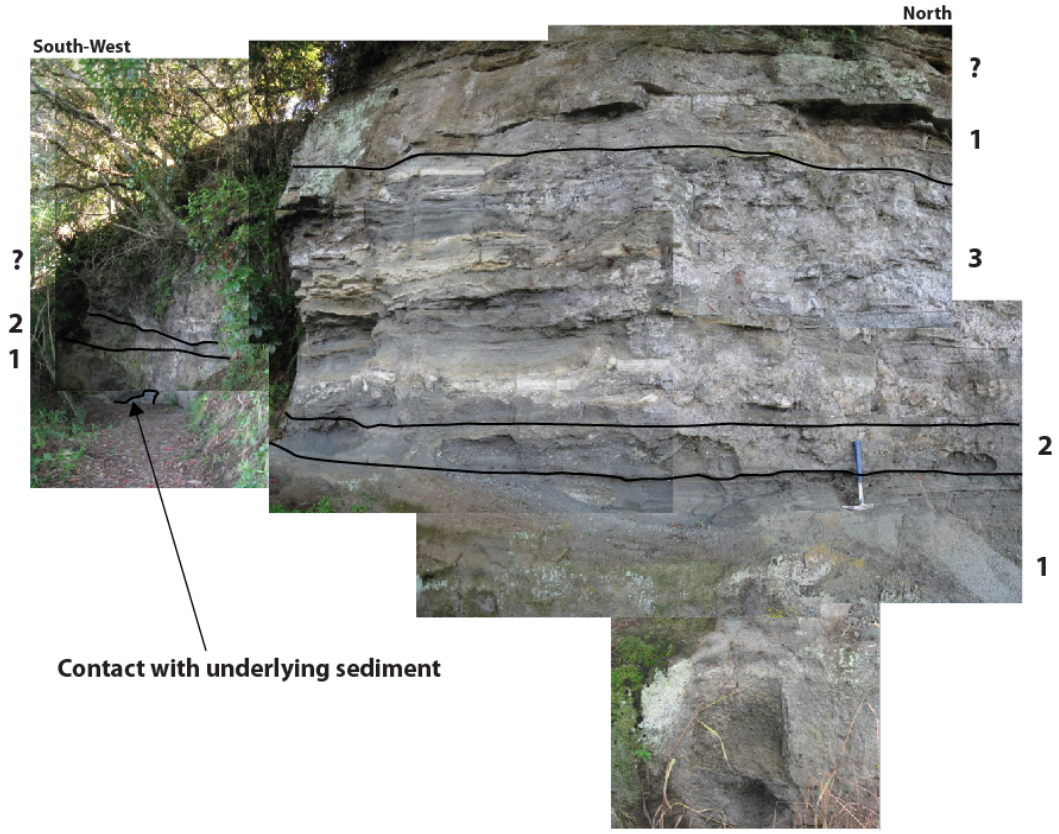

Figure 4.7 Facies of Acacia Bay South. 1 = coarse ash facies, 2 = lapilli- and bomb/block-rich facies, 3 = alternating fine ash-coarse ash/lapilli facies.

2) Lapilli- and bomb/block-rich facies

An overall dark grey, unconsolidated, poorly sorted unit comprised of angular lapilli and block fragments, up to 150 mm across (average of ~ 30 mm), set within a coarse ash matrix is the definition of this second facies (**Figure 4.8**). Noticeable lithics are pumice, purple rhyolite, and brown and light ignimbrite. The unit appears to be internally massive and is weakly reverse graded.

3) Alternating fine ash-coarse ash/lapilli facies

The beds comprising this facies range from white, indurated fine ash through to brown and grey unconsolidated fine lapilli. The fine ash forms thin-medium beds of well to very well sorted consolidated material ranging from soft clay to hard rock. Coarser beds range in thickness from less than 1 cm to more than 15 cm, and are also typically well sorted. Bedding varies greatly within the unit, from weakly laminated crude bedding in the finer-grained layers, to wavy cross-bedding and planar bedding in the coarser layers. Amplitude and wavelength of the cross-beds are 8 cm and 50 cm respectively. Both the finer and coarser beds are

discontinuous across the section, with variation in thickness and height, due to both lensoidal geometries and clean cuts of material that appear to have been broken off and transported from the rest of the bed (**Figure 4.9**). Lapilli within the beds are sub-rounded to angular and include juvenile scoria, pumice and pale rhyolite lithics.

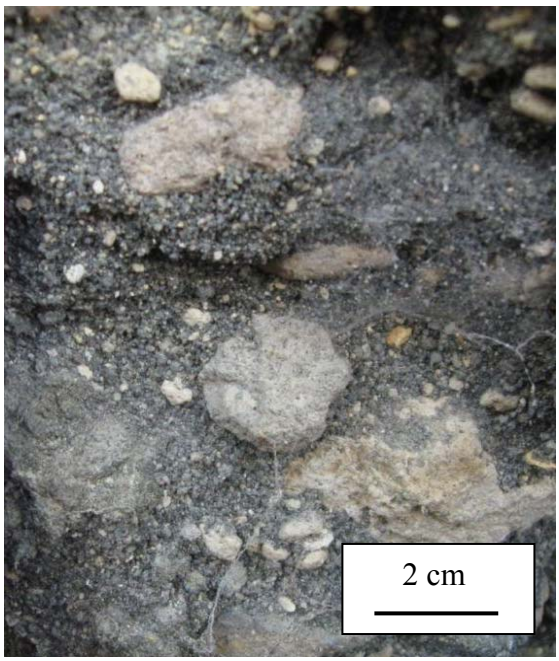

Figure 4.9 Lower section of alternating fine ash-coarse ash/lapilli facies, Acacia Bay South. Note breccia beneath hammer.

The abrupt changes in the three ABS facies are evidenced by the contrast between exposures ~ 10 m to the south (typically thick, rusted dark brown and grey coarse ash beds) and those to the north (medium golden yellow and light grey beds).

This is most clearly seen in the lapilli-rich facies, which has a noticeable increase in grain size to the south and contains bombs and blocks, up to 300 mm across. Within ~ 3 m, the lapilli-rich facies thickens from ~ 30 cm to ~ 1.2 m, forming a wedge. The bed thickness in general increases, and there is an increase in dip to 8 ° to the south, although the lapilli-rich bed dips 11 ° to the north-north-west. To the north, the beds show a different sequence to that found at either of the southern sites, with a noticeable fine-grained layer at its base. This exposure is at a lower elevation, so it is possible that they occur lower in the succession, rather than signifying lateral variation. The massive coarse ash-lapilli layers toward the top of the logged section resemble those of their southern counterparts, but are also thinner, furthering the likelihood of them being related to the coarse ash facies of the other sections. The lowest visible bed is a poorly exposed soft cream unit, possibly lake sediment, with a rip-up clast of it in the overlying bed.

4.1.2 Acacia Bay North

North of Acacia Bay South locality is a small section, reaching a maximum sub-aerial height of just over 1 m, and a lateral extent of a few metres, most of which is inaccessible due to vegetation and its lying directly adjacent to the lake. Here the outcrop shows a thick section of indurated pink and orange-brown fine ash and fine coarse ash layers sandwiched between grey to brown loose coarser-grained units (**Figure 4.10**). The beds at this site are conspicuously thinner than the ABS strata and are sub-horizontal (dipping ~ 4° to the south-east). The deposit here has been divided up into units similar to those at the Acacia Bay South locality:

1) Coarse ash facies

   This is a light brown to grey, coarse ash, tightly packed facies. Slight colour variations indicate composition and induration changes, which are sometimes accompanied by slight normal grading, but otherwise the beds are non-graded. The beds are cm-dm thick, well sorted, cross-bedded, and exhibiting relatively low-angle waves with wavelengths of ~ 40 cm and amplitudes of ~ 2 cm. Thin, wavy white bands are evident in the upper occurrence of the facies, as are bands of white pumice, making up to 10% of the deposit. The darker, coarser ash beds in the upper occurrence often

occur as lensoidal pockets, cut off by the overlying finer layers. Clasts within this facies are sub-rounded to sub-angular.

2) Lapilli-rich facies

   This facies is represented by a single thin bed of angular dark brown juvenile basalt lapilli and yellow pumice lapilli. The bed is moderately to well sorted, fines-poor, massive, and non-indurated. The layer's boundaries are marked by a 5 mm-thick burnt brown band.

3) Alternating fine ash-coarse ash/lapilli facies

   This facies contains a number of weathered orange and grey strongly indurated fine ash to coarse ash beds, which range from thick laminae to thin beds (maximum thickness of 8 cm). These beds frequently alternate with brown coarse ash or fine lapilli beds, which have an average thickness greater than that of the finer-grained beds and are generally tightly compacted but unconsolidated. At some levels, however, these coarser-grained units are lacking, so that the indurated beds are closely stacked. All of the beds are well sorted, non-graded, and matrix-rich, with a scarcity of coarser sub-angular material within each unit. A maximum of a ~ 5 % of lithic material is noted.

Lateral change in phreatomagmatic tuff facies is a well documented phenomenon (Sohn and Chough 1989; Allen *et al.* 1996). Here it is accepted that the facies at Acacia Bay North are likely the more distal lateral variants of those at Acacia Bay South, and the changes in characteristics and correlation of the units between the four logged sites is presented schematically in **Figure 4.1** and discussed further in section **4.6**.

4.2 Grain Size

Acacia Bay grain size analysis was carried out for samples from both Acacia Bay North (2) and Acacia Bay South (10) (**Figure 4.12; Appendix B**). The samples at Acacia Bay South are from the three exposures there.

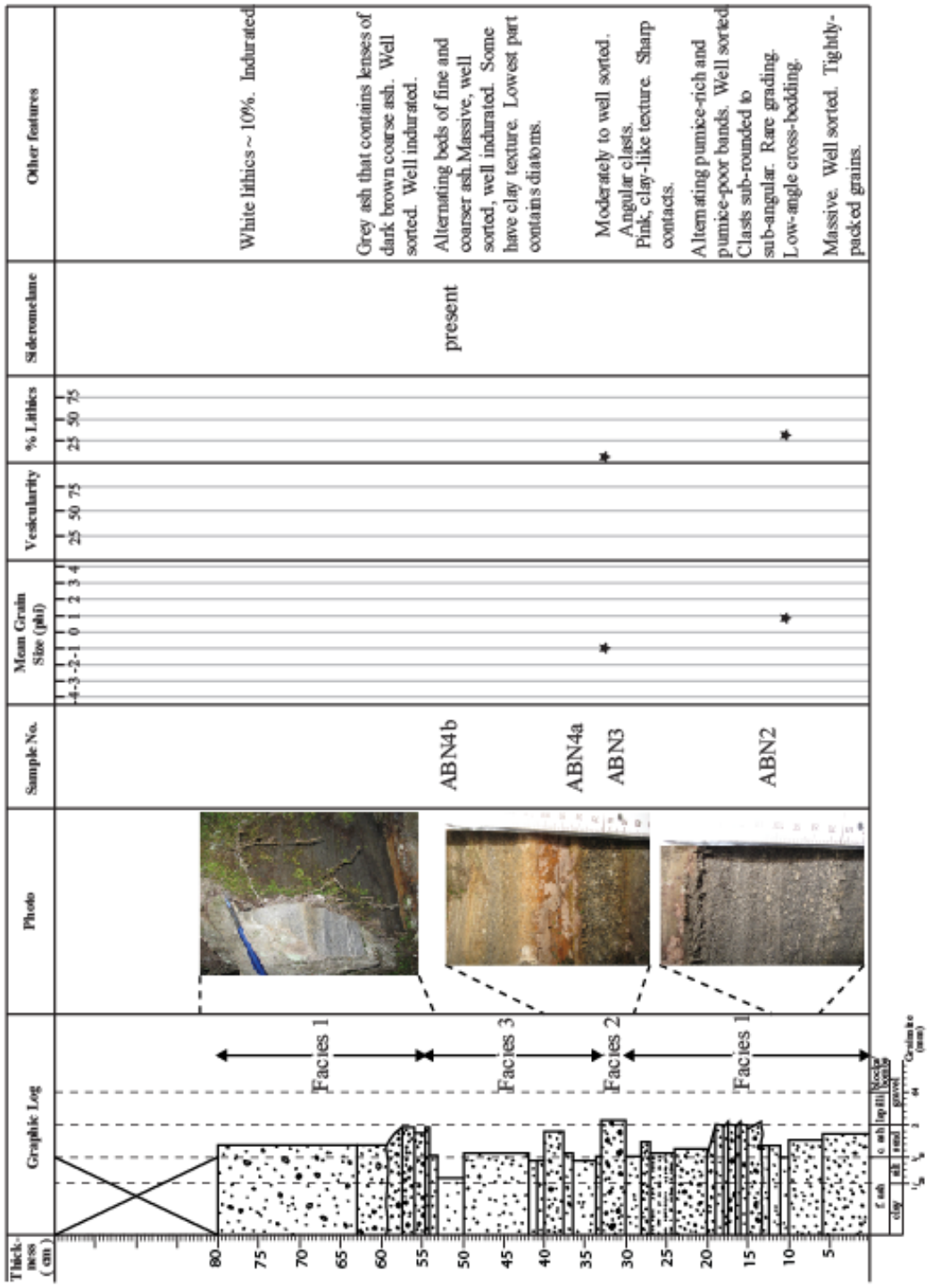

Figure 4.10 Stratigraphic log and data for Acacia Bay North.

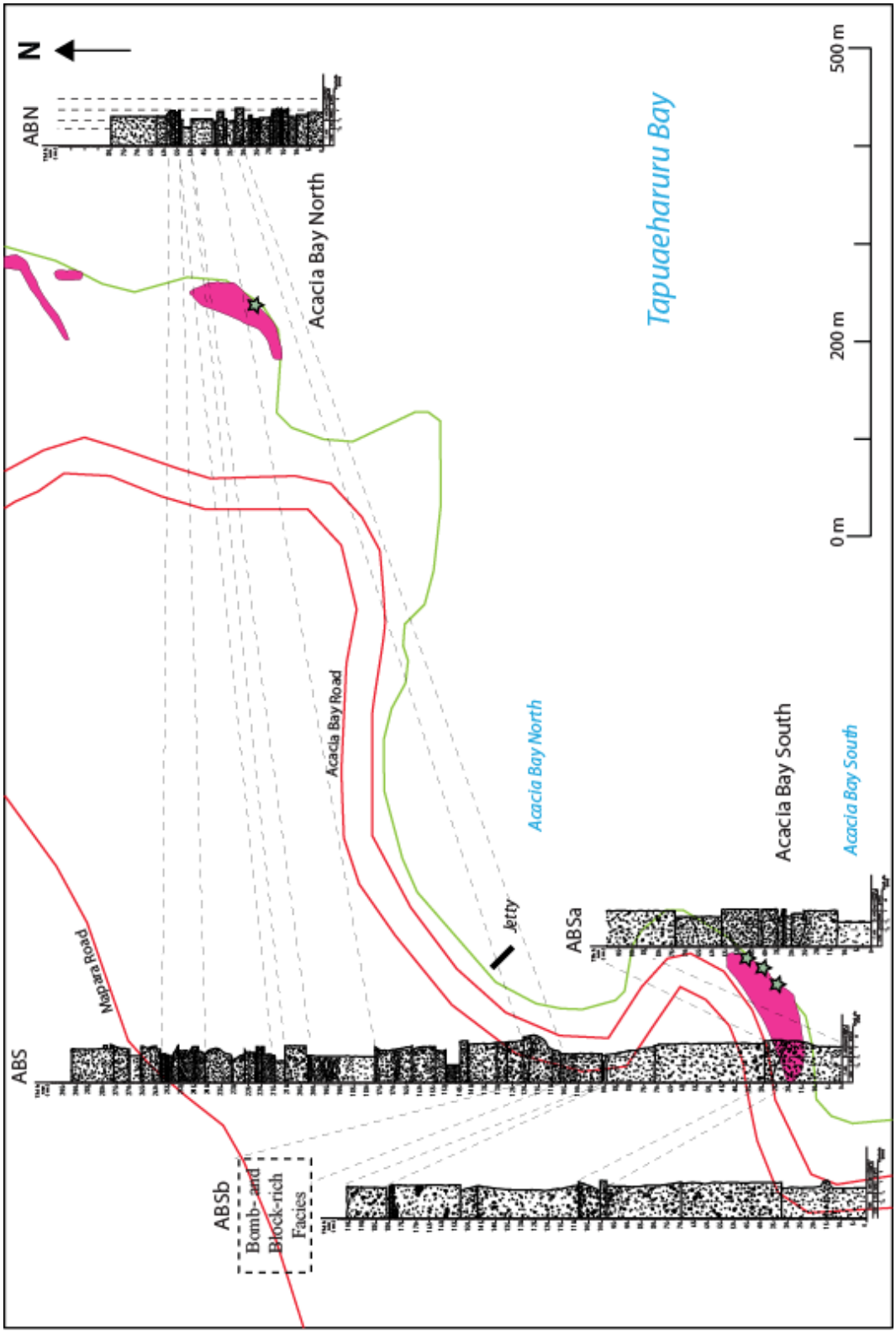

Figure 4.11 Possible correlation of beds between outcrops at Acacia Bay.

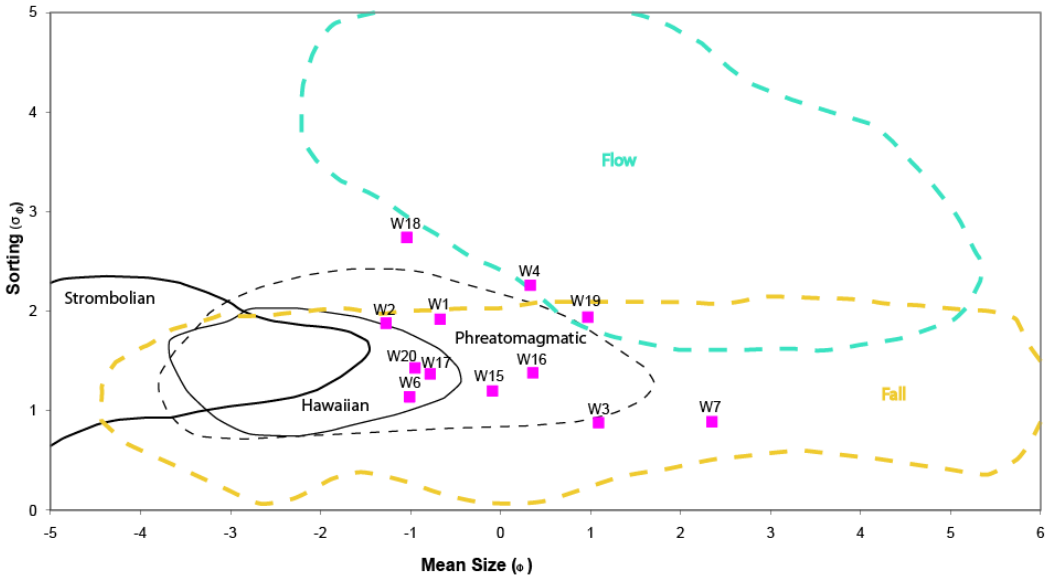

Figure 4.12 Median diameter vs. sorting plot for Acacia Bay samples. Flow and fall fields from Walker (1971), eruption style fields from Houghton and Gonnermann (2008).

There is a relatively wide range of size and sorting values at Acacia Bay South, with beds range from coarser-grained and poorly sorted to finer-grained and well sorted. The two exceptions are W6 and W4. The latter sample comes from the lapilli- and bomb/block-rich facies, which contains several bombs, so the lower mean size likely reflects sieving of the finer fraction, although a graph of size distribution (**Figure 4.13**) reveals a bimodal distribution.

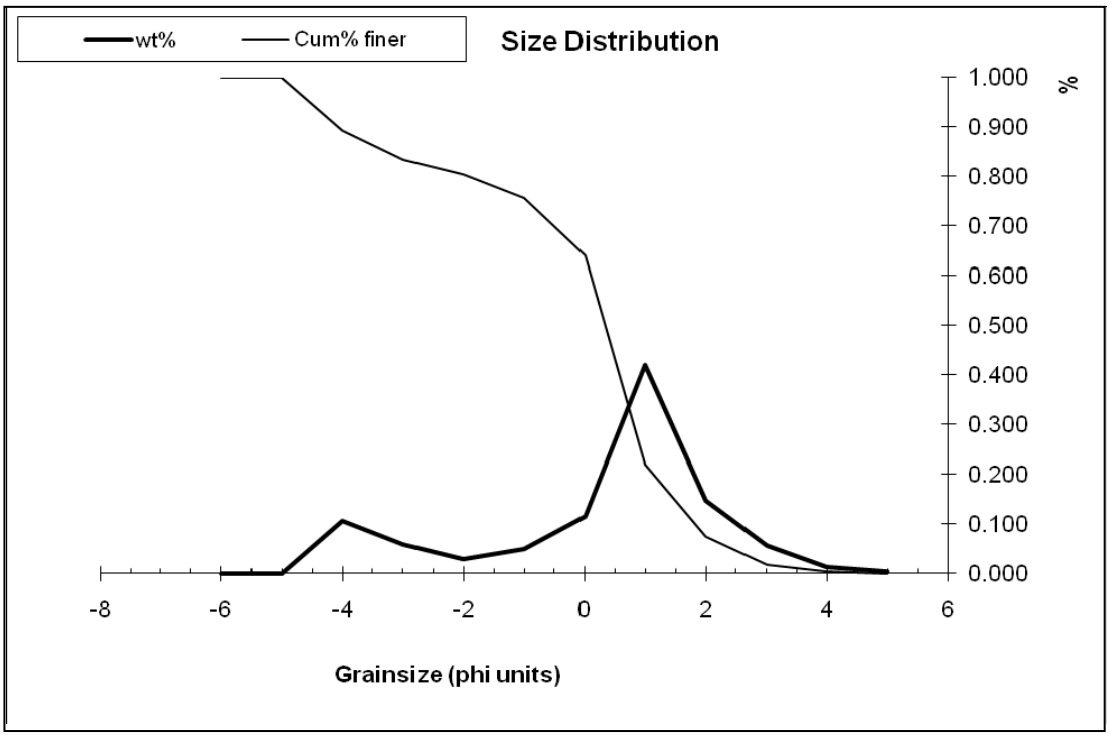

Figure 4.13 Size distribution plot for W4 (lapilli- and bomb/block-rich facies).

The size distribution plot for W6 (**Figure 4.14**), however, shows a unimodal distribution, concentrated around 0 Φ, with a slight positive skew. This relatively coarse, well sorted unit is followed by the finest unconsolidated unit (W7), which is also strongly unimodal, but has near-symmetrical distribution.

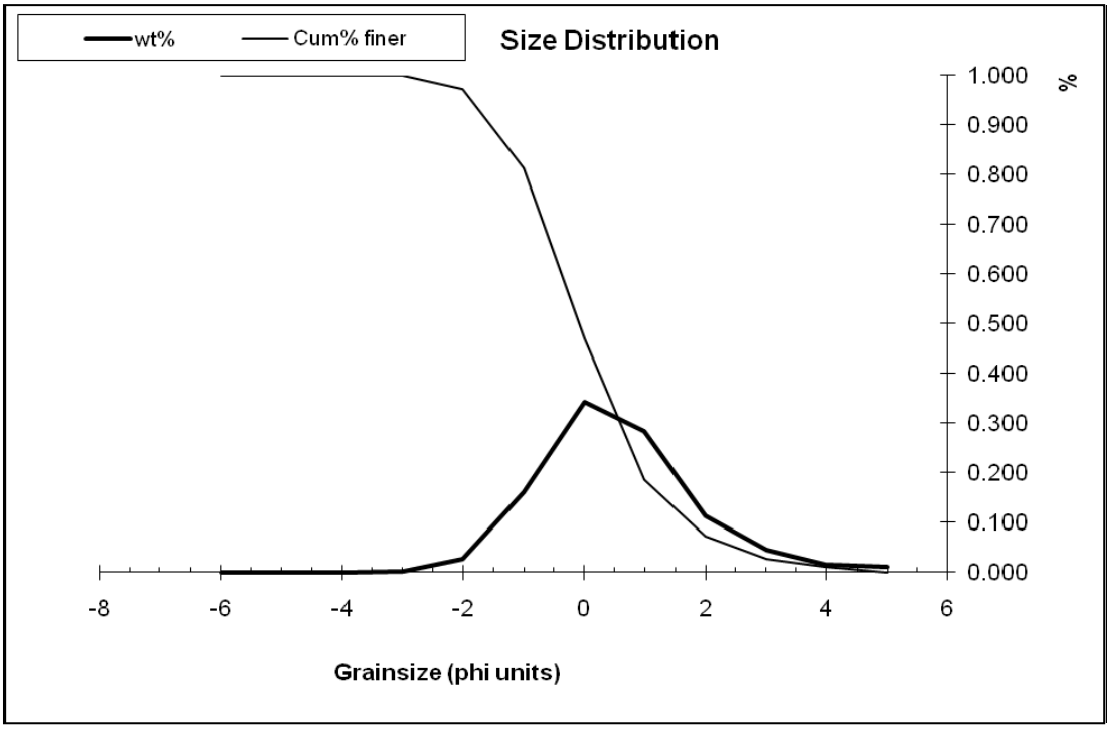

Figure 4.14 Size distribution plot for W6 (alternating fine ash-coarse ash/lapilli facies).

For ABSb, the southernmost site, the three layers sampled are coarse-ash-dominated, and exhibit a subtle increase in grain size with height. Size distribution plots reveal that while the two lower samples (W16 and W17) have unimodal distributions, W18 has a bi-modal distribution, affecting mean grain size (**Figure 4.15**). This larger constituent is actually one piece of consolidated material; if this were to be discounted, then W18 would fit in with its underlying units, with regard to both grain size and sorting.

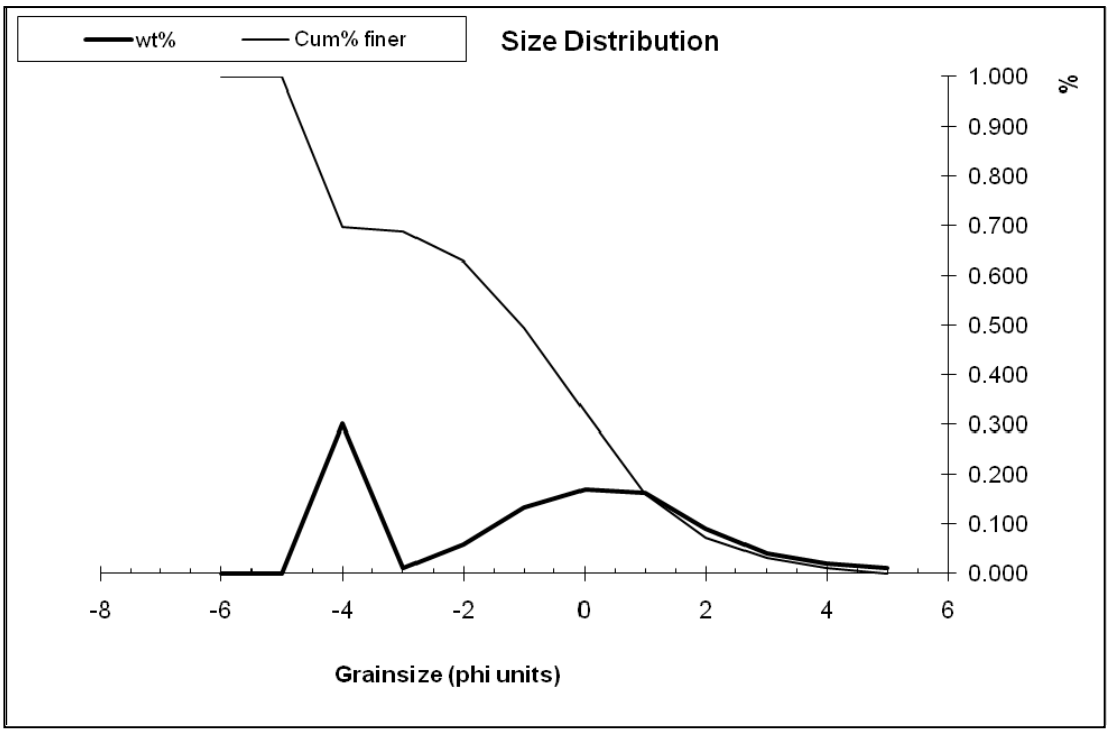

Figure 4.15 Size distribution plot for W18 (coarse ash facies).

4.3 Vesicularity

Due to the dominantly fine-grained nature of the Acacia Bay deposits, vesicularity was only able to be carried out on one sample: W4, from the lapilli- and bomb/block-rich facies found in the main exposure at Acacia Bay South. The ballast method produced vesicularity values of 40-59%, with a mean vesicularity of 54% (**Figure 4.2**, **Appendix C**). The range suggests that the clasts were fragments of a relatively uniformly vesiculated. The mean was skewed toward the lowest value of 40%, with the next lowest value being 51% (**Appendix C**).

4.4 Componentry and Clast Morphology

All units analysed reveal a dominance of juvenile material in the deposit. For the main exposure at Acacia Bay (ABS), it appears that although there is some fluctuation in the deposit, the highest lithic proportions are found in the lowest layer, and the lowest lithic proportions are found in the uppermost sampled layers, indicating a decrease in lithic component during the eruption (**Table 4.1**). The

southernmost outcrop, however, shows uniformly low lithic proportions throughout the deposit.

Table 4.1 Componentry percentages for Acacia Bay tuffs (using binocular microscope, with samples in stratigraphic order).

Sample	Juvenile	Crystal	Lithic
W7	77	6	17
W6	84	2	14
W4	83	0	17
W3	69	2	29
W2	79	6	15
W1	57	3	40
W18	81	2	17
W17	84	1	15
W16	84	2	14
W15	72	3	25
W20	89	<<1	11
W19	65	1	34

4.4.1 Juvenile Clasts

A notable feature of components at Acacia Bay is the distinction between two types of juvenile clasts: a grey, scoriaceous type, and a green-brown glassy type. The presence of two distinct juvenile types is clearest in the southern outcrops. The abundance of these greener, glassy juveniles varies considerably both within and between sites: from <1 % to 34 % of juvenile material at ABS, 2-10 % at ABSb, and 0-5 % at ABN. Scoriaceous clasts have irregular to more angular, blocky morphologies. Although the green juveniles have a glassy, ragged appearance, these grains are actually slightly more vesicular. Vesicularity is generally poor to moderate, with spherical and oval vesicles most common. ABSb is notable for also having a number of distorted vesicles, whereas ABN differs in that it has a couple of scoriae with tubular vesicles that go right through the clast. Nearly all of the clasts of Acacia Bay South are covered with a fine ash coating. At Acacia Bay North, this cover is yellow-brown. SEM images of both types of juvenile components from layer W4 are shown in **Figure 4.16**. The grey clasts have a dense, blocky appearance, with a slightly platy surface. Vesicularity appears low, and vesicles are oval and spherical, with no coalescence visible. The glassy constituents have generally smooth surfaces and shallow (sub-) spherical

cavities of vesicles. One of the clasts shows a ribbon flow-like texture with rare stretched vesicles and has a partial coating of very fine ash.

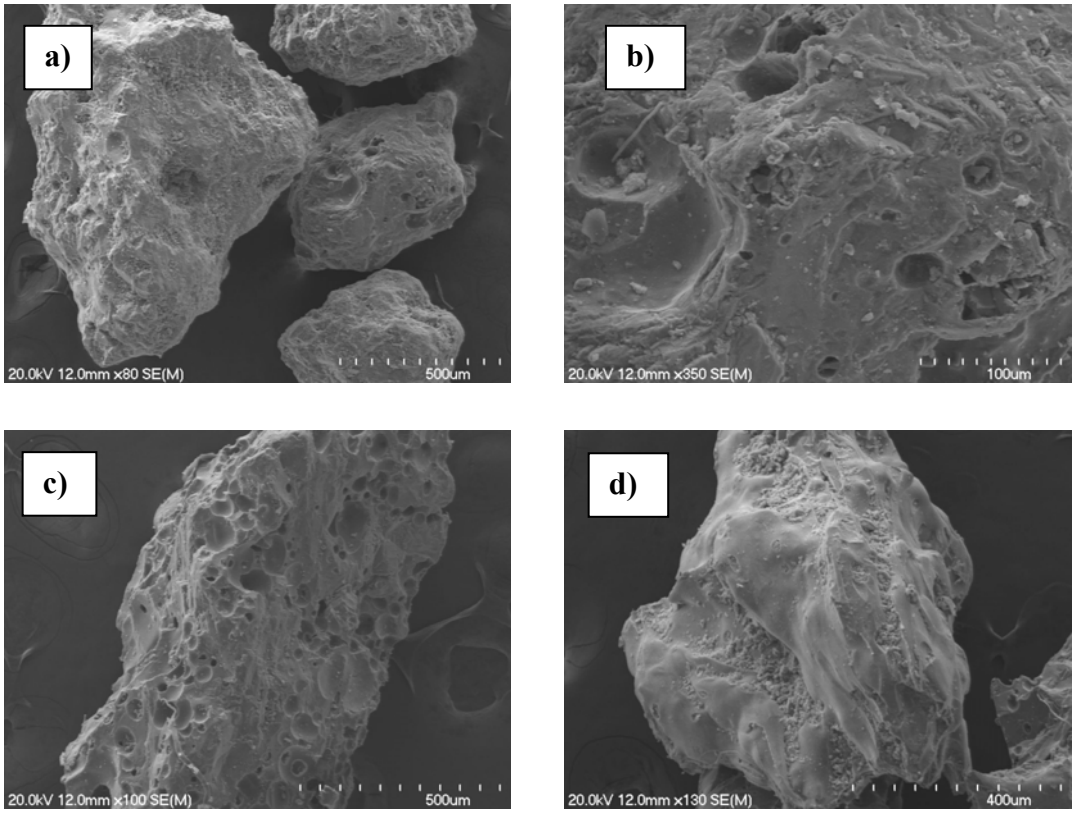

Figure 4.16 SEM images of juvenile clasts from W4: a) scoriaceous clasts; b) scoriaceous clast showing vesicles; c) and d) green glassy clasts. Note relatively high vesicularity of c) and ribbon-like surface of d).

4.4.2 Crystals

Free crystal content, in comparison with the other field sites, is relatively high at Acacia Bay, reaching a maximum of 6% (**Table 4.1**). The majority of crystals are clear and are most likely plagioclase, although cleavage is not always shown. At Acacia Bay South, yellow and brown crystals are also evident, possibly a mix of augite and olivine, with one resembling hornblende. A couple of orange grains in W1 are either crystals or very rare palagonite.

4.4.3 Ltihic Clasts

The most common lithics at Acacia Bay are pumice, ignimbrites and what have been termed as 'flaky' (**Table 4.2**). The latter term is applied to sub-rounded to sub-angular, grey to white to brown flaky rock fragments. The exact nature of

these lithics could not be established, but they are likely to be either a crystal-poor ignimbrite or laminated lacustrine siltstones. Pumice, the most sizable lithic component in most samples, is typically sub-rounded, and occasionally ragged. The pumices vary in colour and texture, from clear to brown, and waxy to powdery, with the most common type being cream and fibrous. A significant proportion of pumices have alternating darker and lighter bands/fibres, with the darker bands sometimes resembling obsidian. Rare pumices at Acacia Bay North contain crystals, whilst two pumices from Acacia Bay South appear to have lithic inclusions. Ignimbrites are sub-rounded to angular in shape, and are generally light grey with lithics and crystals. These ignimbrites commonly have a pink hue, and W1 has green and pink ignimbrite fragments.

Table 4.2 Lithics percentages for Acacia Bay tuffs.

Sample	Pumice	Aggregate	Ignimbrite	Flaky	Other
W7	33	28	5	21	13
W6	50	0	23	0	27
W4	43	10	17	24	6
W3	42	46	6	0	6
W2	44	9	13	19	15
W1	55	34	3	0	8
W18	27	9	24	15	25
W17	33	0	8	0	59
W16	56	0	11	12	21
W15	33	0	31	0	36
W20	23	0	8	50	19
W19	78	6	1	10	5

Aggregates of lithic and juvenile material are relatively rare in the samples. A notable percentage of other lithics are indeterminate, due to the yellow/golden ash/secondary crystalline coating on most of the clasts, which at times have a baked appearance.

4.5 Petrography

4.5.1 Acacia Bay South

Consolidated samples have juveniles and lithics in a crystal- and diatom-rich matrix. W8, which contains no diatoms, is a notable exception.

4.5.2.1 Juvenile Clasts

Juvenile grains include black and dark brown, porphyritic scoriae, and light green-yellow sideromelane, which is sub-equal or secondary in abundance in all samples except W7, where sideromelane comprises ~ 53% of the sample (**Appendix C**). Morphologies are typically irregular. Phenocrysts are plagioclase>olivine>>augite in a felted hyalopilitic groundmass. Plagioclase phenocrysts are subhedral and tabular (0.5 mm), olivine is subhedral to euhedral, with rare iddingsite rims (0.5 mm), and augite is subhedral (0.3 mm). Sideromelane also contains resorbed, polysynthetic twinned plagioclase. Swallow-tailed plagioclase laths are rare, and slightly skeletal olivine is found only in W4.

Several sideromelane clasts contain finer scoria fragments (cognate lithics), while sub-rounded light brown, crystalline accessory lithics (up to 1 mm) resembling those found in scoriae at Acacia Bay North appear in W3, W7, W18 (**Figure 4.17**). Vesicular clear glass is found in one scoria clast in W16.

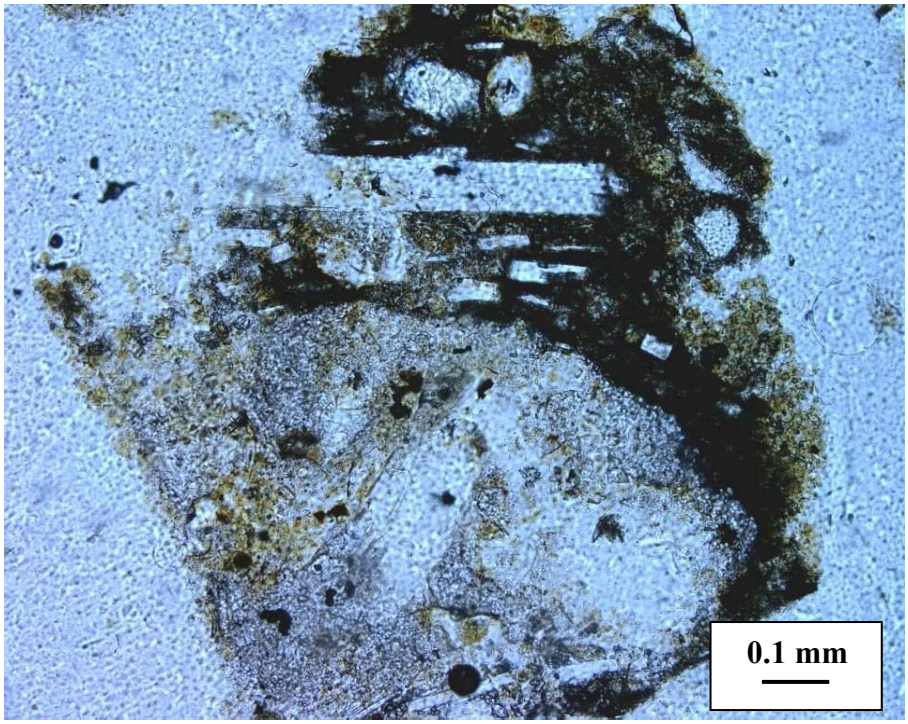

Figure 4.17 Photomicrograph in plane-polarised light of scoria containing unidentified crystalline lithic (W18).

4.5.2.2 Crystals

Free crystals include subhedral plagioclase (0.5 mm), augite (0.9 mm) and olivine (0.7 mm). Xenocrysts account for 0.3-18.6 % of samples, and consist of anhedral to subhedral hornblende (0.1 mm), which is oxidised in W5, anhedral quartz (0.4 mm), and subhedral to euhedral poikilitic orthopyroxene (1 mm). Anhedral to subhedral, oscillatory zoned and polysynthetic plagioclase crystals (0.5 mm) are also present.

4.5.2.3 Lithic Clasts

Xenoliths include various rhyolites (including white-red/grey flow-banded, white-brown spherulitic, grey/brown/orange), pophyritic rhyolite/dacite lava, brown mudstone, beige dolerite with visible hornblende, pumice, peach rhyolite glass shards, and several brown and grey ignimbrites. Unidentified yellow-grey, speckled light brown and brown equigranular lithics also occur. Lithics are sub-rounded to angular, with an average size of ~ 0.6 mm.

Thin sections were made of lithic lapilli and blocks from W1 and W4. These lithics were all found to be light to dark brown ignimbrites. Samples W9 and

W10 both have crystals (~7 %) of oscillatory-zoned plagioclase (1.5 mm) and orthopyroxene (0.7 mm) in a light vitroclastic matrix. W9 is lithic-poor, although the lithic (likely dolerite) matches with one of the lithics found in W10 (**Table 4.3**). Important differences between the two samples are the existence in W10 of devitrified fiamme and subhedral to euhedral augite crystals (0.2 mm). The other three samples (W11, W12, W13) contain subhedral to euhedral crystals (6.6-18%) of oscillatory-zoned plagioclase (1.9 mm), augite (1.2 mm), orthopyroxene (0.9 mm) and hornblende (0.4 mm) in a brown vitroclastic matrix full of devitritied fiamme. Sample W11 differs slightly from the other two samples in that the plagioclase also has sieve textures and occurs in clots, and orthopyroxene is rare.

Table 4.3 Lithics found in ignimbrites of Acacia Bay.

Description of Lithic	Ignimbrite Sample
Brown-blackish scoria?	W11, W12, W13
Dark brown-grey with small laths	W13
Dark grey isotropic	W12
Fine-grained light grey porphyritic	W13
Golden yellow patchy	W11, W12
Grey-brown rhyolite?	W10, W11 ?W13
Grey-white (+red) rhyolite	W11, W12
Grey-white spherulitic rhyolite	W10
Light beige mottled	W9, W10, ?W13
Light beige speckled	W11, ?W12, W13
Light brown crystalline	W12
Light moss-like crystalline with opaques	W13
Light yellow/white crystalline	W13
Messy black with lighter brown ignimbrite lithic	W10
Mottled black and light brown isotropic	W10
Tortoise shell red-brown	W11, W13
White/brown w/orange	W10

Diatoms are a mix of centric and pennate types, with an average size of 0.05 mm (**Figure 4.18**). Frustules are generally very well preserved, with whole frustules present.

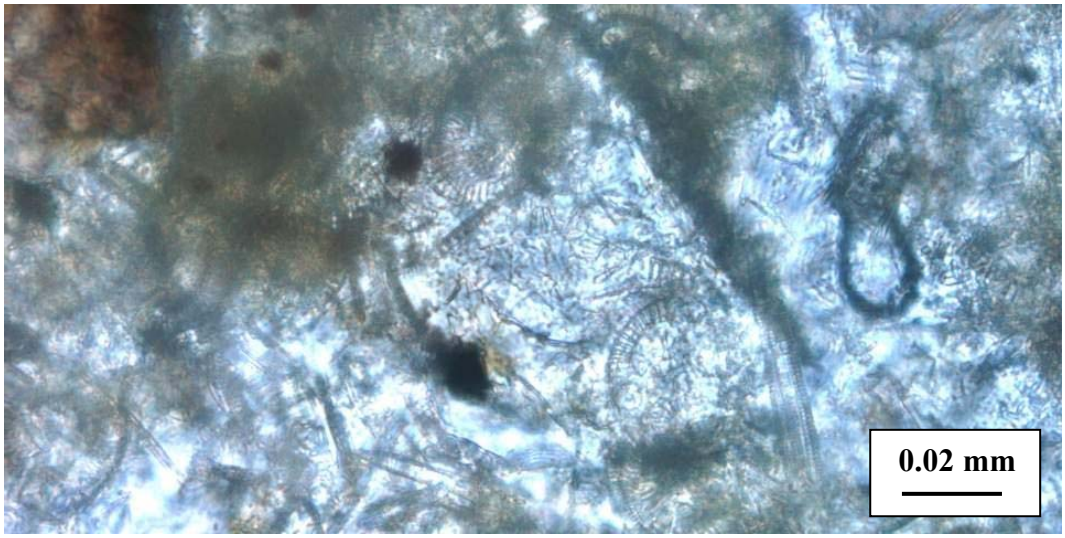

Figure 4.18 Photomircograph of diatoms in basal bed of ABSa (W14) (plane-polarised light).

4.5.2 Acacia Bay North

The finer-grained, indurated samples consist of juvenile clasts, crystals, lithics (± diatoms) set within a palagonite-rich matrix.

4.5.2.1 Juvenile Clasts

In both loose and consolidated samples, juvenile clasts are sometimes ash-covered, and consist of porphyritic black, grey and brown scoriae (up to 1.3 mm across) with subordinate sideromelane. Phenocrysts in juvenile clasts are plagioclase>olivine>augite. Microlites are also common in sideromelane. Tabular plagioclase is subhedral to euhedral, and often resorbed. Olivine occurs as euhedral prismatic or orthorhombic phenocrysts, while augite is anhedral. Swallow-tail plagioclase laths are common in both quenched and non-quenched juvenile clasts. Skeletal olivine phenocrysts occur rarely in sideromelane. Scoria have an irregular or sub-rounded morphology. The irregularly-shaped scoria tend to have higher vesicularities with a felted hyalopilitic groundmass, whilst the rounder clasts are very dense and vitrophyric. Vesicles in W20 are stretched and ragged. Sideromelane is generally fragmental, having an angular/ragged morphology and vitrophyric groundmass. Rare olivine-plagioclase clots (cognate lithics) are found in W19. A few of the juvenile scoriae contain sub-rounded

beige xenoliths lithics that are hypocrystalline and equigranular under crossed-polarised light.

4.5.2.2 Crystals

Free crystals of subhedral plagioclase, olivine and augite are also found in the matrix, with plagioclase (possibly lithic) up to 2.7 mm across. Anhedral to subhedral orthopyroxene (probably xenocryst) is the only other free crystal found.

4.5.2.3 Lithic Clasts

Lithics are grey-pink spherulitic, white-grey/red flow-banded, and red-brown rhyolites, light rhyolite/dacite lava, greywacke, white-green dolerite, grey and brown ignimbrites, brown mudstone, pumice, peach rhyolite glass shards, and unidentified white-yellow/orange lithics. These lithics are dominantly sub-angular to angular, with sizes comparable with that of the juveniles (average of ~ 0.5 mm).

4.6 Correlation of the Acacia Bay Deposits

Of importance to this study is the link between the outcrops at Acacia Bay South and Acacia Bay North. Following Sohn and Chough (1989), and Chough and Sohn (1990), Acacia Bay North's dominance of stratified, undulatory and very thin beds puts the Acacia Bay North deposits as somewhere between 700 and 1100 m from source (**Figure 4.19**). If the southernmost site at Acacia Bay South is indeed very proximal to the vent, as the wedge-shaped lapilli and bomb/block-rich facies indicates (Cas and Wright 1987; Allen *et al.* 1996), then it is viable that Acacia Bay North is related to Acacia Bay South.

Componentry analysis revealed a noticeable lack in the proportion of glassy, quenched juvenile clasts, and greater abundance of pumice for the Acacia Bay North site. Petrography for Acacia Bay North and South shows very similar mineralogy, and scoriae at both sites have the light beige lithic inclusions. The notable exceptions are the ubiquity of quench textures in plagioclase and olivine, existence of palagonite in consolidated samples, vesicularity of juvenile clasts, and reduced xenocryst and xenolith variety. The reduction in lithic types at

Acacia Bay North could result from deposition out of the surge (Sohn and Chough 1989), but uniformity of quench textures might be expected if the northern and southern sites are lateral equivalents of the same eruption deposit, although this could be explained by the smaller grain size at Acacia Bay North (M. D. Rosenberg pers. comm. 2010).

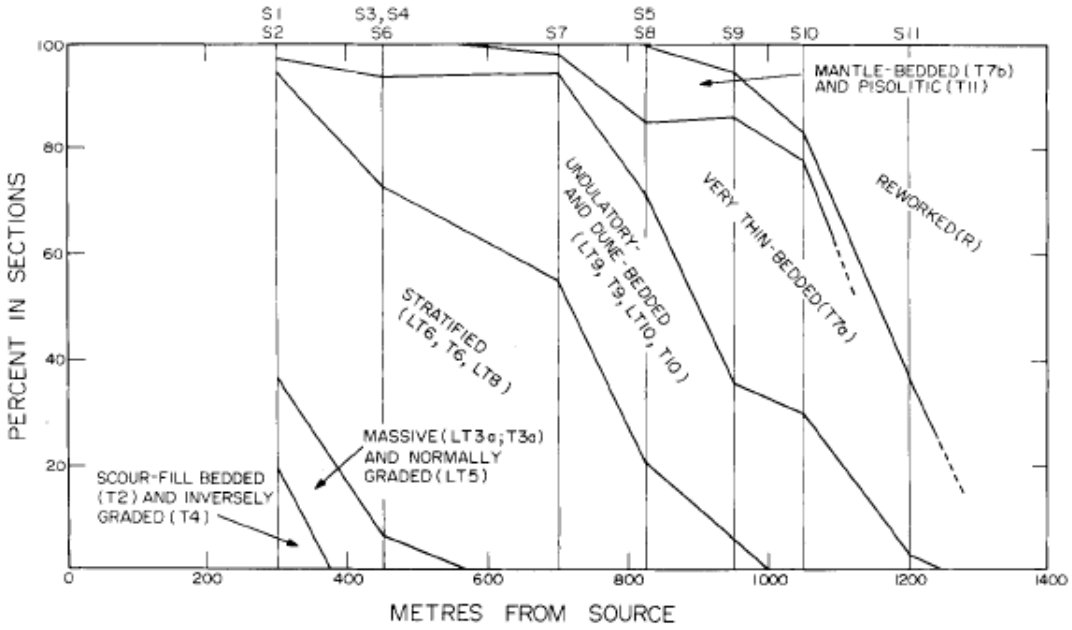

Figure 4.19 Distance-facies diagram for Songaksand tuff ring, Korea, relating abundance of facies type in outcrop with distance from source (Chough and Sohn 1990).

There is also the question of how similar deposits from separate eruptions at nearby locations (with similar geology and hydrology) might be. Nevertheless, it is tentatively proposed that Acacia Bay South and Acacia Bay North are related deposits, and will be treated as resulting from the same eruption in subsequent discussion. With regard to the Purikahou Bluff deposit, the fact that these deposits were not examined here and there is variation within the deposits makes a correlation difficult. However, the thick massive beds containing bombs and blocks at Acacia Bay South indicate a source further south than that proposed by Wilson and Smith (1985). **Figure 4.20** shows a possible vent location for the deposits examined here as inferred from outcrop characteristics, with that of Wilson and Smith (1985) for comparison.

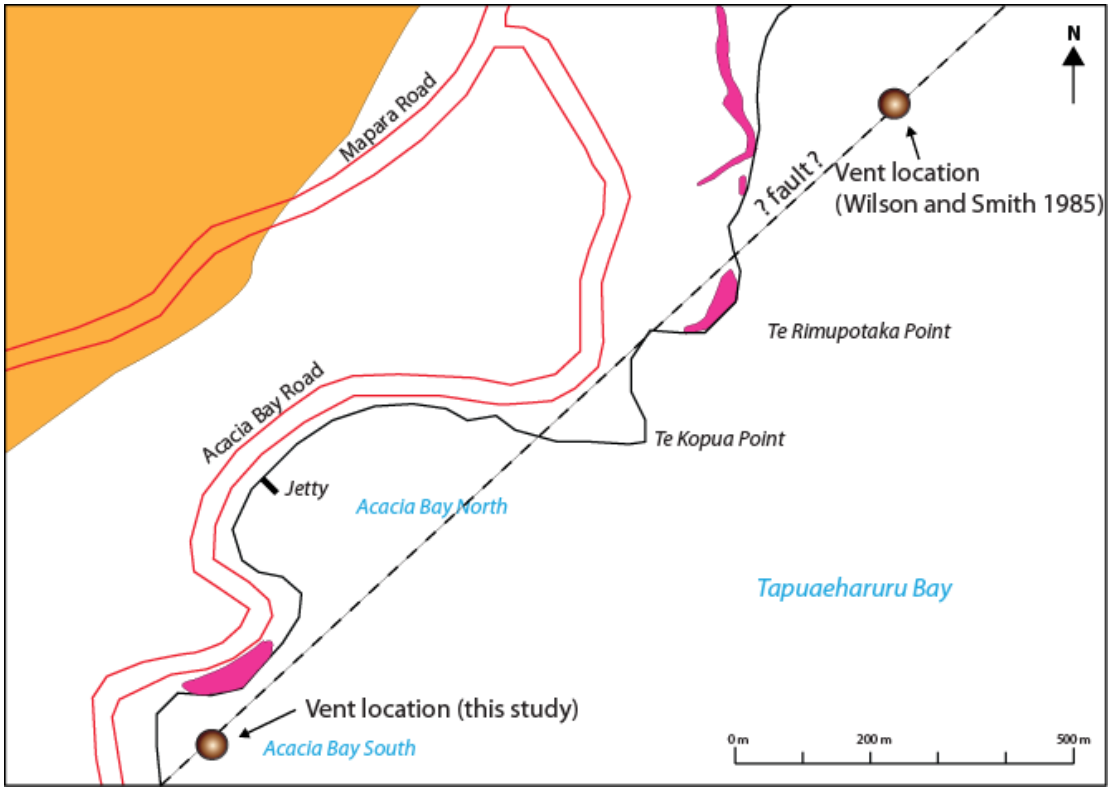

Figure 4.20 Map showing possible vent locations for Acacia Bay basalt eruptions. Modified from NZMS260 Map Series (1: 50 000) Sheet U18.

4.7 Interpretation

4.7.1 Facies

1) Coarse ash facies

The diffusely-bedded, massive, coarse ash and lapilli beds that typify this facies are likely to have resulted from relatively high particle-concentration, rapidly deposited base surges, possibly involving en masse freezing (Cas and Wright 1987; Sohn and Chough 1989; White 2000). The diffuse bedding is thought by Cas and Wright (1987) to represent a transition between planar and dune structures, where internal shear has acted on a highly-concentrated surge), although continuous rain of tephra from jets or dilute currents moving across a water surface, into the underlying surge, is another possible explanation of the nature of the bedding (White 2000; Brand and Clarke 2009). The coarse nature of the grains and grain-supported nature of the beds indicates that the surges were relatively dry (Sohn and Chough 1989; Allen *et al.* 1996). Massive

beds are often associated with wet surges (e.g. Frazzetta *et al.* 1983; Sohn 1996; Büttner *et al.* 1999), but can also indicate proximity to vent (Sohn and Chough 1989; Allen *et al.* 1996) as is deemed to be the case here. W2, which lacks the diffuse bedding, is normally graded, with a coarser grain size and a weakly unimodal distribution, is more likely to be rapidly-deposited fallout (Sohn and Chough 1989). Some of the beds closer to the (inferred) vent have slight reverse and normal grading, probably reflecting the pulsatory nature of eruptions, along with the effects of shear close to the vent (Sohn 1996; Németh and White 2003). The thick and uniform nature of these beds suggests relatively stable eruption conditions.

2) Lapilli- and bomb/block-rich facies/Lapilli-rich facies

This facies, with its poor sorting, wedge-shaped geometry, and coarse grains, most likely resulted from a base surge (Cas and Wright 1987). The reverse grading of the bed suggests that the bed resulted from a high-concentration, relatively dry surge, with the dominant transportation being through grain-dispersive pressure (Sohn and Chough 1989). The dry nature of the surge is supported by the relatively high juvenile content (83 %) (Allen *et al.* 1996). The observed increase in both thickness (to 1.2 m) and grain size to the south indicates that the source was also in that direction, and was very proximal, especially given that base surges are rarely greater than 50 cm thick, and only in near-vent settings (Cas and Wright 1987). A proximal setting is supported by the presence of a similar unit in Auckland that was < 100 m from the vent (Allen *et al.* 1996). The inaccessible nature of the exposure limited ability to see any possible bomb sags, although it is possible that the bombs in the southernmost exposure represent ballistic fall. However, large blocks can be carried by surge deposits without disturbing underlying beds (Sheridan and Wohletz 1983), and bomb sags are more commonly associated with wet surges (e.g. Brand and White 2007).

3) Alternating fine ash-coarse ash/lapilli facies

The diagnostic feature of this facies is the wavy cross-bedding and planar bedding, which is evident in the majority of beds. These features are commonly associated with traction from lateral transportation (e.g. Sohn and Chough 1989; Allen *et al.* 1996), and hence this facies is likely to represent a series of base surges. The cross-bedding of the beds indicates low particle concentration (Sohn and Chough 1989; Zanon *et al.* 2009). The wavy nature of the beds could reflect a wetter type of surge, although slight reverse grading of the beds implies that they are grain-supported, with dispersive pressures playing an important role during transportation (Sohn and Chough 1989; Sohn 1996). W7, which has unimodal sorting (σ_Φ <1) more commonly associated with 'dry' fall (Houghton and Gonnermann 2008), is very fine-grained, forms cross-beds and contains a large amount of sideromelane; therefore, a base surge origin is also proposed, but with less water and more effective fragmentation (e.g. Allen *et al.* 1996; Büttner *et al.* 1999). The decrease in bed thicknesses higher up indicates that eruption conditions were less stable. The finer, well sorted indurated layers that occur sporadically within the facies signify periods of more effective fragmentation (Sohn and Chough 1989; Büttner *et al.* 1999), and a mantling topography exhibited by some of the beds (**Figure 4.21**) implies fall deposition (Sohn 1996; Valentine and Gregg 2008). The lowest fine bed within the facies at the main exposure (W5) is a volcanic breccia containing basaltic material and concentrations of pumice and other lithics, at times marked by a wavy lower contact. An angular piece of fine material also found near the base of this unit precludes a mass-emplaced origin. The clean cuts of the finer-grained bed

Figure 4.21 Mantling fine ash layer within alternating facies, Acacia Bay South. Scale is in mm.

within the rest of the deposit suggest that the bed underwent brittle deformation, and was therefore already consolidated when deformation occurred. The well-preserved diatom-rich nature of the fine-grained bed, the lack of juvenile material and association with high concentrations of pumice and various other lithics imply that this bed represents a vent-clearing phase, possibly with a change in vent location (Németh and Cronin 2009). The broken clast of similar material at the base of the bed, not found underneath the bed at site, makes in situ disruption unlikely.

4.7.2 Role of External Water

Using the age estimate of 100-200 ka for the deposits, and the proximity of the vent to the deposits (likely < 100 m to the south/south-west), the site of both the vent and tuff ring was very likely covered by Lake Huka at the time of eruption (**Figure 2.3**). The consequence of this is that the nature of the deposits could reflect subaqueous eruption and/or deposition. This has implications for which of the deposits' features have resulted from eruption processes (interaction with water at/in the vent) and how many are the product of depositional environment. This has further implications for establishing the volume and source of interactive external water during eruption.

Magma interaction with water during the eruptions that caused the Acacia Bay deposits is proved by the presence of sideromelane and base surge deposits, and is supported by relatively high volumes of accidental lithic components, and the low vesicularity values for the lapilli- and block-rich facies. Several of the beds in the alternating facies show deformational sedimentary features, such as rip-up clasts and slumping. These features are suggestive of wet, dilute base surges, with an overabundance of external water, yet two such beds (W6, W7) are well sorted and unconsolidated, more typical of drier surges. One way to account for this slight contradiction is by subaqueous deposition. Sheridan and Wohletz (1983) note the presence of well-stratified, massive and cross-stratified beds of 'sand-sized' grains in shallow water environments. A subaqueous depositional environment is strengthened by the diatoms found in several of the beds, which indicate a freshwater environment (Leng and Barker 2006), and the facies succession from thicker, massive coarse-grained beds, to thin, fine- and coarse-grained beds, which

has been documented for subaqueous pyroclastic flows, although this is not conclusive (Fisher and Schmincke 1984; Cas and Wright 1991). The presence of well indurated fine ash layers could be due to secondary crystallisation or palagonatisation of basaltic glass in wet sediment (Sheridan and Wohletz 1983; Zanon *et al.* 2009). At Acacia Bay North, several layers have an orange tinge, also thought to reflect palagonite within the bed (Stroncik and Schmincke 2002). Assuming a subaqueous deposition, the vertical changes in the deposit can be related to change in water:magma ratio at the vent.

4.7.3 Source of External Water

The source of water for the eruption at Acacia Bay could be one or both of lake water and groundwater, given the deposits' proximity to water and stratigraphic position above lake sediments. The inferred vent location for the eruption is inconclusive as to source of external water. The mixture of green, glassy and more scoriaceous juvenile clasts, however, suggests that there was a portion of magma that was more rapidly quenched by water, although the vesicular nature of this basalt implies that water interaction occurred following significant magmatic vesiculation, and so did not trigger the eruption. It is likely that these glassy equivalents are sideromelane, found to be relatively abundant in thin section, and which exhibits similar vesicularity to that of its crystalline equivalents. Highly vesicular glass shards are common in the deposits of subaqueous volcanic eruptions (Fisher and Schmincke 1984), yet variably vesicular sideromelane can indicate groundwater sources (Németh and Wilson 2003).

The lithic component, although much higher than expected for dry eruptions, is relatively low. According to White (1996), this would suggest interaction with surface water. The initial high lithic abundance found in W14 likely resulted from vent clearing from the initial explosion. Closer analysis of the lithics, however, reveals an alternative source to lake water. Ignimbrite lithics are rare in the deposits, although the lithic blocks from Acacia Bay South are all ignimbrites. Microscope petrography does not show a high abundance of ignimbrite lithics, but there is strong evidence to suggest that a number of components originated from ignimbrite, and that this ignimbrite was explosively fragmented. This ignimbrite matches very closely with the ~ 220 ka Rangatira Point Ignimbrite (also called the

'brown ignimbrite'; Cole *et al.* 1998), the best exposure of which lies ~ 3 km south of Acacia Bay. According to Cole *et al.* (1998), the Rangatira Point Ignimbrite is a light grey to brown ignimbrite, the lower unit of which is lithic-rich and contains crystals of oscillatory-zoned plagioclase, orthopyroxene, Fe-Ti oxides and trace amounts of quartz and hornblende. Lithics include grey/pink flow-banded felsitic/spherulitic rhyolite, several types of ignimbrite, rare high-silica dacite lava, and rare dark green/black mottled dolerite containing plagioclase, hornblende, Fe-Ti oxides and orthopyroxene. The mineralogy fits well with some lithic samples, as does the presence of dolerite. Strong evidence for the ignimbrite having been explosively fragmented is the peach glass shards found in a significant number of Acacia Bay thin sections, which match the devitrified glass found in W11 and W12. The intimate association of the ignimbrite lithics leaves little doubt that fragmentation of the magma occurred within the Rangatira Point Ignimbrite. The variable vesicularity of the juveniles suggests either that explosive interaction with groundwater was limited or that there was a proportion of the magma that was isolated from the groundwater (at depth) and was rapidly quenched once the magma reached the surface and contacted lake water.

4.7.4 Eruption Phases

The tuff ring deposits at Acacia Bay are interpreted to have resulted from three phreatomagmatic eruption phases. The initial phase consisted of vent-clearing and relatively stable production of base surges and with relatively little interaction with water. This phase was followed by a hiatus and shift in vent position, resulting in another clearing of the vent. A waning in magma supply and/or an increase in water supply lead to a higher water:magma ratio, resulting in short surge pulses of varying composition. The final phase probably involved a reduced water supply, resulting in a return to drier, more stable conditions.

5 *Kaiapo*

5.1 Site and Facies Description

Kaiapo is an extensive tuff ring deposit exposed along Tukairangi Road and is dominated by a northern outcrop covering a length of at least 500 m and a height of nearly 100 m. The rest of its ~ 1.5 km length consists of southern exposures just a few metres thick and up to 10 m across, including an inferred crater fill facies (Smith 1990). Smith (1990) has ascertained that the deposit represents the eastern half of the area covered by the original construct, with the rest having been removed through movement of the Kaiapo Fault (which lies parallel to Tukairangi Road – e.g. Brown *et al.* 1994). The remaining deposit exists on the upthrown side of the fault (Brown *et al.* 1994). The tuff ring overlies the Huka Formation, which outcrops in the northern part of the field area (Smith 1990; Brown *et al.* 1994). In the south-western part of the outcrop, pyroclastic deposits lie adjacent to – and onlap – thick loosely consolidated grey volcaniclastic sediment. Previous work by Smith (1990) and Brown *et al.* (1994) has resulted in the identification of six

eruption phases (P1-P6), within the main northern outcrop, along with an initial vent-clearing facies and reworked lake sediment (R1). Due to accessibility, the focus here is on 23.5 m of the lower units, corresponding to Smith's (1990) R1 and P1-P3 (**Figure 5.1**). Stratigraphic logging was undertaken at five sites along the outcrop, here referred to as KPA (two logs), KPB, KPC, KPD and KPE (from south to north; **Figures 5.2**, **5.3**, **5.4**, **5.5**, **5.6, 5.7**). Observation and sampling was also undertaken at three other localities (**Figure 5.1**). Apart from KPA and KPB, northern to southern sites correspond to an increase in stratigraphic position.

The basal third of the deposit consists of a light orange welded tuff that resembles welded ignimbrite, with pumice lapilli and crystals set within a coarse ash matrix. Further north, this tuff is replaced by yellow, indurated beds and brown coarse ash. Above the welded tuff, the deposit is dominated by a sequence of beds. These are often visible in blocks a few metres across, and have a dip of up to 30° to the south-west. There are some blocks dipping at the 'expected' dip to the north, but the lower beds tend to dip inward, indicating rotational slumping. Fractures in these beds also indicate compactional loading, although some of these could be post-depositional, given the deposit's proximity to the active Kaiapo Fault and the ubiquitous presence of fallen blocks at the site. The deposit shows much lateral variation. In the first few metres of bedding, over a distance of ~ 200 m, beds change from light yellow-grey, non-welded cohesive coarse ash-fine lapilli beds, to dark grey lapilli-rich strongly indurated rock, to golden brown and white lapilli-rich, variably indurated deposits.

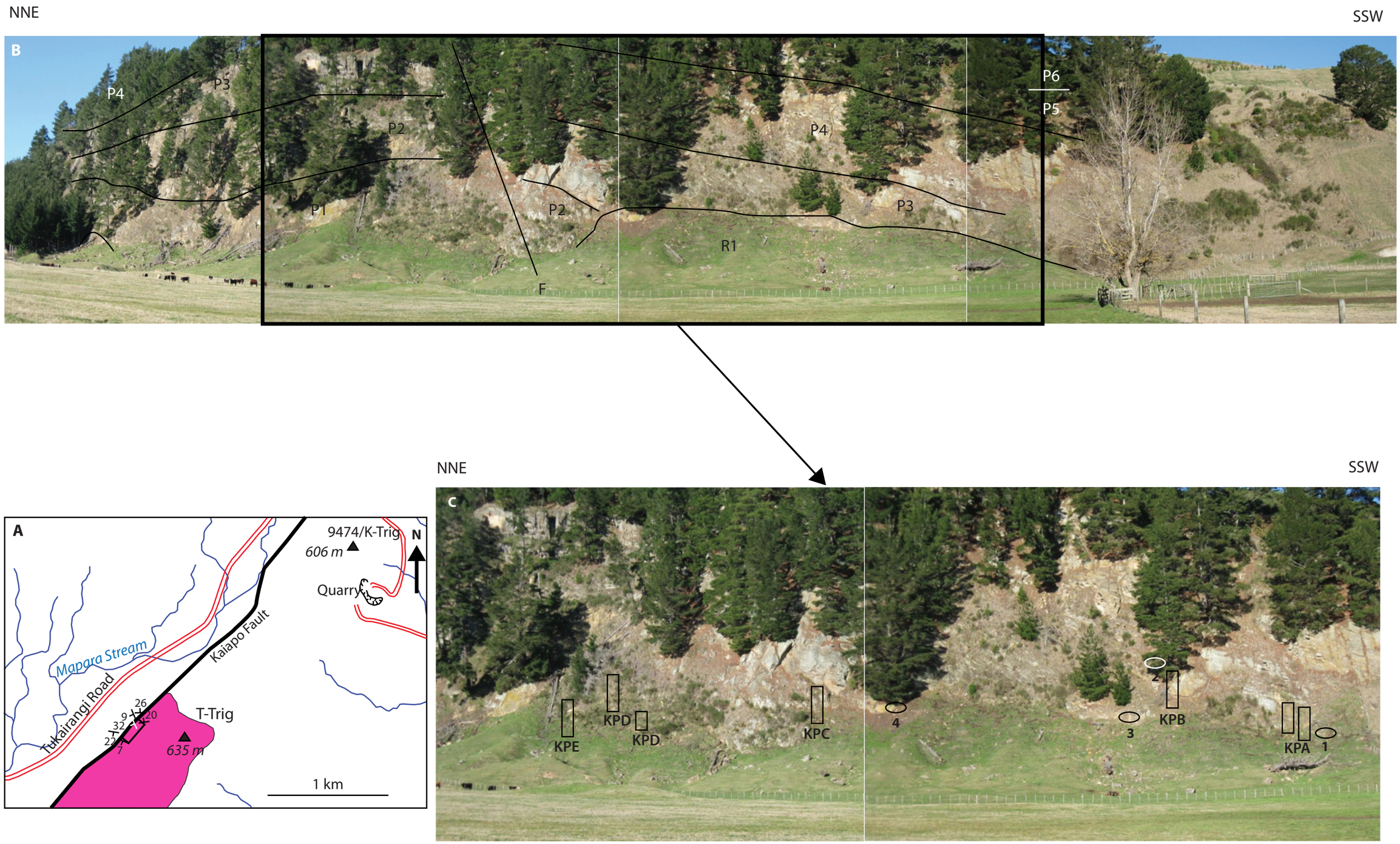

Figure 5.1 Maps and photographs showing area of Kaiapo deposit studied here. A) Map showing location of Kaiapo tuff deposit (in pink). Rectangle shows section studied here. B) Panoramic photograph of studied section showing the stratigraphic units R1, P1-P6 devised by Smith (1990). B) Panoramic photograph showing sites of stratigraphic logs (rectangles) and additional samples (ellipses). Map modified from NZMS260 Map Series (1:50 000) Sheet U18.

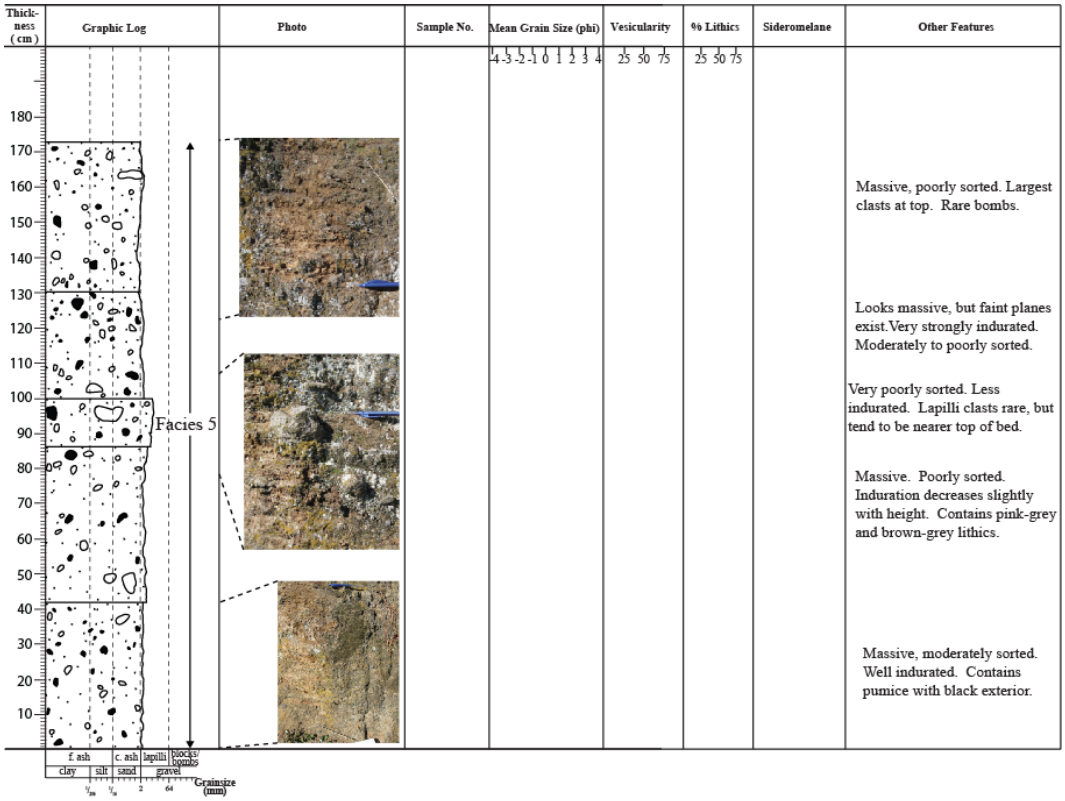

Figure 5.2 Stratigraphic log and data for site KPA-1.

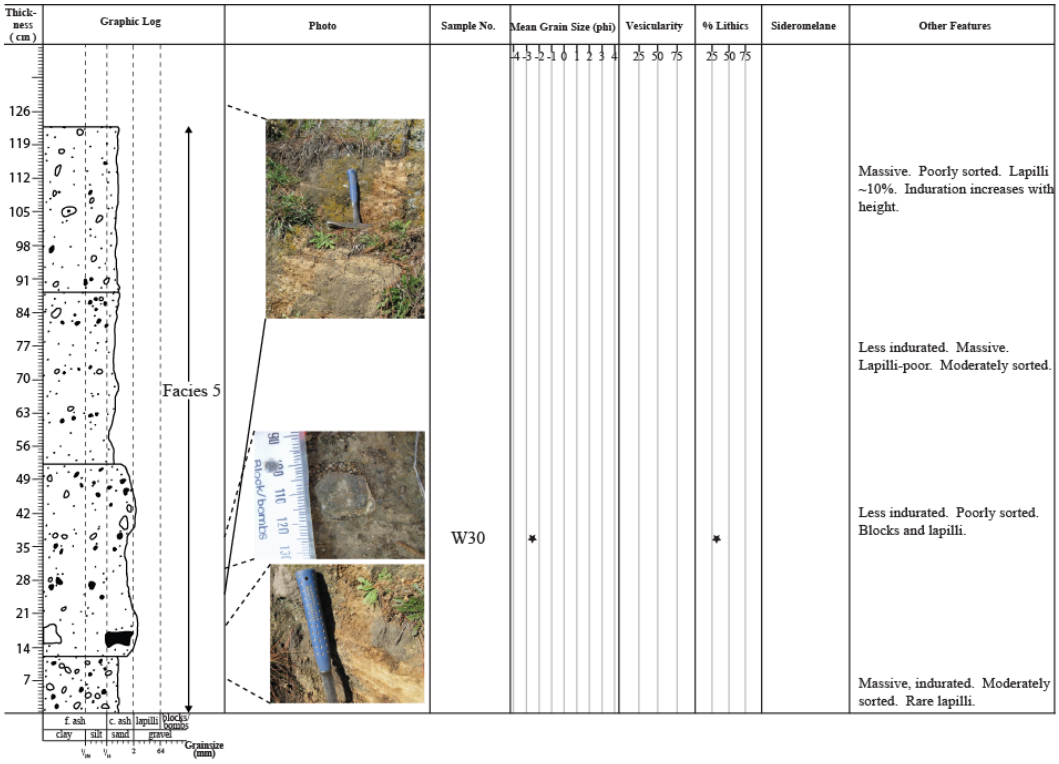

Figure 5.3 Stratigraphic log and data for site KPA-2.

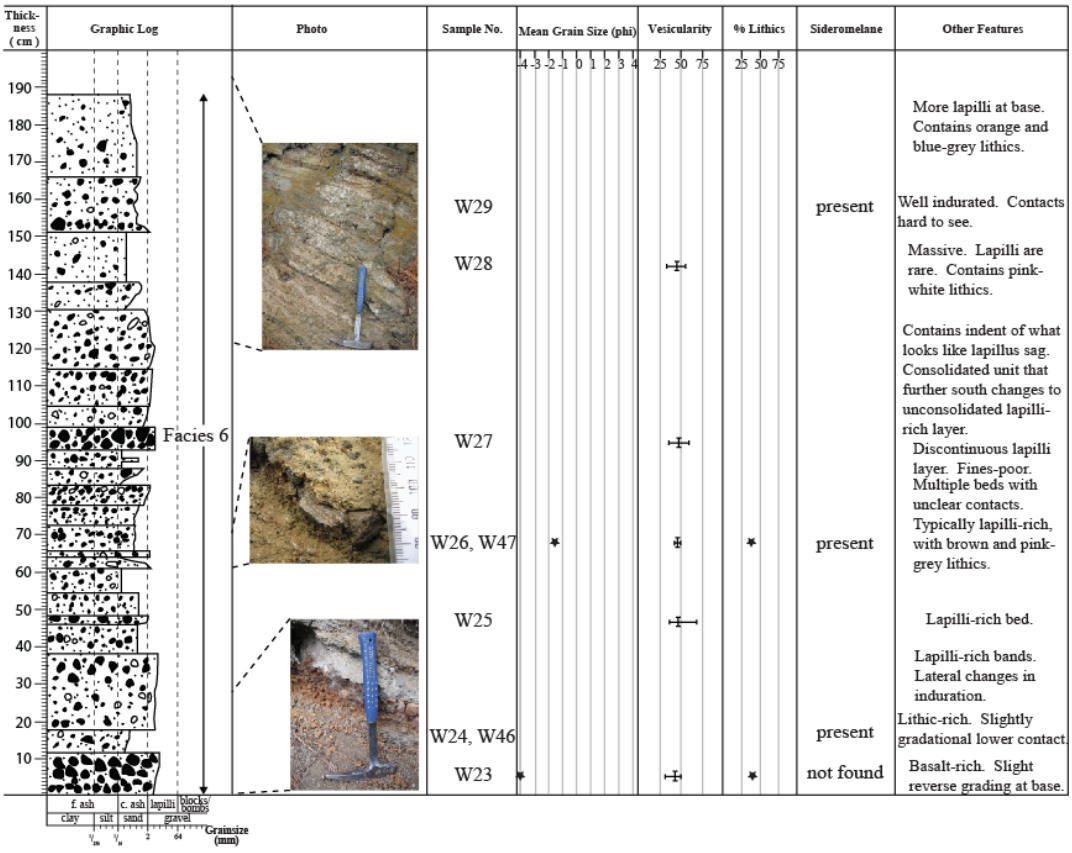

Figure 5.4 Stratigraphic log and data for site KPB.

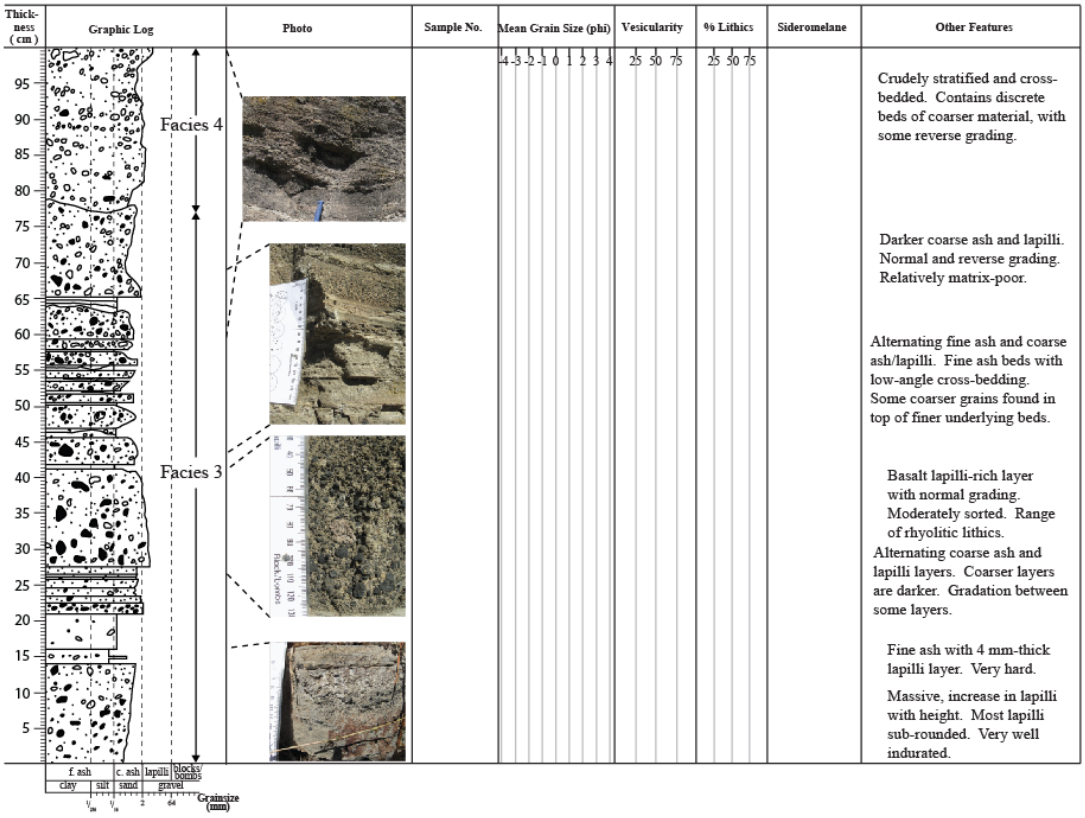

Figure 5.5 Stratigraphic log and data for site KPC.

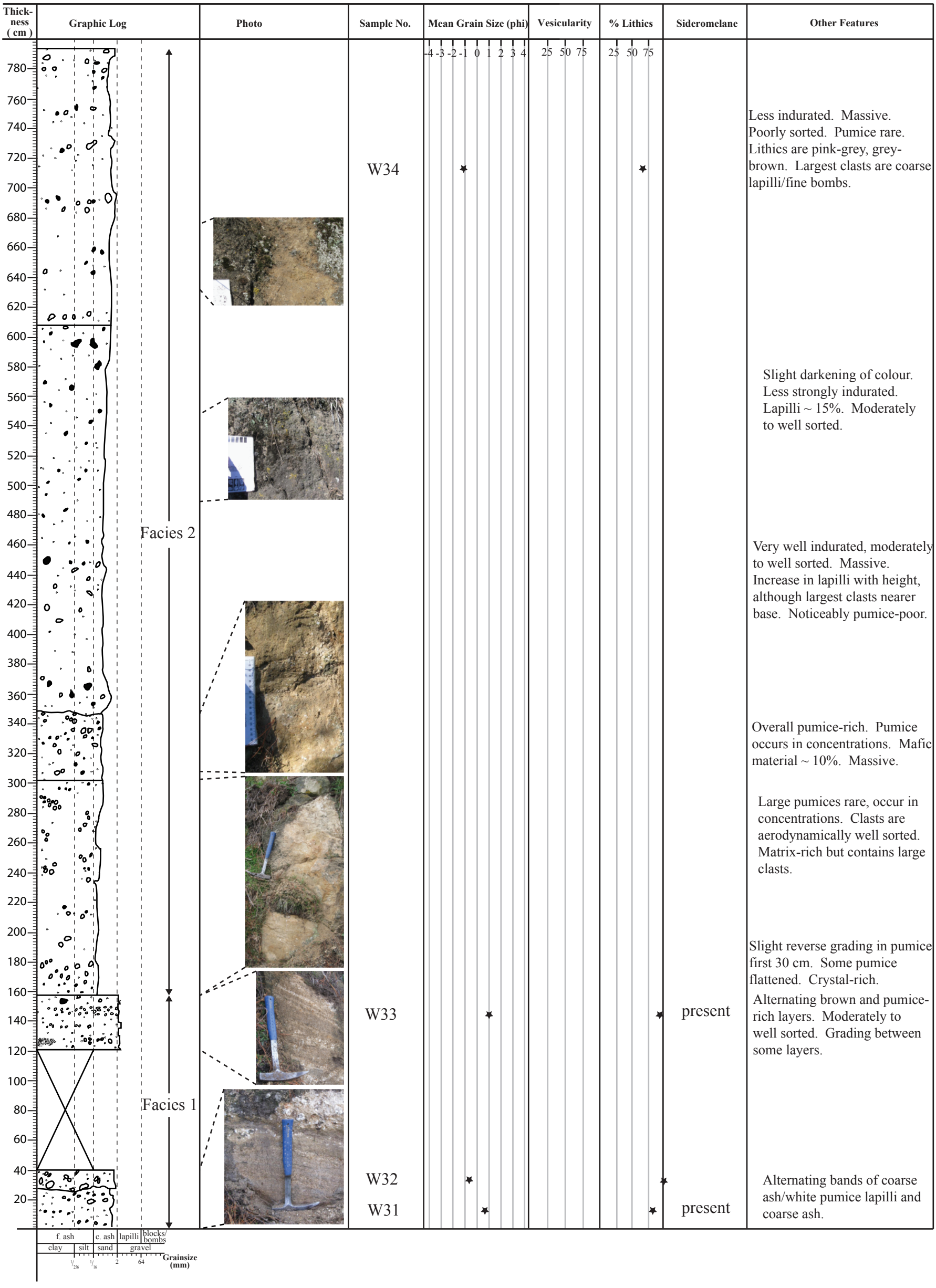

Figure 5.6 Stratigraphic log and data for site KPD.

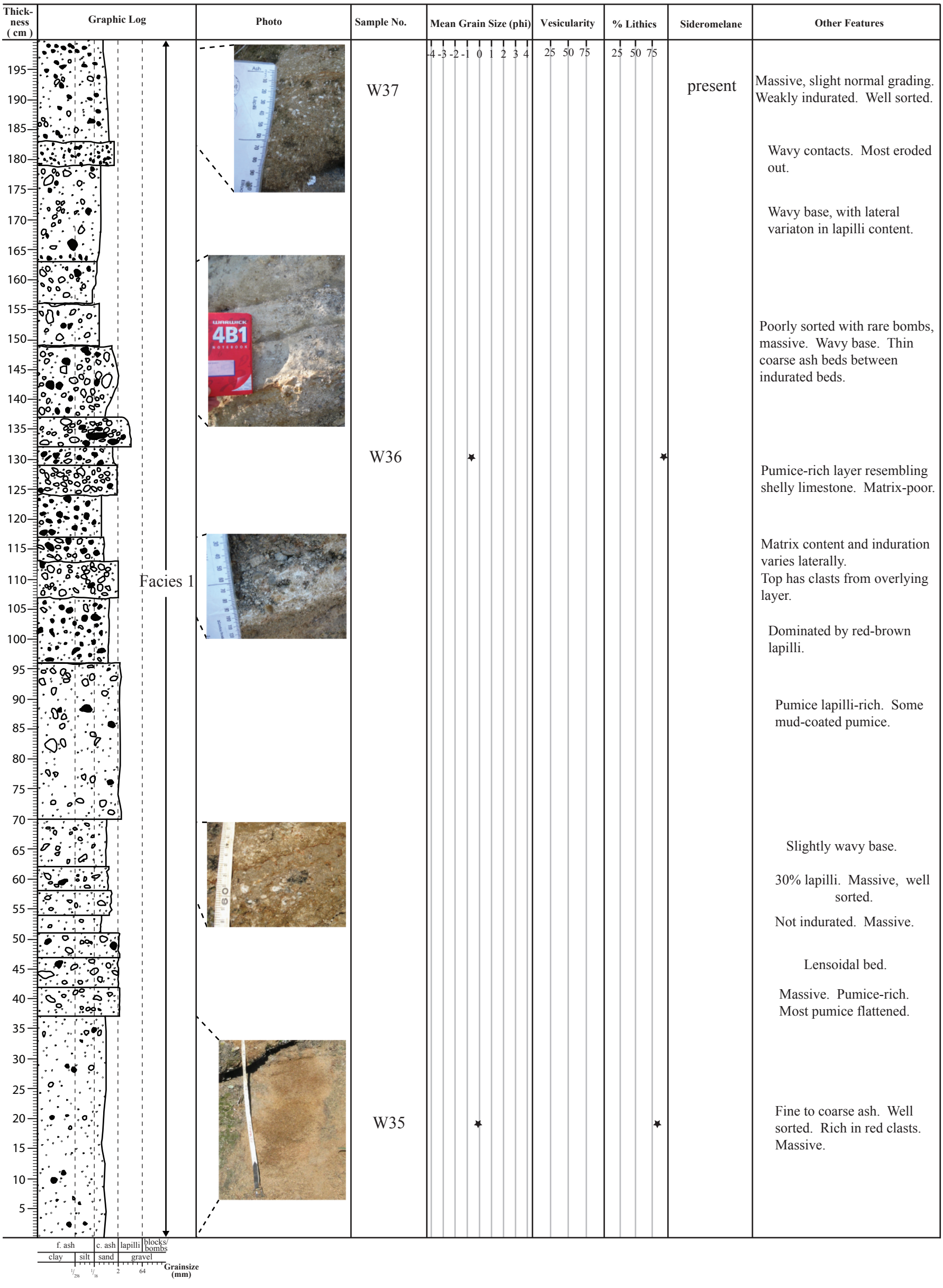

Figure 5.7 Stratigraphic log and data for site KPE.

At a smaller scale, beds often pinch and swell or form small pockets, sometimes visible for only several decimetres.

From analysis of these basal units, the following seven facies can be distinguished (**Figure 5.8**):-

1) Interbedded coarse ash-lapilli and lapilli tuff facies

   This facies is comprised of light golden brown to orange thin to medium beds that alternate between well sorted, unconsolidated coarse ash and lapilli beds and consolidated moderately to poorly sorted, matrix-rich beds containing lapilli and rare bombs. The indurated beds are continuous across section, although induration varies both laterally and vertically, from cohesive but loose material, to hard rock, reflecting relative proportions of coarser-grained material. The unconsolidated beds are at times very thin and have pinch-and-swell geometries. The beds within this facies are notably juvenile-poor and pumice-rich, with some beds consisting almost entirely of pumice. The red-brown clasts are sub-rounded to angular, and are possibly altered juvenile basalt clasts (Smith 1990). Contacts between beds are typically sharp and slightly wavy, although a few beds show a slight gradation, with some larger clasts protruding into the top of underlying layers.

2) Indurated coarse ash and lapilli facies

   This facies consists of beige to golden, thick to very thick massive beds that are poorly to well sorted. Beds consist of varying amounts of lapilli and coarse coarse ash set within a finer coarse ash matrix. Pumice, the most obvious lithic component, tends to occur in concentration clusters, accounting for up to 25% of the deposit. The pumices have both flattened and more rounded morphologies and tend to be larger than the denser components. The lowest bed in the facies shows reverse grading of the pumice, but the other beds show no grading. There is a general decrease in pumice with height, and an increase in red-brown grains, pink-grey rhyolite, and black basalt. Both normal grading and reverse grading occur in some beds, but for the most part the beds are non-graded. Crystals make up a small fraction of the beds.

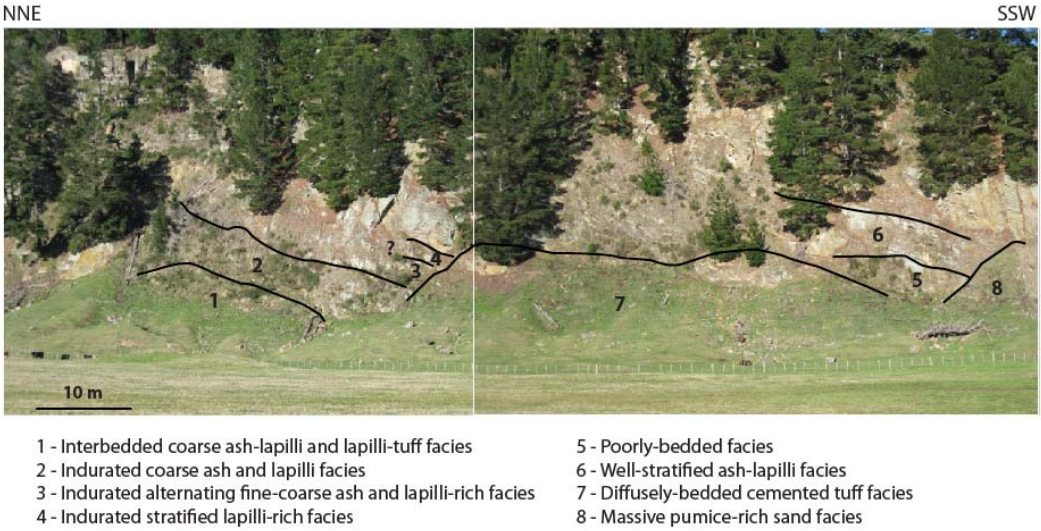

1 - Interbedded coarse ash-lapilli and lapilli-tuff facies
2 - Indurated coarse ash and lapilli facies
3 - Indurated alternating fine-coarse ash and lapilli-rich facies
4 - Indurated stratified lapilli-rich facies
5 - Poorly-bedded facies
6 - Well-stratified ash-lapilli facies
7 - Diffusely-bedded cemented tuff facies
8 - Massive pumice-rich sand facies

Figure 5.8 Facies of the lower section of the Kaiapo deposit. Facies description in text.

3) Indurated alternating fine-coarse ash and lapilli-rich facies

This facies is made up of alternating light grey, thin fine-coarse ash beds and dark grey, medium lapilli-rich beds. There is a mixture of juvenile and lithic clasts, but the dominant component is juvenile basalt. This basalt is typically black, sub-rounded, and rich in white lithic material, probably pumice. Lithics are slightly more angular, and include flow-banded rhyolite, pink-grey ignimbrite and dark green-blue ignimbrite. The lapilli-rich beds are mostly massive and non-graded, although some show slight normal and reverse grading. The fine-coarse ash layers are planar and exhibit thin, low-angle cross-laminations (**Figure 5.9**).

Figure 5.9 Close-up of low-angle cross-laminated fine ash beds in indurated alternating fine-coarse ash and lapilli-rich facies (arrows point to beds).

Sorting ranges from moderately to very well sorted, with better sorting in the finer ash layers; however, some of the fine ash layers contain rare coarser fragments probably derived from overlying beds. All of the beds are extremely well indurated, forming hard, dense rock.

4) Indurated stratified lapilli-rich facies

   A dark brown/black crudely stratified and cross-bedded, well indurated facies. The thin to medium beds are relatively matrix-poor, containing coarse ash and lapilli, along with rare bombs (< 1%). Reverse grading is common, with trains of dominantly sub-angular lapilli marking the top of layers, and discrete pockets of lapilli also occur. Pinch-and-swell of beds gives a channelised appearance to a number of beds. Wavelengths of cross-beds are ~ 60 cm and have low-angle dips (< 10º). From the colour of the facies, a dominance of juvenile material is likely, although some of the coarser clasts are a light colour. It is possible that this facies is a lateral equivalent of the poorly-bedded facies.

5) Poorly-bedded facies

   This is a light buff-brown facies of coarse lapilli and rare bombs (~1-2%) set within a fine coarse ash matrix. Individual beds are massive, and there is little to distinguish bed boundaries, although ridges of weathered sections, used to define boundaries, imply that the beds are mostly thickly bedded. Beds are moderately to poorly sorted. The coarser fragments

within the beds contain juvenile and lithic material in equal proportions. The basalt is black, vesicular, and rounded to angular. One lapillus contains a light yellow-brown pumice armoured in basaltic fine ash, and one brown lithic lapillus also contains smaller angular basalt lapilli. A range of dominantly angular lithic types are found in the facies: pink-grey ignimbrite, and blue-grey and red brown unidentified lithics. Sub-rounded pumice also occurs, but in lower abundance, and tends to have black, iron-pan surfaces. The pink-grey ignimbrite constitutes the largest clasts found in the facies, and in one instance has caused a bedding sag. The deposits are typically indurated, with slight fluctuations to be found with height.

6) Well-stratified ash-lapilli facies

This facies is dominated by light golden, planar, consolidated, thin to thick beds of coarse coarse ash to fine lapilli in finer ash, with rare thin unconsolidated lapilli beds. The consolidated beds are continuous along the section, but show lateral variation with regard to thickness, induration and grain size. In contrast with the consolidated beds, the loose lapilli beds form pockets that only extend across laterally for part of the section. The lapilli beds are noticeably fines-poor, and rich in sub-rounded to sub-angular juvenile vesicular basalt. Rare lithics are sub-rounded pink-grey ignimbrite, yellow, blue-grey and brown unidentified lithics. Beds tend to be either non-graded or slightly reverse graded. Contacts tend to be sharp, but are not always obvious.

In addition to the preceding facies, there are two other markedly different facies:

7) Diffusely-bedded cemented tuff facies

This facies is the orange cemented, diffusely-bedded tuff that comprises the basal third of the deposit. Components include dark lithic material, pumice and crystals set in a coarse ash matrix. A pumice-concentration layer also exists partway up the exposure (**Figure 5.10**). The material is

Figure 5.10 Diffusely-bedded cemented tuff facies. Arrow points to pumice-rich layer.

very well indurated, and individual clasts are unable to be picked out. The facies is lithic-rich, but also contains some black scoria (**Figure 5.11**).

8) Massive pumice-rich sand facies

This facies is found at the southern end of the field area, and forms an angular unconformity with the poorly-bedded facies. It is a dark grey-brown massive sandy unit with a lateral variation in clast content, being well sorted and fine-grained closest to the poorly-bedded facies, but pebble-rich a metre south of there. The unit is pumice-rich, and contains a 'dike' of bomb-sized pumice (**Figure 5.12**). Rip-up clasts of mudstone also occur. The largest grains are found at the base.

Figure 5.11 Close-up of diffusely-bedded cemented tuff facies.

Figure 5.12 Massive pumice-rich sand facies. Note pumice 'dike' and rip-up clasts at bottom-right.

5.2 Grain Size

Grain size analysis was carried out for 11 samples (**Figure 5.13; Appendix B**). The majority of samples come from logged sections (KPA-2, KPB, KPD, KPE). Two other samples (W40, W41) are from a measured concentration zone within the diffusely-bedded cemented tuff facies 5 m south of the KPC log site (sampling site **4** on **Figure 5.1**).

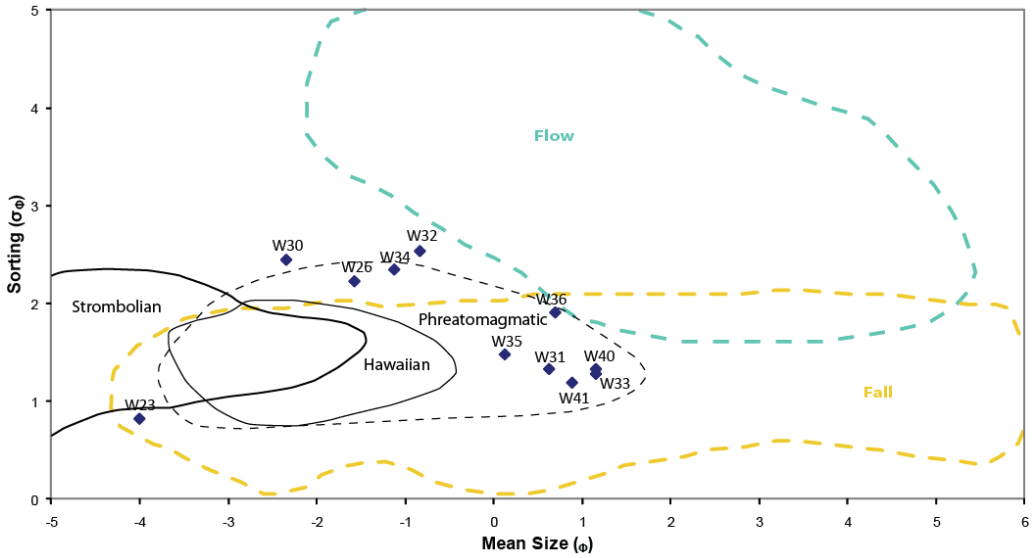

Figure 5.13 Median diameter vs. sorting plot for Kaiapo samples. Flow and fall fields from Walker (1973), eruption style fields from Houghton and Gonnermann (2008).

The data show a broad spread of values for both size and sorting of grains. The samples tend to fall into two groups: coarse-grained and poorly sorted; fine-grained and relatively well sorted. The size distribution for the coarse-grained, poorly sorted beds is represented by sample W32, from the interbedded coarse ash-lapilli and lapilli tuff facies (**Figure 5.14**).

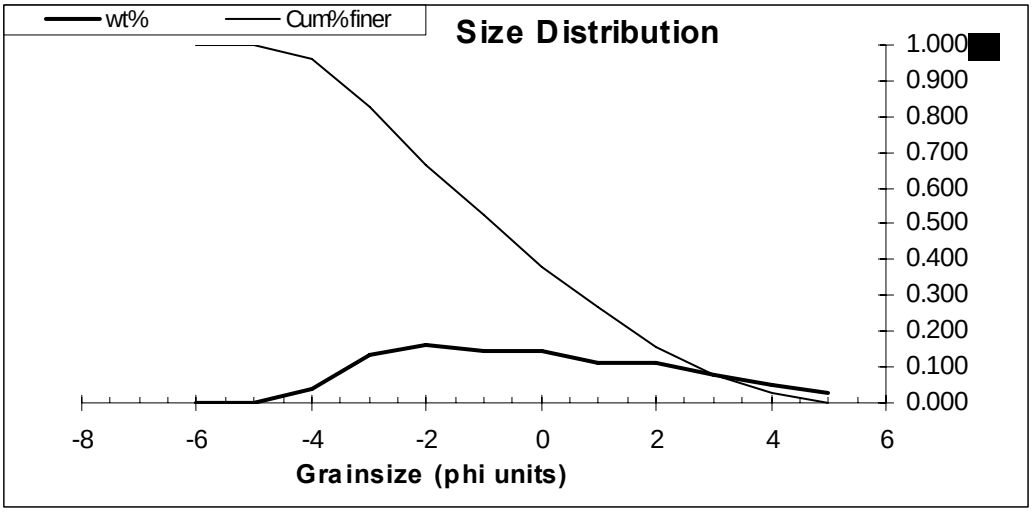

Figure 5.14 Size distribution plot for W32 (interbedded coarse ash-lapilli and lapilli tuff facies).

The fine-grained group of samples have a median grain size of less than 1 mm, with unimodal distributon and a negative skew (**Figure 5.15**), although symmetry of profile varies.

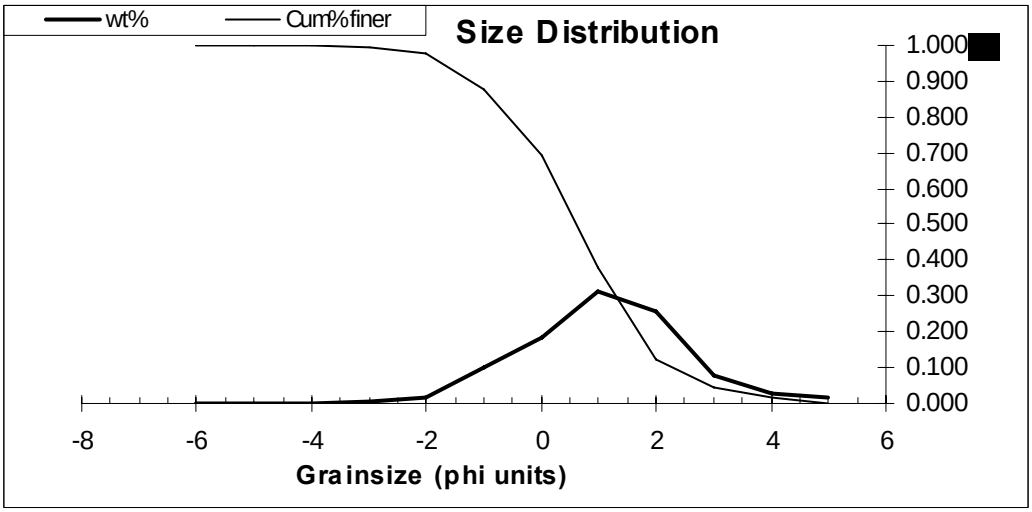

Figure 5.15 Grain size distribution plot for W31 (interbedded coarse ash-lapilli and lapilli tuff facies).

The notable exception in the samples is W23 (well-stratified ash-lapilli facies), which has an average grain size of medium lapilli and is well sorted. The size distribution plot for W23 (**Figure 5.16**) illustrates the dominance of the coarse grains. There is a strong positive skew, but it comprises a very small component of the material.

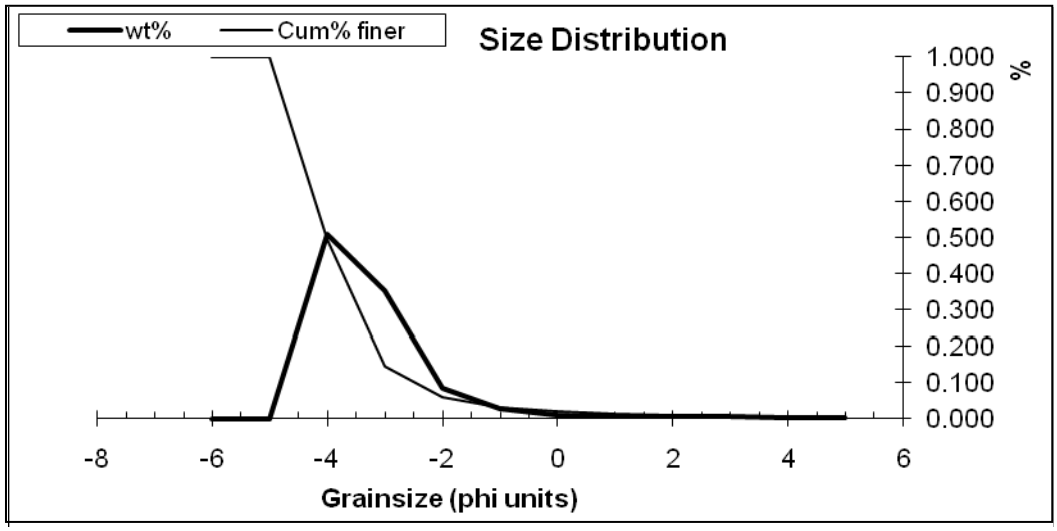

Figure 5.16 Size distribution plot for W23 (well-stratified ash-lapilli facies).

The groups of grain size and sorting do not reflect a clear trend over the course of eruption, as shown in KPD samples, with major fluctuations between the two main groups of size and sorting. However, samples from higher up in the eruption stratigraphy (W30, W23, W26 – well-stratified ash-lapilli facies) are all relatively coarse-grained.

5.3 Vesicularity

Bulk vesicularity values were obtained for five samples from the well-stratified ash-lapilli facies at logging site KPB (**Figure 5.5**, **Appendix C**). Values from the five beds (W23, W25, W26, W27, W28) are remarkably similar, with means ranging from 40 % to 48 % (**Table 5.1**). There are slight fluctuations, but no trend is visible. Variation within the samples is also small, with the largest range being that of W25 (34-68 %). The consistency in values suggests stable vesiculation processes during this stage of the eruption. These values compare well with Smith's (1990) P3 lower vesicularity values, but lack another peak found around 20 % vesicularity.

Table 5.1 Bulk vesicularity data for Kaiapo tuff (beds in stratigraphic order).

Sample	Min.	Max.	Mean	Std. Dev.
W28	31.60	53.97	46.38	6.16
W27	35.77	60.99	47.04	8.73
W26	39.67	49.74	46.34	3.21
W25	34.58	67.86	47.83	9.67
W23	31.54	50.44	40.26	6.27

5.4 Componentry and Clast Morphology

Kaiapo shows a significant contrast in componentry from the basal to upper layers. The lowermost 12 m of the deposit contains >78 % lithics, whereas the lithic abundance in the uppermost units is ~ 30 %, indicating a decrease in lithics with time (**Table 5.2**). The lithic abundance in W34 falls between these values, and observation suggests there is a lower value again at the KPC site (indurated alternating lapilli facies).

Table 5.2 Componentry abundances (%) for Kaiapo tuff (using binocular microscope).

Sample	Juvenile	Crystal	Lithic
W26	64	1	35
W23	61	0	39
W30	67	1	32
W34	35	<<1	65
W33	5	2	93
W32	1	0	99
W31	13	0	87
W36	7	1	92
W35	18	4	78
W41	12	0	88
W40	1	0	99

5.4.1 Juvenile Clasts

Juvenile scoriae at Kaiapo exhibit a range of colours, morphology and textures. Juvenile clasts are typically brown-black, blocky, poorly to moderately vesicular,

and coated with yellow ash, which is baked on several of the clasts, and has been determined by XRD to contain cristobalite/tridymite (Appendix D). Ragged, irregular scoriae with stretched vesicles that go right through the scoria also occur (e.g. W40), and W26 is notable for containing a piece of red scoria. Grains vary from angular to more rounded. Some of the rounded grains in W35 have been broken, resulting from either ground impact or transportation processes. Quenched, glassy scoriae, where present, comprise a negligible proportion of samples, except for W30, where quenched clasts account for 64% of juvenile material. SEM images obtained for juvenile clasts from layers W23 and W26 show a mix of platy, poorly vesicular clasts and more vesicular, ragged scoriae (**Figure 5.17**). The more vesicular variety has wavy fluidal patterns, which can form ridges, reminiscent of Wohletz' type 3 pyroclast (see **1.5**). Vesicles are spherical and oval, with a few coalesced vesicles in the more vesicular variety. The ash-like coating is also visible under SEM. Some of the surface irregularity is due to the vesicle indents, and are usually spherical in shape. The vesicles appear to be dominantly a surface feature, and under the SEM microscope there were no clasts seen with vesicles that were continuous across a clast.

5.4.2 Crystals

Crystals are rare in the samples, with a maximum of 4 % in W35. White tabular or anhedral plagioclase is dominant. Given the large abundance of lithics, it is possible that these crystals are accidental, rather than juvenile. A subhedral yellow crystal found in W26 could be olivine or straight-edged glass.

5.4.3 Lithic Clasts

As noted by Smith (1990), a large proportion of the lithics are pumice, which accounts for up to 96 % in the lowermost units (**Table 5.3**). The pumices vary in both texture and morphology: waxy, glassy, fibrous and swirly, vesicular cream, tan and dark streaked types occur, and pumices range from ragged, torn fragments to rounded clasts. In the lower units, a noticeable proportion (up to a few percent) has an iron-pan coating. The other significant lithic type found at Kaiapo is 'aggregate'. The aggregates are of two types: 1) clusters of individual crystals,

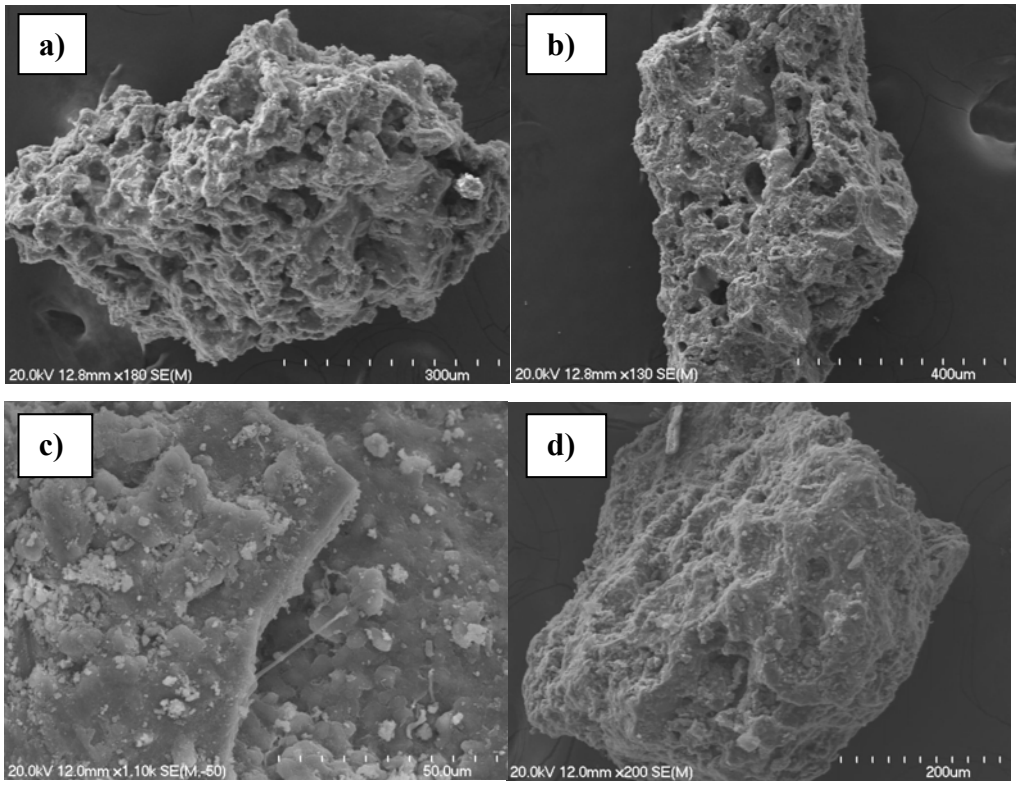

Figure 5.17 SEM images of juvenile scoria from Kaiapo: a) ridged vesicular scoria from W23; b) vesicular scoriae from W23 with visible vesicle-shaped surface; c) close-up of platy clast from W23 showing secondary coating; d) platy clast from W26.

Table 5.3 Abundances of lithic components at Kaiapo tuff.

Sample	Pumice	Aggregate	Other
W26	16	75	9
W23	6	91	3
W30	5	85	10
W34	0	86	14
W33	57	31	12
W32	88	0	12
W31	59	39	12
W36	70	19	11
W35	36	21	43
W41	58	42	<<1
W40	96	3	1

volcanic glass, pumice, scoriae and other volcanic lithics; 2) aggregates of finer-grained material held together in a beige to gold matrix resembling either

ignimbrite or lacustrine siltstones. This matrix looks similar to the cover found on the juveniles, especially for W26. Acicular mafic minerals (possibly hornblende) are also found on a significant number of these aggregates. The aggregates are most common in the upper samples, where the lithic component is much lower. A number of lithics could not be identified due to weathered iron-pan coating, but the other common lithic found is that of a white and grey/pink 'flaky' lake siltstone. Sample W32 is notable for containing no aggregates, with light beige ignimbrite being a common lithic type. The lithics are generally sub-rounded to sub-angular.

5.5 Petrography

Consolidated samples contain varying amounts of scoria, sideromelane, crystals, and lithics in a gold to grey fine ash matrix. Sideromelane is the dominant juvenile clast type in lower sections of the deposit, with scoria being more abundant in the upper sections.

5.5.1 Juvenile Clasts

Brown, grey and black, irregular scoriae contain phenocrysts of subhedral oscillatory zoned, resorbed, polysynthetically-twinned plagioclase (1.7 mm), euhedral olivine (0.8 mm) and subhedral augite (1.6 mm) set in a typically felted hyalopilitic groundmass. Round green/tan sideromelane have the same phenocrysts in a sideromelane groundmass. The largest phenocrysts occur as glomeroporphyritic clots. Upper section juvenile clasts (from KPB site) differ from other sites in that they also contain microcrystals, swallow-tail plagioclase laths and skeletal olivine, tabular plagioclase is rare, and scoria are more abundant than sideromelane. A number of clasts are part-scoria, part-sideromelane. Lower section juvenile clasts are notable for having a red-brown alteration that at times has destroyed the original fabric of the clast. Infilling of vesicles by secondary yellow-red material is also common (**Figure 5.18**).

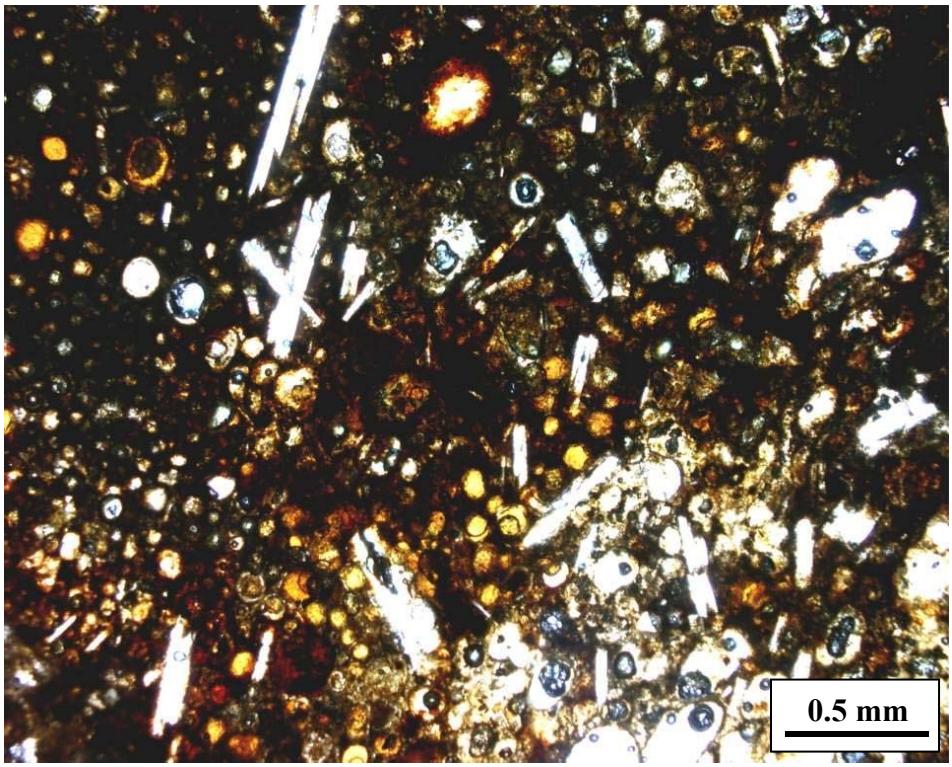

Figure 5.18 Scoria clast from diffusely-bedded cemented tuff facies (plane-polarised light).

Rare sideromelane clasts contain dark scoria fragments, whilst a scoria clast from the well-stratified ash lapilli facies (W46) contains numerous sub-rounded fine-grained beige lithics.

5.5.2 Crystals

Crystals account for up to 42 % and 9 % in lower and upper sections (respectively) (**Appendix E**). Juvenile crystals are oscillatory zoned, resorbed, subhedral to euhedral plagioclase (1.1 mm), anhedral to euhedral olivine (0.3 mm), and anhedral to subhedral augite (1.2 mm). Xenocrysts include oscillatory zoned, resorbed, polysynthetically-twinned anhedral to euhedral plagioclase (1.2 mm), anhedral augite (1.2 mm), subhedral orthopyroxene (0.8 mm), anhedral to subhedral hornblende (0.6 mm), anhedral quartz (1.3 mm), and traces of opaques (0.2 mm) and epidote (0.4 mm).

Some plagioclase crystals have round jagged edges of rhyolitic glass in the interbedded coarse ash-lapilli and lapilli tuff facies samples of W31 and W33, and rare oxidised hornblende is found in W24.

5.5.3 Lithic Clasts

Lithics are a combination of: light grey, brown and orange sparsely porphyritic ignimbrites; a variety of rhyolites, including red-brown 'tortoise shell' rhyolite, orange-grey rhyolite, red-white flow-banded rhyolite, and grey-yellow spherulitic rhyolite; a grey to white rock resembling the 'flaky' lithic found under binocular microscope; silicic lavas; and light-coloured indeterminate intrusive rocks. Fibrous, crystal-rich and black-white pumices are very common and peach glass shards occur rarely. Lithic clasts range from rounded to angular, with an average size of ~ 0.8 mm.

Petrography of several lithic blocks (from sampling sites **1** and **3** in **Figure 5.1**) from revealed: 1) a light brown, devitrified ignimbrite with low amounts of plagioclase, quartz, opaques, orthopyroxene, and augite (W47); 2) a dark 'sandy' ignimbrite containing ~ 34 % crystals (plagioclase, quartz, augite, opaques, orthopyroxene), plagioclase-hornblende clots and beige lithics (W49); and 3) an orange-brown and grey ignimbrite with quartz-rich swirly veins, containing trace amounts of plagioclase, orthopyroxene, (oxidised) hornblende and biotite (W38).

5.6 Interpretation

5.6.1 Facies

1) Interbedded coarse ash-lapilli and lapilli tuff facies

   The mixture of poorly sorted indurated beds and thin unconsolidated ash layers most likely represent the deposits of base surges and coeval ash fall (Fisher and Schmincke 1984; Cas and Wright 1987; Sohn and Chough 1989; Martin and Németh 2005). The matrix-rich nature of the indurated beds denotes a low-concentration surge that was wet at the point of deposition (Sheridan and Wohletz 1983; Allen *et al.* 1996). Wavy bedding is often associated with medial base surge deposits (Brand and White 2007; Gençalioğlu-Kuşcu *et al.* 2007), but also supports a wet, dilute type of surge (Brown *et al.* 1994; Allen *et al.* 1996). The small-scale lateral variation reflects the pulsatory deposition of unsteady surges

due to subtle changes in suspension and traction (Németh and White 2003). The high abundance of pumice in these beds indicates that fragmentation occurred within a permeable pumice-rich horizon. The dominance of sideromelane and the poorly sorted character of the beds support their being wet (e.g. Martin and Németh 2005; Brand and White 2007), and the red alteration of juveniles clasts (Smith 1990), possibly from iron-water interaction could also support this. The very low juvenile clast content in the facies is due to a low magma supply or overabundance of water. (Allen *et al.* 1996; Ort and Carrasco-Núñez 2009).

2) Indurated coarse ash and lapilli facies

The beds comprising this facies, with compacted pumice and variable sorting, are deemed to be from more voluminous base surges. The fact that the pumice clasts are larger than their denser counterparts could indicate that these beds are fall deposits (Walker *et al.* 1971), yet grain size analysis shows relatively poor sorting more typical of surge deposits. It is possible that these beds are a mixture of fall and surge, termed 'surge modified fall deposits', which are common in proximal settings, where arrival times of the surge and fall are almost simultaneous (Gençalioğlu-Kuşcu *et al.* 2007). The slight reverse grading at the base of the lowest bed in this facies could indicate subaqueous deposition (White 2000) or basal shearing or traction carpet dispersal pressures of highly-concentrated, near-vent surge (Sohn and Chough 1989; Allen *et al.* 1996; Sohn 1996). The decrease in pumice and corresponding increase in juvenile clasts indicates an increase in magma supply with time or a shallowing of fragmentation (Németh and White 2003). The appearance of different lithic types also points to a change in fragmentation depth. The well indurated nature of this facies indicates that the beds were at least moist when deposited (Sheridan and Wohletz 1983).

3) Indurated alternating fine-coarse ash and lapilli-rich facies

The alternation between coarse- and fine-grained beds are interpreted to represent a succession of base surge and fall deposits (Sohn and Chough 1989; Zanon *et al.* 2009). The cross-laminations of the indurated fine beds indicate lateral transportation of finely-fragmented pyroclasts in a surge (Sohn and Chough 1989). The lapilli-rich beds are deemed to be fall, due

to their being relatively well sorted, rich in coarse, relatively vesicular juvenile clasts and showing a lack of a matrix (Frazzetta *et al.* 1983; Zanon *et al.* 2009), although they could represent high-concentration dry surges (Sohn and Chough 1989; Allen *et al.* 1996; Zanon *et al.* 2009). These coarser beds are also well-indurated, which points to the material being wet or sticky at the time of deposition (Sheridan and Wohletz 1983). This could either be due to conditions in the tephra jet (Sohn 1996), or depositional environment. Variations in thickness and grain size probably reflect subtle changes in fragmentation and eruption energy, often due to magma supply rates (Houghton and Gonnermann 2008). The high juvenile content in these beds indicates a high supply rate of magma relative to that of water (Ort and Carrasco-Núñez 2009),

4) Indurated stratified lapilli-rich facies

   This facies, with its reverse grading and low-angle cross-beds, is most likely the result of a series of high-concentration base surges (Sohn and Chough 1989). The grain-supported matrix, dominated by coarse grains, suggests a dry surge (Allen *et al.* 1996). The crude stratification is typical of channelised deposits (Sohn and Chough 1989). The wetness of the deposit as indicated by induration (Sheridan and Wohletz 1983) could reflect environment of deposition, rather than water content of the surge. The coarse grain size, in conjunction with the dark colour of the deposit, if not an effect of weathering, also supports a drier, unoxidised magmatic-rich eruption phase (following facies of Allen *et al.* 1996).

5) Poorly-bedded facies

   The poorly sorted, massive, and matrix-supported characteristics of these poorly-defined beds denote a rapid succession of relatively wet medium-concentration base surges (Sohn and Chough 1989; Brown *et al.* 1994; Allen *et al.* 1996). The occurrence of armoured (pumice) lapilli, often associated with accretionary lapilli (e.g. Brand and Clarke 2009) suggests at least damp conditions (Allen *et al.* 1996; White 2000), possibly in a water-exclusion zone of an eruption column (White 2000) or surge cloud (Sohn 1996), although a lack of any noticeable wavy contacts implies that the surges were not as wet as those responsible for Facies 1.

6) Well-stratified ash-lapilli facies

The consolidated beds of this facies, with their poor sorting and lateral variation in thickness and grain size, are interpreted as medium-concentration base surges (e.g. Sohn and Chough 1989). The unconsolidated, well-sorted lapilli beds are considered to be short-lived fall deposits. Grain size analysis of the basal lapilli bed (KP1) shows a plot typical of strombolian fall deposits (cf. **7.2**), with only the small lithics component and angular morphology suggestive of involvement of water (e.g. Barberi *et al.* 1989; Martin and Németh 2006). In comparison with previous facies, the planar contacts and marked increase in scoriaceous juvenile clasts in consolidated beds, and the unconsolidated lapilli beds point to much drier conditions, with brief alternation between wetter and drier conditions (e.g. Frazzetta *et al.* 1983; Sohn 1996). The pumice inclusions observed in the juvenile clasts indicate intimate mixing with a silicic source (as discussed by Smith 1990).

7) Diffusely-bedded cemented tuff facies

This facies, with its mix of volcaniclastic and sedimentary material, and a 'welded' ignimbrite-like texture and appearance, is very similar to the 'crystal tuff' deposits of Cas and Wright (1987). The indurated nature of the facies renders it more like a volcaniclastic sandstone. The indurated nature of the facies, given the low juvenile basalt content, is unlikely to be primary (R. M. Briggs pers. comm.. 2010), but rather post-depositional, either from hot springs, or simply consolidation of material leading to lithification. The alignment of crystal grains evident in some thin sections points to either lateral transportation or a layering effect from background accumulation of material. The facies is also diatom-rich, indicating that it was subaqueous (lacustrine) and supporting an epiclastic origin (Cas and Wright 1987). The undulatory nature of the facies could represent pre-eruption lake-floor topography, given the natural variation that exists at the base of lakes (Nelson and Lister 1995), but could have been modified during eruption. The existence of rare basaltic scoria at depth supports a theory of reworking of the lake sediments (as proposed by Smith 1990; also Cas and Wright 1987).

8) Massive pumice-rich sand facies

This facies' sandy texture and dark appearance, which looks muddy in thin section, suggests a sedimentary origin. The high amount of volcanic material within the deposit can be explained by the volcaniclastic nature of lake sediments found within the region (Nelson and Lister 1995), and the basalt contained within the facies could be mixed in from the eruption. The unit also shows signs of major disruption, however, with the pumice 'dikes' and rip-up clasts, and lacks the diatoms present in diffusely-bedded welded tuff facies. A more likely explanation is that of Smith (1990) that it represents a vent-clearing phase. Given the sandy nature of this facies, it is possible that the majority of material originates from the 'sandy' black ignimbrite found as lithics higher up in the Kaiapo section. Vent-clearing can result in a decrease in lithic proportions from by causing more efficient fragmentation near the surface (Németh and White 2003), which could help the decrease in lithics with height at Kaiapo. Lorenz and Kurszlaukis (2007), however, can only envisage a single, most likely initial, vent-clearing phase, and for shallow, rather than deep, maar craters (if the eruption at Kaiapo initially formed a maar). This makes an initial vent-clearing phase more conducive, although this facies could also indicate a change in vent location.

5.6.2 Role of External Water

The lower part of the Kaiapo deposit exhibits marked variation in external water involvement. There is evidence in the deposit for both active and passive interaction with water, affecting both magma fragmentation and deposition.

The first phases of the eruption were very wet, with the presence of wet surges and sideromelane being the dominant juvenile clast type (e.g. Sheridan and Wohletz 1981; Frazetta *et al.* 1983; Fisher and Schmincke 1984). There is also an extremely high abundance of lithic material in these units, almost to the point of being phreatic (Sheridan and Wohletz 1983; Petrinovic and Colombo Piñol 2006). The possibility exists that some of the features of the beds, such as alteration of juvenile clasts and wavy contacts are also due to subaqueous deposition (as

suggested by Smith 1990; Brown *et al.* 1994). There is no obvious density grading of pumice, which can indicate subaqueous deposition (Fisher and Schmincke 1984; White 2000), although some of the pumice concentrations could actually represent the tops of separate eruptive units.

There is evidence of a decrease in water with time, with a change to drier eruption deposits, as indicated by the sharper contacts between beds and an increase in juvenile material (Brown *et al.* 1994; Allen *et al.* 1996). The planar contacts could reflect a drier depositional environment (cf. Wohletz 1983; Brown *et al.* 1994), whereas the increase in juvenile material could be due to one or more of: drying-up of the water source (Allen *et al.* 1996; Ort and Carrasco-Núñez 2009), change in fragmentation depth to a shallower level (Németh and White 2003), change in fragmentation depth to a harder aquifer (Carey *et al.* 2007) or an increase in magma supply and ascent rate (Houghton *et al.* 1999). The indurated facies at the KPC site have a high amount of coarse juvenile material, associated with drier eruptions, but, despite the vertical variation, all of the units are very well indurated, indicative of moist conditions (Sheridan and Wohletz 1983). This combination of features is interpreted to represent deposition of relatively dry deposits into a wet environment. This would help explain the variation in induration along the length of the deposit. The KPB site, which represents the latest eruption phase looked at in this study, involved much less water than previous phases, with lapilli fall accompanying relatively dry base surges. Sideromelane is present, but is very much subordinate to scoriaceous clasts, suggesting that water supply was relatively low, so only interacted with a small proportion of magma (e.g. Martin and Németh 2005; Ort and Carrasco-Núñez 2009). The alternation between surges and lapilli fall therefore likely reflects an unstable water supply, although slight changes in magma ascent rate could be responsible by affecting ability of water to mix with magma (Houghton *et al.* 1999; Martin and Németh 2006). Nevertheless, it is likely that a small amount of water was present during the lapilli fall, given the blocky, angular nature of the clasts, the relatively low vesicularity values, and the fact that lithic clasts are also found in greater abundance in many of the lapilli beds than would be expected for a purely magmatic eruption (Barberi *et al.* 1989; Houghton and Wilson 1989; Carey *et al.* 2007). The red scoria found in W26 is unusual, and could reflect the

relatively dry nature of the eruption at this point, or it could have originated from another vent.

5.6.3 Source of External Water

Given that the Kaiapo deposit overlies diatomaceous lake siltstones, and the eruption is inferred to have taken place in the late Pleistocene when Lake Huka existed (Smith 1990; Brown *et al.* 1994), the probability of lake water being the source of external water is strong. Evidence for this is found in the basal units, where dark and white pumice, also found in the diatomaceous diffusely-bedded welded tuff facies, is ubiquitous. The presence of sideromelane and very wet nature of the beds also suggest that magma met with a large volume of water. The very high lithic values, however, are more often associated with maars, which involve groundwater and subsurface explosions (e.g. Cas and Wright 1987; Brand and Clarke 2009; Ort and Carrasco-Núñez 2009). Furthermore, the lack of clear evidence of subaqueous deposition in the basal units lessens the likelihood of a significant lake level at the site of deposition and, given the proximity of deposits to the vent, site of eruption. It is therefore proposed that during the initial stages of eruption, fragmentation occurred at a shallow level within very wet, semi-consolidated lake sediment (as is the case with 'soft-substrate' maars – Németh and Martin 2006; Auer *et al.* 2007), and involved explosive interaction of magma with water in this sediment and overlying lake water. This lake water was likely quite shallow.

The eruption phases responsible for the upper units, by contrast, may have involved water from a different source (Brand and White 2007). These units all show an increase in juvenile material (and scoria content), which could be simply due to a reduced (lake) water supply, but the lithic components differ markedly from the basal units, being relatively pumice-poor, and containing rhyolite and ignimbrite. Pink-grey ignimbrite lapilli and blocks were commonly found. The alternation between fall and surge deposits near the top of the section suggests fluctuating magma:water interaction, with a reduced water supply and/or increased magma supply rate (e.g. Zanon *et al.* 2009). Together, these characteristics point to a groundwater source, with fragmentation of magma occurring at a progressively greater depth (Auer *et al.* 2007; Ort and Carrasco-

Núñez 2009). Such a scenario is possible for maar eruptions that begin in shallow soft-substrate (Auer *et al.* 2007). The pink-grey ignimbrite is identified by Cole *et al.* (1998) as being part of the Rangatira Point Ignimbrite, and the dark, 'sandy' ignimbrite matches with their description of a 'sandy' black ignimbrite member. These water sources are similar to those of Smith (1990), who proposed an initial phreatomagmatic eruption through magma interaction with water from a pumice-rich horizon within the upper Waiora Formation (of which the Rangatira Ignimbrite is a member - Brown *et al.* 1994) and the soft sediments of the Huka Formation. A change in fragmentation depth and aquifer source during the course of the eruption was not explicitly discussed.

5.6.4 Eruption Phases

The section of Kaiapo studied here is interpreted to have resulted from five phreatomagmatic phases. The initial phase involved eruption of base surges with coeval ash fall from fragmentation of magma with water within a soft substrate and subsequent non-explosive interaction with lake water. The second phase was marked by a more voluminous magma discharge rate, which was followed by subsequent draining of the magma. A progressive deepening of the fragmentation level resulted in a drier eruption phase, with eruption of large amounts of basalt lapilli in dry surges, although deposition was at least partly subaqueous. The fourth phase was marked by explosive interaction of the magma with a deeper ignimbrite aquifer, with vent-clearing and subsequent moderate-concentration base surges, deposited subaerially. The final phase, with angular basalt lapilli fall deposits and surges, was the product of low, fluctuating degrees of magma: water interaction, either due to an unsteady magma supply rate or an intermittent water supply.

6 *Kinloch*

6.1 Site and Facies Description

The Kinloch deposit consists of one outcrop of tuff exposed in a cliff section along the edge of Lake Taupo (**Figure 6.1**). The tuff is situated adjacent to spherultic rhyolite eruptives and the Whangamata Fault, and is south of the possibly-related basalt deposits of Ben Lomond and Marotiri (see **Figure 2.2**). The exposed cliff face lies ~ 6 m both horizontally and vertically from the current lake edge, where a wide range of typically hydrothermally-altered outsize volcanic and sedimentary boulders, along with smaller rocks and crystal fragments, are situated.

In contrast to the Acacia Bay, Kaiapo and Punatekahi deposits, the stratigraphy below and above the basalt at Kinloch is well exposed. A succession of tephra and paleosol layers underlies the basalt. The youngest dated tephra layer is that of the Opepe Tephra (~ 9.95 ky cal. B.P.; Wilson 1993; **Figure 6.2**, identified at Kinloch by M. D. Rosenberg pers. comm. 2008; supported by the mineralogy of

samples W67 and W68). The tuff is overlain by a ~ 4 m-thick, very poorly sorted unit containing unidentified blocks and what appear to be rounded fragments of the underlying altered Oruanui ignimbrite. This layer could represent some late-stage mass flow that originated from the vent, but it is also possible that this unit was caused by the breakout flood following the Waimihia eruption (c. 3.55 ky cal. B.P.; Wilson 1993; Manville *et al.* 2007). This would render the age of the basalt to be somewhere between 9.95 ky and 3.5 ky B.P., making it the youngest known basalt in the TVC by more than 100 ky. The existence of paleosols also suggests that the site has been subaerial since at least the Oruanui eruption (c. 26.5 ka), despite its close proximity to the lakefront.

The extent of the deposit along the shoreline is likely to be less than 50 m given that, in close proximity to the exposed tuff, at the same elevation, poorly sorted fluvial deposits are found, and further east again of these deposits, only rhyolite tephra are found (**Figures 6.3, 6.4**). The rapid change in stratigraphy over a short distance strongly suggests the presence of another fault. The total thickness of the preserved tuff is ~ 7 m. Inferring a length of 50 m and an inward extent of ~ 10 m, an estimated volume of ~ 5 x 10^{-6} km^3 remains, but it is likely that this was originally much higher.

The tuff deposit is cut by three main faults: a pair of high-angle conjugate faults (008/70 ° E and 172/70 ° E) along the main face, both down-faulting to the east with an offset of ~ 1 m; and further east, a lower-angle fault (000/58 ° E) down-faulting ~ 2 m to the north. These appear to have been produced near the end of the eruption or shortly after, as they cut into all of the Kinloch units and visible preceding stratigraphy, but not the overlying massive deposit. There are also smaller faults of a few cm to be found, which are clearly syn-depositional.

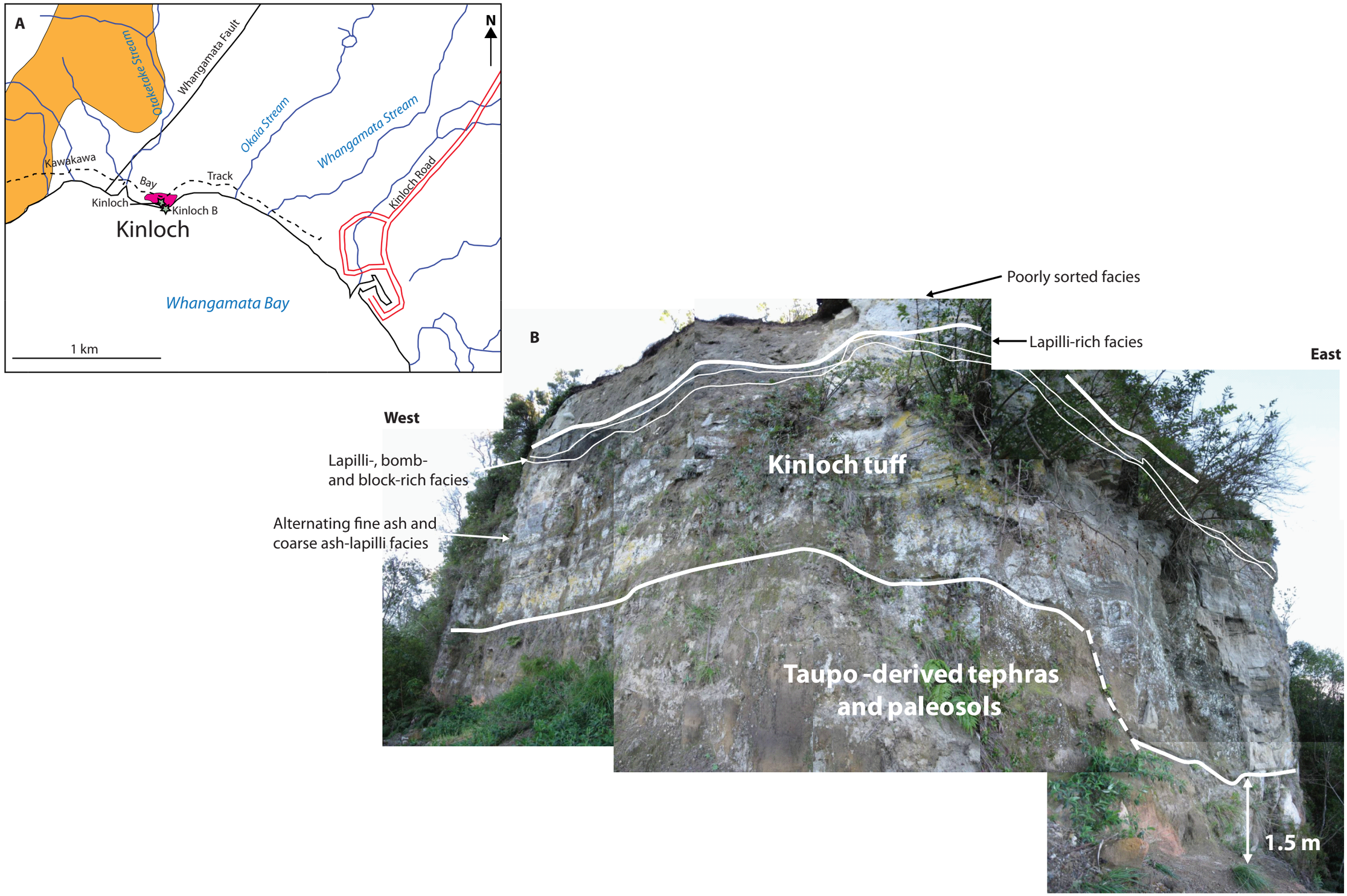

Figure 6.1 Location and appearance of the Kinloch tuff deposit. A) Map showing location of Kinloch tuff. Ornage is rhyolite, pink is basalt. Stars on map refer to stratigraphic log locations. B) Photograph showing main cliff exposure and facies described in text. Map modified from NZMS260 Map Series (1:50 000) Sheet T18.

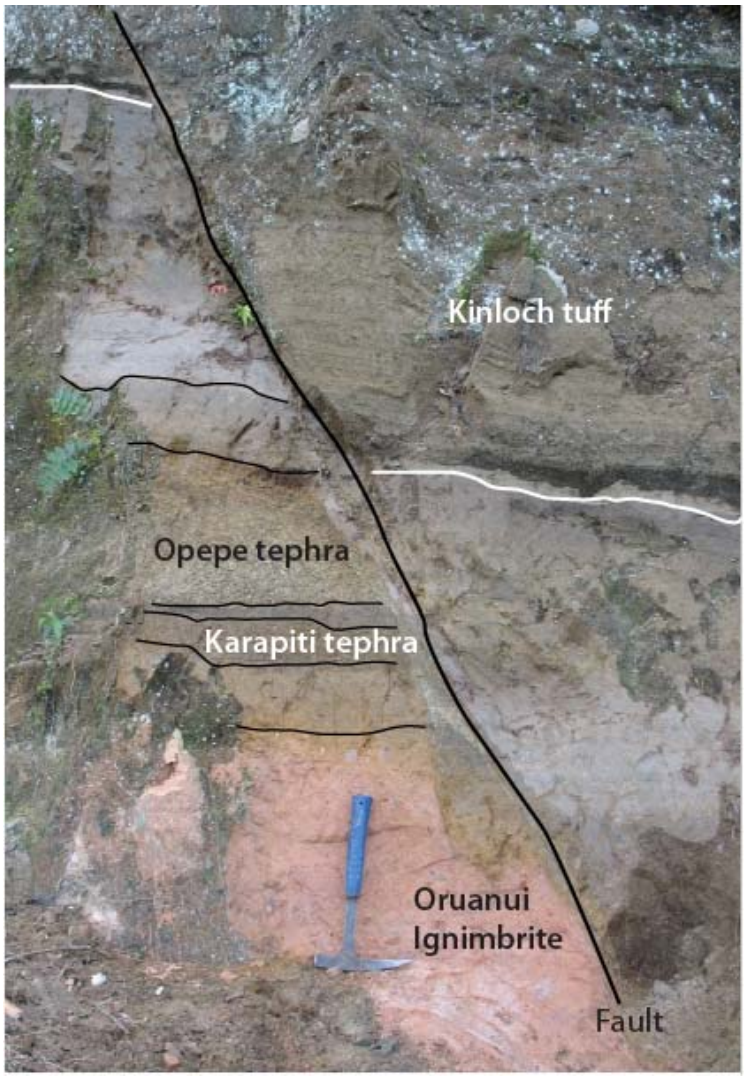

Figure 6.2 Pre-Kinloch stratigraphy. Unmarked layers are palaeosols. (Photo: R. M. Briggs)

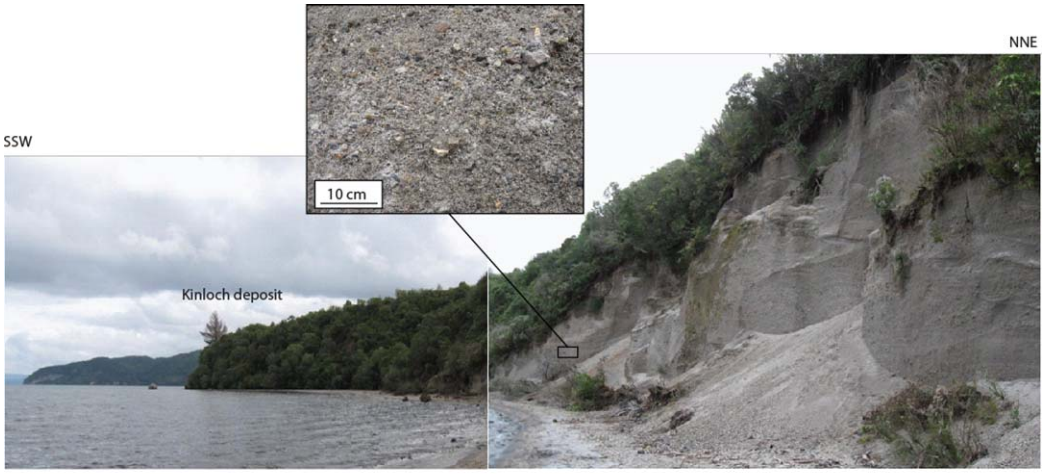

Figure 6.3 Fluvial deposits ~ 50 m east of Kinloch basalt.

Figure 6.4 Rhyolite tephra east of Okaia Stream, Kinloch. Height of outcrop is 5 m.

The Kinloch tuff is dominated by a 5.5 m-thick succession of alternating lighter fine ash and darker coarse ash-fine lapilli layers. This is overlain a black bomb-rich layer, which is further overlain by several dark, finer-grained beds. The deposit can be divided into three broad facies, as follows (**Figures 6.1, 6.5**). It should be noted that the third facies is not accessible and was described from a distance.

1) Alternating fine ash and coarse ash-lapilli facies

   This facies is a sequence of light, consolidated thick, faintly bedded, consolidated, well sorted fine ash-fine coarse ash, and darker, unconsolidated, thin to medium bedded coarse ash to coarse lapilli. Small proportions of lapilli are also found in the second-lowest fine-grained bed, but dissipate higher up. The coarse ash-lapilli beds are often erosional, cutting into underlying finer ash layers with U-shaped channels. Low-angle cross-bedding is also common, and flame structures underlie the first coarse ash bed. The finer-grained layers contain thick laminations of planar fine ash that is in places vesiculated. Some of these vesicles are elongated, directed parallel to flow, possibly the result of shear by overlying units (**Figure 6.6**). The coarser units have varying proportions (up to 20%) of pale pumice and rhyolite lithics.

Kinloch (Main Site)

(GPS No.) E 2762895 N 6278658

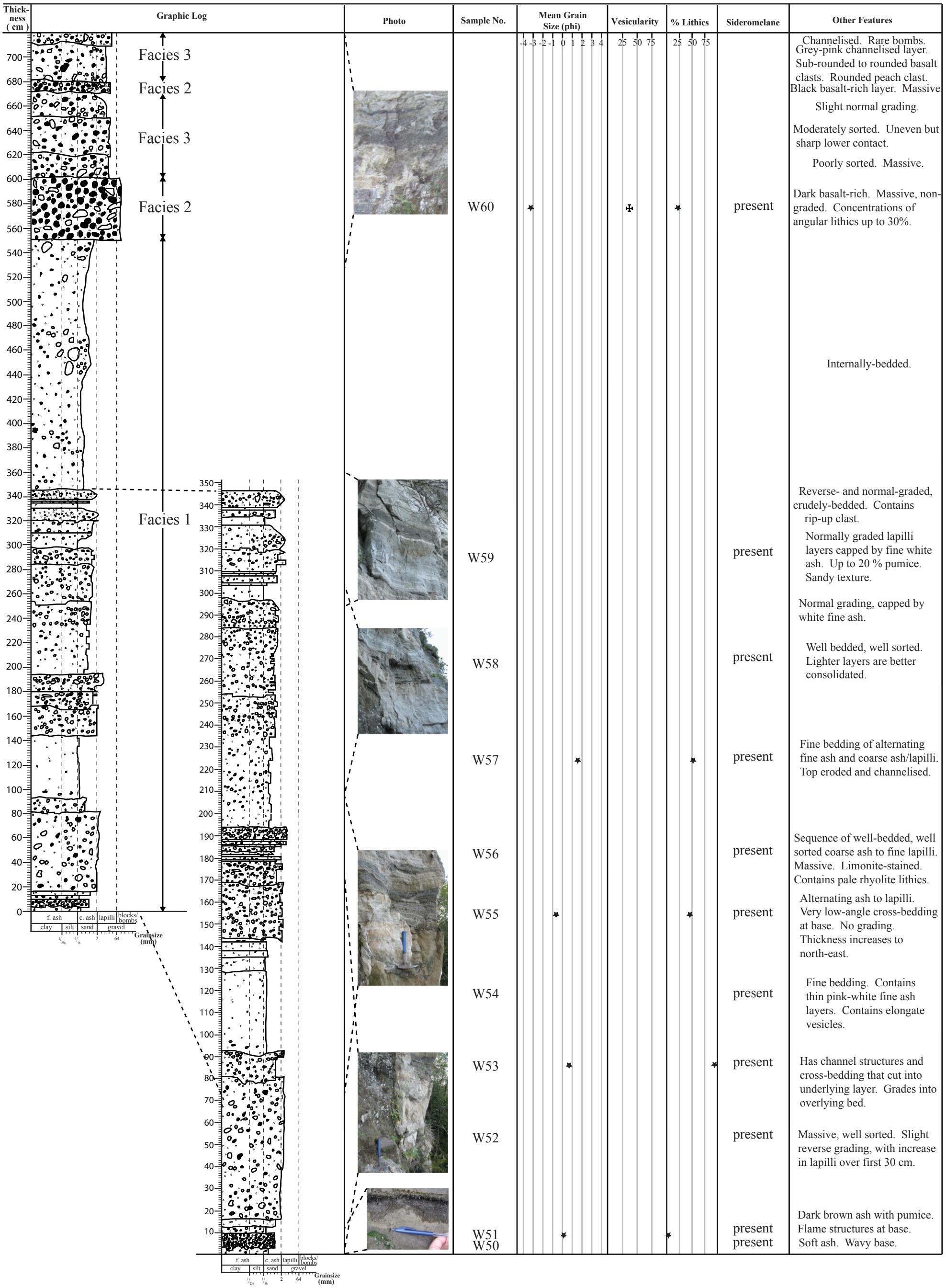

Figure 6.5 Stratigraphic log and data for the Kinloch tuff deposit (main site). (Top 3.7 m logged by sight.)

Thickness of both types of beds tends to increase with height.

Figure 6.6 Close-up of vesiculated tuff, Kinloch. Scale is in mm.

2) Lapilli-, bomb- and block-rich facies

This facies consists of dark, massive, thick beds rich in lapilli, blocks and bombs. The two layers that comprise this facies are unconsolidated, and appear to be non-graded and well sorted. The diagnostic feature of this facies is the presence of black sub-spherical lava balls (similar to 'pelletal lapilli' – Kurszlaukis *et al.* 1998; Lorenz and Kurszlaukis 2007; Carracedo Sánchez *et al.* 2009; **Figure 6.7**). These balls are generally of coarse lapilli/bomb size, exhibit breadcrust textures and contain visible crystals of olivine and plagioclase. Numerous sub-rounded to rounded pumice inclusions, up to several mm in size, are included within the glassy groundmass of the balls. The blocks within the facies are angular lilac to white spherulitic rhyolite lithics. Lithics make up 5-30% of the deposit, and occur in concentrations. Contacts with other facies are sharp but undulate, and the beds show variable thickness, giving a slight channelised geometry.

3) Lapilli-rich facies

Golden-brown to grey, massive, thick, lapilli-rich beds characterise this facies. The beds are non-graded, matrix-rich and look poorly sorted. Bed thickness varies across the section, with a channelised geometry. Across the northernmost fault in the section, the thinner beds seem to disappear. Juvenile content cannot be accurately estimated, although darker beds are inferred to have higher juvenile content than the lighter beds. Both light angular lithics and dark juvenile clasts are visible, with lithic clasts seemingly the larger constituent. A rounded peachy fragment in a higher part of the facies is likely to be part of the hydrothermally-altered Oruanui ignimbrite found at the base of the deposit.

Figure 6.7 Sub-spherical lava balls. Ruler scale is in mm.

Overlying the pyroclastic succession, is the following unit, the relationship of which to the other facies is uncertain. It is described here for completeness:

4) Poorly sorted facies

This very thick unit (~ 4 m) contrasts strongly with the other facies at Kinloch, in its combination of very light colour, matrix-rich nature, and very large lithic clasts, with no visible basalt content. Lithics include large rounded fragments of the underlying Oruanui ignimbrite and what look like rounded sedimentary cobbles (**Figure 6.8**). The unit is very poorly sorted and looks loosely compacted, and the degree of landslide material at the base of the section provides some testament to that.

Figure 6.8 Close-up of poorly sorted facies. Arrows point to likely Oruanui ignimbrite fragments.

Two stratigraphic logs were completed: one for the main cliff section (bar the poorly sorted facies) ('KL' - **Figure 6.5**), and one much smaller section north of the cliff that faces east, referred to as KLb (**Figure 6.9**). The data collected refer to samples taken from both of those log sites.

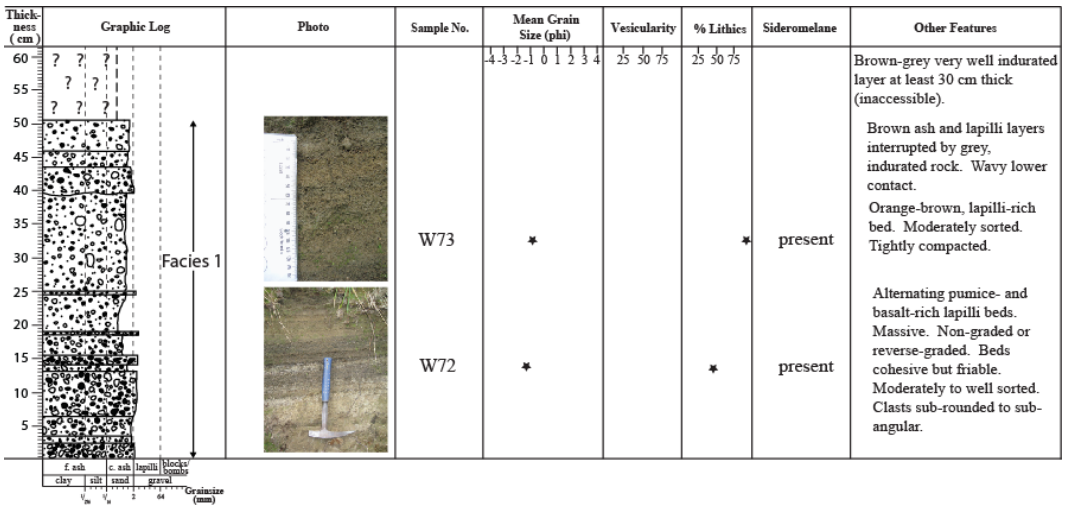

Figure 6.9 Stratigraphic log and data for site Kinloch B (KLb).

6.2 Grain Size

Grain size analysis was carried out on seven samples from Kinloch (**Appendix B**): four from the main face, and three from the down-faulted, mostly inaccessible section perpendicular to the main face. The majority of analyses come from the unconsolidated fractions of the alternating facies found in the basal two-thirds of the deposit. The two exceptions are W57, taken from a friable part of the consolidated finer fraction, and W60, from the lower bomb-rich layer.

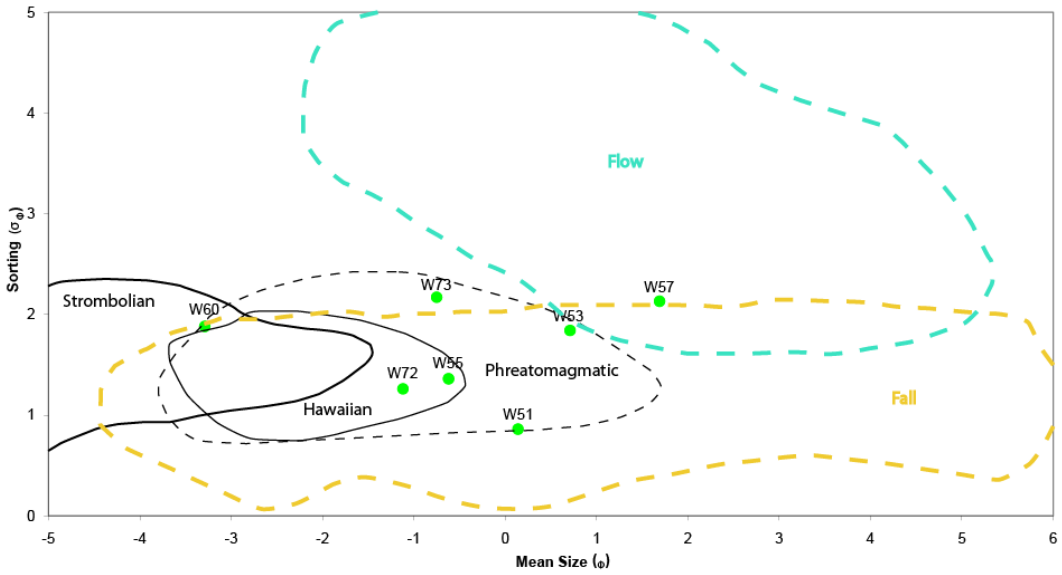

Figure 6.10 Median diameter vs. sorting plot for Kinloch samples. Flow and fall fields from Walker (1971), eruption style fields from Houghton and Gonnermann (2008).

The sorting versus grain size plot (**Figure 6.10**) show variations in both grain size and sorting in the lower part of the succession (alternating fine ash and coarse ash-lapilli facies): the initially well sorted, coarse ash was followed by a finer, less well sorted unit; a change to a much coarser, moderately sorted deposit was then also followed by a finer and more poorly sorted deposit. Despite the fluctuations, the grain size is consistently within a coarse ash range. In contrast, W60, the uppermost unit able to sampled (from lapilli, bomb- and block-rich facies), shows a marked change to a mean grain size of medium lapilli (excluding > 5 Φ clasts, which were not bulk-sampled). Unlike the samples from the alternating facies, however, W60 doesn't fit the general pattern of coarser beds having better sorting. The grain size distribution plot for W60 (**Figure 6.11**) reveals a positive skew,

which is also different from those of the other units, and almost a mirror image of W57 (**Figure 6.12** and **Figure 6.13**).

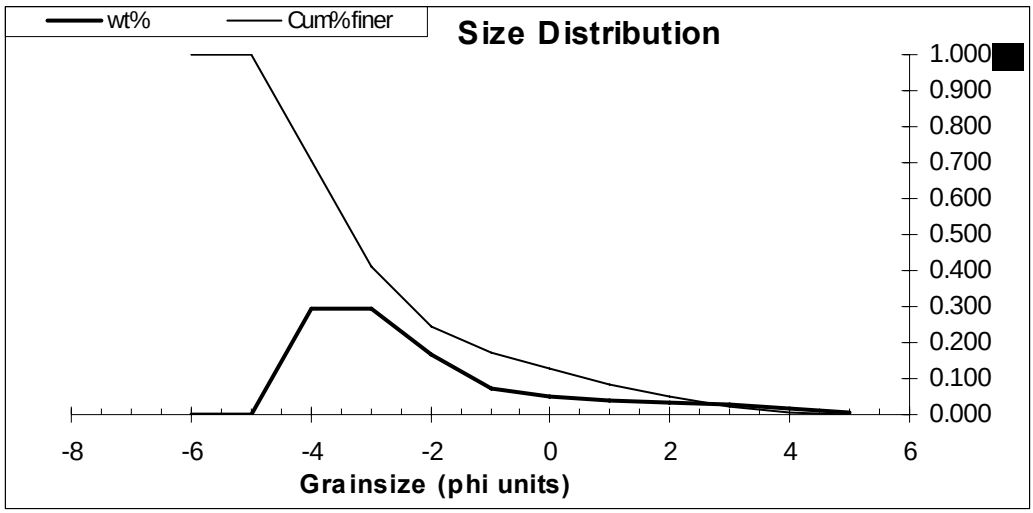

Figure 6.11 Grain size distribution plot for W60.

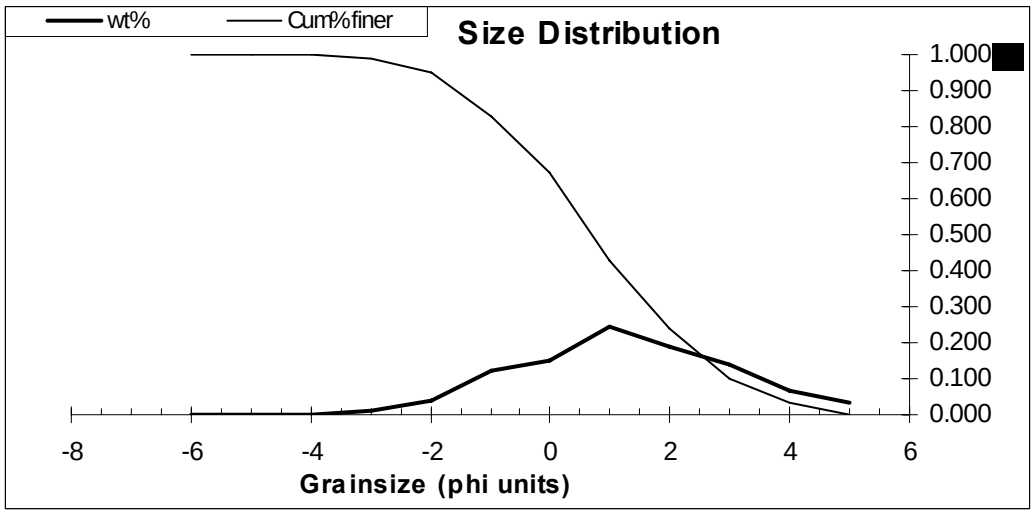

Figure 6.12 Grain size distribution plot for W53.

Samples W72 and W73 are from the same down-faulted section as that of W60, a cliff face that lies close to 90° from the main exposure (KLb). It is likely that they represent a lateral equivalent of W55 and W56 (given the similarity between W72 and W55 in **Figure 6.10**), or W59 and the bed above W59 (given the height in relation to W60). Their data also show a marked difference from layer to layer, with W73 a lot less sorted than its preceding bed.

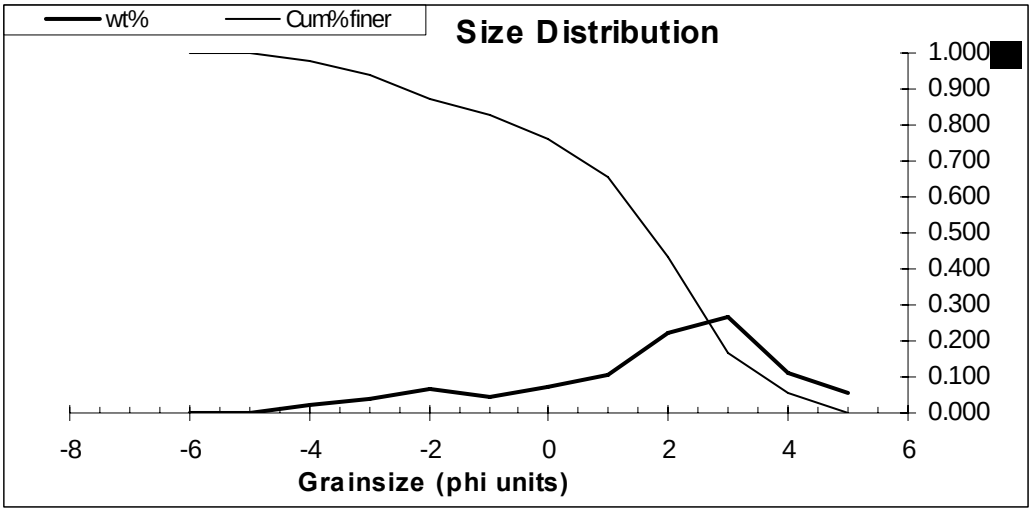

Figure 6.13 Grain size distribution plot for W57.

6.3 Vesicularity

Due to the inability to sample above 4 m and the fine-grained nature of the basal beds, only one sample, that of the initial bomb-rich layer (sample W60), was able to be tested for vesicularity. Bulk vesicularity results (**Appendix C**) show remarkably consistent values of poor to moderate vesicularity, at 35-43%. The mean vesicularity is just over 36 %, indicating dominance at the lower end of values.

6.4 Componentry and Clast Morphology

Binocular microscrope analysis of the 1 Φ fraction of samples from the alternating facies shows a generally high lithic content, although it fluctuates, being initially low, then very high, before stabilising at around 50 %. There is a marked decrease in lithic content in the bomb- and block-rich facies (**Table 6.1**).

6.4.1 Juvenile Clasts

Juvenile clasts are typically black, with ragged and blocky morphologies. Spindle-shaped grains are present in W51. Vesicularity ranges from poor to moderately

high, containing oval, spherical and elongate vesicles. Vesicles are generally small, and are smallest in W60. W51 and W60 have scoria clasts where tubular

Table 6.1 Componentry values (%) for Kinloch using binocular microscope (in stratigraphic order).

Sample	Juvenile	Crystal	Lithic
W60	73	4	23
W57	49	2	49
W55	55	0	45
W53	8	0	92
W51	95	<<1	5
W73	5	0	95
W72	54	1	45

vesicles go right through the clast. Crystals are visible in most samples, but size and abundance varies. Green, quenched glassy clasts are present, but are rare, only contributing a significant proportion of juveniles in W53, where juvenile content is very low. Pumice inclusions in juvenile clasts are rare, with a few scoria fragments adjoining what looks like waxy, clear pumice. An ash coating exists on all of the lower facies' clasts, although its appearance dissipates with height. W60 differs from lower facies samples in that juvenile clasts are very vesicular, ragged, angular black scoria, speckled with orange hydrothermal precipitate.

SEM images were obtained for scoria clasts of W51 and W60, and a piece of tuff from W54 (**Figure 6.14**). W51, which is the most juvenile-rich bed, contains a mix of blocky, almost platy, ash-covered grains and smoother, fluidal clasts (**Figure 6.14a-b**). Vesicularity is relatively poor for both clast types. Vesicles form ragged, deep structures in the blockier grains, whereas vesicles in the fluidal clasts have stretched oval morphologies and are more clearly defined.

The W54 sample is a piece of consolidated vesiculated tuff. In the SEM images (**Figure 6.14c-e**), several vesicles are clearly visible, and are a lot larger than the matrix. Vesicles are shallow and slightly oval. The tuff itself is an aggregate of loose crystals and sub-angular to angular ash grains, which show a range of morphologies (**Figure 6.14d**). Intergranular porosity is visible in SEM (**Figure 6.14e**).

In contrast with W51, the juvenile basalt clasts from W60 (**Figure 6.14f-h**), consist of grains that show a friable texture (**Figure 6.14f**), at times with broken surfaces showing rare coalesced vesicles (**Figure 6.14g**). Also visible are stretched, branching strings of material, possibly lava (**Figure 6.14h**).

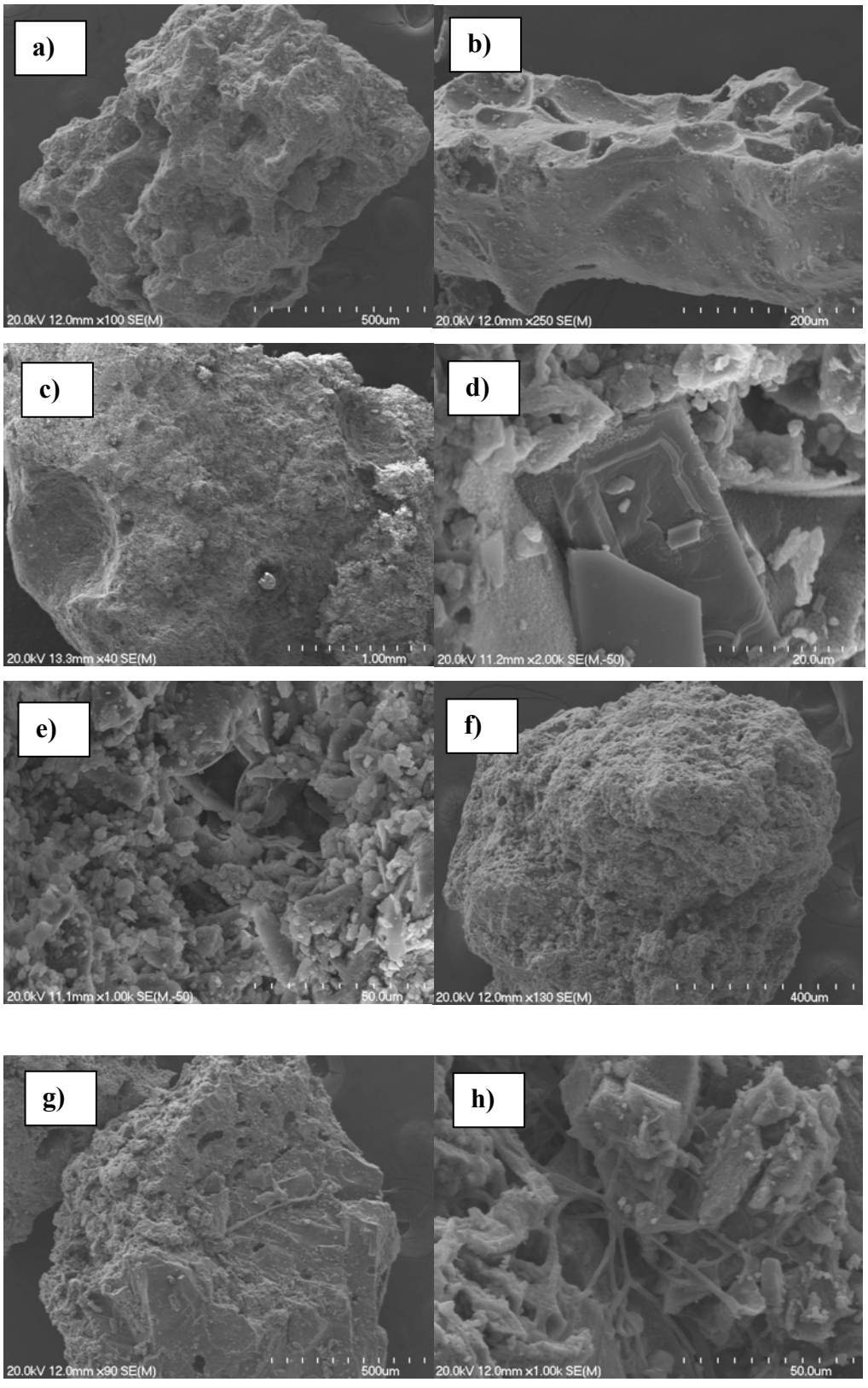
a)
20.0kV 12.0mm x100 SE(M)
500um
b)
20.0kV 12.0mm x250 SE(M)
200um
c)
20.0kV 13.3mm x40 SE(M)
1.00mm
d)
20.0kV 11.2mm x2.00k SE(M,-50)
20.0um
e)
20.0kV 11.1mm x1.00k SE(M,-50)
50.0um
f)
20.0kV 12.0mm x130 SE(M)
400um
g)
20.0kV 12.0mm x90 SE(M)
500um
h)
20.0kV 12.0mm x1.00k SE(M)
50.0um

Figure 6.14 (previous page) SEM images of juvenile eruptives from Kinloch: a) blocky, ash-covered scoria (W51); b) fluidal scoria (W51); c) fragment of consolidated tuff (W54); d) close-up of consolidated tuff showing plagioclase crystal amongst ash grains (W54); e) close-up of tuff pores (W54); f) friable, vesicle-poor grain (W60); g) broken clast showing smooth surface and rare coalesced vesicles (W60); h) close-up of broken clast with stretched 'strings' between ash particles (W60).

6.4.2 Crystals

Crystal contents are low, reaching a maximum of 4%. Nearly all of the crystals are plagioclase, although some quartz is found in the bomb facies (KL14). Some crystals are difficult to distinguish from rhyolitic glass.

6.4.3 Lithic Clasts

The most abundant lithic type found is the aggregate of scoria, crystals, lithics and ash (**Table 6.2;** see **5.4** for definition of aggregate). Interestingly, there is a strong positive relationship between total lithic contents for a sample, and aggregate lithic contents ($R^2 = 0.9386$; see **9.2.1.4**), indicating that aggregates strongly affect lithic values at Kinloch.

Table 6.2 Lithics percentages for Kinloch using binocular microscope.

Sample	Pumice	Aggregate	Ignimbrite	Flaky	Other
W60	12	7	1	0	80
W57	32	47	15	0	6
W55	17	41	18	23	1
W53	4	95	0	1	0
W51	33	7	13	47	0
W73	<1	95	<1	3	1
W72	21	60	1	13	5

The other common lithic types are pumice and ignimbrite. Pumices are a mix of brown and creamy, ragged and rounded clasts, which are typically fibrous, sometimes waxy and often have a baked appearance. Ignimbrites are light beige, sub-angular to sub-rounded speckled fragments, sometimes containing visible lithics and pumice. The flaky component consists of grey, sometimes pinkish sub-angular to angular grains with a flaky-looking surface texture. It is possible

that these relate to the grey and orange rhyolite found in thin section. The other lithics are dominantly comprised of grains that are indeterminate due to an ash-like cover. In the case of W60, the high 'other' constituent is mainly comprised of clear to frosted grey, glassy/pumice-like ragged fragments and quartz crystals.

6.5 Petrography

Consolidated samples comprise (typically) juvenile basalt, crystals and lithics in a sparsely vesiculated, light brown, fine-grained matrix.

6.5.1 Juvenile Clasts

Juvenile clasts are of two types: dark brown to black scoria and yellow-green sideromelane. Sideromelane is subordinate to scoria in all but one sample, averaging ~23 % of juvenile clasts. Clasts have irregular, blocky or rounded morphologies. Vesicularity is low in both scoria and sideromelane juvenile clasts, with vesicles up to 0.3 mm in size. Scoria and sideromelane are porphyritic, with crystals set in a rarely microcrystalline felted hyalopilitic groundmass. Phenocrysts are subhedral plagioclase (0.6 mm), euhedral olivine (1.1 mm), subhedral to euhedral augite (0.7 mm) and subhedral epidote (1.4 mm). Tabular plagioclase phenocrysts are rare. Plagioclase laths commonly exhibit swallow-tail textures, and olivine is skeletal in W51, W54, W58 and W60 (**Figure 6.15**). In one of the lava balls (W70), phenocrysts form aligned phenocryst chains. Cognate lithics occur in the form of plagioclase-olivine and augite glomeroporphyritic clots, and accessory lithics of light beige material, rhyolite and clear vesicular rhyolitic glass (pumice). Lithic scoria fragments were also found in juvenile clasts from W56 and W60.

6.5.2 Crystals

Juvenile crystals of subhedral plagioclase, olivine and augite are commonly found in the matrix of consolidated samples, but are rare in loose fractions. Xenocrysts of anhedral to subhedral oscillatory zoned plagioclase (1.2 mm), subhedral orthopyroxene (1.1 mm), subhedral hornblende (0.9 mm) and anhedral quartz (1.3 mm) are also found.

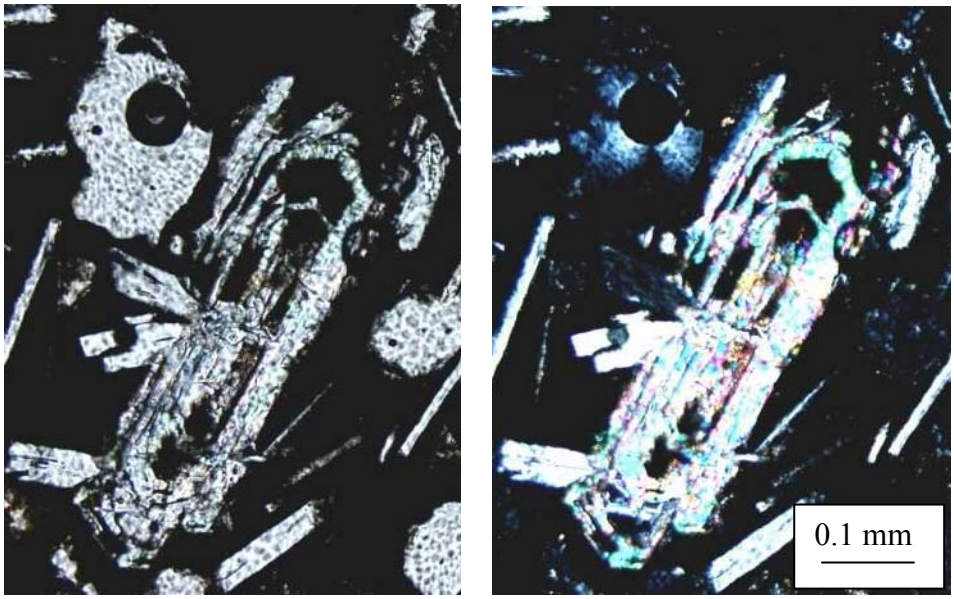

Figure 6.15 Photomicrograph of skeletal olivine within scoria (W51). Left: plane-polarised light, right: crossed-polarised light.

6.5.3 Lithic Clasts

The lithics at Kinloch, which account for up to 40 % of samples (**Appendix E**) consist of rounded to angular red-brown/white spherulitic rhyolite, rhyolite lava, brown/grey/white rhyolite, variously coloured ignimbrite, pumice, unidentified beige and yellow lithics, and greywacke. There is little change in lithic type with stratigraphic height (**Table 6.3**), with only the clear rhyolite lava being restricted to higher samples. W57 is notable for being relatively ignimbrite-rich, whilst the unidentified porphyritic yellow lithic is found in every second unit, and generally constrained to the finer, consolidated units.

Table 6.3 Main lithic types, Kinloch tuff.

	Sample (W..)										
Lithic type	**60**	**59**	**58**	**57**	**56**	**55**	**54**	**53**	**52**	**51**	**50**
Red-brown/white spherulitic rhyolite	+	+	+	+	+	+	+	+	+	+	+
Yellow crystalline lithics	-	+	+	-	+	-	+	-	+	-	+
Ignimbrites	+	-	-	+	+	-	+	-	+	+	-
Grey/brown/ white rhyolite	-	+	+	+	+	-	+	+	-	+	-
Rhyolitic glass from grey/orange rhyolite	+	+	+	+	+	-	+	-	-	+	-
Light brown/beige w/peachy spher rhy	-	-	+	+	+	-	+	-	-	-	+
Grey with orange rhyolite	+	-	-	-	+	+	-	-	-	+	+
Light mottled lithic, possibly dolerite	-	+	-	-	-	+	+	-	-	-	-
Greywacke	-	-	-	-	-	-	-	-	-	+	-
Clear perlitic rhyolite lava	+	+	+	+	+	-	-	-	-	-	-

Thin sections of three lithic blocks from the bomb- and block-rich facies and an ex situ block (found at the base of the main log site) containing a basalt bomb reveal up to three types of rhyolite. Two of the blocks from the bomb- and block-rich facies (W61, W62) consist of red brown/beige and white radiating spherultic rhyolite containing lithophysae (15 %), plagioclase (~ 20%) and traces of hornblende, orthopyroxene, opaques, and augite (**Figure 6.16**). Plagioclase typically occurs as glomerocrysts. A number of crystals in one of the samples are red/limonite-stained. The third sample (W63) has bands of orange spherulite within a grey groundmass, and is crystal-poor (3%), dominated by plagioclase,

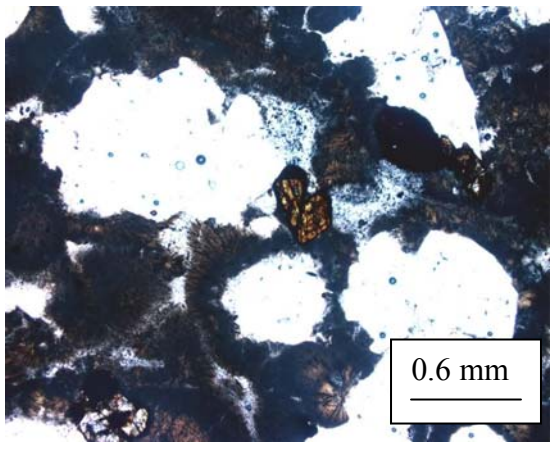

Figure 6.16 Photomicrograph of spherultic rhyolite lithic, Kinloch (plane-polarised light).

and pyroxene. The ex situ rhyolite (W64) is a clear, perlitic lava showing obvious flow texture and has a moderate crystal component (16.7%) consisting of plagioclase (mostly glomerocrysts), quartz, and traces of hornblende, orthopyroxene, opaques, and augite (**Figure 6.17**). One irregular plagioclase lath-rich dark scoria lithic (7.1 mm) is present in one of the thin sections.

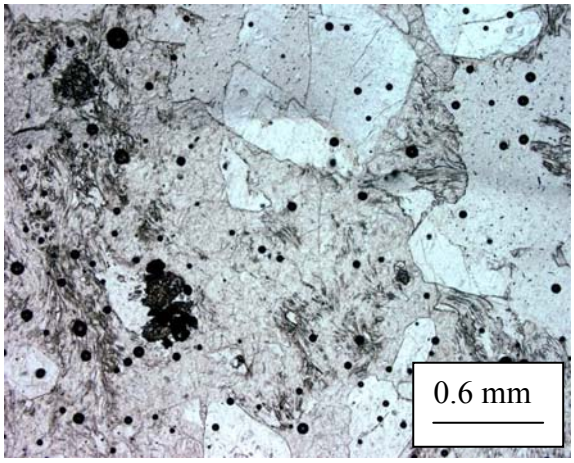

Figure 6.17 Photomicrograph of perlitic rhyolite, Kinloch (plane-polarised light).

Thin sections of several tuffs in the alternating facies revealed that thin (mm-thick), finer-grained bands within the beds are actually free of basalt (that is, phreatic; **Figure 6.18**). W54 and W59 contain fragments of an unidentified yellow lithic (1.5 mm), pumice (1.1 mm) in a felsic crystal- and glass-rich matrix. In W57 the fine-grained section is a mottled, crystal-rich band that is free of larger, identifiable clasts.

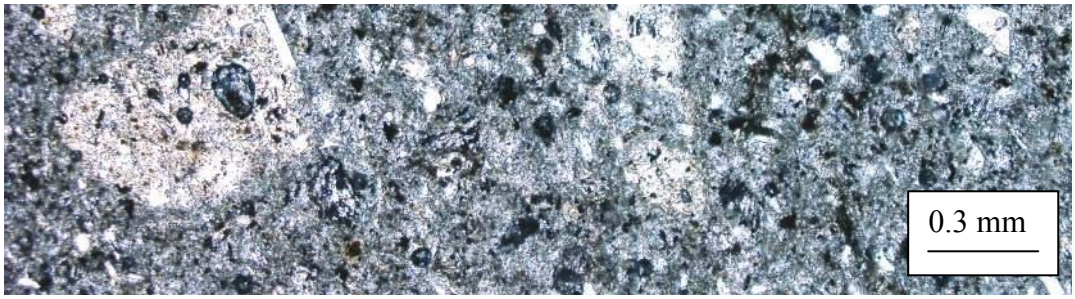

Figure 6.18 Photomicrograph of basalt-free (phreatic) band in alternating fine ash and coarse ash-lapilli facies (plane-polarised light). Larger clasts are light beige lithics and pumice, set within a crystal-rich matrix.

6.6 Interpretation

6.6.1 Facies

1) Alternating fine ash and coarse ash-lapilli facies

   This lower facies, which comprises the majority of the deposit, is inferred to result primarily from base surges. The darker,coarser ash-lapilli beds within this facies, which initially resemble fall deposits, (such as is the

case in Németh and White 2009) are often erosional, causing U-shaped channels and exhibit cross-bedding that indicate tractional emplacement, along with near-vent deposition (Sheridan and Wohletz 1983; Brand and White 2007). Given the relatively coarse, clast-supported fabric and moderate sorting of the majority of samples, a relatively dry base surge is inferred (Allen *et al.* 1996). Sideromelane, although present, is also rare, supporting a dry base surge origin. The first unconsolidated layer, however, which has a much higher juvenile content, is well sorted, lacks erosional structures and forms a laterally continuous and consistently-thick layer, is more likely to be a water-poor fall deposit (Brand and White 2007; Houghton and Gonnermann 2008). It also is poor in aggregate material, which seems to be more abundant in wetter samples. Interestingly, however, it also has one of the highest sideromelane:scoria ratios of the lower beds, similar to the vesiculated tuff (W54). The layer beneath the fall deposit exhibits flame structures, indicating that this layer was saturated with water, and that the fall was deposited while the bed was unconsolidated (Brand and Clarke 2009). The vesiculated texture of the fine-grained tuffs indicates that these base surges were at least moist when deposited (e.g. Frazzetta *et al.* 1983; Sheridan and Wohletz 1983; Brand and Clarke 2009), and the stretched form of the vesicles, parallel to flow, makes it likely that the surge deposits were soon covered by rapidly-sedimented currents. The diffuse bedding in an otherwise massive deposit is suggestive of internal shearing within a highly-concentrated base surge (Cas and Wright 1987). Slight variations in grain size within the tuffs reflect either slight variations in water (and hence effectiveness of fragmentation) and/or energy fluctuations of the pulse creating the surge. Internal grading is rare, which indicates that eruption conditions were steady (Jurado-Chichay and Walker 2001).

The increased thickness of coarse- and fine-grained units with height indicates longer periods of stable conditions and/or a greater magma discharge rate. Finer-grained horizons of W54, W57 and W59 are free of perceptible juvenile basalt are suggestive of phreatomagmatic phases where country rock was preferentially fragmented, almost to the point of

being phreatic (Sheridan and Wohletz 1983; Petrinovic and Colombo Piñol 2006).

2) Lapilli-, bomb- and block-rich facies

The open framework of these beds, lacking any sedimentary structures, indicates that this facies is a fall deposit (Sohn and Chough 1989; Allen *et al.* 1996; Brand and White 2007; Gençalioğlu-Kuşcu *et al.* 2007). The coarse nature of the material suggests that they were ballistics, and therefore that the site is proximal to the vent (Valentine and Gregg 2008). The lack of clast flattening or welding indicates that the material was relatively cold before contact with the ground (Carracedo Sánchez *et al.* 2009). The dark colour, in conjunction with the clast size, is typical of a more magma-rich eruption phase (Allen *et al.* 1996), although there are several features of the deposit that together point to the involvement of at least some water during the eruption of this facies. The sorting (1.88 σ_Φ) is poorer than to be expected for the coarse grain size, although the distribution plot still shows a basically unimodal distribution, and it fits within the strombolian field of Houghton and Gonnermann (2008 – see **Figure 6.10**). The low vesicularity lapilli within the bomb facies can signify either significant degassing or fragmentation induced by interaction with water (Houghton and Wilson 1989). The vesicularity values are remarkably homogeneous, without the variability that is thought to typify products of phreatomagmatic eruptions (Houghton and Wilson 1989), and close inspection of the clasts often revealed many smaller, spherical vesicles, which may support a degassing theory. The presence of lithic blocks are stronger indications of water involvement, but could merely be a sign of weak conduit wall (Carey *et al.* 2007). The strongest evidence for the interaction of magma with water is the presence in thin section of the quench textures evident on the plagioclase laths and olivine phenocrysts (although these could be caused by rhyolite – see **6.6.4**), and rare sideromelane (Fisher and Schmincke 1984; Shelley 1993). Cognate lithics in the juvenile clasts suggest that small volumes of magma that had cooled and crystallised in the chamber were ripped from the walls by rapid ascent of fresh magma. Given the homogeneous vesicularity of the basalt, it is likely that the ascending magma at this time represented a fresh

supply. The lack of bedding sags or soft deformation in the underlying fine-grained base surge and the resorbed tabular plagioclase (Mangan *et al.* 2009) may support a period of quiescence prior to the formation of this facies. The morphology of the grains is mixed, with coarser fractions being spheroidal and dense with breadcrust textures, and the 1 Φ fraction being dominated by angular, ragged scoriaceous grains with hydrothermal coating. In hand specimen, the bombs appear to be rich in pumice inclusions, which in thin section is found to be accompanied by beige crystalline lithics. The irregular boundaries of the pumice and other lithic material suggest that they have an intimate relationship with the basalt. The finding of one of the spherical basalt lapilli within the rhyolite lava also indicates a close eruptive relationship (see **6.6.4**).

3) Lapilli-rich facies

The interpretation of this facies is hindered by the fact that only distal observation was possible, but it is evident that the beds within this facies represent a type of reversion to conditions that existed for the alternating facies, in that they appear to be matrix-rich and have channelised geometries that point to a confined, base surge origin (Sohn and Chough 1989; Allen *et al.* 1996). The distinguishing feature of this facies is the much larger, average lapilli grain size, which may suggest that this stage of the eruption was more energetic (Houghton and Gonnermann 2008). The inferred phreatomagmatic nature of the deposit is slightly at odds with the lapilli-rich nature of the beds, given that theory dictates that an increase in water (up to a point) should result in more efficient (finer) fragmentation (Büttner *et al.* 1999), although coarser-grained facies have been described at near-vent locations (e.g. Sohn and Chough 1989). Without closer inspection of the beds and identification of the larger constituents, inferring the underlying processes is speculative at best. One possible scenario is that the larger clasts are accessory lithics from the bomb facies that have been dragged up with the eruption mixture.

4) Poorly sorted facies

The very poorly sorted, matrix-rich nature of the facies strongly indicates that it is a mass-emplaced unit. The appearance of rounded cobbles suggests that it was a debris flow. The very different nature of the deposit,

with no visible juvenile basalt components, indicates that the facies is not related to the eruption, and likely originates from another source. There are, however, clasts of the hydrothermally-altered Oruanui ignimbrite fragments in the unit, which are also presumed to occur in a higher section of the lapilli-rich facies. As mentioned previously, given the inferred maximum age of the Kinloch tuff deposit at ~ 9.5 ky cal. B.P., a debris flow resulting from a breakout flood, possibly that following the Waimihia eruption (Manville *et al.* 2007), is proposed.

6.6.2 Role of External Water

The Kinloch tuff deposit is rife with evidence of water being involved in all stages of the eruption. Explosive interaction of magma with water is inferred to be responsible for the production of the base surges, which comprise the majority of the deposit. This is evidenced by the presence of sideromelane, sedimentary and soft deformation structures, moderate to poor sorting and relatively high lithic values. The initial fall deposit also involved a small volume of water, as indicated by the presence of sideromelane, although the low lithic contents in W51 are more consistent with magmatic fragmentation (Fisher and Schmincke 1984; Cas and Wright 1987).

In the case of the initial bomb layer of the lapilli-, bomb- and block-rich facies , establishing the role of water is more complicated, as the layer exhibits a range of characteristics that are associated with both 'dry' and 'wet' eruptions. The coarse average grain size, ragged vesicular finer clasts, spherical bombs and lack of matrix or sedimentary structures more closely represent drier eruptions (e.g. Houghton and Wilson 1989; Allen *et al.* 1996; White 2000), whilst the low vesicularity, poor sorting, quench textures, presence of sideromelane and significant lithic component imply interaction with water (e.g. Houghton *et al.* 1999). Given the strong evidence for sudden quenching of the basalt, it is most likely that water was present, although the role (active/passive) or volume of this water is uncertain. The mix of the finer-grained scoriaceous clasts and denser, rounded coarser-grained clasts indicates that the layer is comprised of two sub-populations, which originated in different circumstances (similar to that described by Miyabuchi *et al.* 2006). The low amount of sideromelane, at least, points to a

low interactive magma:water ratio. The minerals' quench textures found in the bombs could be due to quenching from contact with cold rhyolite lava. Such a situation has been proposed to explain the round bombs from the Rotomahana (Tarawera) eruption of 1886 (Rosseel *et al.* 2006).

6.6.3 Source of External Water

The vent for the eruption at Kinloch is likely to have been very close to the deposit, but the lack of outcrop (and accessible outcrop) prevents the estimation of a vent location. (The direction of the stretched vesicles in one of the tuffs though, if indicative of flow direction, constrains the vent position to either north or south of the deposit.) The deposit is situated very close to the lake, and this is likely to be the same shoreline as at the time of eruption (see **2.3**). The presence of fluvial deposits close by to the site, although likely to be younger than the tuff, also renders river water as a possibility. The source of water could therefore either be surface water or groundwater. It should be noted that this discussion is restricted to the beds up to and including the first bomb layer, as data were not able to be collected from higher up in the stratigraphy.

Evidence for interaction with surface water is minimal. The inference of a lake source is compatible with the ongoing interactive role that water had during the eruption and the lava balls in the bomb layer, which share similarities with submarine pillow lavas (e.g. Palankis *et al.* 2008). The rare occurrence of green, glassy juveniles could also indicate some interaction with lake water (see **4.7.4**). The change to a more magmatic eruptive unit could be due to emergence of a subaqueous eruption, with the following units representing breaching and influx of water into the newly-formed volcanic construct (Kokelaar 1986). The flame structures in the basal unit, however, indicates the presence of very shallow water (Brand and White 2007; Brand and Clarke 2009).

There is stronger evidence for interaction with groundwater. The dominance of scoria over sideromelane clasts implies that only a small proportion of the magma was rapidly quenched by water prior to cooling and crystallisation could take place (Fisher and Schmincke 1984). The relatively high lithic component, which is known to be very high for subsurface eruptions like that which form maars (e.g. Cas and Wright 1987) and has been associated with other groundwater eruptions

(Carey *et al.* 2007), increases the likelihood of groundwater being involved. There is a dominance of spherulitic rhyolite throughout the deposit, which is to be expected given the ubiquity of the spherulitic Haparangi rhyolites in the area. An abundance of one lithic type can simply reflect weakness of the conduit wall rock (Carey *et al.* 2007). This could be the case here, given that the site shows strong evidence of hydrothermal alteration, but the rhyolite samples show no sign of any alteration, so a weak conduit wall is considered to be unlikely, although it is possible that faults have weakened the rhyolite.

If groundwater is indeed the water supply, there are two possible sources: local spherulitic rhyolite (referred to as either Whakaroa-like Rhyolite, or by the more generic term of Haparangi Rhyolite – Sutton *et al.* 1995) and the Whangamata Fault. As mentioned in **2.3**, Whakaroa-like rhyolite around Kinloch has recently been found to have a high fracture-dependent permeability, whereas the Whangamata Fault, in close proximity to the deposit (and likely pathway for the basalt to reach the surface), also has a high water flow. Due to the fact that spherulitic rhyolite is ubiquitous in the field area, there is no way to determine whether the external water came from the rhyolite itself or from the fault within/beside the rhyolite.

6.6.4 Association with Rhyolite

There are two features of the Kinloch tuff deposit that point to an intimate syn-eruptive association with a silicic source: basalt scoria and sub-spherical lapilli and bombs containing pumice inclusions with ragged boundaries and perlitic rhyolite lava containing basalt lapilli. The pumice and unidentified beige lithic inclusions within the basalt, which are identified at several levels in the deposit, could simply be lithics that have been absorbed by ascending magma, and even the ragged boundaries of the inclusions could simply point to melting due to the temperature of the magma at depth (prior to quenching by water). The finding of basalt within the ex situ rhyolite block, however, suggests a more intimate relationship. A possible explanation is that hot basaltic magma rose up through a rhyolite dome and caused partial melting and extrusion of the rhyolite. It seems likely that this rhyolite was responsible in some way for the lava balls and the quench textures found within the lava balls could be due to contact with the

rhyolite (Streck and Grunder 1999; Rosseel *et al.* 2006). Mixing of basalt and rhyolite in the Rattlesnake Tuff of Oregon resulted in ubiquitous quench textures in the phenocrysts of basalt inclusions (Streck and Grunder 1999). A reason for choosing an internal, limited melting is the fact that there is no obvious rhyolite lava outcrop visible at the field site. If the basalt had triggered a full rhyolite eruption, then a significant volume of rhyolite would be expected (although it is possible that this rhyolite is hidden). The angular nature of the rhyolite blocks in the bomb layer also suggests that melting was not widespread. The relationship of the rhyolite to the basalt is discussed further in **Chapter Eight/Geochemistry**.

6.6.5 Eruption Phases

It is inferred that the basaltic eruption at Kinloch consisted of at least three eruption phases: one phreatomagmatic phase, one dominantly magmatic phase and one mostly-phreatomagmatic phase. The initial phase involved interaction of magma with a significant volume of water, resulting in relatively wet and dry base surges. Eruption conditions were relatively constant, but magma discharge rate increased during this phase, as the eruption grew in intensity, leading to thicker surge units. This was followed by a dominantly magmatic phase, possibly following a period of quiescence, where magma supply rate overwhelmed any water present, resulting in ballistic fall. The last (certain) phase of the eruption consisted of several thick, dilute base surges, interrupted by a much smaller ballistic unit. The dominance of dilute wet surges reflects a waning of magma supply.

7 *Punatekahi*

Punatekahi is a scoria cone complex that has been quarried for at least 20 years. There are two cones exposed in the quarry: a larger, northern scoria cone that dominates the western sector of the quarry (Punatekahi A), and a much smaller cone to the south-east (Punatekahi B) (**Figure 7.1**). Since the study of Brown (1990), the depth of the quarry has increased by 20 m to ~ 60 m. The lower contact of the scoria cone is not visible, but is inferred to be with the Huka Formation (~ 300-27 ky cal. B.P.; Henley and Stewart 1983; Manville *et al.* 2007), which underlies the other K-Trig volcanoes to the south-west (Brown 1990). Atop Punatekahi A lie numerous tephra layers that have been identified by Brown (1990). The oldest tephra is the Tihoi tephra (~ 45 ky cal. B. P.), which sits directly above a paleosol formed on scoria, thereby constraining the age of Punatekahi between ~45-300 ky. As noted by Brown (1990), this is consistent with the K-Ar date of 140 ky (Stipp 1968).

7.1 Site and Facies Description

The southern half of Punatekahi cone is dominated by orange to red brown scoria, which forms packets of steeply-dipping (~ 30°) reversely graded, coarse ash-lapilli beds. The coarser fractions are often covered in a white coating. The beds originate from both western and eastern directions, forming a concave pattern where they interlock. The interlocking of these beds marks the surface boundary between Punatekahi A and Punatekahi B. To the east, the beds of Punatekahi B cut off thinner, lower beds, and are gradually replaced by a ~ 8 m-thick domed, massive/crudely-bedded purple scoria lapilli and bomb unit. This lapilli and bomb unit overlies two closely-spaced grey welded beds with regular vertical jointing and is adjacent to a mass of grey lava. The lava appears to occupy the internal part of the Punatekahi B cone, and extends north to the quarry track. The western set of beds (Punatekahi A) shallow to the north-west. Here, as with Punatekahi B, the change in bed dips is associated with a dome-shaped, massive, poorly-sorted, non-welded bomb-rich unit, with bombs up to 1.5 m across. Interbedded with these layers, at various levels, are 1 m-thick grey beds, which are welded and show clear vertical fractures. These beds are mostly sub-horizontal, but in places change to a strong vertical dip, possibly due to slumping. The northern sector also contains a sub-horizontal yellow-brown ash layer, visible laterally over only a few metres.

At three-quarters of the total height above the quarry floor, the southern part of the Punatekahi A cone changes markedly from an orange-red to a purple scoria deposit across a wavy unconformity (**Figure 7.2**).

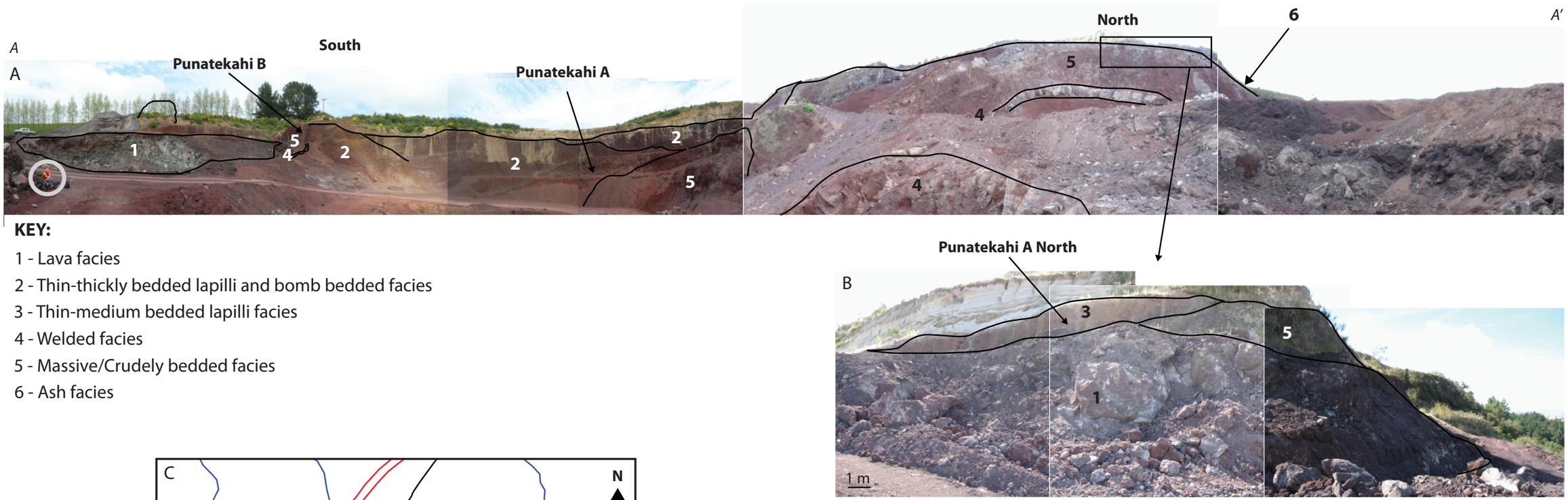

KEY:

1 - Lava facies
2 - Thin-thickly bedded lapilli and bomb bedded facies
3 - Thin-medium bedded lapilli facies
4 - Welded facies
5 - Massive/Crudely bedded facies
6 - Ash facies

Figure 7.1 Topographic and photographic maps of Punatekahi. **A**) Photomap showing distribution of facies described in text. **B**) Photomap of northernmost outcrop. **C**) Topographic map showing location of Punatekahi. Lilac shows official quarry area. **D**) Map of quarry, showing sites of stratitraphic logs and site from which photomap **A** is taken (looking south). (Maps **C** and **D** modified from NZMS260 U18, Brown 1990 and Brown *et al.* 1994.)

Figure 7.2 Angular unconformity between red scoria and purple scoria, Punatekahi A. Note change in bedding dip and disappearance of white coating above unconformity. Hammer for scale.

There is a slight increase in bed angle (8º), and the white coating disappears. This purple unit, which darkens toward the top of the cone construct, appears to extend further northwards, but has been severely affected by post-depositional faulting and/or erosion; this is evidenced by vertical contacts between the scoria and the overlying tephrostratigraphy. The northernmost part of the Punatekahi A cone is capped by several small multi-coloured, medium scoria beds that overlie a dark, partially-welded, lapilli unit. Associated with this unit is a small mass of light welded lava. Although there is a clear thickening of scoria to the north-west of the quarry, there are no visible outcrops to the west of the summit, and a pit dug into the slope reveals only post-Punatekahi tephra. This absence of scoria to the west suggests the presence of a splay fault off the Kaiapo Fault, trending north-north-east. Three stratigraphic logs were constructed at Punatekahi: (1) the massive/crudely-bedded construct at Punatekahi B (**Figure 7.3**); (2) along the southwestern quarry face ('Punatekahi A' – **Figure 7.4**); and (3) in the northernmost exposure ('Punatekahi A North' - **Figure 7.5**). The two cones at Punatekahi are comprised of the following six facies (**Figure 7.1**):-

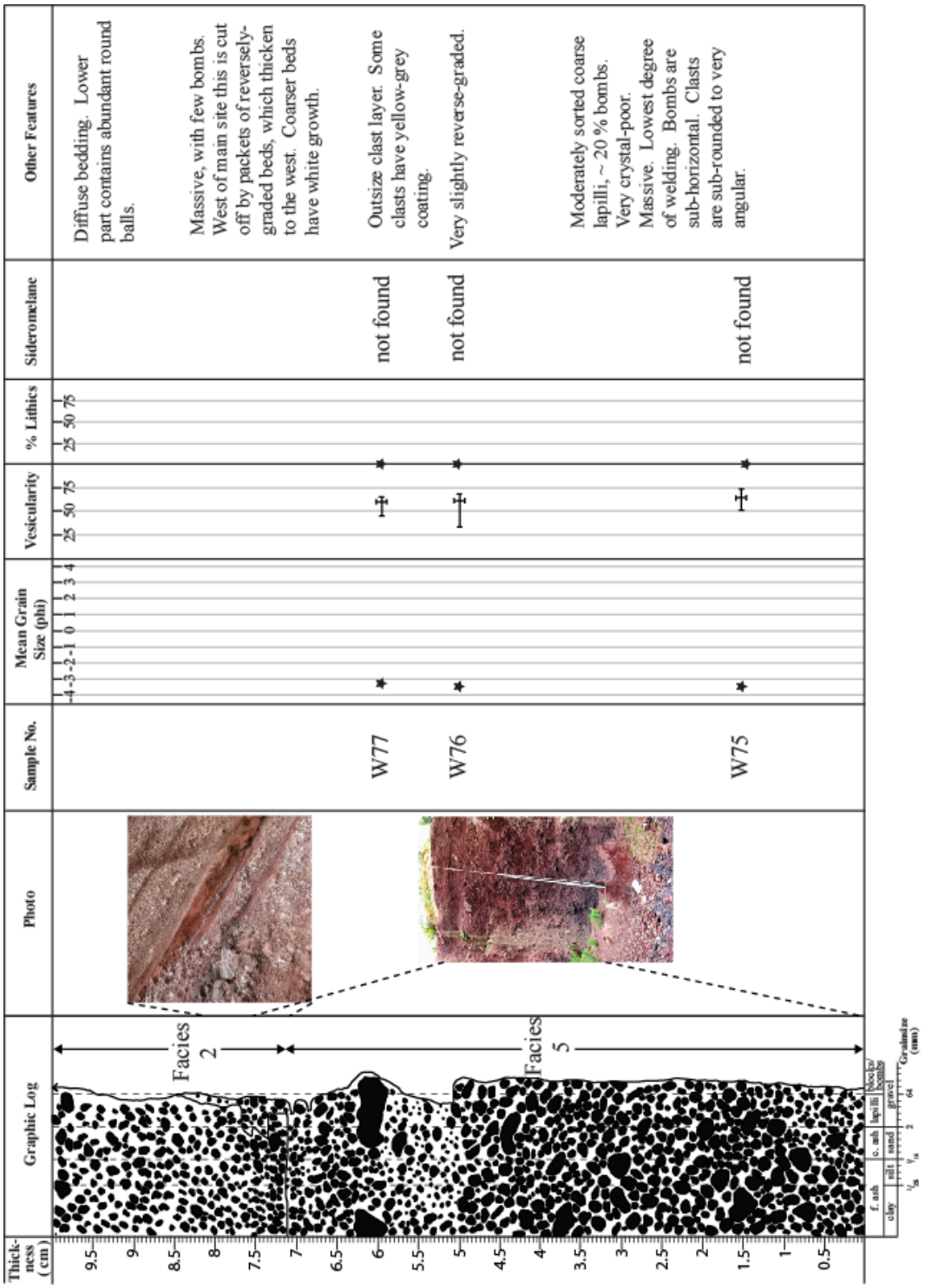

Figure 7.3 Stratigraphic log and data for Punatekahi B.

Punatekahi A

N6278428 E2773594

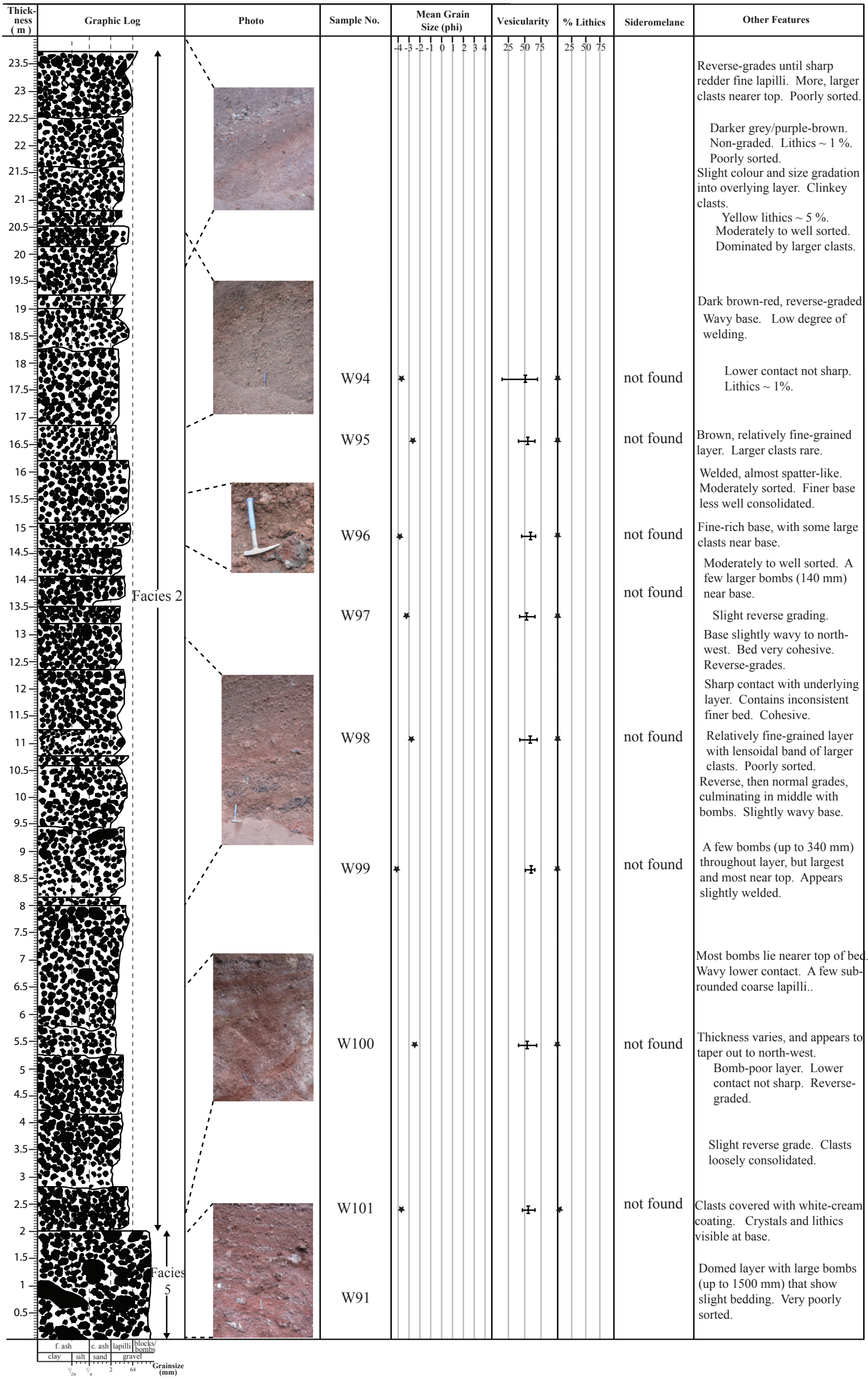

Figure 7.4 Stratigraphic log and data for Punatekahi A.

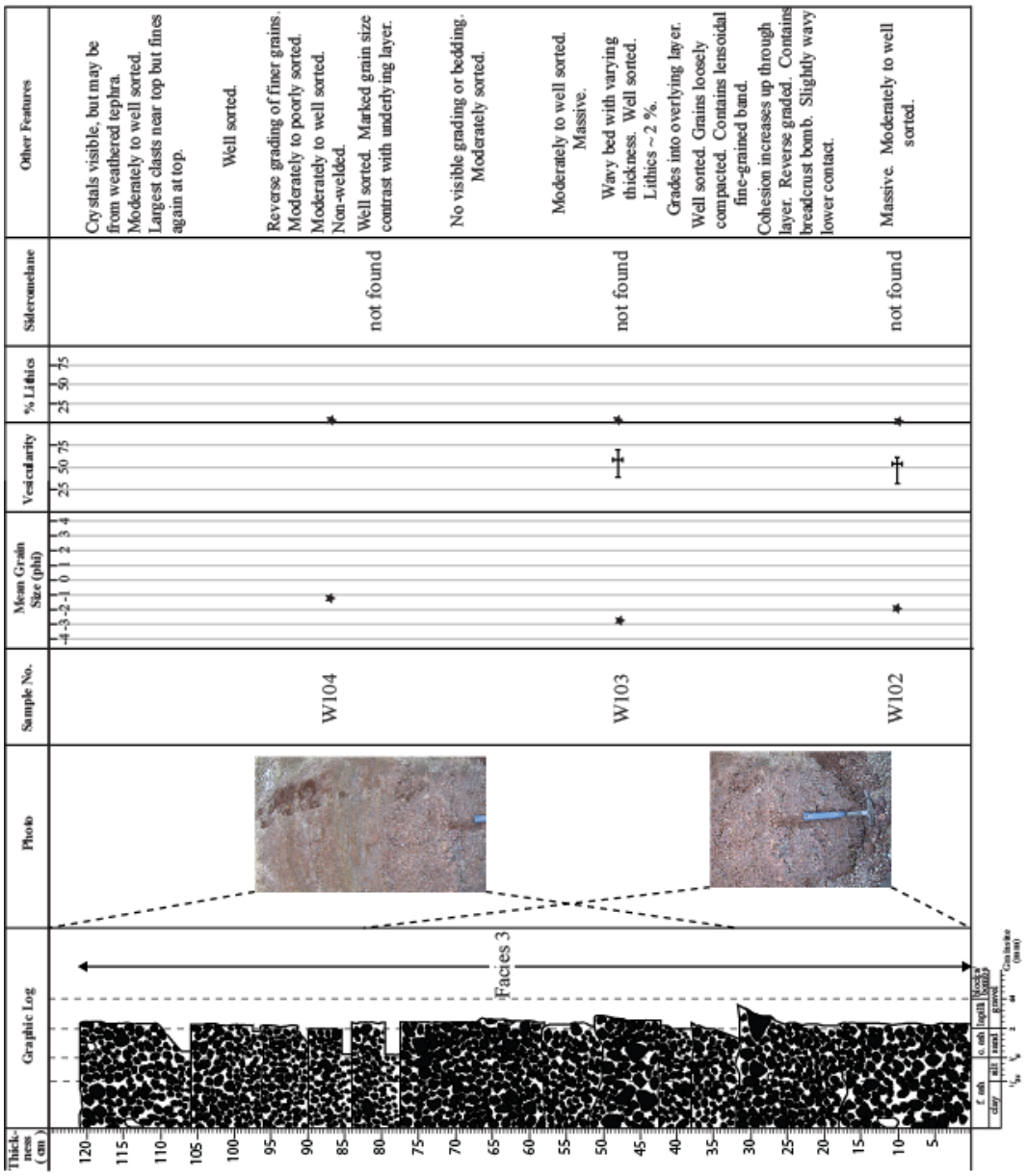

Figure 7.5 Stratigraphic log and data for Punatekahi A North.

1) Lava facies

This facies consists of grey, massive hard basalt rock containing visible phenocrysts of plagioclase and olivine. The lava at Punatekahi B has a flat top to the east, but slopes to the west. The western exposure reveals a rubbly a'a top section, the clinkery blocks of which appear sub-horizontal to the north, but further south suggest a dip to the west (**Figure 7.6**). Its total thickness is as of yet unknown, but its exposed thickness is ~ 5 m, and drilling has revealed a further 13 m in the southern sector (G. Seay pers. comm. 2009). In the northern part, where it meets a quarry track, the lava is sharply abutted against red scoria. This scoria produces a vertical contact with the lava to the

south. This lava originally joined up with the eastern-most jointed welded unit that is associated with Punatekahi A (G. Seay pers. comm. 2009). There is a much smaller lava facies at Punatekahi A, where a ~ 10 m-long section is exposed, with an approximate thickness of ~ 3 m.

2) Medium-thickly bedded lapilli and bomb facies

This facies consists of multiple thin-thick beds of red or purple scoria lapilli that typically exhibit reverse grading from very thin basal horizons of red coarse ash and are internally massive. Bombs account for ≤ 20% of a bed, but in one horizon they reach up to 30%, with clasts looking more fragmented (**Figure 7.4**). Beds tend to dip at the angle of repose (~ 30º), but dips shallow closer to the crudely bedded facies. Beds are non-welded, although clasts are tightly packed, and are poorly to well sorted.. Lithic clasts are very rare (< 1%), and are represented by small fragments of cream indurated ash. The juvenile scoria are moderately to highly vesicular, and generally have a ragged morphology. Bombs with broken, angular faces reveal a black interior, and lava slabs are common. A significant number of scoria within specific areas in the lower part of the cone exhibit a white-cream crystalline or powdery coating of crystobalite and/or tridymite (**Appendix D**).

Figure 7.6 Lava facies, Punatekahi B. Notebook for scale is 17 cm long.

3) Thin-medium bedded lapilli facies

This facies is made up of a series of non-welded thin-medium beds containing moderately to well sorted red, purple, brown and yellow scoria lapilli. In contrast with the other lapilli facies, the clasts are noticeably blocky, and bombs, displaying a more ragged morphology, are rare (~ 1%). The facies could be a scoria flow deposit, because it contains wavy beds which pinch and swell. Beds tend to be slightly reversely graded. Due to the multicoloured nature of the scoria, identifying lithics is problematic, although a small proportion of pale yellow material (<1% of the deposit), appearing slightly different to the golden altered juvenile lapilli, is considered to be lithic. Dips are variable, but relatively gentle.

4) Welded facies

This facies is represented by light grey to red indurated rock that forms m-thick beds at various levels in the quarry. Welded facies beds are conformable with underlying contours and show regular vertical jointing. At a distance these beds have the appearance of lava. Closer inspection reveals a melding of rubbly lava bombs and clasts, reminiscent of clinkery a'a lava (**Figure 7.7**), and faint outline of clasts are sometimes visible (**Figure 7.8**).

Figure 7.7 Welded facies, Puntekahi B.

Figure 7.8 Welded facies overlying crudely-bedded facies, northern end of Punatekahi A. Note outlines of clasts (indicated by arrows). Hammer for scale.

The rock is light, clinkery, and variably vesicular. No minerals are visible. In addition to the regular vertical jointing, whole blocks of this welded agglutinate are seen detached from the main beds, particularly where they cross the crudely-bedded facies. One of these units contains within it a jumbled layer of pale blocks and an indurated tubular mass of black juvenile material, possibly a dike (**Figure 7.9**).

Figure 7.9 Jumbled, dense black intrusion (circled) through welded facies, Punatekahi A.

5) Massive/crudely-bedded lapilli and bomb facies

This facies contains several thick-very thick beds of dark red-brown or black scoria lapilli and bombs. Lapilli are crystal-poor and highly vesicular. Bombs, which comprise ~20 % of the deposit, are mostly angular and have a sub-horizontal orientation, giving the appearance of crude internal bedding. Unbroken breadcrust bombs are rare, with lava slabs dominant (**Figure 7.10**). Broken bombs show a vesicular inner core, with a denser outer skin. An outsize layer near the top of the facies at Punatekahi B contains yellow-grey-coated scoria up to 20 cm in size. Some smaller bombs consist of scoria surrounding darker, rounded lava fragments. Grains are tightly compacted, and the face of the sections are stable.

Figure 7.10 Lava slabs and dense bombs occurring in crudely-bedded facies, Puntekahi A. Hammer for scale.

6) Ash facies

This facies forms a single medium bed of cohesive yet friable yellow ash near the top of Punatekahi A cone. The layer is massive and moderately sorted, containing clasts of purple scoria lapilli. An overall mantling geometry is observed, although thickness varies and the bed tapers out at either end of its ~ 6 m length. No visible grading occurs within the bed. The lower contact is with scoria that melds into agglutinate. The ash is overlain by a massive lapilli and bomb unit (**Figure 7.11**).

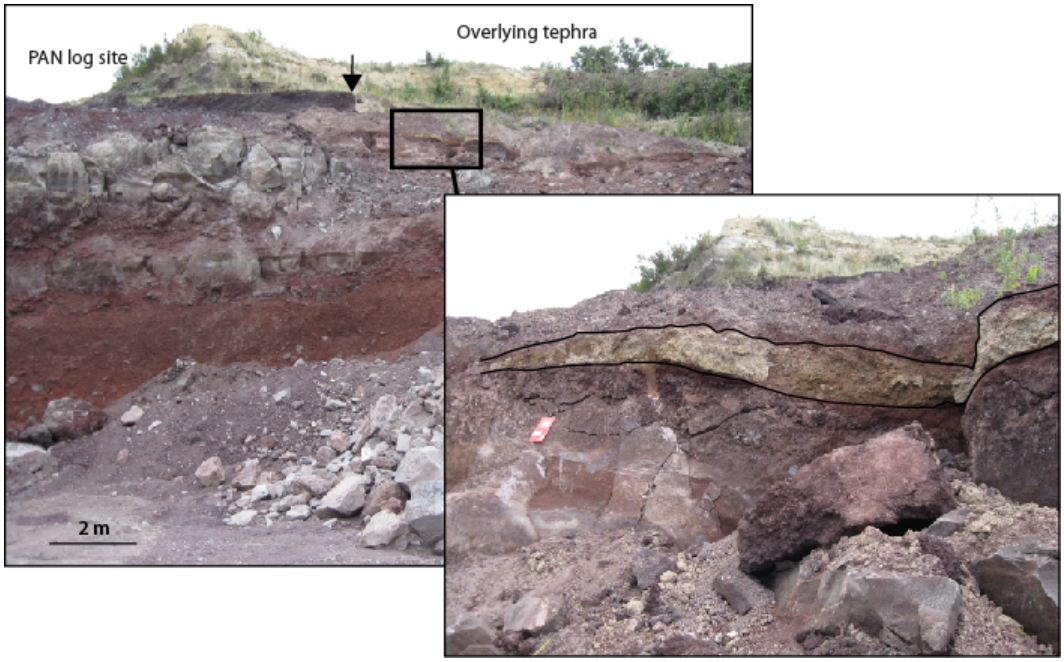

Figure 7.11 Ash facies at Punatekahi. Enlarged section shows tephra between black lines. Notebook is 17 cm long. Arrow in backset photo points to vertical contact between scoria and post-Punatekahi rhyolitic tephra.

7.2 Grain Size

Grain size analysis was undertaken on 18 samples (**Appendix B**): 15 from Punatekahi A, and three from Punatekahi B. The majority of samples come from logged sections, but four come from other sites at Punatekahi A, including the above-unconformity equivalent of W97 (W107), and W83, which possibly represents a dike location and has a strong smell of sulphur.

From the median diameter vs. sorting plot of the samples (**Figure 7.12**), it is clear that all of the samples occupy a small area of the graph, and there is a general association of finer median sizes with poorer sorting.

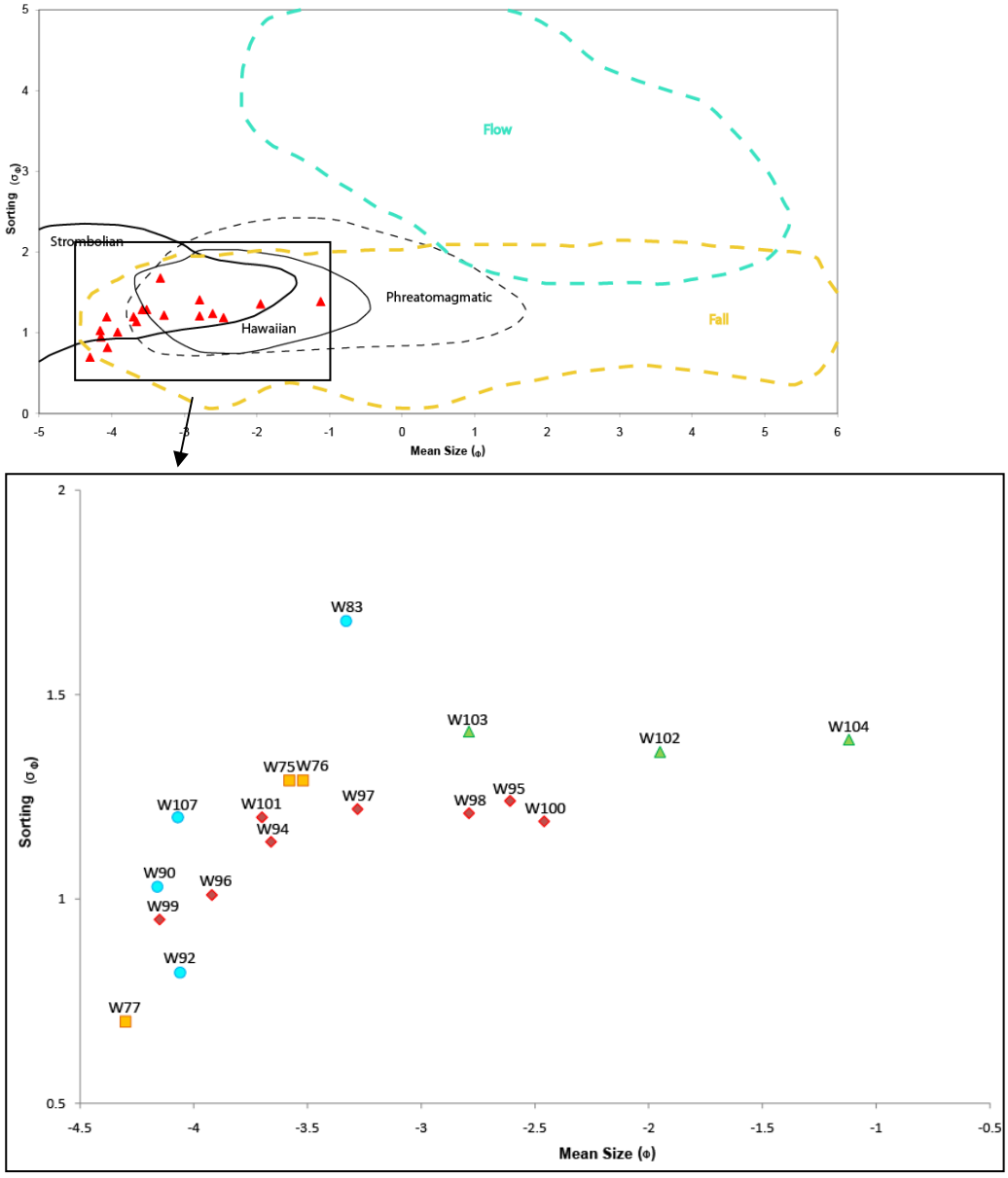

Figure 7.12 Median diameter vs. sorting plot for Punatekahi samples. Flow and fall fields from Walker (1973), eruption style fields from Houghton and Gonnermann (2008).

The samples that originate from the medium-thickly bedded lapilli and bomb facies of Punatekahi A are all well sorted, with W99 and W96 being slightly better sorted. Most of the samples have a strong coarse peak with unimodal distribution (**Figure 7.13**) as to be expected, but W97 and W101 are weakly bimodal (**Figure 7.14**). This weak bimodality for W97 contrasts with its above-unconformity equivalent (W107), which in all other respects is very similar to W97.

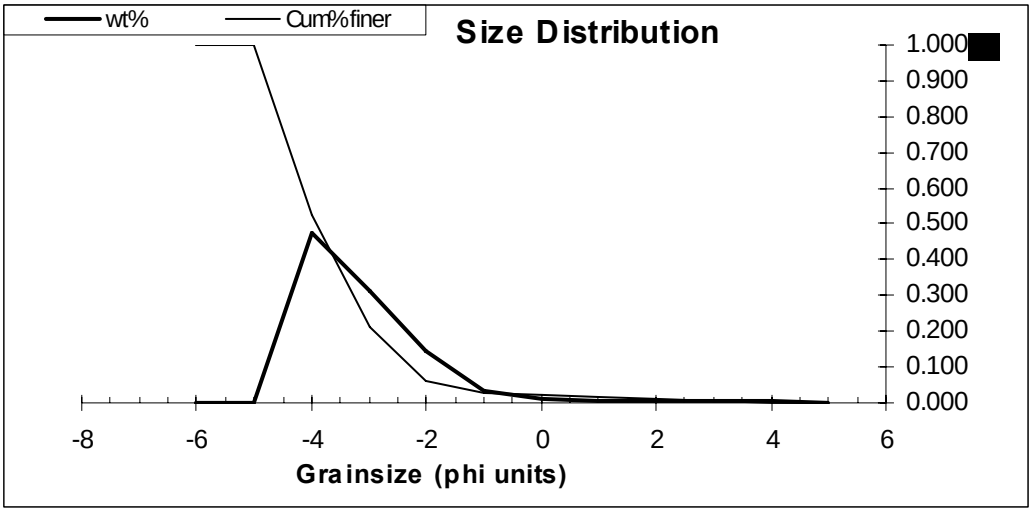

Figure 7.13 Grain size distribution plot for W96 (medium-thickly bedded lapilli and bomb facies).

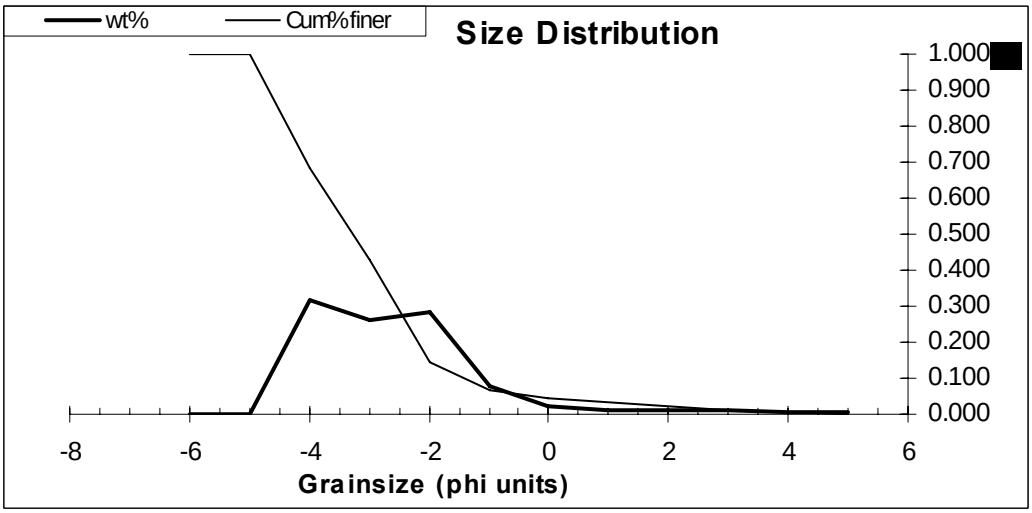

Figure 7.14 Grain size distribution plot for W97 (medium-thickly bedded lapilli and bomb facies.

Fluctuations in grain size are noticeable and random, with no clear trend in grain size with stratigraphic height. W95, W98 and W100 form a tight cluster of finer-grained beds, reflecting what was observed in the field. These beds are all strongly unimodal with positive skew (**Figure 7.15**).

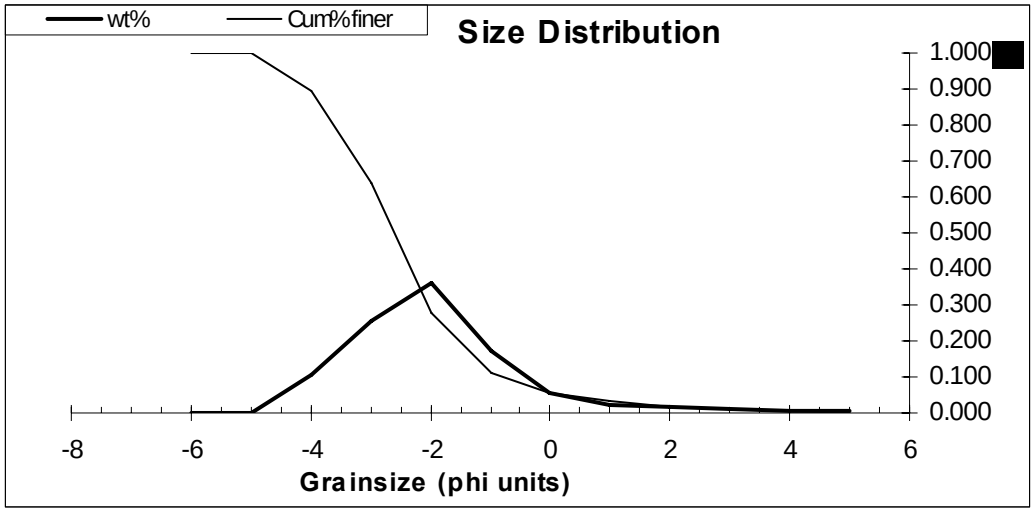

Figure 7.15 Grain size distribution plot for W95 (medium-thickly bedded lapilli and bomb facies).

For the massive/crudely-bedded lapilli and bomb facies samples of Punatekahi B (W75-W77), the two lower beds are nearly identical, but the higher unit (W77 – **Figure 7.16**) reveals a marked change to a much better sorted and coarser bed.

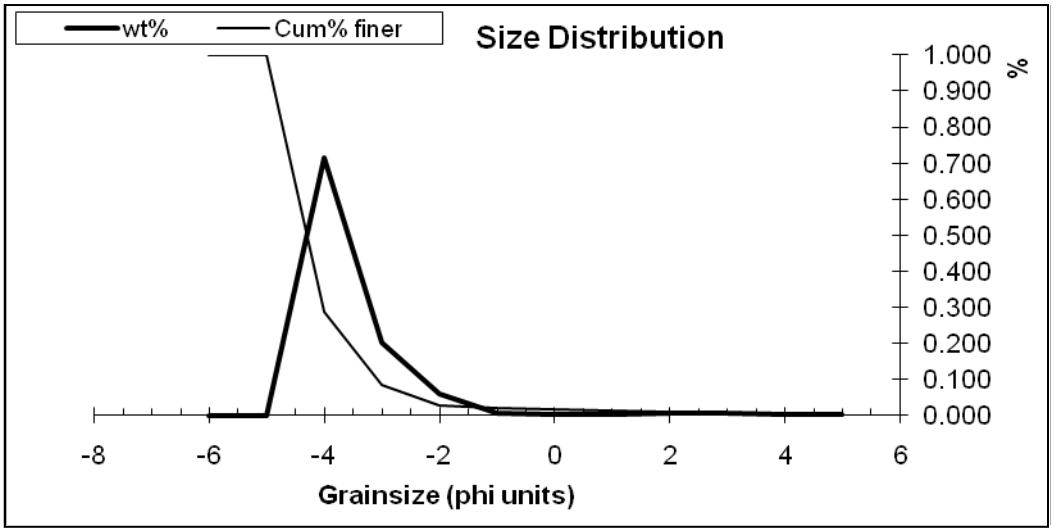

Figure 7.16 Grain size distribution plot for W77 (massive/crudely-bedded lapilli and bomb facies).

The thin-medium bedded lapilli facies samples are notable in that they constitute a separate group with poorer sorting and generally finer median clast diameters. Sorting between the three samples is remarkably similar, but there is a noticeable fluctuation in grain size.

All of the samples are unimodal, although both W103 and W104 (**Figure 7.17**) look almost bimodal.

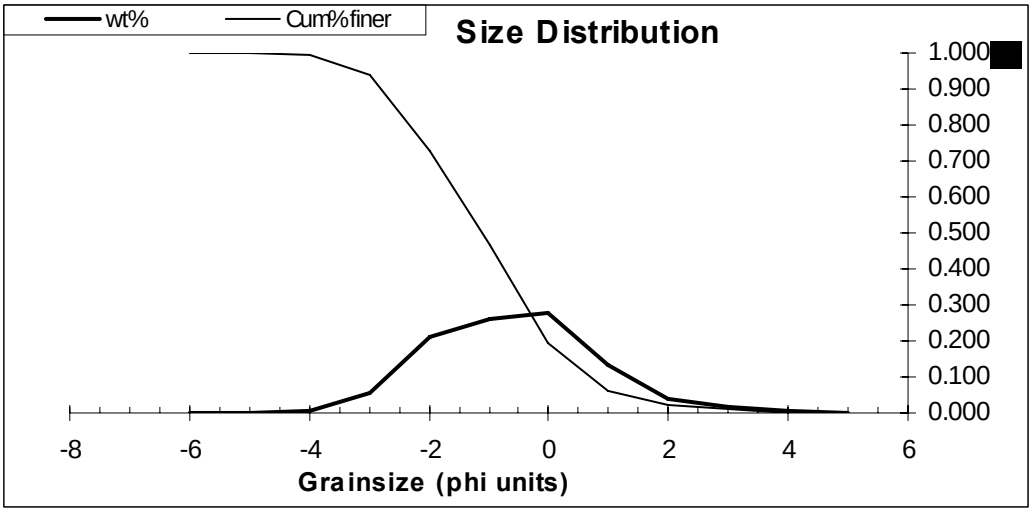

Figure 7.17 Grain size distribution plot for W104 (thin-medium bedded lapilli facies).

The other point of interest is that of W83, which has the poorest sorting of all 18 samples, yet still has a coarse median grain size. The size distribution plot for this unit (**Figure 7.18**) shows a clear decline in abundance of clasts with decreasing grain size, and a strong positive skew.

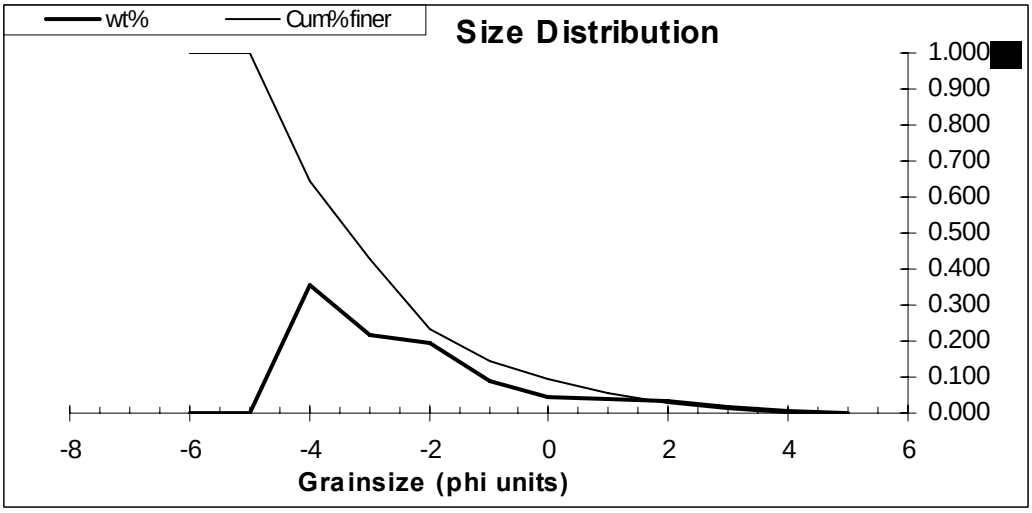

Figure 7.18 Grain size distribution plot for W83 (possible 'dike' in massive/crudely-bedded facis of Punatekahi A).

7.3 Vesicularity

Bulk vesicularity was measured for most samples for which grain size analysis was undertaken, with the exception of the uppermost sample from the thin-

medium bedded lapilli facies, which was too fine-grained. Results are shown in **Table 7.1** (also **Figures 7.3**, **7.4**, **7.5**, **Appendix** C).

Table 7.1 Bulk vesicularity values for Punatekahi scoria cones. Facies: 2 = medium-thickly bedded lapilli and bomb facies; 3 = thin-medium bedded lapilli facies; 5 = massive/crudely bedded lapilli and bomb facies. Samples W75-W77 are from Punatekahi B, W102-W103 are Punatekahi A North. The rest are from Punatekahi A.

Sample	Facies	Min.	Max.	Mean	Std. Dev.
W75	5	51.88	74.91	67.31	7.19
W76	5	31.87	71.49	60.51	11.86
W77	5	47.71	65.19	60.1	7.01
W83	5	46.54	65.75	56.2	7.18
W92	5	50.65	67.89	61.38	5.37
W90	5	44.72	71.21	59.96	8.57
W94	2	15.84	69.35	51.28	15.89
W95	2	39.43	64.23	55.35	8.03
W96	2	47.5	67.33	59.45	6.19
W97	2	38.64	65.05	52.97	9.04
W107	2	52.3	65.77	59.74	5.04
W98	2	41.8	71.29	58.77	8.65
W99	2	50.88	65.55	59.44	4.64
W100	2	38.66	69.9	53.78	8.87
W101	2	45.51	66.37	56.28	7.51
W102	3	31.24	60.64	53.02	9.22
W103	3	37.07	70.95	57.68	12.06

Clasts are incipiently to highly vesicular (Houghton and Wilson 1989). Mean vesicularity ranges from 51 to 67%, with standard deviations of 5-12%. The highest standard deviations are found for W76 and W94, where single dense clasts occur. W103, with the third highest deviation, differs in that it has several clasts of moderate vesicularity. Overall, the highest vesicularities are found at Punatekahi B cone (W75-W77), and the lowest are found at Punatekahi A North. No relationship between vesicularity and sorting was found.

7.4 Componentry and Clast Morphology

As to be expected for a scoria cone, all of the samples from both cones contain at least 97% juvenile material (**Table 7.2**), consisting of ragged fragments, fluidal spindle shapes and irregular blocky clasts, with smooth or rubbly surfaces.

Table 7.2 Componentry values (%) for Punatekahi cones in approximate stratigraphic order (using binocular microscope).

Sample	Juvenile	Crystal	Lithic
W75	>>99	<<1	0
W76	>>99	<<1	0
W77	>>99	<<1	0
W83	>>99	0	<<1
W92	100	0	0
W90	99	0	1
W94	>99	0	<1
W95	100	0	0
W96	100	0	0
W97	>>99	0	<<1
W107	100	0	0
W98	100	0	0
W99	100	0	0
W100	>>99	<<1	0
W101	97	1	2
W102	99	0	1
W103	98	0	2
W104	99	0	1

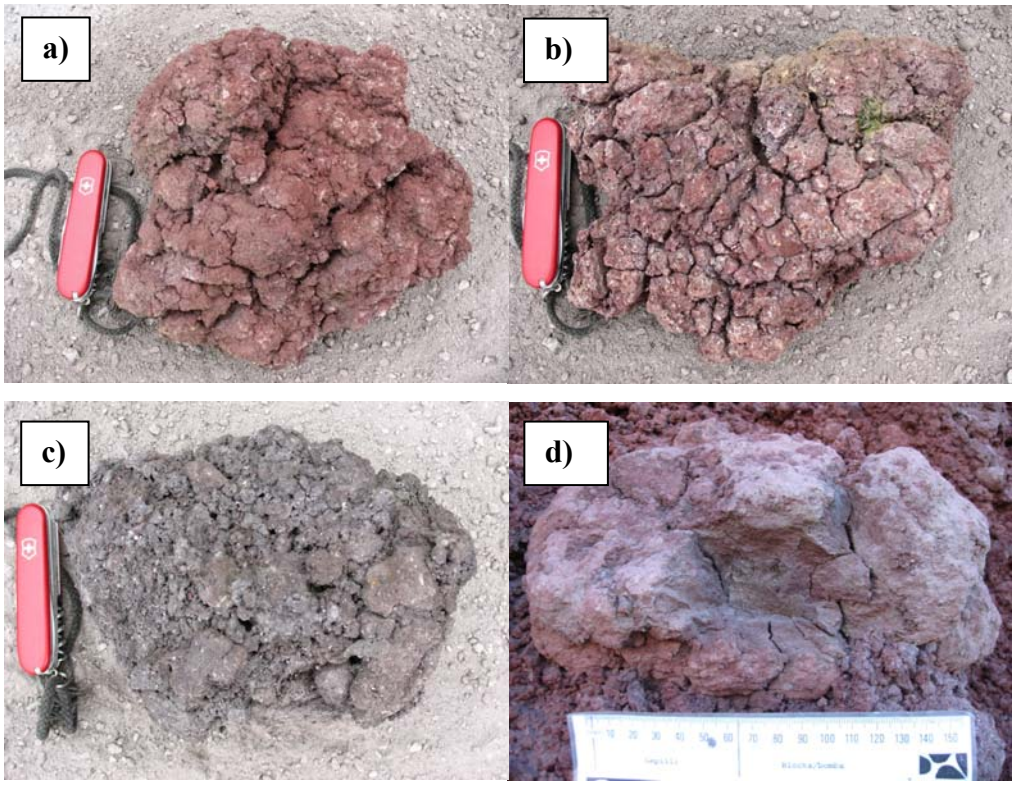

Figure 7.19 Range of bombs at Punatekahi: a) cauliflower-type bomb; b) breadcrust bomb; c) composite bomb; d) dense bomb. a) to c) are from Punatekahi B, d) is from Punatekahi A.

The range of morphologies visible in the 1Φ fraction are similar to that found in the bombs (**Figure 7.19**). The exceptions to this are the samples W94 and W95, where the lapilli are blocky and smooth, and the scoria from the thin-medium bedded lapilli facies (from Punatekahi A North), which, whilst still vesicular, are notable for both the variety in colour and dominantly blocky morphology.

7.4.1 Juvenile Clasts

The majority of juvenile clasts contain visible felsic and mafic crystals. Samples from Punatekahi B exhibit a pink or yellow coating, whilst a significant number of samples from Punatekahi A show a white powder or crystalline coating, as well as a yellow ash-like cover. The white coating and part of the outer layer of a sample from the thin-medium bedded lapilli facies were analysed using XRD (**Appendix D**) and both were found to be quartz polymorphs of cristobalite and/or tridymite. SEM images of scoria from W76, W83 and W104 reveal the differences between sites (**Figure 7.20**). Clasts from W76 are a mix of ragged, fluidal and blocky shapes (**Figure 7.20a-c**). Vesicles are clearly defined and spherical in the more ragged clasts, and smaller, oval vesicles occur in the blocky grains. W83 clasts, in comparison with W76, are vesicle-poor, with sharper, planar surfaces (**Figure 7.20d-f**). Close up, these surfaces appear to be smooth and ridged, although a significant number of surfaces are covered in a semi-crystalline coating, most likely the white coating seen in hand specimen. Scoriae from W104 are distinguishable from both W76 and W83 by being noticeably platy, with a soft, granular appearance (**Figure 7.20 g-h**). Vesicularity of these clasts is low.

7.4.2 Crystals

Crystals comprise a negligible fraction (< 1 %) of the deposit. Clear plagioclase is most common, but W76 also contains a speckled yellow-brown crystal, which could be olivine altered to iddingsite.

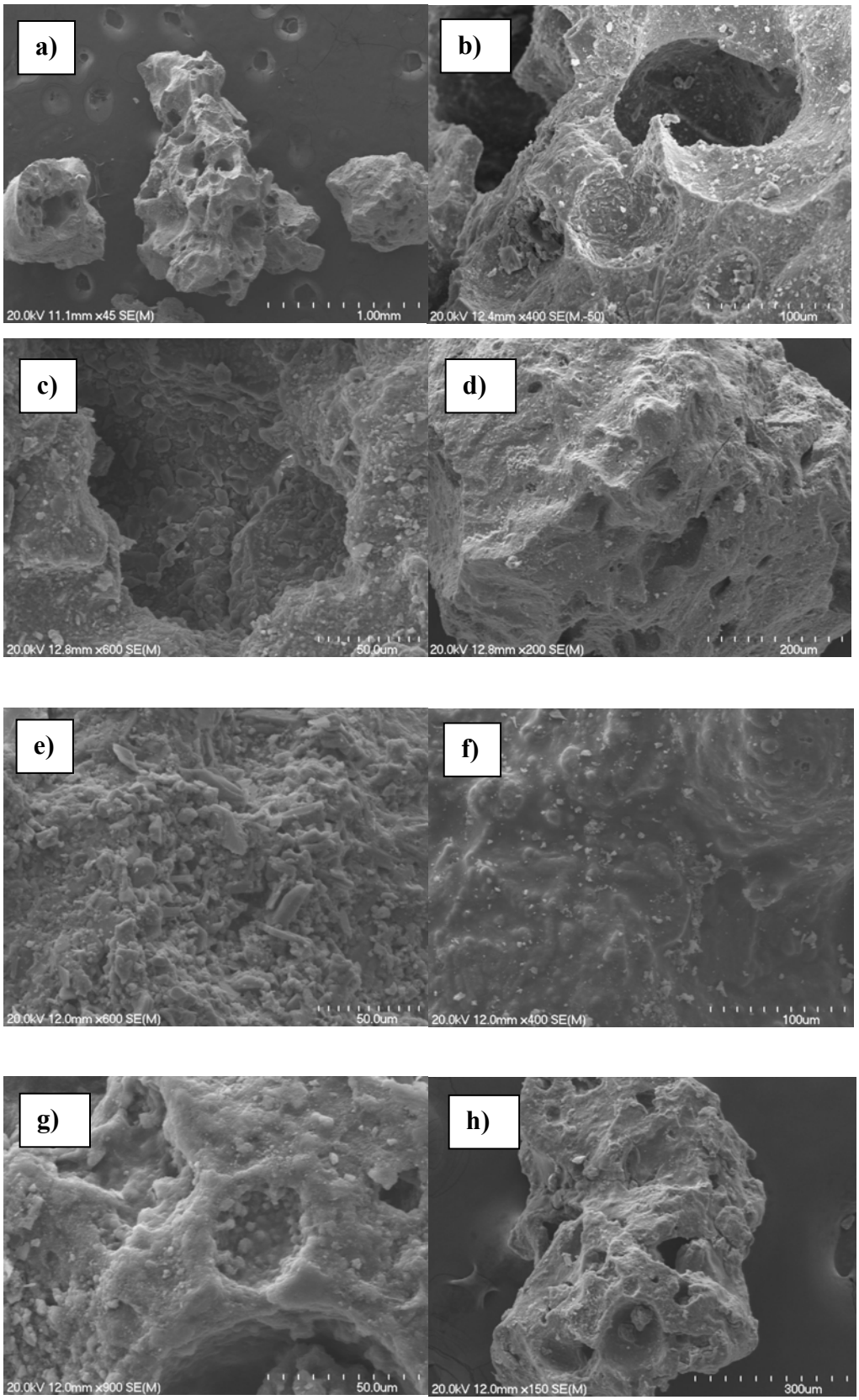

Figure 7.20 SEM images of scoriae from Punatekahi. a) range of morphologies seen in W76; b) ragged surface with spherical vesicles (W76); c) ragged vesicle outline (W76); d) blocky, vesicle-poor scoria (W83); e) granular texture of scoria (W83); f) ridged, vesicle-free surface (W83); g) thick-walled vesicles of relatively vesicle-poor scoria clast (W104); h) smooth, blocky and vesicular scoria clast (W104).

7.4.3 Lithic Clasts

The rare lithic component (< 2 modal %) consists of a yellow ash/ignimbrite containing crystals and lithics, creamy crystal-bearing pumice, and loose quartz polymorph growths. Lithics are dominantly restricted to the finer fractions, although rare, larger fragments, comparable in size to the juvenile scoria, are to be found in the lower, southern part of Punatekahi A cone.

7.5 Petrography

7.5.1 Juvenile Material

Analysis of lava and welded agglutinate reveals anhedral to subhedral, highly resorbed, polysynthetically twinned, rarely oscillatory zoned plagioclase (2.5 mm), anhedral to euhedral augite (0.9 mm), and rare anhedral to euhedral iddingsite-rimmed olivine (0.7 mm) set in a trachytic hyalopilitic groundmass. Two samples from the lava facies also appear to contain anhedral to euhedral Fe-Ti oxides (0.2 mm). The vesicles are spherical to oval, and vesicularity varies from 3-44 % (**Appendix E**). Glomeroporphyritic clots, typically plagioclase-augite, are common. Two dense rounded bombs from Punatekahi B cone differ by containing skeletal olivine (0.3 mm). One of the bombs also has a felted groundmass and contains a red scoria lithic (3.8 mm) with phenocrysts that show strong resorption textures (**Figure 7.21**). Sample W104 contains porphyritic juvenile clasts with a much higher abundance of olivine, which is rarely skeletal and exhibits resorption, groundmass laths of swallow-tail plagioclase (**Figure 7.22**), and vesicles infilled with yellow-orange secondary alteration.

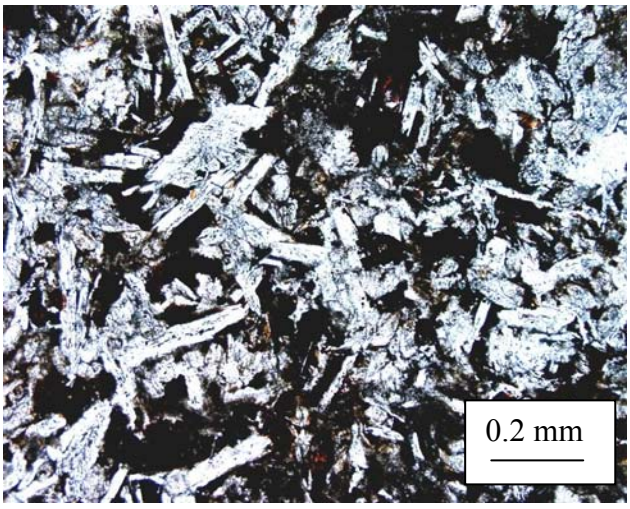

Figure 7.21 Photomicrograph of red scoria lithic within bomb from Punatekahi B (plane-polarised light).

The ash found at Punatekahi A cone contains juvenile black scoria with subhedral highly resorbed plagioclase (0.5 mm) and euhedral skeletal olivine (0.3 mm), covered with ash and yellow-orange material, possibly palagonite.

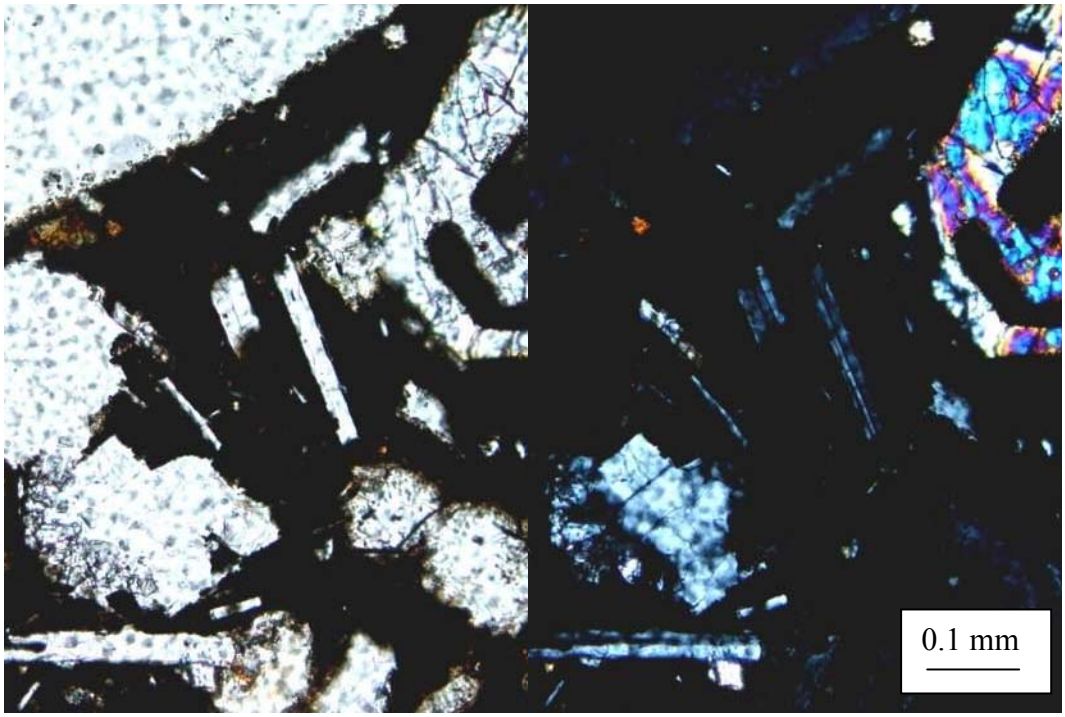

Figure 7.22 Resorbed olivine and swallow-tail plagioclase, W104. Left image: plane-polarised light, right image: crossed-polarised light.

7.5.2 Crystals

In the ash facies, subhedral plagioclase (0.9 mm), augite (0.7 mm), euhedral olivine with iddingsite rims (0.3 mm) and orthopyroxene (xenocryst – 0.6 mm) are found.

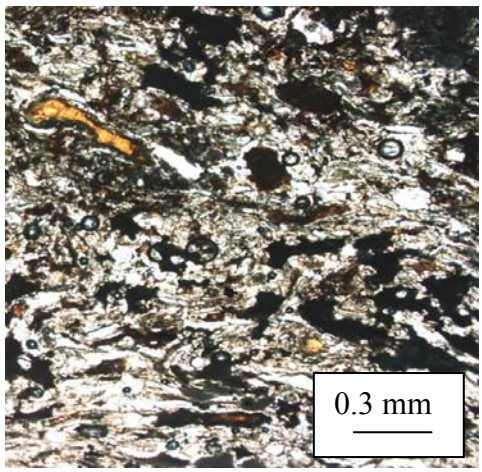

Figure 7.23 Matrix of ex situ, thermally-altered ignimbrite, Punatekahi (plane-polarised light) (W105).

7.5.3 Lithic Clasts

Sub-rounded to sub-angular grey-white flow-banded rhyolite, brown ignimbrite with orthopyroxene, plagioclase and opaques, and loose glass shards and yellow-orange fragments are present (likely some form of secondary growth) within the ash facies. A lithic that looks

hydrothermally-altered was found to be a light brown ignimbrite with oscillatory zoned subhedral plagioclase, opaques, pumice and devitrified glass shards (**Figure 7.23**). This ex situ ignimbrite could be the same as that found in the ash, given that devitrification of glass is related to temperature (e.g. Streck and Grunder 1995).

7.6 Interpretation

7.6.1 Facies

The facies evident at Punatekahi are similar for both cones, and are likely produced by the same processes.

1) Lava facies

   The trachytic groundmass and horizontal fracturing indicate a lava flow, although the presence of scoria lithics in bombs in the vent deposit of Punatekahi B suggests fallback into a lava lake (Houghton and Gonnermann 2008; Valentine and Gregg 2008). The flat-top geometry of the lava facies, although possibly affected by quarrying, also suggests a lava lake, as does the sub-horizontal alignment of blocks. Some samples from the top of the lava have felted groundmass and are vesicular, further supporting a static pool of lava. It is therefore proposed that the lava was a lake that breached its walls and formed a flow to the west. The vertical contact with the scoria represents either the wall of the channelised flow (Cas and Wright 1987), or an unbreached part of the pre-existing cone construct.

2) Medium-thickly bedded lapilli and bomb facies

   The steep dips, at or near the angle of repose suggest that these beds represent outer wall deposits of undisturbed scoria airfall deposits (Houghton and Schmincke 1989). The reverse grading evident in most of the beds could be due to either an increase in eruption intensity (e.g. Jurado-Chichay and Walker 2001), or the material rolling downslope before coming to rest (Fisher and Schmincke 1984; Cas and Wright 1987).

The finer ash layers could reflect either less energetic explosions (Patrick *et al.* 2007) or part there-of, or vent-clearing of a blocked vent (Houghton and Schmincke 1989). Fall from ash plumes is proposed by Riedel *et al.* (2003) and Patrick *et al.* (2007) to be more common than originally proposed for 'strombolian'eruptions. The ash-rich layers are not, however, traditionally considered to be strombolian, and their origin is still debated (Houghton and Gonnermann 2008). The evidence for water involvement is low (see **7.6.2**), so the range of vesicularities found for the beds at Punatekahi A (15-71 %) are likely the result of heterogeneous magma supply, being variously affected by degassing related to magma ascent rates (Houghton and Wilson 1989). The presence of lava slabs indicates that this degassing occurred within the lava lake, and the variable rates are likely to be mostly due to fresh, vesiculating magma mixing with the degassed lava in the lake (Houghton and Schmincke 1989). The interfingering of bedded facies from Punatekahi A and Punatekahi B indicate that two vents were concurrently active during the construction of the lower and upper parts of Punatekahi A and B cones, respectively.

3) Thin-medium bedded lapilli facies

   The lapilli beds that dominate the Punatekahi A North site are very similar to the other bedded facies, indicating that these beds are the result of ballistic fall. The difference in bed thickness and grain size possibly reflects waning conditions that mark the final phase of cone-building at Punatekahi. The relatively poorer sorting could indicate closer proximity to the vent (Ort and Carrasco-Núñez 2009), whereas the lighter colours exhibited by the clasts, which are the result of hydrothermal alteration, and the blockier morphology suggest that this facies has been modified by the presence of external water (e.g. Sheridan and Wohletz 1983; Di Traglia *et al.* 2009, either during or following eruption. The proximity of the facies to a crudely-bedded facies unit and shallow orientation of the beds are consistent with an inner wall position.

4) Welded facies

   This welded light grey rock, with its regular vertical jointing and trachytic groundmass indicate that it is the product of mobile material (Tucker and Scott 2009). The majority of welded light rock that comprises this facies

is vesicular and in some instances outlines of clasts are visible, which suggest that the rock was not formed by coherent lava directly from the crater (Cas and Wright 1987; Németh and White 2003; Riggs and Duffield 2008). However, the original joining of the welded facies to the lava at the northern end of Punatekahi B supports a lava flow origin. It is therefore proposed that the welded facies has two origins: lava flow from breaching or overflow of coherent lava from a lava lake (Cas and Wright 1987; Head and Wilson 1989), and rapidly erupted lava blobs from fountaining (hawaiian eruption style) that became mobile and behaved like a lava flow (clastogenic; the 'rootless flows' of Head and Wilson 1989; Fisher and Schmicnke 1984; Cas and Wright 1987; Riggs and Duffield 2008; Valentine and Gregg 2008). Where outlines of clasts are visible, the latter process is inferred. The formation of welded agglutinate requires an increase in magma ascent rate, associated more with hawaiian-style eruptions than strombolian (Head and Wilson 1989; Houghton *et al.* 1999; Houghton and Gonnermann 2008). Breaks in the agglutinate at sites of the crudely-bedded facies suggest rupture from magma moving up through cooled lava in subsequent eruption phases. The black dense tubular concretion found in one of the facies' outcrops is inferred to be the remnant of a dike. It is possible that this is part of the same dike described by Brown (1990). It is the only obvious dike-like structure found at the quarry. Welding is a feature of the inner walls of a scoria cone (Houghton and Schmincke 1989).

5) Massive/crudely-bedded lapilli and bomb facies

The domed geometry, proportion of large bombs and thick, crude beds indicate that this facies represents the inner wall or vent area (Fisher and Schmincke 1984; Houghton and Schmincke 1989). The proximity of this facies to both the bedded facies and, in the case of Punatekahi B, the lava facies, implies that this facies represents an inner wall facies. It does however lack the high angles found at Rothernberg (Houghton and Schmincke 1989), but this could be due to the compact nature of the cone, with nearby emplacement of magma affecting dips (Houghton and Schmincke 1989). The large bombs are likely ballistics from the vent and explain the poor sorting observed in the field. The occurrence of bomb

sub-horizontal bomb layers also supports that this facies was close to the vent, lacking the slopes that outer sections of the cone would be expected to have, whereas the rounder, cored bombs at Punatekahi B, reminiscent of the 'cannonball' bombs of Houghton and Schmincke (1989), indicate that the facies there is a crater fill facies. The very high vesicularities found at Punatekahi B (≤ 75 %) suggest that magma ascent rate was greater than degassing rates. In addition to degassing in the lake, the range in values could result from recycling at the vent, which is evidenced by the cored bombs at Punatekahi B (Patrick *et al.* 2007).

6) Ash facies

The ash in the northern part of the Punatekahi A cone, in part due to its association with welded and massive facies, comprises part of the inner wall of Punatekahi A. Ash falls from eruptions at scoria cones are rarely preserved (Riedel *et al.* 2003), and this is likely reflected in the very localised exposure of it at Punatekahi A. The fact that the ash is preserved indicates that it was shortly covered by subsequent eruptives. This is further supported by the existence of large scoria clasts found mixed in with the finer ash fraction and the semi-gradational upper contact. The significant amount of lithic material in the ash, along with the sideromelane indicate that the ash has resulted from phreatomagmatic activity (Barberi *et al.* 1989).

The correlation of facies to parts of a scoria cone model (following Houghton and Schmincke 1989) results in the identification of at least four vents at Punatekahi: three at Punatekahi A and one at Punatekahi B (**Figure 7.24**). Evidence suggests that there was a northward shift in vent position with time from vent 1 to vent 4.

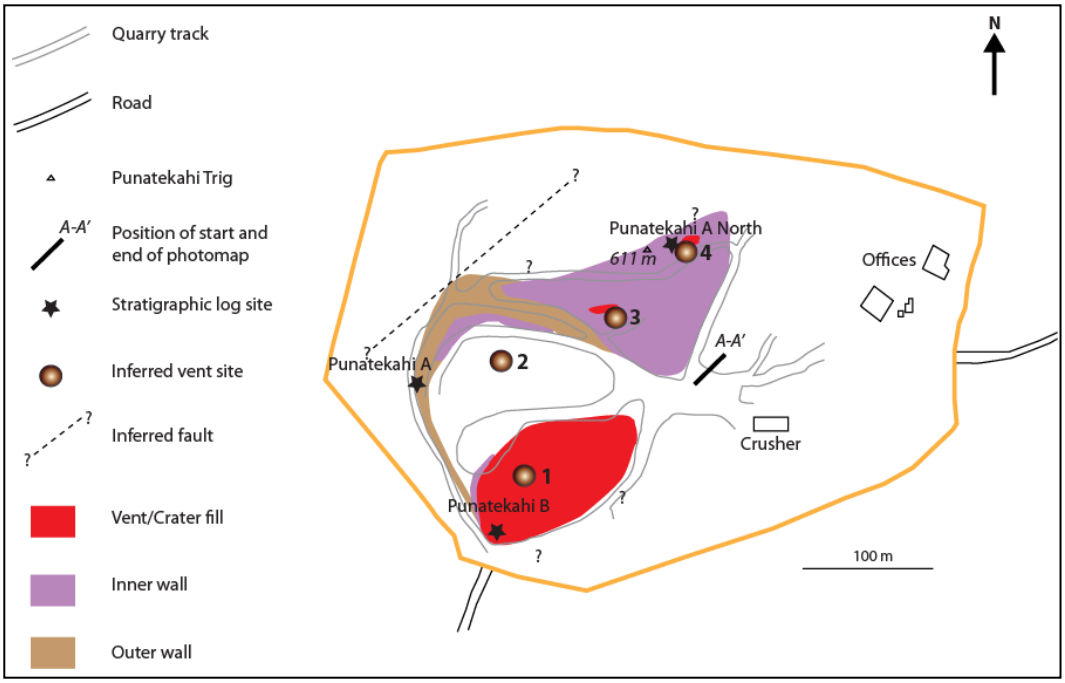

Figure 7.24 Interpretation map showing inferred parts of the scoria cone and vent positions during construction of the cone complex. Numbers 1-4 are vents in chronological order (Modified from Brown 1990).

7.6.2 Role of External Water

At first look, Punatekahi resembles a typical scoria cone, with beds of red-black scoria lapilli and bombs, and lava forming a positive cone construct (e.g. Houghton and Schmincke 1989; Riedel *et al.* 2003). The coarse-grained nature and morphology of the scoriae, the low lithic content and the typically good sorting of the beds all indicate that water was absent or was negligible at Punatekahi (e.g. Barberi *et al.* 1989; Houghton *et al.* 1999). There is some evidence to suggest, however, that water was present during the construction of the Punatekahi A cone. This evidence includes: the morphology of the thinly-medium bedded lapilli facies, the ash facies, and the white coating found on juvenile clasts within medium-thickly bedded lapilli and bomb facies.

The beds within the thin-medium bedded lapilli facies consist of blocky, relatively fine-grained clasts that form among the most poorly sorted beds at Punatekahi. The clasts are hydrothermally altered (with cristobalite/trydimite coating), have the overall lowest vesicularities found at the cone complex (mean of 55 %) and quench textures, although rare, do exist. Considering that this facies, from the northernmost part of the cone, represents the last known stage of eruption, it is possible that the finer grains, quench textures and lower vesicularities reflect

older, degassed magma in the waning part of eruption (Houghton and Wilson 1989; Houghton *et al.* 1999; Di Traglia *et al.* 2009). The hydrothermal alteration of the clasts could also be post-depositional. However, the coincidence of all of these features together, in close proximity to the lithic-rich ash facies, is better explained by the presence of water, although the timing of magma interaction with water relative to fragmentation is unclear. The morphology of the clasts in this facies, as revealed in SEM, more closely resembles the pyroclasts of phreatomagmatic phases at the other field sites (see **Figure 5.17a**) than the morphology of the other pyroclasts of Punatekahi, meaning either that water was concurrent with eruption, or that some of the features of the phreatomagmatic deposits' clasts are post-depositional.

The ash facies, though, which is rich in lithic material, shows strong evidence for water being present in an 'active' role during the construction of Punatekahi A. The presence of sideromelane shows not only that there was definitely water present during the eruption of the material, but also, importantly, that the ash was juvenile, and not some concurrent rhyolitic or phreatic ash (the latter being a strong possibility due to the inference of hydrothermal activity – Riggs and Duffield 2008).

The white coating that is found on juvenile clasts of the medium-thickly bedded lapilli and bomb facies, concentrated in discrete zones of the construct, is evidence only of passive water presence. This white coating, which has been identified as quartz polymorphs, could have two possible origins. The first is the rhyolitic tephra which overlies the scoria cone, which has obviously washed down quarry wall faces. This is however, deemed unlikely, given the fact that the quartz polymorph growth is visible only in a certain area of the cone, whereas wash-downs are ubiquitous, the white coating is found not only on clasts exposed to the surface, but those deeper within the quarry face, and rhyolite tephras do not usually contain quartz polymorphs (R. M. Briggs pers. comm. 2010). The possibility of the tephra seeping in through the top of the cone is also not a viable explanation, given that the quartz growth disappears above the unconformity between the basal red bedded facies and the upper purple bedded facies. Temperatures needed for growth of these crystals (more than ~ 200 º C – Ohba and Kitade 2005) also renders the tephra as a source following cooling of the lava very unlikely. The second, more likely explanation is that this cover formed via

hydrothermal precipitation. The quartz polymorph coating on the thin-medium bedded lapilli facies' scoria supports a hydrothermal source. The restriction of hydrothermally altered zones to the basal and upper eruptive deposits, close to the inferred vent sites, implies that the magma itself was the driver for short-lived hydrothermal systems (Ohba and Kitade 2005). Furthermore, the coating only being found on the coarser clasts suggests that this hydrothermal system was in place during or shortly after eruption, given that larger clasts would be hotter and retain their heat for longer, thereby allowing sufficient time for the quartz to crystallise. It is possible that the rather low, wide-ranging vesicularity of the medium-thickly bedded lapilli and bomb facies is in part explained by the presence of hydrothermal water (following Houghton and Wilson 1989), but there is little evidence from morphology of the clasts to support this, with a blocky morphology only evident on the lapilli fraction of one of the beds (W95) (Sheridan and Wohletz 1983).

7.6.3 Source of External Water

Given its inferred stratigraphic position above Huka Falls Formation (Brown 1990) and lake sediment settings of the other K-Trig basalts (Brown 1990; Smith 1990; Brown *et al.* 1994), external water could be surface or ground water. Brown (1990), with the surmising of an initial phreatomagmatic phase (see **1.4**), suggested the source of groundwater was a saturated shallow lake margin. Here, the source of external water for both the active and passive interaction with the basalt appears to be the same. There is support for this inference from the observation that only those parts of the cone that have hydrothermal alteration also show active interaction of water with magma. Indication of source of this external water is most clearly seen in the phreatomagmatic ash. This ash has a high lithic content (~ 69%), and a small sideromelane:scoria ratio, suggestive of a groundwater source. The overriding lithic type found in the ash is a light brown ignimbrite. This ignimbrite matches with that found in the Rangatira Ignimbrite in most respects, except for the lack of hornblende (Cole *et al.* 1998), so is suggested as a possible source of the water.

7.6.4 Eruption Phases

There is evidence at Punatekahi for four eruption phases: three magmatic phases and one phreatomagmatic phase. Due to the nature of the exposure, the initial eruption phases at Punatekahi are not able to be determined, so this number is likely to be higher. The first phase was initiated at Punatekahi A (vent 2 in **Figure 7.24**) in the south-west, with magmatic eruption of scoria lapilli and bombs. At Punatekahi B (vent 1), lava was erupted from a lava lake, producing ballistic bombs and lapilli, with some recycling of bombs. The latter part of the eruption phase involved a breach of the lava lake, which resulted in a reduced magma supply and fining of eruptives. During this phase, a hydrothermal system was initiated by the basaltic magma and some aquifer fragmentation possibly occurred. The second magmatic phase followed a period of quiescence, during which erosion took place. This second magmatic phase involved more powerful/longer eruption blasts from vent 3, but the phase was of a shorter duration. Magma discharge rate at one point was great enough to produce clastogenic lava flows. The vent for this second phase was further north and Punatekahi B had ceased to be active by this time, as had the hydrothermal system. This was followed by a slight change in vent position (to vent 4) and the only phreatomagmatic phase, which produced a fine ash from interaction of magma with groundwater. Reactivation of the hydrothermal system or activation of a new hydrothermal system occurred, resulting in blocky, hydrothermally altered scoria lapilli.

8 Geochemistry

8.1 Introduction

Geochemical analysis for major and trace elements has been done on six samples: five basalts (one from each of Kinloch and Kaiapo, three from Punatekahi) and one rhyolite (from Kinloch) (**Table 8.1**).

8.2 Basalts

8.2.1 Classification

Using a simple SiO_2 vs. K_2O classification plot, the Punatekahi samples are low-K tholeiites, Kaiapo is borderline low-K tholeiite/medium-K basalt, and Kinloch is a borderline low-K/medium-K basaltic andesite (**Figure 8.1**). All of the 'basalts'

can be classified as high-alumina (**Figure 8.2**), with Kaiapo having the highest Al_2O_3 content (18.21%) and Kinloch the lowest (16.67%).

Table 8.1 Major and trace element data for the five basalts and the rhyolite (W64). Major elements in wt. %, trace elements in ppm. *Fe_2O_3 = total iron.

Element	Kinloch W60	Kaiapo W23	Punatekahi W93	Punatekahi W84	Punatekahi W74	Kinloch W64
SiO_2	50.94	48.88	49.58	49.52	48.69	71.47
TiO_2	1.17	0.94	0.99	1.00	1.00	0.27
Al_2O_3	16.29	17.94	17.43	17.56	16.95	13.79
Fe_2O_3*	9.83	9.14	10.38	10.38	10.25	2.39
MnO	0.16	0.15	0.17	0.16	0.16	0.06
MgO	5.47	6.37	6.84	6.78	6.68	0.51
CaO	10.33	12.06	12.21	12.22	11.91	2.22
Na_2O	2.74	2.23	2.26	2.27	2.31	4.10
K_2O	0.51	0.47	0.32	0.35	0.36	2.97
P_2O_5	0.25	0.34	0.12	0.28	0.15	0.07
LOI	-0.07	0.12	-0.19	-0.04	-0.35	1.87
TOTAL	97.63	98.64	100.11	100.49	98.11	99.71
S	178	269	154	157	143	215
Cl	172	508	53	-	-	855
V	337	303	378	350	380	11.3
Cr	73	182	109	119	120	7.6
Co	45	49	42	38	34	23
Ni	28	40	33	33	38	1.3
Cu	45	34	36	24	36	3.6
Zn	86	73	76	80	77	44
Ga	18.7	18.9	17.9	16.7	18.5	16.1
Rb	11.9	11.1	6.9	7.3	7.2	115
Sr	310	381	337	334	343	164
Y	23	20	20	20	20	23
Zr	102	68	64	61	61	156
Nb	4.9	3.7	3.5	3.3	3.0	6.6
Ba	154	116	91	90	84	545
La	7.6	6.2	-	8.2	5.2	24
Ce	18.2	15.9	10.5	14.1	13.7	42
Nd	9.4	9.1	-	-	-	21
Pb	2.6	2.4	2.1	1.2	1.9	15.0
Th	2.0	1.7	1.1	1.7	2.4	14.6
U	3.1	3.4	2.6	3.4	3.9	5.7

8.2.2 Magma Type

A plot of the trace elements, normalised to primitive mantle (**Figure 8.3**), has been constructed for the five basalts. Average N-MORB (Normal Mid-Ocean

Ridge Basalt) and OIB (Ocean Island Basalt) concentrations have been added for comparison. All of the basalts show a similar pattern, being enriched in

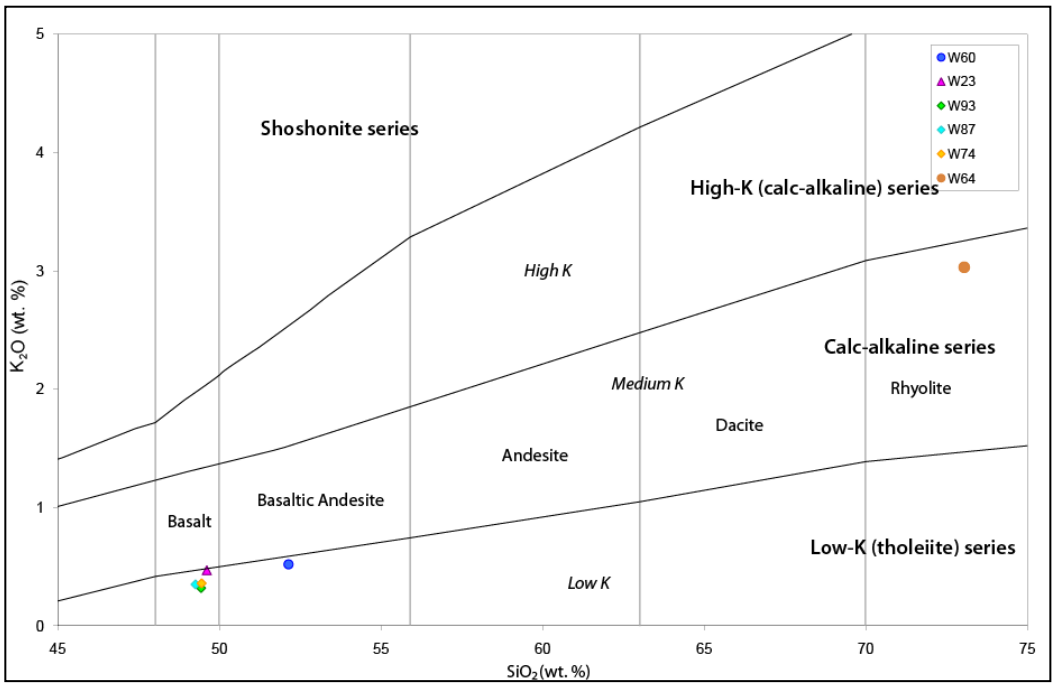

Figure 8.1 SiO_2 vs. K_2O (wt. %) rock classification plot for basalt and rhyolite samples. Series divider lines show variation in divisions (from Rollinson 1993).

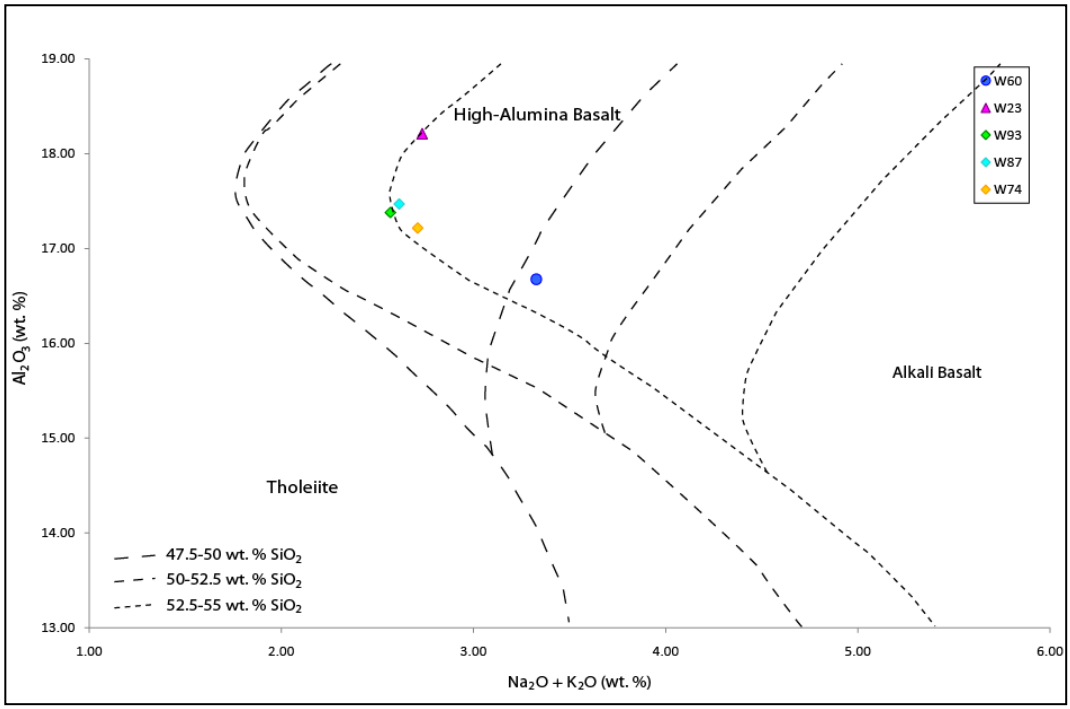

Figure 8.2 High-alumina classification Al_2O_3 – Na_2O + K_2O – SiO_2 plot for basalts (Kuno 1960 as cited in Cole 1973).

incompatible elements relative to N-MORB, and depleted relative to OIB. The trough formed by all basalts for Nb is indicative of an arc type of setting. There is a relative depletion in Zr, Ti and Y. Kinloch has typically higher values than the other basalts, although Punatekahi sample TS14 is higher in La, and Kaiapo is higher in Sr and P.

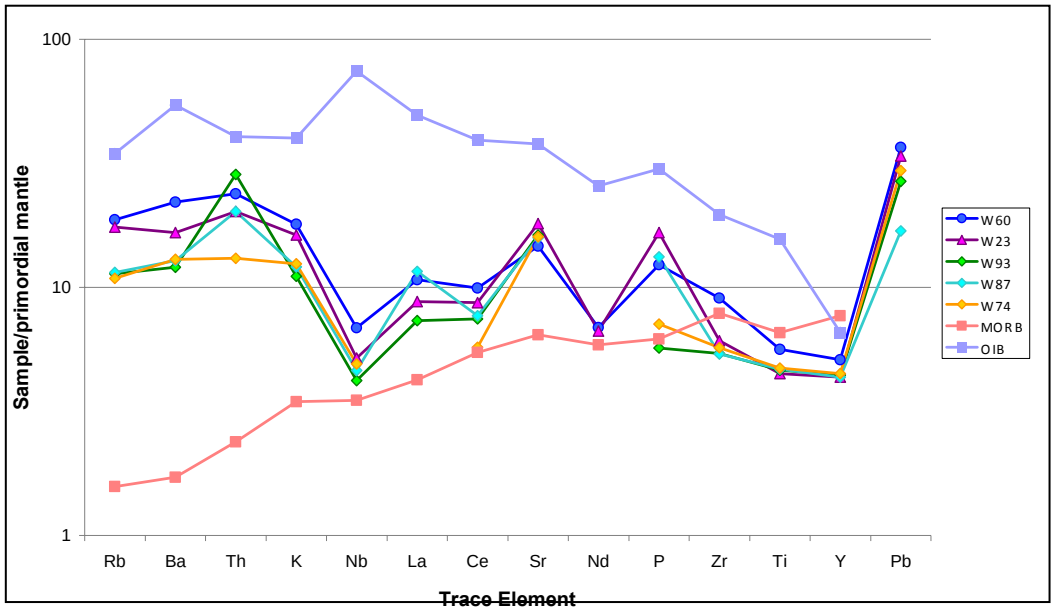

Figure 8.3 Multiple element spider diagram for basalts. Trace element concentrations normalised to primordial mantle using values from McDonough et al. (1992). N-MORB and OIB values from Saunders and Tarney (1984) and Sun (1980) (cited in Rollinson 1993).

A comparison between the five basalts is made clearer by incompatible trace element plots. The Zr vs. Sr plot (**Figure 8.4**) shows that Sr is relatively similar between the basalts, but that Kinloch is distinguishable by its much higher Zr. The Zr vs. Rb plot (**Figure 8.4**) also clearly identifies the Punatekahi samples as being distinct from Kaiapo and Kinloch.

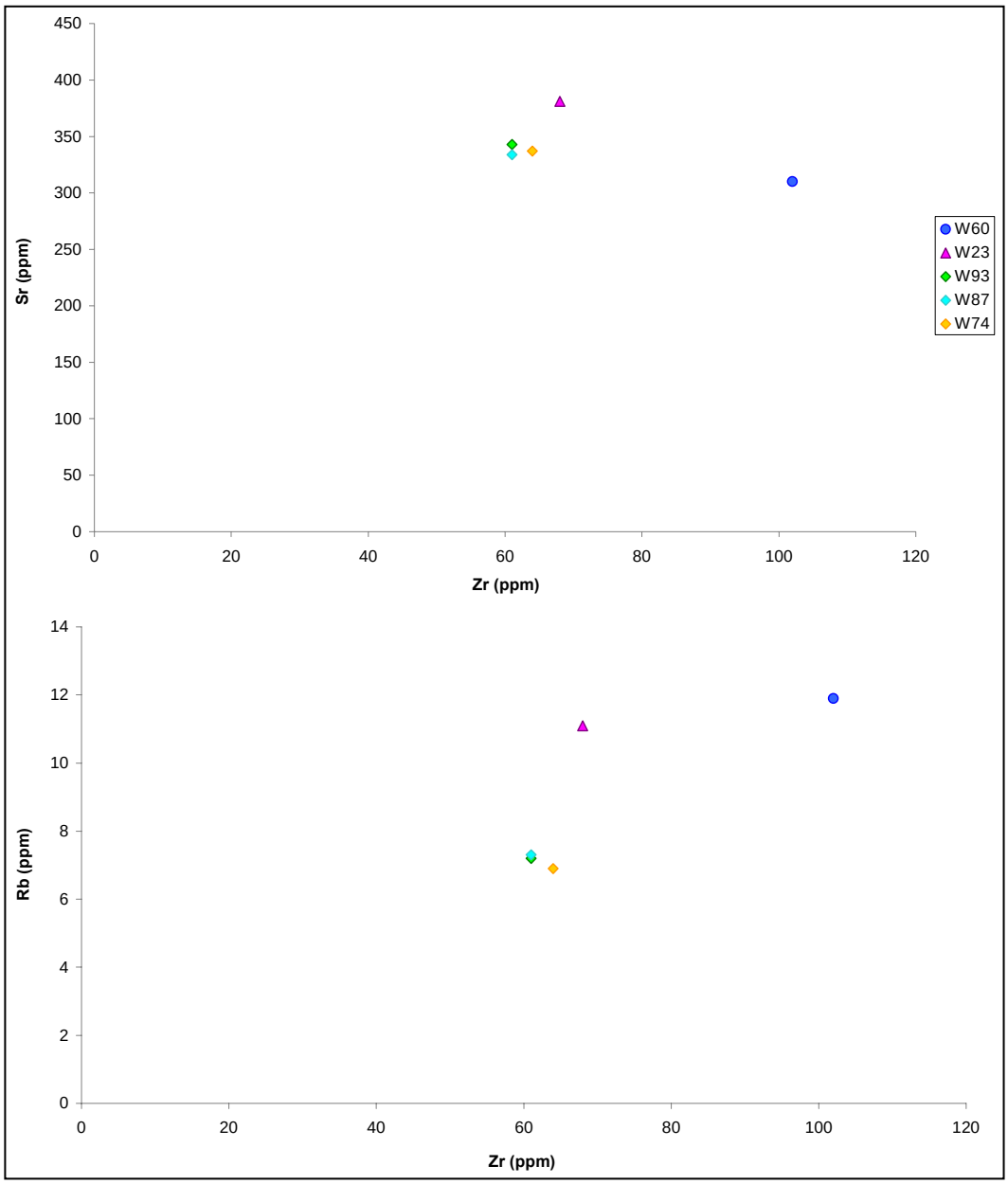

Figure 8.4 Zr vs. Sr and Zr vs. Rb incompatible plots for the basalts.

8.2.3 Magmatic Processes

A determination of magmatic processes operating in the basalts in TVC is hindered by the lack of samples able to be geochemically analysed. The three samples at Punatekahi, though, taken from Punatekahi B (W74) and the northern part of Punatekahi A (W93, W87), originate from three different stratigraphic levels of the cone complex, thereby offering a restricted view into changes in magma composition/magma source with time. Within analytical error (1% for major elements, 5% for most trace elements), there are no systematic changes in composition with stratigraphic position at Punatekahi.

8.2.4 Comparison With Other Taupo Volcanic Zone Basalts

A trace-element comparison with other TVZ basalts (**Figure 8.5**) shows that the TVC basalts studied here follow the same general trend suggestive of arc basalts (Gamble *et al.* 1993), although the TVC basalts have lower Pb. Interestingly, the Acacia Bay data (Wilson and Smith 1985), which are likely similar to that of the Acacia Bay deposit studied here, produce a different trend from the other basalts, both in TVC and TVZ as a whole, having higher Ba, Sr, Pb, a much higher Th value, and lower Zr.

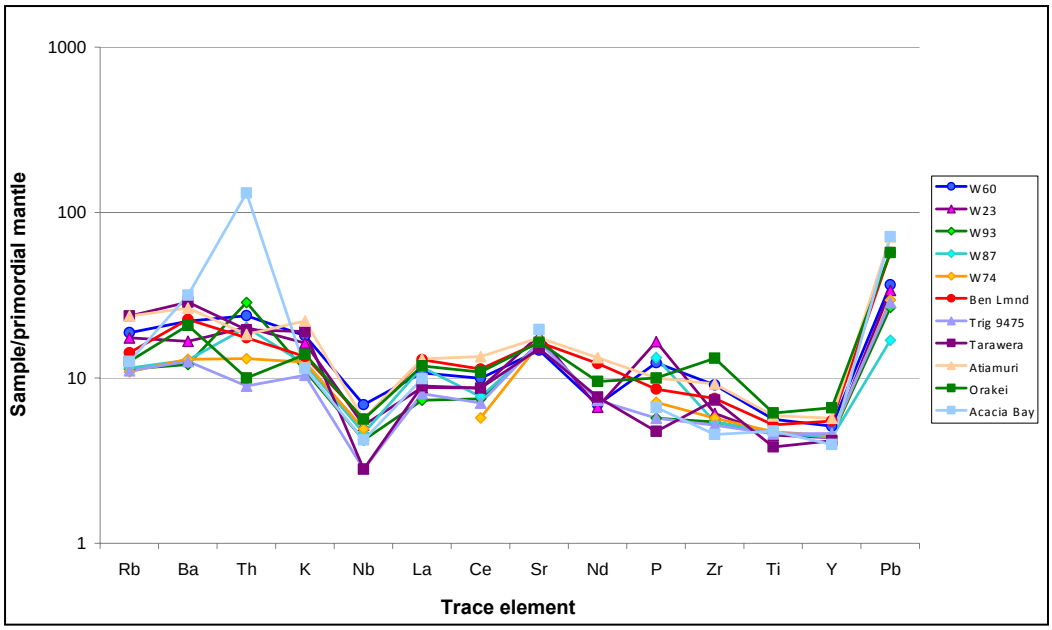

Figure 8.5 Multi-element plot of TVC basalts (this study) with other TVZ basalts for comparision. (Additional data from Gamble et al. 1993; Acacia Bay – Wilson and Smith 1985.)

Additionally, the Ben Lomond basalt, which is the closest basalt to Kinloch, does not show a particularly strong correlation with Kinloch relative to the other basalts. The overall similarity between the basalts lends support to the theory that all of the TVZ basalts are ultimately derived from the same source (Graham *et al.* 1995).

8.3 Rhyolite (Kinloch)

8.3.1 Classification

The perlitic rhyolite of Kinloch is a calc-alkaline rhyolite (**Figure 8.1**).

8.3.2 Comparison With Other TVC Rhyolites

Trace element comparison of the Kinloch rhyolite with selected rhyolites from Sutton *et al.* (1995) is given in **Figure 8.6**. As the multi-element plot illustrates, all of the TVC rhyolites have the same trend, with very little variation in K, Nb, La, Ce and Nd. Kinloch rhyolite falls within most of the other values, although it has slightly higher values for Th and U.

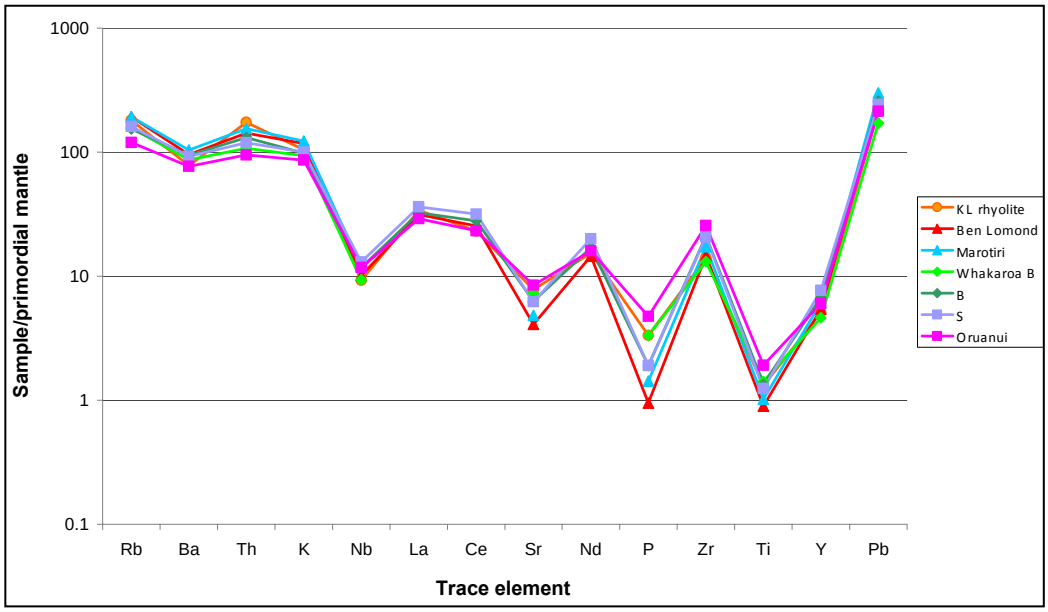

Figure 8.6 Multi-element plot for Kinloch and other nearby rhyolites. Additional data from Sutton *et al.* (1995). Primordial mantle normalising values are the same as used for the basalts.

Of particular interest is whether there is any correlation with the Whakaroa-type rhyolites, which are abundant in the area. Kinloch is plotted against three such rhyolites in **Figure 8.7**. Neither Whakaroa samples from Sutton *et al.* (1995) are from the dome adjacent to the Kinloch basalt deposit, but the Te Kauwae Point sample is from the same dome complex that is adjacent to the Kinloch tuff (see Sutton *et al.* 1995 for locations). The similarity between all rhyolites indicates

that they all originate from similar magma batches. The differences to be found between them though, particularly the higher Th value for Kinloch, indicate that they are all distinct rhyolites. It is interesting to note that Kinloch has a closer match with the two 'Whakaroa' rhyolites than it does with its closer Te Kauwae Point neighbour.

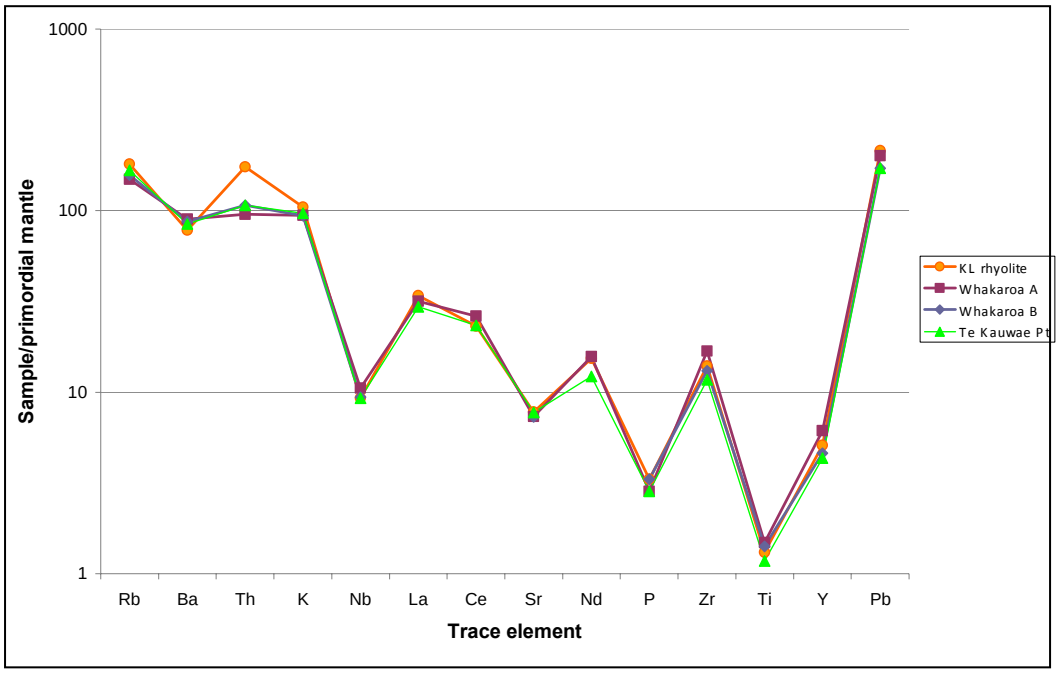

Figure 8.7 Multi-element plot for Kinloch rhyolite and three Whakaroa-type rhyolites. (Additional data from Sutton *et al.* 1995).

8.3.3 Relationship to Kinloch basalt

Given the finding of the basalt lapilli within the rhyolite, and pumice within the basalt, the primary motivation for analysing the rhyolite is to determine which, if any, correlations can be made between the two rocks that would support a theory of contamination or assimilation. The SiO_2 vs. K_2O classification plot illustrates the slight enrichment in these major elements for Kinloch basalt relative to the other basalts. A plot of trace elements (**Figure 8.8**) also seemingly shows a trend toward the rhyolite, although the degree to which the basalt is similar to the rhyolite fluctuates. The possible degree of contamination by the rhyolite is quite small, and therefore the differences in the Kinloch basalt relative to the other basalts could be due to contamination from pumice in the bombs (similar to that found by Streck and Grunder 1999), or simply natural variation from assimilation of a continental source at depth.

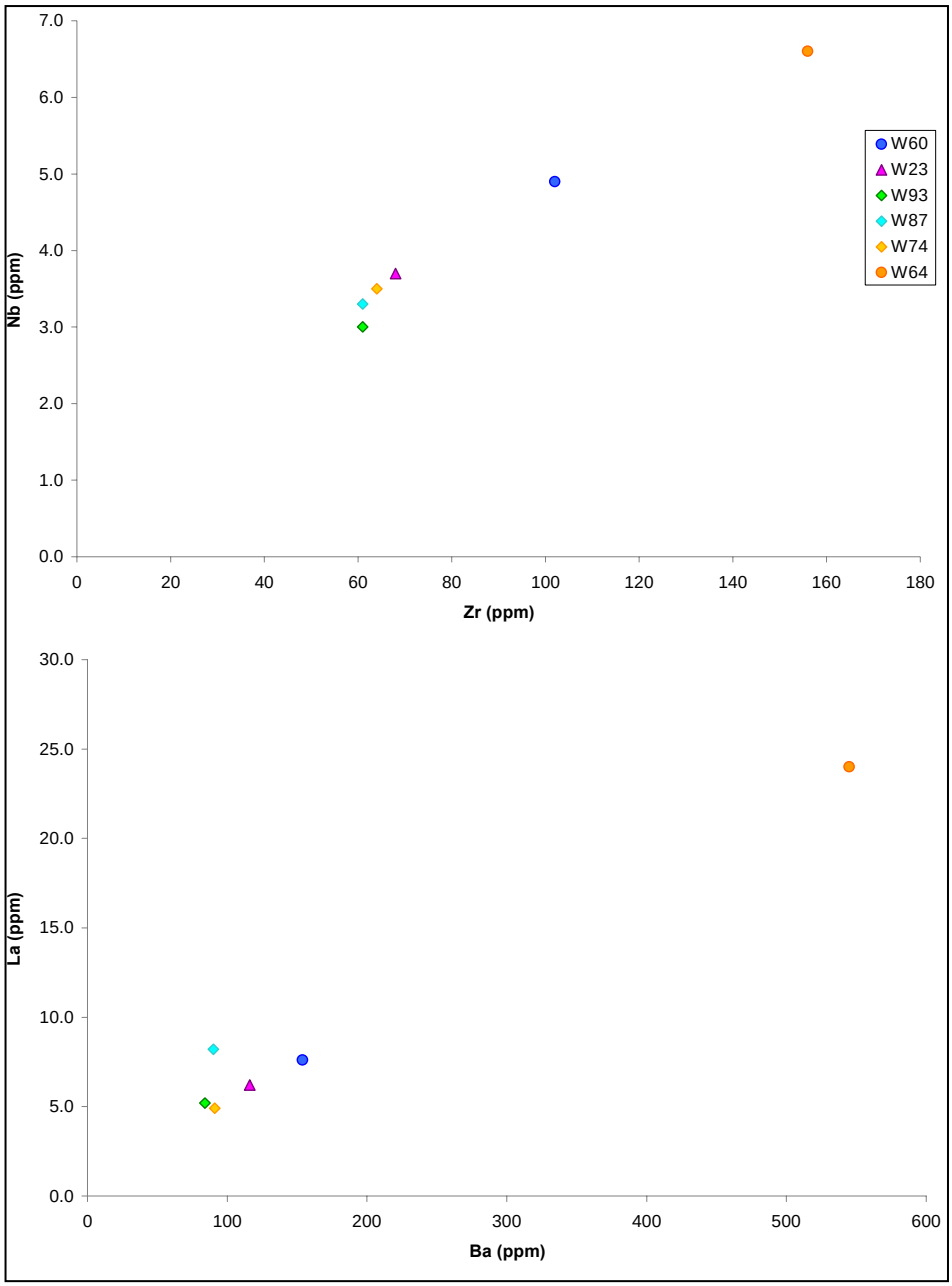

Figure 8.8 Zr vs. Nb and Ba vs. La incompatible plots for the basalts and rhyolite.

8.4 Summary

The geochemical analysis undertaken shows that all of the TVC basalts are (borderline) low-K and can be categorised as high-alumina. Discrimination plots indicate that they are low LILE arc magmas, with very low LILE (Rb, Ba, Th, K) and low HFSE (low Nb, Ti). Kinloch is shown to be quite different from the other basalt samples, being classified as a basaltic andesite and having increased Zr, Rb, Ti and decreased Sr. Apart from Ti, these changes can be explained in part by

contamination by rhyolite, although the data are inconsistent, which implies assimilation of a different continental source at depth. The rhyolite itself has a strong agreement with all of the nearby spherulitic rhyolites, which confirms an association with those rhyolites. Slight differences, however, indicate that this rhyolite is distinct from the other rhyolites.

9 Discussion

9.1 Introduction

Despite the fact that all of the deposits studied resulted from eruption of basaltic magma from the Taupo Volcanic Centre, and three of them involved magma interaction with a significant amount of water, each deposit possesses characteristics that make it unique. The first half of this discussion looks at the similarities and differences between each site, and an eruption model for each site is postulated. The second half of this discussion considers the volcanological, hydrological, and hazard implications of this study.

9.2 Comparison of the Four Basalt Volcanic Centres

9.2.1 Physical and Chemical Characteristics

9.2.1.1 Deposit Geometry

The preserved geometry of both the Kaiapo and Punatekahi deposits has been strongly affected by movement of the Kaiapo Fault (Brown 1990; Smith 1990; Wilson 1993; Brown *et al.* 1994). Preservation of the Acacia Bay and Kinloch tuff deposits are poor compared with Kaiapo and Punatekahi, resulting from their proximity to Lake Taupo, with tectonic activity also likely having had an impact at the sites. The incomplete preservation of the four volcanic centres complicates assessment of deposit geometries. From the widespread deposits at both Acacia Bay and Kaiapo, comprised mostly of base surges, a tuff ring deposit is inferred (Kokelaar 1986; Sohn 1996; see **9.2.3.2**). The thickness of the Kaiapo deposit, however, is more characteristic of a tuff cone (Sheridan and Wohletz 1983). A dip of 29 º obtained at Kinloch is also suggestive of a tuff cone (Sheridan and Wohletz 1983; Sohn 1996), although this may not be an original dip, given the numerous faults at the site. The presence of erosional U-shaped channels may support a tuff cone deposit (Brand and Clarke 2009). The scoria cone complex of Punatekahi is reminiscent of a parasitic scoria cone (possibly a multiple superimposed or coalesced cone; Corazzato and Tibaldi 2006), suggesting that Punatekahi A is the main construct, with Punatekahi B only slightly modifying the geometry of the deposit. The part of Punatekahi that has not been lost from faulting is well-preserved, given the moderate bed dips found at the site (Riedel *et al.* 2003), suggesting that the remaining cone construct closely resembles that at the time of eruption. Using the radially-expanding nature of base surges (Cas and Wright 1987; Martin and Németh 2005), their dips, and inferred vent locations (from Smith 1990 for Kaiapo), estimates of original deposit geometries are given in **Table 9.1**.

Table 9.1: Deposit geometry parameters for the four basalt deposits.

Parameter	Acacia Bay	Kaiapo	Kinloch	Punatekahi
Radius (km)	1	0.5	0.125	0.2
Dispersal (km^2)^	1.57	0.39	0.03	0.1
Height (m)	4	100	7	100
Rim* (m)	500	250	62.5	?
Height:rim†	0.008	0.4	0.112	?
Dips (º)	2-8	9-32	29	7-30

^ Dispersal calculated using radius of exposure to work out area.

*** Rim diameter was estimated by assuming that the surge runout length is no more than one crater diameter from crater rim (following Fisher and Schmincke 1984).**

† According to Vespermann and Schmincke (2000), tuff cones have height:rim ratio of 0.2-0.5 and tuff rings have height: rim ratios of 0.05-0.13.

9.2.1.2 Grain Size

The grain size data from the four sites shows a wide range of size and sorting values (**Figure 9.1**; **Table 9.2**). Punatekahi deposits are typically much more coarse-grained and better sorted than the phreatomagmatic deposits, showing a clear positive relationship between grain size and sorting. There is one data point, however, that lies very close to some of the Kinloch and Acacia Bay samples.

Table 9.2 Comparison of physical characteristics of the four basalt deposits.

Volcanic Centre	Grain Size Range (MdΦ)	Mean Grain Size (MdΦ)	Sorting Range (σΦ)	Mean Sorting (σΦ)	Vesic.† Range (%)	Vesic. Index (%)	%J/%L/%C*
Acacia Bay	-3.62	-0.6	0.88-2.74	1.59	41-60	54	77/2/21
Kaiapo	-5.16	-0.48	0.82-2.54	1.72	31-68	46	26/01/73
Kinloch	-4.98	-0.46	0.86-2.17	1.37	30-43	36	48/1/51
Punatekahi	-3.01	-3.3	0.70-1.68	1.19	15-75	58	99/0/1

†Vesic. = bulk vesicularity.

***%J/%L/%C is overall (average) componentry. J = juvenile clasts, L = lithic clasts, C = crystals.**

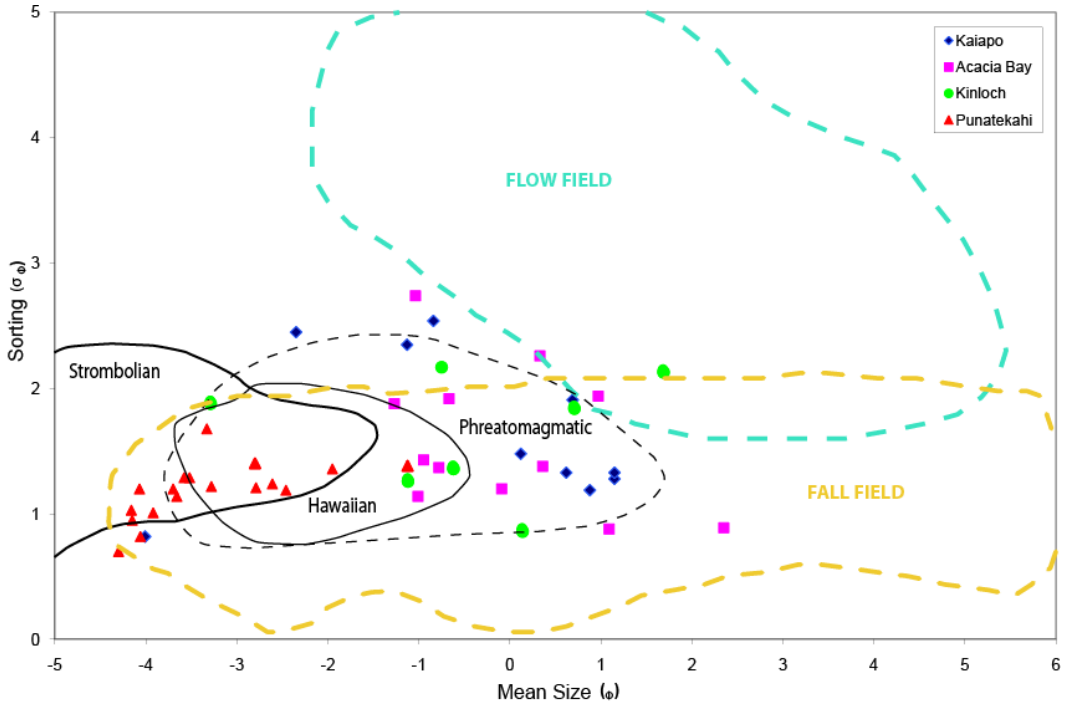

Figure 9.1: Median diameter vs. sorting plot for all four TVC basalts. (Flow and fall fields from Walker 1971; other fields from Houghton and Gonnermann 2008.)

This data point is from the thin-medium bedded lapilli facies in the northern part of the Punatekahi A cone, which exhibits other evidence of low magma:water interaction (see **9.2.3.1**). The next finest Punatekahi sample, also from the same facies, is slightly anomalous in an otherwise relatively tight grouping of data. In contrast to the tight cluster of values seen at Punatekahi, the samples from each phreatomagmatic centre form a wide range of values, and the relationship of better sorting with coarser grain size becomes non-existent, almost with a slight negative trend, although it is not statistically significant (maximum $R^2 = 0.176$ for Acacia Bay). Three notable data points on the graph are the poorly sorted, coarse-grained Kinloch bomb layer, the very well sorted, fine-grained layer from Acacia Bay, and the well sorted, coarse-grained bed from Kaiapo. The Kinloch sample falls directly on the border of the phreatomagmatic field of Houghton and Gonnermann (2008), whereas the Kaiapo sample falls among the best sorted beds of Punatekahi, well within the magmatic fall field. The very fine, well-sorted Acacia Bay sample likely indicates very efficient fragmentation, and therefore it is inferred that all of these units represent magma:water values close to the magmatic/phreatomagmatic transition zone. According to the flow and fall fields of Walker (1971), a large proportion of samples are fall deposits, which in part would reflect the fact that grain size analysis was only carried out on

unconsolidated (or friable) samples (therefore not including many base surge deposits – e.g. Sheridan and Wohletz 1983). Several of the samples that lie within the fall field showed features in the field associated with lateral transportation, such as cross-bedding (Sohn and Chough 1989; see **9.2.3.3**). This seems to confirm the difficulty in distinguishing fall and flow deposits in the field, especially at sites proximal to the vent (as discussed by Fisher and Schmincke 1984; Zanon *et al.* 2009). A comparison of the grain size data obtained in this study with other magmatic and phreatomagmatic basalt deposits is given in **Figure 9.2**. The plot shows that the fields of magmatic and phreatomagmatic centres are similar to those found at other centres. Punatekahi has a close fit with the magmatic samples from Crater Hill and one of the sample sets from Rothenberg. All of the samples overlap with the phreatomagmatic samples from Crater Hill and Cora Maar. Only Acacia Bay has significant overlap with Fossa Cone (Vulcano), and both Kaiapo and Kinloch have overlap with the strombolian fields of Rothenberg (Houghton and Schmincke 1986).

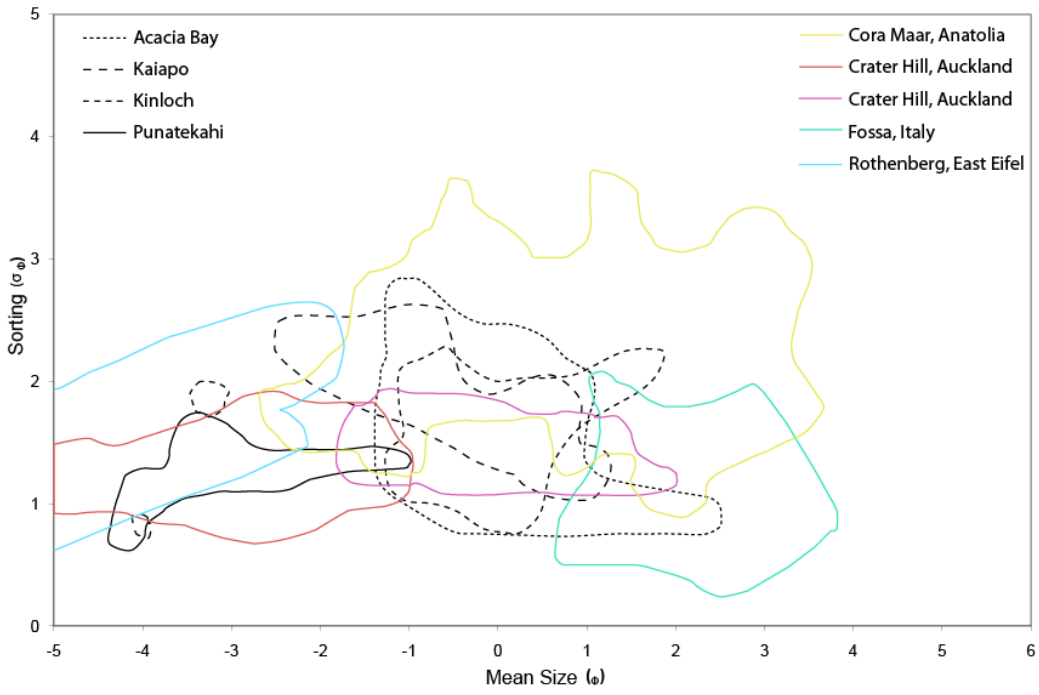

Figure 9.2 Median diameter vs. sorting plot for the four basalt deposits in this study, with Cora Maar (Gençalioğlu-Kuşcu *et al.* 2007), Crater Hill (Houghton *et al.* 1999), Fossa cone (Frazzetta *et al.* 1983) and Rothenberg (Houghton and Schmincke 1986) for comparison.

It is interesting to note that although these samples of Kaiapo and Kinloch seem rather anomalous, all but one of the Kaiapo samples actually lie close to some of

the coarser-grained surge samples of the Cora Maar deposit. This indicates that overlap of phreatomagmatic and magmatic deposits may be quite common. Houghton and Gonnermann (2008), who created the phreatomagmatic, strombolian and hawaiian fields shown in **Figure 9.1**, have noted that there are few quantitative grain size data sets in the literature.

9.2.1.3 Vesicularity

Due to the dependence of bulk vesicularity data on having a sufficient number of 16-32 mm-size juvenile clasts (Houghton and Wilson 1989), the majority of values were obtained from Punatekahi, with the other three deposits being poorly represented (only one set of data from both Acacia Bay and Kinloch). Comparison of the four basalt deposits (**Tables 9.2, 9.3**) shows that vesicularity values are very similar in terms of mean vesicularity, although Punatekahi has the highest mean vesicularity, and Kinloch has the lowest (although this is biased to one sample). Punatekahi also has the highest vesicularity, which is to be expected for a scoria cone (Houghton and Wilson 1989; Houghton *et al.* 1999). According to Houghton and Wilson (1989), assuming that the sample represents the fragmentation surface during eruption, the arithmetic mean of vesicularity for 30 (or, less preferably, 10) analysed juvenile clasts should be 70-80 % for 'dry' eruptions, and much lower (≥ 4 %), for 'wet' eruptions. Additionally, the range of vesicularity values should in theory be greater for 'wet' than for 'dry' eruptions, as the interruption by water of magmatic fragmentation processes will freeze the heterogeneous nature of the magma (Houghton and Wilson 1989). The data in **Table 9.2** are rather anomalous, then, as Punatekahi, which is dominated by magmatic processes (see **9.2.3.1**), shows the greatest range in data, and the lowest vesicularity of any of the samples. There is a slight decrease in vesicularity with stratigraphic height (**Table 9.3**), which could add support to degassing as being an important factor in the lower vesicularity values (Houghton and Wilson 1989; Houghton *et al.* 1999) or could simply reflect waning eruption conditions (Di Traglia *et al.* 2009). Recycling of clasts could also affect these values (Houghton and Smith 1993). The other possibility is that there has been some water:magma interaction, leading to disruption of heterogeneous magma fragmentation (Houghton and Wilson 1989). The very low vesicularity value of 15 % from

sample W94 at Punatekahi, could possibly be explained as a broken lava slab, but samples W102 and W103 from the thin-medium bedded lapilli facies also show poorer sorting and have blocky morphology and thick vesicle walls, more typical of phreatomagmatic deposits (Sheridan and Wohletz 1983), implying that for this part of the eruption, magma:water interaction affected magmatic fragmentation

Table 9.3 Bulk vesicularity values for the four basalt deposits.

Log Site	Sample	Min.	Max.	Mean	Std. Dev.
PAN	W103	37.07	70.95	57.68	12.06
PAN	W102	31.24	60.64	53.02	9.22
PA	W107	52.30	65.77	59.74	5.04
PA	W90	44.72	71.21	59.96	8.57
PA	W92	50.65	67.89	61.38	5.37
PA	W94	15.84	69.35	51.28	15.89
PA	W95	39.43	64.23	55.35	8.03
PA	W96	47.50	67.33	59.45	6.19
PA	W97	38.64	65.05	52.97	9.04
PA	W98	41.80	71.29	58.77	8.65
PA	W99	50.88	65.55	59.44	4.64
PA	W100	38.66	69.90	53.78	8.87
PA	W101	45.51	66.37	56.28	7.51
PA	W83	46.54	65.75	56.20	7.18
PB	W77	47.71	65.19	60.10	7.01
PB	W76	31.87	71.49	60.51	11.86
PB	W75	51.88	74.91	67.31	7.19
ABS	W4	41.14	59.63	54.22	5.10
KPB	W28	31.60	53.97	46.38	6.16
KPB	W27	35.77	60.99	47.04	8.73
KPB	W26	39.67	49.74	46.34	3.21
KPB	W25	34.58	67.86	47.83	9.67
KPB	W23	31.54	50.44	40.26	6.27
KL	W60	30.12	42.59	36.25	4.20

processes. Conversely, the phreatomagmatic centres of Acacia Bay, Kaiapo and Kinloch all show rather narrow vesicularity ranges, which are also not to be expected. For Acacia Bay and Kinloch, these values could reflect limited

sampling. Nevertheless, low vesicularity with relatively small ranges are not uncommon (e.g. Allen *et al.* 1996; Houghton *et al.* 1999). This probably results from a homogeneous magma supply (Houghton *et al.* 1999).

9.2.1.4 Componentry and Clast Morphology

Binocular microscope componentry values (summarised in **Table 9.2**) for the four basalt centres illustrates the difference between Punatekahi and the other volcanoes, with lithic percentages clearly attesting to the relative amount of sub-surface fragmentation that occurred and, by extension, the existence of water-induced fragmentation during the eruption. The magmatic centre of Punatekahi has consistently low lithic values averaging 1 %, whereas all of the other sites have fluctuating values, with a total span from 5 % to 95 %. Kaiapo has the overall highest lithic value of 77 %. This value of 77 % is strongly influenced by the lower part of the deposit, where lithic material comprises up to 99 % of a sample, indicative of a maar-like eruption, likely within a soft substrate (Cas and Wright 1987; Auer *et al.* 2007; Ort and Carrasco-Núñez 2009; Pardo *et al.* 2009). Of the phreatomagmatic deposits, Acacia Bay has the lowest average lithic percentage, at just 26 %. This could reflect (near-) surface magma:water interaction with shallow groundwater or lake water in an open vent (Allen *et al.* 1996; Németh and White 2003). The intermediate value exhibited by Kinloch therefore suggests magma interaction with groundwater within a harder lithology than that at Kaiapo.

Juvenile clasts cover a full spectrum of colours, shapes and vesicularities, although brown-black, blocky, poorly-moderately vesicular clasts are most common at Acacia Bay, Kaiapo and Kinloch, and red, ragged and fluidal, moderately-highly vesicular clasts dominate at Punatekahi. Juvenile clasts from the three phreatomagmatic centres often exhibit an ash coating, whilst at Punatekahi, a significant proportion of juvenile clasts have a quartz polymorph growth.

Crystal values are low for all sites, but slightly higher for the phreatomagmatic centres, being highest at Acacia Bay. Nearly all the crystals are plagioclase, but it is quite likely that a number of these are lithic, not juvenile, given the ubiquity of plagioclase in Taupo Volcanic Centre volcanic deposits (e.g. Sutton *et al.* 1995).

The lithic values at Acacia Bay, Kaiapo and Kinloch have been affected by the presence of aggregate material (aggregates of juvenile basalt, crystals, ash, lithic fragments, pumice, rhyolite glass). At Acacia Bay, there is no clear relationship, but in the case of Kinloch, the lithic value is strongly related to the aggregate count (**Figure 9.3**), suggesting that 'actual' lithics (rock fragments, pumice, rhyolite glass) should have a lower value. At Kaiapo, the relationship is actually negative, with aggregates having greater abundance in the upper sections where lithic content is much lower.

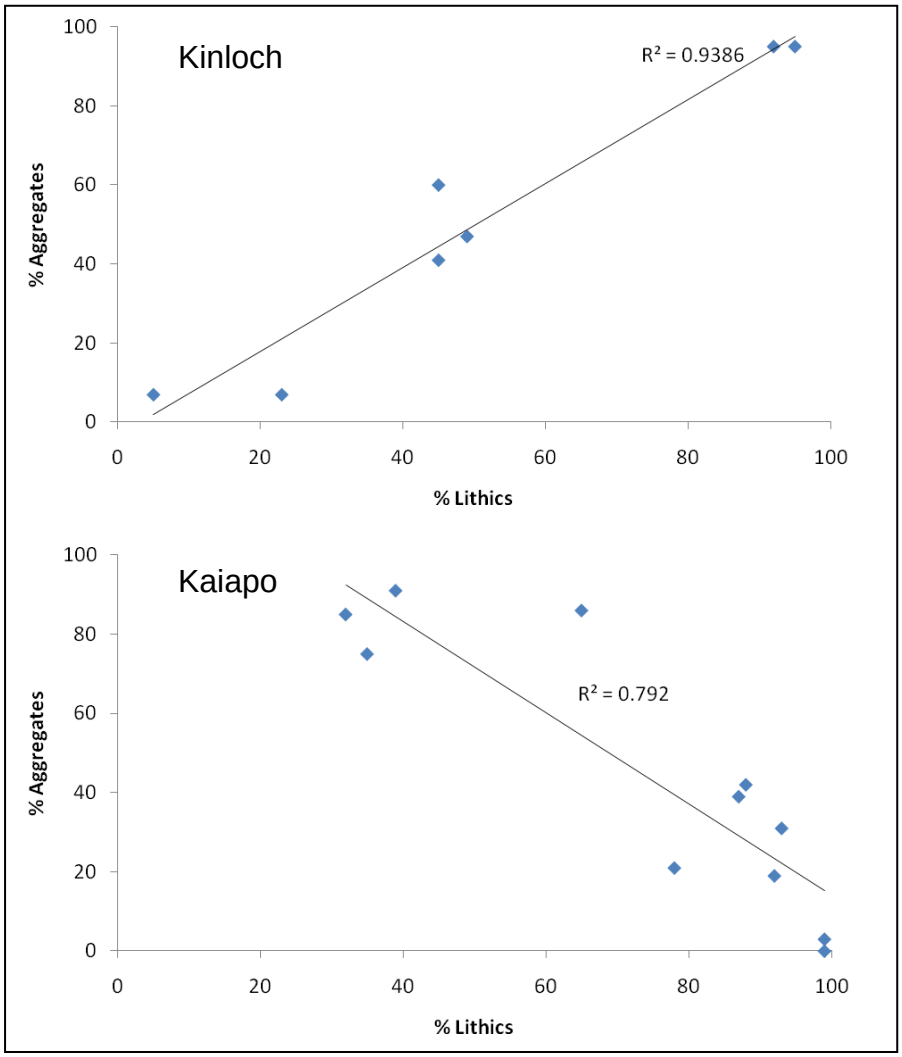

Figure 9.3 Scatter plots showing relationship between lithic proportions and aggregates for Kinloch and Kaiapo tuff deposits.

The reason for this could be a change in induration of the beds, related in part to wetness of the material that formed the deposit (e.g. Sheridan and Wohletz 1983; Zanon *et al.* 2009).

9.2.1.5 Petrography

Basalt from the four centres all share a similar mineral assemblage of plagioclase, olivine and augite set in a hyalopilitic groundmass. As has been previously noted by Cole (1973), the K-Trig volcanoes of Kaiapo and Punatekahi have a relative lack of olivine. Kinloch, on the other hand, differed in the lack of tabular plagioclase, with olivine being more abundant than augite. Quench textures of juvenile minerals were found at all sites. At Punatekahi these are restricted to samples from the thin-medium bedded lapilli facies that typifies the northernmost vent area and exhibit other characteristics associated with magma:water interaction. The quench textures at Acacia Bay and Kaiapo likely result from interaction with water, due to a lack of other likely cool sources of quenching. At Kinloch, however, the ubiquitous quench textures evidenced by the swallow-tailed plagioclase and skeletal olivine in the lava balls (of the bomb-and block-rich facies) could be the result of contact with rhyolite, which had an intimate relationship with the erupted basalt (see **9.3.1**; Rosseel *et al.* 2006). Hypersthene, hornblende, plagioclase and quartz are commonly found as xenocrysts in samples from all of the tuff deposits and in the ash facies of Punatekahi, with biotite being very rare. This is a reflection of the common assemblage of minerals found in the rhyolites and ignimbrites of Taupo Volcanic Centre (Sutton *et al.* 1995). Pumice inclusions were found in juvenile clasts from Kaiapo and Kinloch, with unidentified beige xenoliths also occurring in basalt at Acacia Bay, Kaiapo and Kinloch. These unidentified xenoliths have a yellow tinge in plane-polarized light and are often crystalline, making it possible that they are reworked/altered lake sediment. Lithics at Kinloch are dominated by spherulitic rhyolite. Rhyolite is also common at Acacia Bay and Kaiapo, but the lithic assemblage clearly differs from Kinloch in the existence of dolerite and a stronger ignimbrite component. Petrographic analysis revealed the presence of basalt-free layers at Acacia Bay and Kinloch. At Acacia Bay, this is consolidated diatomaceous lake sediment within a volcaniclastic breccia, whereas the basalt-free layers of Kinloch represent phreatic phases (Sheridan and Wohletz 1983; Petrinovic and Colombo Piñol 2006) (**9.2.3.1**).

9.2.1.6 Geochemistry

The geochemical data obtained for Kaiapo, Kinloch and Punatekahi indicates that all of the basalts are relatively similar, belonging to the low-K series, and showing enrichment of large ion lithophile elements and depletion of Nb, characteristic of arc magmas (Gamble *et al.* 1993; Rollinson 1993). Kinloch is noticeably different from the other basalts in terms of its higher SiO_2 and K_2O, lower Al_2O_3, higher Zr, Ti, Rb and Ba. These differences are possibly the result of contamination of the basalt by pumice inclusions, although it is more likely that contamination and assimilation of a crustal source at depth is responsible. There is a marked change in surface geology west of the Kaiapo Fault, and the numerous other faults between there and the Kinloch tuff deposit suggest that tectonic processes could have affected the underlying geology to greater depth (Grindley 1960: Brown *et al.* 1994; Hadfield *et al.* 2001; Hiess *et al.* 2007). The volcanic arc trace element patterns of Kaiapo, Kinloch and Punatekahi match that of other Taupo Volcanic Zone basalts (Gamble *et al.* 1993).

9.2.2 External Water Involvement

9.2.2.1 Role of External Water During Eruption

All four basalt deposits exhibit characteristics that point to involvement of water during eruption. There are several features of deposits that point to an 'active' involvement of water during eruption (that is, a phreatomagmatic eruption with fragmentation induced by magma:water interaction – e.g. Wohletz and Zimanowski 2000). The main features utilised in this study for inferring explosive interaction with water are summarised in **Table 9.4**.

The construction of the scoria cone complex of Punatekahi included little explosive interaction with water. Evidence for interaction with water comes from the ash facies, which contains, along with juvenile scoria, sideromelane (Fisher and Schmincke 1984) and a considerable lithic component of mostly ignimbrite fragments and glass shards (Barberi *et al.* 1989; Wohletz and Zimanowski 2000). The swallow-tail plagioclase and skeletal olivine in the juvenile clasts within that ash could also reflect magma:water interaction (Shelley 1993).

There is also evidence for possible active magma:water interaction in the thin-medium bedded lapilli facies of the northernmost site at Punatekahi A. There, blocky, hydrothermally-altered scoria containing rarely-quenched plagioclase and olivine phenocrysts form finer-grained, moderately to poorly sorted beds. There is a noticeable lack of lithic material though, which could be explained by interaction with water that lay close to the surface (Allen *et al.* 1996; Németh and White 2003), but the quench textures and finer grain size can be explained through waning eruption conditions (A. Pittari pers. comm. 2010), suggesting that hydrothermal alteration was post-depositional.

Table 9.4 The key features used in this study for determining explosive magma:water interaction.

Feature	Inference	Key Reference(s)
Deposit:		
Base surge	Phreatomagmatic explosion	Sheridan and Wohletz 1981; Cas and Wright 1987
Bed:		
Lithic component > 5 %	Magma fragmentation is sub-surface	Barberi *et al.* 1989
Armoured lapilli	Environment was sticky/wet allowing ash to adhere to clast	Allen *et al.* 1996; White 2000
Sideromelane	Rapid cooling of basalt before crystallisation can begin	Fisher and Schmincke 1984;
Poor Sorting	Fragmentation of more than just magma (i.e. wall rock)	Walker and Croasdale 1971
Fine grain size	More efficient fragmentation	Walker and Croasdale 1971; Houghton and Gonnermann 2008
Clast:		
Blocky morphology	Clasts were cold prior to flight through air and contact with ground	Wohletz 1983
Low vesicularity	Vesiculation of magma is halted due to cooling and fragmentation by external water	Houghton and Wilson 1989; Houghton *et al.* 1999
Quench textures on minerals	Rapid cooling of basalt	Shelley 1993

Indication of explosive interaction at the other three volcanic centres of Acacia Bay, Kaiapo and Kinloch is much greater. Each of the three deposits are

comprised of a significant base surge component and nearly all of the samples were found to contain sideromelane, arguably two of the strongest indicators of explosive magma:water interaction (Fisher and Schmincke 1984). The relative water content of the surges (wet or dry) can be estimated by the features found within the base surges. Wet surges, which are formed with cooler water (in a liquid phase), are identifiable from being matrix-rich, with vesicles, contain accretionary lapilli and armoured lapilli, and typically have massive or planar bedding (often disturbed) that can stick to steep-sided structures (Sheridan and Wohletz 1981; Frazzetta *et al.* 1983; Allen *et al.* 1996; Brand and White 2007; Gençalioğlu-Kuşcu *et al.* 2007; Gisbert *et al.* 2009). Dry surges, which are formed with superheated steam (gas phase only), form unconsolidated, clast-supported deposits, which tend to be well-bedded, and often exhibit reverse grading, reflecting grain dispersal processes (Sheridan and Wohletz 1981; Sheridan and Wohletz 1983; Wohletz 1983; Sohn and Chough 1989; Allen *et al.* 1996).

Kaiapo has a mixture of matrix-supported base surge deposits containing armoured lapilli and disturbed bedding in the basal part of the deposit, and drier, clast-supported, well-bedded base surge deposits. The Kinloch deposit shows erosional channels in well-bedded, clast-supported layers (dry surge) that alternate with finer-grained, vesiculated tuffs that indicate emplacement by wet surge. Acacia Bay appears to have a dominance of dry base surges, as most of the layers are clast-supported.

As Sohn (1996) has noted, the correlation of types of base surge and deposit type (cone versus ring) with water:magma ratio is common (following work by e.g. Sheridan and Wohletz 1983; Frazzetta *et al.* 1983; Kokelaar 1986), but the resulting surge type reflects more than simply the relative amounts of water and magma, instead suggesting that morphological variations are the dominant control. **Figure 9.4** shows an estimation of the water:magma ratios for the four basalts examined in this study using the correlation diagram of Morrissey *et al.* (2000) (see **9.2.3.2** for discussion of eruption styles).

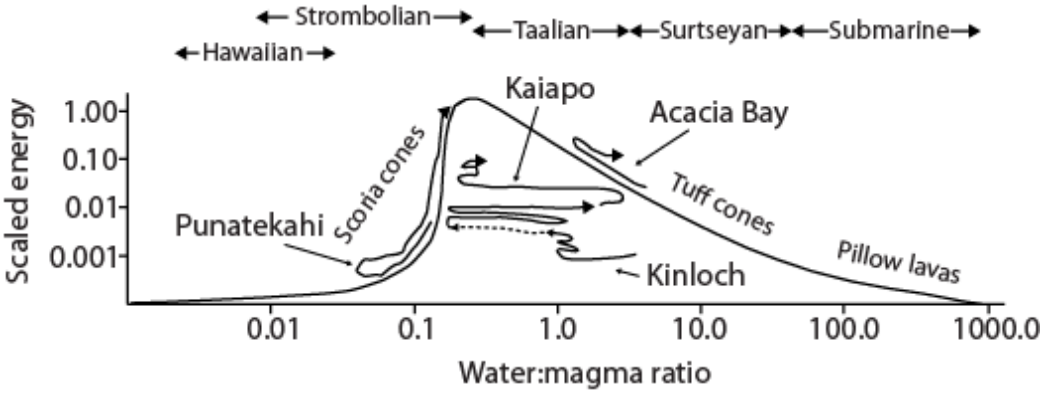

Figure 9.4: Water:magma ratio diagram with suggested variation in the course of the four basalts added (modified from Morrissey et al. 2000).

Using **Figure 9.4**, the water:magma ratios of the four basalts' eruptions are as follows: ~ 0.05 to 0.3 for Punatekahi, ~ 0.2 to 5 for Kaiapo and Kinloch, and ~ 2 to 5 for Acacia Bay. It is clear that assessing water:magma ratios using the vague parameters of landform and eruption style is inaccurate (following Sohn 1996; White 1996), but enables a comparison of 'wetness' of the eruptions. From this it follows that the eruption(s) at Punatekahi were the 'driest' and the eruption at Acacia Bay was the 'wettest', with the Kaiapo and Kinloch eruptions having similar, intermediate 'wetness'.

As demonstrated by Befus *et al.* (2009) and the occurrence of pillow lavas (Kokelaar 1986; Palinkas *et al.* 2008) and peperites (e.g. Skilling *et al.* 2002; Befus *et al.* 2009), interaction of magma with water is not always explosive, and Kokelaar (1986) discussed the effect of water depth on explosivity of basalt magma:water eruptions. Given the depths needed to constrain explosivity (possibly 1 km – Kokelaar 1986; **Figure 1.3**), depth was not considered to be a factor for the TVC basalt eruptions. The possibility of subaqueous deposition, however, given the proximity of all of the volcanic centres to the lake at the time of eruption, is a further consideration. Both of the Acacia Bay and Kaiapo tuff rings contain a number of beds with wavy contacts and there are rare occurrences of density grading of pumice, which indicate subaqueous deposition (Brown *et al.* 1994; White 2000). Diatomaceous sediments, which occur as part of a volcaniclastic breccia within the tuff and contain basalt scoria at the two centres, respectively, provide tenuous support to subaqueous deposition (following Cas and Wright 1991). The variable concentration in the basal surges at Kaiapo is further evidence of subaqueous deposition (Sheridan and Wohletz 1983). The

absence of any of these features in the Kinloch tuff, along with its stratigraphic position above well-developed palaeosols, lessens the probability of subaqueous deposition, although it is accepted that a lack of clear evidence for subaqueous deposition is not authoritative, especially given the flame structures evident in the basal bed of the tuff, which can indicate a very shallow subaqueous environment (Brand and White 2007; Brand and Clarke 2009). The lack of evidence for subaqueous deposition higher up in the succession (similar to the case at Kaiapo) suggests that, if present, the (lake) water level was indeed shallow at the time.

9.2.2.2 Source of External Water

Trying to identify the source of external water from deposit information is complicated by two factors: 1) little work has been done on distinguishing volcanic deposit features between surface and ground water sources (see **1.4**);
2) little is known regarding the subsurface geology of the Taupo region, being mostly restricted to discoveries from geothermal drilling (e.g. Browne *et al.* 1992). All of the basalt deposits' proximity to past or present lake boundaries (Manville and Wilson 2004) means that the source of external water during eruption could have been lake and or ground water. For the Acacia Bay and Kaiapo deposits, the inference of subaqueous deposition (see **9.2.2.1**) denotes the lake as a source of water. The juvenile clasts of Acacia Bay samples contain a significant green, quenched juvenile basalt component, likely to be sideromelane, given the similarity with clasts in thin section. Interestingly, though, these clasts are typically more vesicular than the accompanying scoria. Magma:water interaction should lead to lower vesicularity than is evident in these clasts (Houghton and Wilson 1989), therefore one way to explain the nature of these clasts is quenching following magmatic fragmentation. Vesicular sideromelane has been associated with submergent volcanoes (Fisher and Schmincke 1984), lending support to the lake being a source of water.
The Kinloch tuff, in comparison, has little evidence for subaqueous deposition, and has a relatively high lithic content (although this has been skewed by aggregate lithics – **9.2.1.4**), which indicates magma interaction with groundwater was the dominant magma:water interaction that took place (Barberi *et al.* 1989; Carey *et al.* 2007). The abundance of spherulitic rhyolite in the Kinloch tuff

samples suggests that fragmentation occurred within rhyolite situated close to the tuff deposit (following e.g. Barberi *et al.* 1989; Martin and Németh 2005). Abundance of one type of lithic can point to weakness of conduit wall rock (Carey *et al.* 2007), but this is considered unlikely due to the indurated nature of the rhyolite.

In contrast with the Kinloch centre, the other volcanoes have evidence of explosive magma:water interaction involving an ignimbrite groundwater source. The tuff deposits at Acacia Bay contain lithics and xenocrysts that match well with those found in the Rangatira Ignimbrite (as described by Cole *et al.* 1998), as do brown lithic blocks from within the lapilli- and bomb/block-rich facies, suggesting fragmentation from within the Rangatira Ignimbrite. The best known surface exposure of the Rangatira Ignimbrite lies close to the Acacia Bay deposit, strengthening the likelihood that this inference is correct. At the K-Trig volcanoes of Kaiapo and Punatekahi, the source is less clear, although there is also an abundance of glass shards and lithic rock fragments that are similar to that found at Acacia Bay, leaving open the possibility that the Rangatira Ignimbrite was also the source of water for the Kaiapo and Punatekahi eruptions. Smith (1990) proposed that the pumice horizon within the Waiora Formation (which includes the Rangatira Ignimbrite – Brown *et al.* 1994) was one of the groundwater sources for the Kaiapo eruption. The high pumice content found in the basal beds of the Kaiapo deposit could also, however, be from the pumice-rich Unit J of the Huka Falls Formation (Henley and Stewart 1983). The Huka Falls Formation outcrops near the studied area at Kaiapo (Grindley 1960; Smith 1990; Brown *et al.* 1994; Hadfield *et al.* 2001) and the lake sediments at the site support lake sediment as a water source.

9.2.3 Eruption Characteristics

9.2.3.1 Eruption Mechanisms

The mechanics of magma fragmentation during an eruption can be either magmatic or phreatomagmatic. Magmatic fragmentation is driven by exsolution of volatiles out of the magma as a consequence of a change in pressure, and occurs when bubbles rupture from excess strain (Houghton and Wilson 1989;

Cashman *et al.* 2000). In contrast, phreatomagmatic eruptions *sensu lato* (e.g. Lorenz 1987; Starostin *et al.* 2005) occurs when ascending magma interacts with external water, which causes heating and rapid vaporisation and expansion of the water, leading to brittle fragmentation of the magma (e.g. White 1996; Wohletz and Zimanowski 2000). This process, termed (Molten) Fuel-Coolant Interaction (FCI or MFCI; White 1996; Wohletz and Zimanowski 2000; Rosseel *et al.* 2006; Grunewald *et al.* 2007; Befus *et al.* 2009), interrupts magmatic fragmentation and, due to the violent water expansion phase, results in a more explosive eruption style. The main difference between magmatic and phreatomagmatic eruptions is therefore the presence of external water (Sheridan and Wohletz 1983), although not all eruptions where water is present results in a phreatomagmatic eruption, due to such factors as volume of water relative to magma, water depth, timing of interaction and density and viscosity contrasts between water and magma (Kokelaar 1986; White 1996; Wohletz and Zimanowski 2000; Skilling *et al.* 2002: Mastin *et al.* 2009). The products of magmatic eruptions are typically well sorted, thick, coarse-grained, clast-supported, and scoriaceous, and lava flows are also commonly present (Walker and Croasdale 1971; Wilson and Head 1989; Carey *et al.* 2007; Houghton and Gonnermann 2008). Phreatomagmatic eruptions, in comparison, are relatively poorly sorted, fine-grained, matrix- or clast-supported (Walker and Croasdale 1971; Allen *et al.* 1996; Houghton and Gonnermann 2008). Lava flows are absent, beds are often thin and, as well as scoria, sideromelane (quenched basaltic glass), accretionary lapilli, and significant wall rock lithics are typically found (Sheridan and Wohletz 1983; Wohletz and Zimanowski 2000; Martin and Németh 2005). The dominance of lateral transportation and emplacement processes associated with phreatomagmatic eruptions also leads to bed structures such as cross-bedding and erosional channels, and pinch-and-swell geometries (Sohn and Chough 1989; Brown *et al.* 1994; Houghton *et al.* 1999; Brand and Clarke 2009). Using these distinguishing features as a guide, the scoria cone complex of Punatekahi, which is dominated by thickly-bedded scoria deposits with a scarcity of lithic components and contains several lava flows, has been formed predominantly by magmatic fragmentation mechanisms. At the three other sites of Acacia Bay, Kaiapo, and Kinloch, the beds have an ubiquity of sideromelane, are typically poorer sorted and are finer-grained than Punatekahi (see. **Figure 9.1**). The beds also have a much higher

lithic content (**Table 9.1**) and sedimentary structures such as cross-bedding, erosional channels, and are often laterally discontinuous, which point to phreatomagmatic mechanisms as being dominant. The fine-grained, basalt-free layers at Kinloch also suggest a small amount of phreatic activity (Sheridan and Wohletz 1983; Nairn *et al.* 2005; Ohba and Kitade 2005), which is not found at any of the other sites. As has been noted, however, the transition between magmatic and phreatomagmatic is not fixed, and the above-mentioned characteristics of such eruption mechanisms are more accurately end-members on a continuum (Houghton *et al.* 1999), where small changes in eruption conditions (for example, magma ascent rate) can cause sharp transitions in eruption mechanism (e.g. Houghton and Schmincke 1986; Ort and Carrasco-Núñez 2009). Although Punatekahi is dominated by magmatic fragmentation, the presence of a lithic-rich ash facies containing small amounts of sideromelane in the highest part of the complex indicates that MFCI also played a role during the later stages of eruption. Likewise, the relatively lithic-poor coarse-grained lava balls of Kinloch and the well sorted lapilli fall deposits of Kaiapo have a mix of both traditionally magmatic and phreatomagmatic characteristics. The presence of sideromelane indicates magma:water interaction (Fisher and Schmincke 1984), but this is very low, and the presence of lithics could be explained in part by weak conduit wall rock (Carey *et al.* 2007), with the implication that these fall products of Kinloch and Kaiapo are borderline magmatic-phreatomagmatic. Given the growing acknowledgement that resulting deposits and characteristics are a function of more than purely magma:water ratios (Sohn 1996), and that MFCI cannot accurately account for the complex processes that occur during phreatomagmatic eruptions (White 1996; Mastin *et al.* 2009), establishing the exact cause for these deposits' characteristics is problematic.

9.2.3.2 Eruption Styles

Eruption of basalt magma is typically divided into the magmatic styles of strombolian and hawaiian, and the phreatomagmatic style of surtseyan (e.g. Wohletz 1983; Hougton and Gonnermann 2008). Strombolian eruptions involve intermittent bursts of fragmentation of lava material as a result of movement of gas 'slugs' that move up the conduit, resulting in eruption of coarse scoria, bombs

and solidified lava lake slabs (Houghton and Schmincke 1989; Parfitt 2004; Houghton and Gonnermann 2008). The production of finer ash is controversial and not traditionally associated with strombolian eruptions (Houghton and Gonnermann 2008). Recent observations of Etna and Stromboli, however, included production of ash plumes (Riedel *et al.* 2003; Patrick *et al.* 2007), and deposition of ash up to tens of kilometres from a cinder cone has been identified at several South American volcanoes, including Cerro Negro (Riedel *et al.* 2003). Production of fine ash has been attributed to 'violent' strombolian eruptions (Riedel *et al.* 2003; Martin and Németh 2006; Valentine and Gregg 2008; Di Traglia *et al.* 2009), but recent research by Patrick *et al.* (2007) provides evidence that fine ash falls are a second type ('Type 2') of normal strombolian activity. The formation of finer ash can result from less energetic explosions (Patrick *et al.* 2007) or vent-clearing of slump material (Houghton and Schmincke 1989; Riedel *et al.* 2003). An hawaiian eruption style, in contrast to strombolian, occurs when gas moves freely up through the eruption column in a continuous manner, resulting in fountaining of finer blobs of lava that are often shaped during flight through the air (Head and Wilson 1989; Parfitt 2004; Houghton and Gonnermann 2008). Lava flows can result when discharge rates exceed cooling rates of the ejected lava, so that clasts remain molten at deposition, meld and mobilise (clastogenic lava flow), or lava can flow straight from the vent (Fisher and Schmincke 1984; Cas and Wright 1987; Wilson and Head 1989; Riggs and Duffield 2008; Valentine and Gregg 2008). A change in eruption style from strombolian to hawaiian during a single eruption is a common occurrence (e.g. Houghton *et al.* 1999). An increase in magma ascent rate can cause an eruption style to change from strombolian to hawaiian by affecting the ability of gas bubbles to coalesce and form slugs (Houghton *et al.* 1999; Parfitt 2004; Houghton and Gonnermann 2008), although viscosity of magma and fragmentation efficiency are also cited as points of difference between the two eruption styles (Houghton and Gonnermann 2008; Valentine and Gregg 2008; Di Traglia *et al.* 2009). A change between eruption styles may be able to be inferred from a change in deposit features and characteristics such as grain size (Houghton and Gonnermann 2008), but deposits from hawaiian and strombolian eruptions are not mutually exclusive (Riedel *et al.* 2003; Valentine and Gregg 2008). Punatekahi, which is a scoria cone complex, has evidence of both strombolian and hawaiian

eruption styles during the construction of the cones. The bedded and massive/crudely bedded facies (representing outer and crater sections of the cone) (Houghton and Schmincke 1989), are dominated by irregular, ragged scoria lapilli, with significant breadcrust bombs and lava slabs, consistent with a strombolian eruption. The coarse ash that often separates the coarser-grained beds, following Riedel *et al.* (2003) and Patrick *et al.* (2007), are here interpreted to also indicate strombolian activity. The cone also contains several lava flows, likely a mixture of clastogenic and vent-fed lava flows, given the vesicularity and visible clast outlines, and evidence of lava lake breaching (respectively) (Head and Wilson 1989; Németh and White 2003; Riggs and Duffield 2008). The clastogenic lava flows, at least, indicate hawaiian activity. The fact that (welded) lava beds are found at different stratigraphic levels throughout the cone complex suggests ongoing fluctuations in eruption conditions such as magma ascent rate and hence eruption style (Parfitt and Wilson 1994). The presence of the phreatomagmatic ash points to a further eruption style at Punatekahi.

Basaltic phreatomagmatic eruption styles are commonly referred to as surtseyan, in a similar vein to how phreatomagmatic has become synonymous with eruptions involving magma interaction with water (Wohletz 1983; Lorenz 1987; Houghton *et al.* 1999). A surtseyan eruption *sensu stricto* is where bulk interaction of magma with a slurry of water and unconsolidated sediment (and later, recycled erupted clasts) results in steam explosivity (Kokelaar 1986). A continuous magma supply leads to uprush activity, and intermittent supply causes tephra jets (Kokelaar 1986; Sohn 1996). Surtseyan eruptions produce a large amount of tephra, most of which accumulates close to the vent to build up a tuff cone (Kokelaar 1986). As pointed out by Kokelaar (1986), observed eruptions at Surtsey were predominantly subaqueous and did not produce many base surges (cf. Sheridan and Wohletz 1983). More violent explosions, which can occur on land, and involve magma:water interaction at depth, with little jetting and major base surge production, differ markedly from the 'surtseyan' style of eruption (Kokelaar 1986; although underlying processes may not – White 1996). Tuff rings result, but maars are also common, and juvenile content can be low (Kokelaar 1986). This eruption style is commonly referred to as taalian, following observation of Taal in 1965 (Kokelaar 1986).

The Acacia Bay deposit is thin and extends laterally for almost 1 km, and is comprised mostly of bed surges, which would suggest a taalian eruption. However, there are several features of the deposit that indicate surtseyan activity. These include the highly vesicular, quenched juvenile clasts, which have been associated with submergent volcanoes (Fisher and Schmincke 1984), and the subaqueous eruption environment, inferred from the wavy contacts, pumice horizons and volcaniclastic breccia (containing indurated diatomaceous mudstone) (Brown *et al.* 1994; White 2000). It therefore seems probable that the eruption at Acacia Bay involved both surtseyan and taalian styles of eruption.

The extensive tuff ring deposit at Kaiapo is dominated by a succession of base surges, with minor fall and initially very high lithic values, which therefore signifies a taalian eruption style, rather than surtseyan. The evidence for subaqueous deposition, though (see. **9.2.2.1**), is more compatible with surtseyan style of eruption (Kokelaar 1986), but this can be explained by a relatively shallow water depth. Indeed, higher up in the Kaiapo stratigraphy, evidence for subaqueous deposition disappears (see **9.2.2.1**). However, it is very likely that surtseyan activity also occurred at Kaiapo (as proposed by Smith 1990 and Brown *et al.* 1994), given the presence of surface water, but this was probably restricted to the initial eruption phases.

The phreatomagmatic ash at Punatekahi, which involved interaction with groundwater in a dry environment, without the formation of base surges, is technically neither surtseyan nor taalian (Kokelaar 1986), but can only be referred to as a short-term phreatomagmatic phase interrupting hawaiian/strombolian activity (following Houghton *et al.* 1999). Like Punatekahi, it is inferred from lack of wavy bedforms, pumice concentrations and freshwater indicators (such as diatoms) that the eruption of Kinloch was not subaqueous (Brown et al. 1994; White 2000). The implication is that the Kinloch basalt eruption is also technically not surtseyan. The volumetrically significant base surge component suggests instead a taalian type of eruption (Kokelaar 1986). The lava balls of the bomb- and block-rich facies, however, is unusual in its mixture of round morphology, coarse grain size and poorly sorted, unconsolidated bedding, which suggests underlying processes of an, as of yet, undefined eruption style.

9.2.3.3 Emplacement Processes

Emplacement of erupted material is either via fall or lateral transportation along the ground. Emplacement by fall can be classified as being one of the following three types:-

- ballistic: clasts are deposited proximal to the vent, where explosive energy is too low to form buoyant plumes, which is common in basalt eruptions given the relatively low viscosity and gas content of magma that reaches the surface (Patrick *et al.* 2007; Houghton and Gonnermann 2008: Namiki and Manga 2008), or pyroclasts are too heavy to be transported higher above the gas thrust region, being decoupled from the gas phase (Cas and Wright 1987; Riedel *et al.* 2003);
- plume: finer clasts are forced up into the atmosphere above the jet thrust region and are carried to more distal regions, with distance being related to clast-support envelopes based on power of eruption and density of the clasts (Riedel *et al.* 2003);
- surge fall: pyroclasts fall out of a base surge's accompanying cloud (from separation of denser and more dilute components), either simultaneously or following surge emplacement, depending on distance from the vent (Cas and Wright 1987; Sohn and Chough 1989). Similar to this is fallout from surge travelling across a water surface in subaqueous environments (White 2000; Brand and Clarke 2009).

Fall deposits tend to mantle existing topography, form a continuous layer, are grain-supported, moderately to well sorted, show reverse or normal grading and lack sedimentary structures such as cross-bedding (Fisher and Schmincke 1984; Sohn and Chough 1989; Martin and Németh 2005; Houghton and Gonnermann 2008). At Punatekahi, the magmatic fall deposits are clearly distinguishable as they form reverse-graded, well sorted, beds that have a typically continuous thickness. The presence of lava slabs reflects ballistic emplacement of a fragmented solidified lava lake cap (Houghton and Schmincke 1989). The finer, coarse ash that forms thin beds between the layers, which are similar in all respects except grain size, are also interpreted as being fall deposits, although it is possible that they represent fall from plumes. Distinguishing between fall and flow deposits of phreatomagmatic eruptions is more complex than for magmatic

eruptions, especially in proximal settings, where both fall and flow deposits can have planar contacts, without sedimentary structures (Fisher and Schmincke 1984; Cas and Wright 1987), and often classifying a bed as being emplaced by fall or flow is an arbitrary one (Zanon *et al.* 2009). At each of the three phreatomagmatic centres, emplacement of pyroclasts by fall is inferred to be insignificant relative to flow. At Acacia Bay, a relatively thick bed within the coarse ash facies that exhibits normal grading in an otherwise massive, weakly unimodal, grain-supported bed is interpreted as a fall deposit (Sohn and Chough 1989). Several of the thinner, finer-grained grain-supported beds within the alternating ash/lapilli facies, exhibit a mantling topography that is also indicative of fall emplacement. These beds, which alternate with thicker flow deposits (as described below), most likely represent coeval surge ash fall (Sohn and Chough 1989). At Kaiapo, fall deposits were identified within all but the indurated stratified lapilli-rich facies and the poorly-bedded facies. Coeval surge ash fall within the alternating lapilli-rich facies is inferred from the presence of thin, unconsolidated, better sorted beds amongst matrix-rich, poorly sorted surge deposits (Sohn and Chough 1989). Density grading possibly indicates fall emplacement simultaneous with flow in the indurated coarse ash and lapilli facies, whilst ballistic fall in both the indurated alternating lapilli-rich facies and well-stratified ash-lapilli facies is indicated by the good sorting, coarse grain size, and clast-supported fabric of the beds. Kinloch contrasts strongly with Kaiapo, in that only three beds in the section are identifiable as having been emplaced by fall. The first is in the basal part of the alternating coarse ash/lapilli facies, being a well-sorted, laterally continuous bed with a high juvenile content (Brand and White 2007). The other two beds belong to the bomb- and block-rich facies, inferred to be from ballistic fall due to the coarse size of the rounded clasts and the open framework (Sohn and Chough 1989; Allen *et al.* 1996; Brand and White 2007; Gençalioğlu-Kuşcu *et al.* 2007). The other coarser-grained beds within the alternating facies at Kinloch have the appearance of a series of fall deposits, except for the erosional U-shaped channels and low-angle cross-bedding that characterise the base of the beds (Sheridan and Wohletz 1983; Brand and White 2007). However, given the inferred proximity of the Kinloch tuff deposit to the vent, a greater volume of fall deposits might be expected (Kokelaar 1986), so it is possible that some of the unchannelised beds represent fall. Another possibility is

that the vesiculated tuffs are actually fine-grained tephra fall, with the vesicles resulting from wet material that did not undergo significant lateral movement (Kokelaar 1986).

Laterally transported deposits, in comparison with deposits emplaced by fall, are topographically controlled, and in the case of base surges, thin rapidly with distance from the vent, have relatively poor sorting, and can be matrix-supported (Fisher and Schmincke 1984; Sohn and Chough 1989; Allen *et al.* 1996). Deposits of basalt eruptions can be emplaced by two broad types of flow, relating to degree of water involvement (e.g. Cas and Wright 1987):-

- lava flow: results from overflow of a lava lake, breach of cone holding lava, or rapid accumulation of spatter from lava fountains that meld and form a flow (clastogenic lava flow; Fisher and Schmincke 1984; Cas and Wright 1987; Head and Wilson 1989; Riggs and Duffield 2008; Valentine and Gregg 2008);
- base surge: radially-expanding cloud and slug of water, lithic rocks and (usually) juvenile basalt that originates directly from the vent (lateral blast) or collapse of an eruption column that is too dense to rise above the jet thrust region (Sheridan and Wohletz 1983; Kokelaar 1986). A base surge can be 'wet' or 'dry', depending on temperature (and phase) of the water in the eruption mixture (Sheridan and Wohletz 1981, 1983).

At Punatekahi, both lava lake-derived and fountain-derived, clastogenic lava flows occurred. The evidence for this assessment is the presence of jointed, welded beds that either join directly to remnants of lava lakes or are variably vesicular and show clast outlines (Cas and Wright 1987; Németh and White 2003; Riggs and Duffield 2008; Valentine and Gregg 2008). At Acacia Bay, Kaiapo and Kinloch, emplacement via base surge is inferred from the presence of diffuse bedding, cross-beds/-laminations, erosional channels, pinch-and-swell or channelised geometries (Sohn and Chough 1989). At Kaiapo, there is dominance of matrix-supported, variably-concentrated beds in the lower facies, implying emplacement by wet surges (Sohn and Chough 1989; Brown et al. 1994; Allen *et al.* 1996). Higher up in the eruption stratigraphy, surges become more grain-supported and fall deposits also increase, suggesting dry surges (Frazzetta *et al.* 1983; Allen *et al.* 1996; Zanon *et al.* 2009). At Acacia Bay nearly all of the base surges are grain-supported, indicating emplacement by dry surge (Allen *et al.*

1996). Most of the base surges at the southern deposit (Acacia Bay South) are diffusely bedded, although some ripple and cross-bedding is evident, and one thicker bed containing lithic blocks that exhibits wedge-shaped geometry with rapid thinning along the outcrop. These features indicate that the deposit is very close to the vent (Cas and Wright 1987; Allen *et al.* 1996). The lower facies of the tuff deposit at Kinloch is also comprised predominantly of dry or relatively dry (following Allen *et al.* 1996) base surges based on the observation of clast-supported beds and low sideromelane: scoria ratios (**Appendix E**). The finer-grained beds, however, rarely contain larger lapilli fragments (therefore matrix-supported) and are vesicular, indicating wetter conditions (Fisher and Schmincke 1984; Kokelaar 1986; Brand and Clarke 2009). No thinning of beds is visible at Kinloch, although U-shaped channels and the massive or diffuse bedding that typifies the beds indicates that, like at Acacia Bay, the deposit is close to source (Sheridan and Wohletz 1983; Chough and Sohn 1990; Allen *et al.* 1996; Sohn 1996). In contrast, the well-developed planar beds and cross-laminations found at Kaiapo suggest more of a medial setting (Sohn 1996; Martin and Németh 2006; Di Traglia *et al.* 2009; Zanon *et al.* 2009).

9.2.4 Eruption Models

The previous sections illustrate that each of the sites represent unique eruption conditions. A separate eruption model for each of the four sites will be presented, taking into account previously discussed data.

9.2.4.1 Acacia Bay

Eruption at Acacia Bay is considered to have been triggered by movement of basaltic lava through a NNE-trending fault underneath Lake Huka (**1** – see **Figure 9.5**). Vesiculation of magma was halted by explosive interaction of magma with groundwater in the Rangatira Ignimbrite (**2**). The mixture of rock, lake sediment, magma and steam intersected lake water during rapid ascent, quenching basalt along the margins of the ascending material, and forming fall deposits. This was subsequently followed by production of dry base surges (**3**). Partway through the eruption, fragmentation occurred within consolidated lake sediment, as a result of

vent migration or change in fragmentation depth (**4**). Eruption conditions became unstable either due to water supply, magma ascent rate, or changes in vent geometry, with several thinner base surges and some coeval fall. The final phase of the eruption involved a reversion to more stable, magmatic-rich conditions, with thicker, coarser dry surge and fall production.

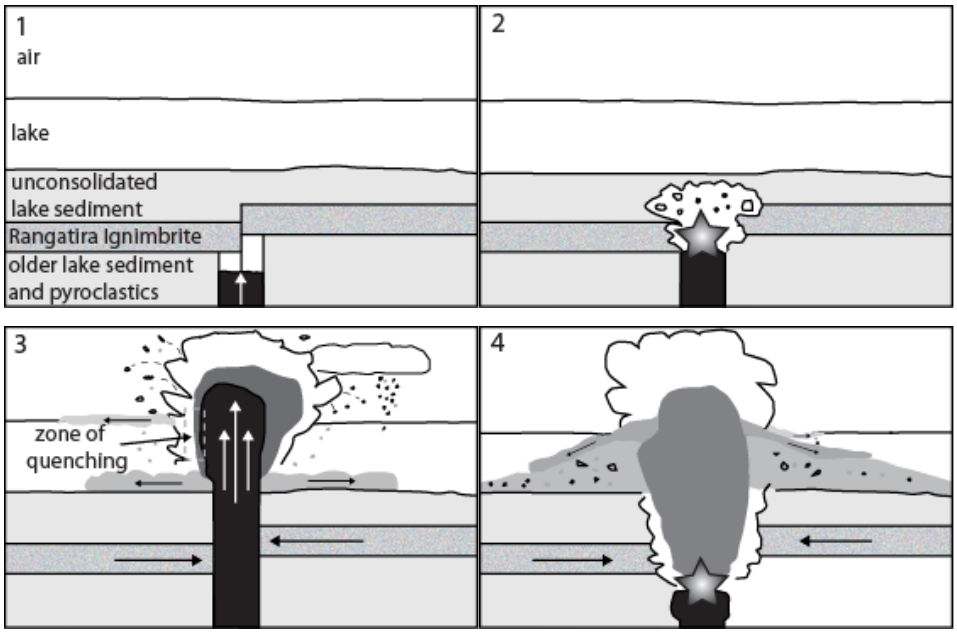

Figure 9.5: Schematic of basalt eruption at Acacia Bay. Explanation in text.

9.2.4.2 Kaiapo

The eruption at Kaiapo has several possibilities with regard to eruption model, regarding aquifers (and fragmentation level). Smith (1990) originally proposed that fragmentation initially occurred in the Waiora Formation, and then at a shallower level met with water-saturated lake sediment. This model is retained here, except that the fragmentation dominantly occurred from contact with the lake sediment, with the high pumice content being derived solely from the sediments. The possibility of more than one vent during eruption has not been previously discussed, although the onlapping of later eruption stages on what looks like vent debris also leaves that as another viable option. For simplicity, an eruption model without vent migration is presented in **Figure 9.6**. The initial phase of eruption began with ascent of magma along the Kaiapo Fault. This magma, water and rock mixture mixed with saturated semi-consolidated lake sediment (**1 – Figure 9.6**). The water within the lake sediment resulted in

phreatomagmatic eruption of the material, forming subaqueous base surges (subaqueous eruption-fed density currents – White 2000) with coeval fall, which was deposited in shallow lake water (**2**). The majority of coeval fall was displaced by subsequent surges. As the eruption progressed, the thickness of deposits around the vent exceeded lake level, leading to drier surges and a larger ballistic fall component. Fragmentation level also dropped, causing the rupture of another, harder aquifer (**3**), which produced a vent-clearing phase. The resulting base surges were relatively dry, and coarse ballistic fall deposits became common, a consequence of reduced water:magma interaction, with fluctuations between surge and fall reflecting changes in water supply or magma ascent rate (**4**).

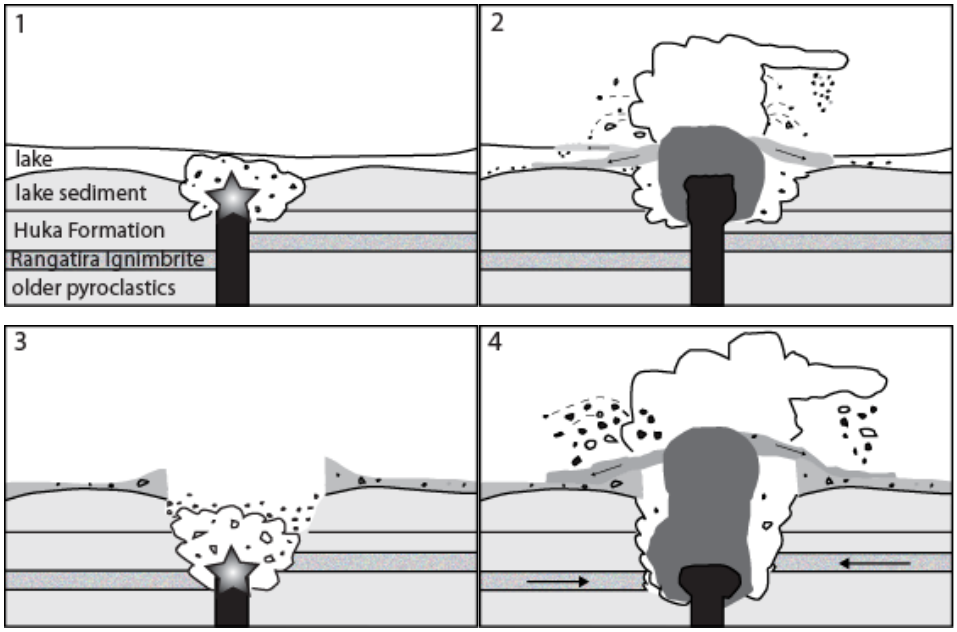

Figure 9.6: Schematic of basalt eruption at Kaiapo. Explanation in text.

9.2.4.3 Kinloch

The eruption at Kinloch began with rise of magma within a rhyolite dome along a fault, probably the Whangamata Fault (**1** – **Figure 9.7**). During ascent, the magma came into contact with groundwater (either along a fault or in fractures in the dome), causing brittle fragmentation of the magma. Once the magma reached the surface, the rock, water an d magma hit very shallow lake water, which quenched a small portion of the basalt (**2**). A base surge with coeval ash fall was produced. The initial surge was deposited along the lake margin, with the fall forming flame structures. The rupture of the aquifer caused a strong head

gradient, leading to increased flow toward the conduit (indicated by arrows), resulting in a series of 'wet' surges. Consequent changes in 'wetter' and 'drier' surges resulted from subtle changes in magma ascent rate, accompanied by drier eruption conditions from the depletion of lake water. The heat of the basalt caused partial melting of the rhyolite in the dome, which assimilated with the basalt. It is also possible at this time that hydrothermal circulation was initiated, causing phreatic explosions. A period of quiescence followed, allowing material in the conduit to degass and partially solidify (**3**). At depth, magma began to vesiculate. Pressure built up, eventually forcing the magma to the surface, interacting with external geothermal groundwater, excavating more rhyolite and extruding the older magma (**4**). The excavation of more rhyolite allowed greater water movement, resulting in wetter surges.

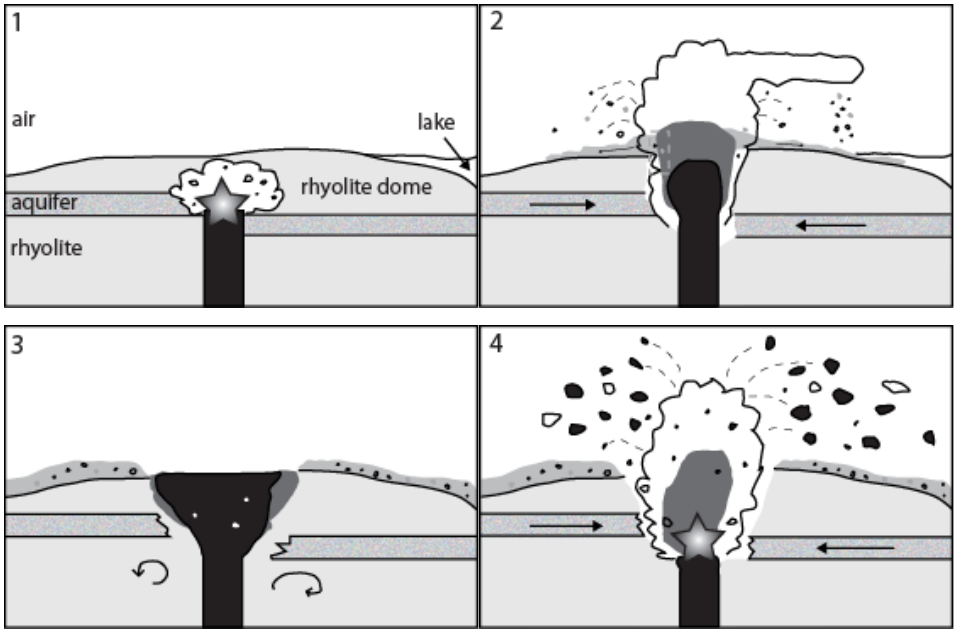

Figure 9.7: Schematic of basalt eruption at Kinloch. Horizontal arrows = groundwater movement, circular arrows = hydrothermal circulation. Explanation in text.

9.2.4.4 Punatekahi

At Punatekahi, the eruption was initiated by magma ascent along the Kaiapo Fault (Brown 1990; Brown *et al.* 1994). The first stage of eruption involved concurrent eruption from two vents (**1 – Figure 9.8**), possibly via intrusion of a shallow dike (Houghton *et al.* 1999). Intermittent strombolian eruptions through solidified lava lake crusts produced lava slabs, whilst a breach in the lava lake wall at Punatekahi

B formed a lava flow. Production of ash plumes were common, relecting more "Type 2" eruptions (Patrick *et al.* 2007), although these abated with time. Intrusion of the magma created a temporary geothermal system (quasi volcanic-hydrothermal system – Hochstein and Browne 2000), which resulted in growth of quartz polymorphs on still-hot erupted clasts in the southern section of the cone. The majority of fragmentation occurred within the cone construct. A period of quiescence followed, with erosion and slumping of material (**2**). Activity renewed further to the north-west, with Punatekahi B and the geothermal system inactive (**3**). Strombolian activity dominated, with production of ballistic scoria lapilli fall through reposes between explosions of up to a few minutes, resulting in lava slab extrusion. It is likely that all fragmentation occurred within the pre-existing construct. Another vent shift came with upwelling of a fresh magma source (**4**). Magma discharge rates were initially rapid, forming welded flows. A waning in magma ascent rate allowed contact and mixing with groundwater, producing a phreatomagmatic ash fall, and creating another temporary geothermal system, which resulted in blocky ballistic fall.

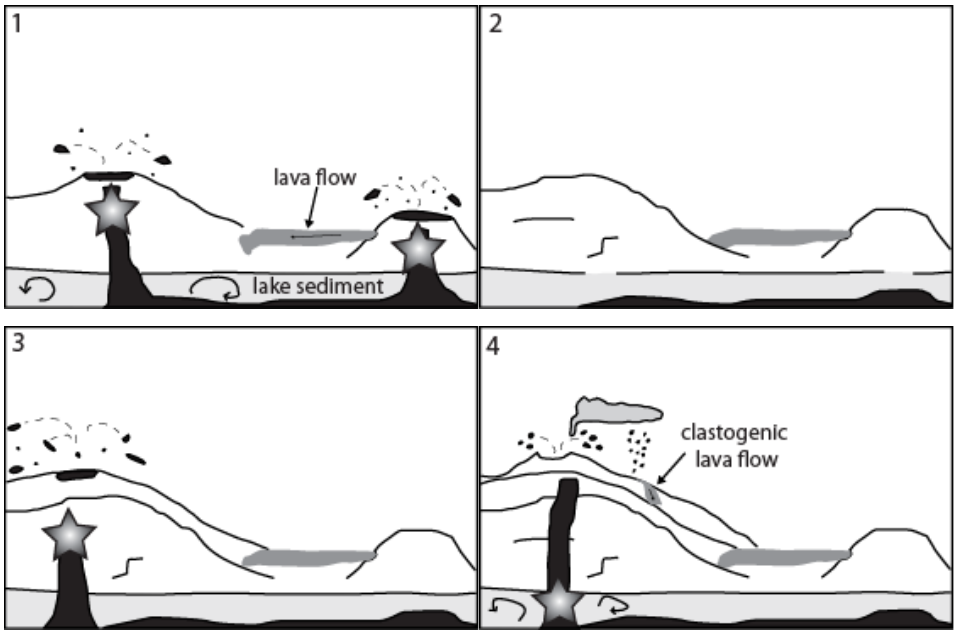

Figure 9.8: Schematic of basalt eruption at Punatekahi. Circular arrows = hydrothermal circulation. Explanation in text.

9.3 Implications for the Taupo Volcanic Centre (TVC)

9.3.1 Volcanological Implications

The tuff deposits at Acacia Bay examined here are different from those studied by Wilson and Smith (1985). The piecemeal nature of the Acacia Bay deposits makes the inference of the relationship with those of Purikaou Bluff difficult, although the massive, thick and coarse-grained beds point to the existence of another, more southern vent in the vicinity of Acacia Bay, several hundred metres to the south-west of that inferred for Purikahou Bluff (Wilson and Smith 1985; **Figure 4.20**). This second vent also produced a phreatomagmatic eruption, but unlike the Purikahou Bluff eruption, pumice does not feature highly in the deposits, and the significant presence of ignimbrite suggests at least some groundwater:magma interaction, although lake water likely also featured in an active role. The implications of a second vent are that Acacia Bay could not be considered a random offshoot of the K-Trig volcanoes, and it is possible that the Acacia Bay deposits form another NE-SW lineament of volcanoes, strengthening the role of faults in the creation of basalt volcanoes in the Taupo Volcanic Centre (Hiess *et al.* 2007). Further work is required, however, to determine the relationship between the deposits.

The K-Trig volcanoes of Kaiapo and Punatekahi have previously been studied (Brown 1990; Smith 1990; Brown *et al.* 1994). Originally, it was proposed that the eruption of Kaiapo was surtseyan, although a maar-type eruption was considered. Smith (1990) decided on a surtseyan eruption type based on the presence of underlying lacustrine sediments (and hence a lake), attributing the very high pumice lithic component in the lower section of the deposit to a pumice-rich horizon in the Waiora Formation (the aquifer). This is a reasonable assumption, although, as discussed in **9.2.3.2**, an initial taalian or maar-type of eruption cannot be ruled out, given that lithic percentages are so high (e.g. Cas and Wright 1987) and underlying lacustrine sediments do not necessarily correlate with the presence of a deep lake at the time of eruption. Initial magmatic fragmentation within a soft substrate, such as unconsolidated wet lake sediments, which would also likely have been rich in pumice (following Henley and Stewart 1983; Nelson and Lister 1995), is also a valid possibility. Greater excavation of

the Punatekahi cone complex due to quarrying has lead to an updating of the history of the volcano. Brown (1990) previously found evidence of only one vent within the quarry, but proposed the existence of another vent ~ 500 m south-east of the main vent based on a lava flow deposit outside of the quarry (not looked at in this study). Possible easterly vent migration during the middle stages of the eruption was also suggested. In contrast, the distribution of facies within the quarry as described here indicates the presence of four different vents, two of which were concurrently active, and two of which point to vent migration. At least one of the vent shifts followed a period of quiescence. Furthermore, Brown (1990) found no evidence of phreatomagmatic activity at Punatekahi, instead merely purporting an initially phreatomagmatic phase based on personal findings of K-Trig and knowledge of the Kaiapo eruption. In this study, a phreatomagmatic ash was discovered near the top of the northernmost part of the Punatekahi A cone. There is also evidence for the existence of a short-lived, ephemeral geothermal system, probably resulting from hot, ascending basaltic magma (Ohba and Kitade 2005).

The Kinloch deposit has important implications for the nature of the chronology of the Taupo Volcanic Centre. From its stratigraphic position, a maximum age of ~ 9.5 ky (given its position above the Opepe Tephra; Wilson 1993; M. D. Rosenberg pers. comm. 2008) makes it the youngest basalt deposit in the TVC by ~ 100 ky. The evidence of such a young basalt eruption proves that basalt eruptions were not confined to late Pleistocene (Houghton *et al.* 1987), but have continued through to the Holocene, meaning that there is the real possibility that basalt could again erupt from TVC, and that the inference of older ages for the other basalts may not be correct. If the inferred age of Acacia Bay at ≤ 200 ky (Wilson and Smith 1985) is correct, and the young age of Kinloch is representative of its associated basalts of Ben Lomond and Marotiri, then it is possible that there is a migration of basaltic activity to the west with time. As far as the rock record shows (Wilson 1993; Sutton *et al.* 1995), eruptions of basalt have occurred within the same geological timeframe as rhyolite. Before the discovery of Kinloch, it might have been plausible to suggest that basaltic volcanism waned as rhyolite eruptions became more explosive, and perhaps was restricted to pre-65 ka (following information from Sutton *et al.* 1995), but the age of Kinloch (< 9.5 ky), although is proof that basaltic volcanism in the TVC has

continued through to the post-Oruanui phase. The finding of melted rhyolite in basalt and basalt balls within a rhyolite block at the base of the Kinloch tuff section indicates a close relationship of rhyolite and basalt at Kinloch. It is possible that the basalt was a trigger for a rhyolite eruption, as was the case for the Kaharoa eruption (Leonard *et al.* 2002), although evidence is not conclusive. The close association does, however, support that there is a link between basaltic and rhyolitic volcanism (Houghton *et al.* 1987). The K-Trig line of volcanoes (including Punatekahi, K-Trig and Kaiapo) do not seem to have any close alignment with rhyolite volcanoes (see **Figure 2.2**), however, and it is possible that the same faulting that removed part of the deposits also removed the associated rhyolites. Another possibility is that the typical spatial and temporal relationship of the basalts with rhyolite is testament to the TVC being a very active volcanic centre and the importance of faults in allowing magma ascent to the surface (e.g. Sutton *et al.* 1995; Hiess *et al.* 2007), rather than there being a special basalt-rhyolite relationship.

The finding of Rangatira Ignimbrite (-like) lithics at all of the eastern sites (Acacia Bay, Kaiapo, Punatekahi) indicates that, although surface exposure of the ignimbrite is minimal (e.g. Cole *et al*. 1998), the ignimbrite was indeed initially widespread, at least as far north as Punatekahi.

9.3.2 Hydrological Implications

The inferred subaqueous deposition of the Acacia Bay and Kaiapo tuffs indicates that the area was covered by a lake at the time of eruption. The inference of a lake presence at Kaiapo has been previously proposed by Smith (1990) and Brown *et al.* (1994). The presence of lake water at Acacia Bay, if the eruption is 100-200 ky cal. B. P. (as inferred for the Purikahou Bluff eruption by Wilson and Smith 1985), fits in well with the configuration of Lake Huka at that time (**Figure 2.3**; Manville and Wilson 2004). At Kinloch, subaqueous deposition is considered possible for the basal beds, thereby leaving open the possibility that the lake boundary was slightly further inland that at present, and that faulting has subsequently uplifted the block west of the Whangamata Fault. This would mean that, although the site of the tuff deposit was mostly subaerial between the breakout floods following the Oruanui (~26.5 ka) and Waimihia (~3.55 ka)

eruptions (as evidenced by the well-developed paleosols in the underlying stratigraphy), there have been slight fluctuations in lake level. The scoria cone complex of Punatekahi has no evidence of the presence of lake water, although the inability to see to the base of the scoria cones prevents a definitive answer. The presence of the scoria cone complex, however, suggests that, if lake water was present at the time of eruption, it would have been very shallow. Brown (1990) and Brown *et al.* (1994) have suggested that the area between Punatekahi and the K-Trig and Kaiapo deposits marks the margin of Lake Huka at ~ 140 ky BP, and evidence from this study is in agreement with this assessment.

In terms of subsurface hydrology, the abundance of Rangatira Ignimbrite (-like) lithics in the deposits of Acacia Bay, Kaiapo and Punatekahi indicates that the Rangatira Ignimbrite is/was a productive aquifer. At Kinloch, the inference is that a groundwater source exists within the spherulitic rhyolite that lies close to the Kinloch tuff. Due to the proximity of the Whangamata Fault to the field site, establishing whether the fault or the rhyolite is the source of water is difficult. The recent hydrological work undertaken in the Kinloch area has established that both the fault and the rhyolite are probable groundwater sources: the Whangamata Fault is a significant groundwater pathway (**Figure 2.4**), whilst Whakaroa rhyolite in the area has fracture-dependent permeability of up to 120 m d^{-1} in (Hadfield 2007). This means that, whilst the inferences made from the Kinloch deposit are therefore not groundbreaking, they demonstrate that, for more recent eruptions, deposits can indeed provide insight into the hydrology of a region.

9.3.3 Hazard Implications

The age of the Kinloch basaltic tuff deposit (< 9.5 ky cal. B. P.) illustrates that there is the real possibility of another basaltic eruption in the future. It is likely that any further eruption will take place along a fault, and, given both the presence of Lake Taupo and the ability of faults to act as a pathway for water (e.g. Bahati *et al.* 2005) and increase permeability in otherwise relatively dense lithologies (Forster and Smith 1989), it is probable that the eruption would be at least partly phreatomagmatic. A phreatomagmatic eruption similar to those inferred from the deposits in this study would produce a mixture of wet and dry base surges accompanied by plume and ballistic fall, with the towns of Kinloch, Acacia Bay

and Taupo (north of Lake Taupo) most likely to be affected. The base surge would be a fast-moving mix of basalt scoria, ash, lithic fragments and steam that could be fatal to anyone within a one kilometre-radius of the vent. Depending on location of the vent, roads could be blocked off, farms could be ruined, power lines knocked down. Ash plumes could initially cause minor disruption of tourist operations in the air and in the lake, and could halt airport activity, with the wet, heavy, ash causing collapse of roofs. Waste water treatment plants could also be affected (Houghton *et al.* 2006). Movement of magma along a fault would likely cause earthquakes, with possible landslides and new geothermal activity, displacing people and property. A magmatic eruption would result in localised ballistic emplacement of scoria. Lava flows could destroy vegetation and block roads, while ash plumes would have a similar impact to that by a phreatomagmic eruption. A more serious implication would be if basalt induced a rhyolite eruption (Houghton *et al.* 1987), which could result in rhyolite lava domes, ash fall and/or pyroclastic flows, with the possibility of a 'super eruption' like that of Taupo 232 A. D

10 Conclusions

The basalts of Acaica Bay, Kaiapo, Kinloch and Punatekahi illustrate the diversity in basaltic volcanism to be found in the Taupo Volcanic Centre (TVC), covering a time range of ~ 200 ky to 9.5 ky and a range of eruption styles (hawaiian to taalian), which reflect both the geological and hydrological setting of the basalts.

The deposits of the four centres reflect the differing degrees of water involvement during each eruption. The scoria cone complex of Punatekahi is dominated by thick beds of coarse-grained, relatively well sorted scoria lapilli beds, intercalated with (typically) clastogenic lava flows, indicative of magmatic strombolian and Hawaiian eruptions (respectively). One bed of lithic-rich ash containing sideromelane near the top of the cone also points to a minor phreatomagmatic eruption phase during construction of Punatekahi. The tuff deposits at Acacia Bay, Kaiapo and Kinloch, in comparison, have a significant base surge component, formed predominantly by phreatomagmatic taalian eruptions. All of the tuff ring deposits show evidence of having been partly subaqueously

deposited, indicating that a) the eruptions were in part surtseyan, and b) that at the time of eruption, the areas were covered by lake water. At Acacia Bay, the lake water was fairly deep, whilst at Kinloch this water was very shallow, representative of a lake margin.

According to lithic components, the basalt eruptions of Acacia Bay,
Kaaipo and Punatekahi all involved explosive interaction with an ignimbrite groundwater source. Given the similarity of lithic components with the Rangatira Ignimbrite (by Cole *et al.* 1998), it is likely that this was the aquifer at those three sites. The Kinloch tuff deposit contains abundant spherulitic rhyolite lithics from the Whangamata rhyolite dome, suggesting that fragmentation occurred within the rhyolite that is ubiquitous in the Kinloch area, rather than the Rangatira Ignimbrite. Both the Whangamata rhyolite and the Whangamata Fault are strong possibilities as the aquifer for that eruption.

The four basalt centres all share a similar mineralogy with phenocrysts of plagioclase, olivine and augite, with augite greater in abundance than olivine in the Kaiapo and Punatekahi deposits. Geochemical analysis shows that Kaiapo and Punatekahi are tholeiitic basalts and Kinloch is a basaltic andesite, with all three basalts being derived from an arc magmatic source.

In addition to differing geochemical characteristics, the Kinloch tuff is anomalous among the four basalt deposits with regard to both its very young age (< 9.5 ky) and its inferred close syn-relationship with rhyolite, by causing melting of the rhyolite that it intruded.

The presence of monogenetic basalts within the TVC rhyolite caldera system (with voluminous plinian and phreatoplinian eruptions forming ignimbrites and rhyolite lava domes) indicates that further unique hazards from magmatic and phreatomagmatic basaltic volcanism need to be considered. The young age of the Kinloch basaltic tuff suggests that further basalt eruptions from the TVC are a real possibility. Given the important role of faults in allowing basaltic magma to ascend to the surface (e.g. Hies *et al.* 2007), it is quite likely that the next eruption will take place along a fault, and closer to the lake, a phreatomagmatic eruption

would be expected, with inland phreatomagmatic eruptions dependent on the presence of permeable aquifers.

References

Abrams, M. J.; Siebe, C. 1994: Cerro Xalapaxco: an unusual tuff cone with multiple explosion craters, in central Mexico (Puebla). *Journal of Volcanology and Geothermal Research 63*: 183-199.

Allen, S. R.; Bryner, V. F.; Smith, I. E. M.; Ballance, P. F. 1996: Facies analysis of pyroclastic deposits within basaltic tuff-rings of the Auckland volcanic field, New Zealand. *New Zealand Journal of Geology and Geophysics 39*: 309-327.

Auer, A.; Martin, U.; Németh, K. 2007: The Fekete-hegy (Balaton Highland Hungary) "soft-substrate" and "hard-substrate" maar volcanoes in an aligned volcanic complex – Indications for vent geometry, subsurface stratigraphy and the paleoenvironmental setting. *Journal of Volcanology and Geothermal Research 159*: 225-245.

Bahati, G.; Pang, Z.; Ármannsson, H.; Isabirye, E. M.; Kato, V. 2005: Hydrology and reservoir characteristics of three geothermal systems in western Uganda. *Geothermics 34*: 568-591.

Barberi, F.; Cioni, R.; Rosi, M.; Santacroce, R.; Sbrana, A.; Vecci, R. 1989: Magmatic and phreatomagmatic phases in explosive eruptions of Vesuvius as deduced by grain-size and component analysis of the pyroclastic deposits. *Journal of Volcanology and Geothermal Research 38*: 287-307.

Befus, K. S.; Hanson, R. E.; Miggins, D. P.; Breyer, J. A.; Busbey, A. B. 2009: Nonexplosive and explosive magma/wet sediment interaction during emplacement of Eocene intrusions into Cretaceous and Eocene strata, Trans-Pecos igneous province, West Texas. *Journal of Volcanology and Geothermal Research 181*: 155-172.

Bibby, H. M.; Caldwell, T. G.; Davey, F. J.; Webb, T. H. 1995: Geophysical evidence on the structure of the Taupo Volcanic Zone and its hydrothermal circulation. *Journal of Volcanology and Geothermal Research 68*: 29-58.

Bradley, R. H.; Witte, L. C. 1972: Explosive interaction of molten metals injected into water. *Nuclear Science and Engineering 48*: 387-396.

Brand, B. D.; Clarke, A. B. 2009: The architecture, eruptive history, and evolution of the Table Rock Complex, Oregon: From a Surtseyan to an energetic maar eruption. *Journal of Volcanology and Geothermal Research 180*: 203-224.

Brand, B. D.; White, C. M. 2007: Origin and stratigraphy of phreatomagmatic deposits at the Pleistocene Sinker Butte Volcano, Western Snake River Plain, Idaho. *Journal of Volcanology and Geothermal Research 160*: 319-339.

Brown, S. J. A. 1990: Strombolian deposits of the K-Trig basalts Taupo. Unpublished B.Sc. (Hons) project, lodged in Geology Department, University of Canterbury. 89 p.

Brown, S. J. A.; Burt, R. M.; Cole, J. W.; Krippner, S. J. P.; Price, R. C.; Cartwright, I. 1998: Plutonic lithics in ignimbrites of Taupo Volcanic Zone, New Zealand: sources and conditions of crystallisation. *Chemical Geology 148*: 21-41.

Brown, S. J. A.; Smith, R. T.; Cole, J. W.; Houghton, B. F. 1994: Compositional and textural characteristics of the strombolian and surtseyan K-Trig basalts, Taupo Volcanic Centre, New Zealand: implications for eruption dynamics. *New Zealand Journal of Geology and Geophysics 37*: 113-126.

Browne, P. R. L.; Graham, I. J.; Parker, R. J.; Wood, C. P. 1992: Subsurface andesite lavas and plutonic rocks in the Rotokawa and Ngatamariki

geothermal systems, Taupo Volcanic Zone, New Zealand. *Journal of Volcanology and Geothermal Research 51*: 199-215.

Büttner, R.; Dellino, P.; Zimanowski, B. 1999: Identifying magma-water interaction from the surface features of ash particles. *Nature 401*: 688-690.

Carey, R. J.; Houghton, B. F.; Sable, J. E.; Wilson, C. J. N. 2007: Contrasting grain size and componentry in complex proximal deposits of the 1886 Tarawera basaltic Plinian eruption. *Bulletin of Volcanology 69*: 903-926.

Carracedo Sánchez, M.; Sarrionandia, F.; Arostegui, J.; Larrondo, E.; Gil Ibarguchi, J. I. 2009: Development of spheroidal composite bombs by welding of juvenile spinning and isotropic droplets inside a mafic eruption column. *Journal of Volcanology and Geothermal Research 186*: 265-279.

Cas, R. A. F.; Wright, J. V. 1987: Volcanic Successions: Ancient and Modern. London, Unwin Hyman. 538 p.

Cas, R. A. F.; Wright, J. V. 1991: Subaqueous pyroclastic flows and ignimbrites: an assessment. *Bulletin of Volcanology 53*: 357-380.

Cashman, K. V.; Sturtevant, B.; Papale, P.; Navan, O. 2000: Magmatic fragmentation. In Sigurdsson, H. (Ed.), Encyclopedia of Volcanoes. San Diego, Academic Press. pp. 421-430.

Charlier, B. L. A.; Wilson, C. J. N.; Lowenstern, J. B.; Blake, S.; Van Calsteren, P. W.; Davidson, J. P. 2005: Magma generation at a large, hyperactive silicic volcano (Taupo, New Zealand) revealed by U-Th and U-Pb systematics in zircons. *Journal of Petrology 46*: 3-32.

Chough, S. K.; Sohn, Y. K. 1990: Depositional mechanics and sequences of base surges, Songaksan tuff ring, Cheju Island, Korea. *Sedimentology 37*: 1115-1135.

Cioni, R.; Sbrana, A.; Vecci, R. 1992: Morphologic features of juvenile pyroclasts from magmatic and phreatomagmatic deposits of Vesuvius. *Journal of Volcanology and Geothermal Research 51*: 61-78.

Clement, A. J. H.; Fuller, I. C. 2007: Fluvial responses to environmental change in the North Island, New Zealand, during the past c. 30 ka recorded in river terrace sequences: a review and model for river behaviour. *New Zealand Journal of Geology and Geophysics 50*: 101-116.

Cole, J. W. 1973: High-alumina basalts of the Taupo Volcanic Zone, New Zealand. *Lithos 6*: 53-64.

Cole, J. W. 1981: Genesis of lavas of the Taupo Volcanic Zone, North Island, New Zealand. *Journal of Volcanology and Geothermal Research 10*: 317-337.

Cole, J. W.; Brown, S. J. A.; Burt, R. M.; Beresford, S. W.; Wilson, C. J. N. 1998: Lithic types in ignimbrites as a guide to the evolution of a caldera complex, Taupo Volcanic Centre, New Zealand. *Journal of Volcanology and Geothermal Research 80*: 217-237.

Corazzato, C.; Tibaldi, A. 2006: Fracture control on type, morphology and distribution of parasitic volcanic cones: An example from Mt. Etna, Italy. *Journal of Volcanology and Geothermal Research 158*: 177-194.

Dabell, K.; Hendy, C.; Hadfield, J.; Kim, N. 2006: Initial stages of effluent plume development, Kinloch water treatment plant (WTP), Kinloch, Taupo, New Zealand. *Journal of Geochemical Exploration 88*: 15-18.

de Ronde, C. E. J.; Stoffers, P.; Garbe-Schonberg, D.; Christenson, B. W.; Jones, B.; Manconi, R.; Browne, P. R. L.; Hissman, K.; Botz, R.; Davy, B. W.; Schmitt, M.; Battershill, C. N. 2002: Discovery of active hydrothermal venting in Lake Taupo, New Zealand. *Journal of Volcanology and Geothermal Research 115*: 257-275.

Di Traglia, F.; Cimarelli, C.; de Rita, D.; Gimeno Torrente, D. 2009: Changing eruptive styles in basaltic explosive volcanism: Examples from Croscat complex scoria cone, Garrotxa Volcanic Field (NE Iberian Peninsula). *Journal of Volcanology and Geothermal Research 180*: 89-109.

Fisher, R. V.; Schmincke, H. U. 1984: Pyroclastic Rocks. New York, Springer-Verlag. 472 p.

Forster, C.; Smith, L. 1989: The influence of groundwater flow on thermal regimes in mountainous terrain: a model study. *Journal of Geophysical Research 94*: 9439-9451.

Frazzetta, G.; La Volpe, L.; Sheridan, M. F. 1983: Evolution of the Fossa Cone, Vulcano. *Journal of Volcanology and Geothermal Research 17*: 329-360.

Gamble, J. A.; Smith, I. E. M.; Graham, I. J.; Kokelaar, B. P.; Cole, J. W.; Houghton, B. F.; Wilson, C. J. N. 1990: The petrology, phase relations and tectonic setting of basalts from the Taupo Volcanic Zone, New Zealand and the Kermadec Island Arc - Havre Trough, SW Pacific. *Journal of Volcanology and Geothermal Research 43*: 235-270.

Gamble, J. A.; Smith, I. E. M.; McCulloch, M. T.; Graham, I. J.; Kokelaar, B. P. 1993: The geochemistry and petrogenesis of basalts from the Taupo Volcanic Zone and Kermadec Island Arc, S. W. Pacific. *Journal of Volcanology and Geothermal Research 54*: 265-290.

Gençalioğlu-Kuşcu, G.; Atilla, C.; Cas, R. A. F.; Kuşcu, İ. 2007: Base surge deposits, eruption history, and depositional processes of a wet phreatomagmatic volcano in Central Anatolia (Cora Maar). *Journal of Volcanology and Geothermal Research 159*: 198-209.

Gisbert, G.; Gimeno, D.; Fernandez-Turiel, J. L. 2009: Eruptive mechanisms of the Puig De La Garrinada volcano (Olot, Garrotxa volcanic field, Northeastern Spain): A methodological study based on proximal

pyroclastic deposits. *Journal of Volcanology and Geothermal Research 180*: 259-276.

Glover, R. B.; Stewart, M. K. 1996: Chemical and isotopic changes in shallow groundwater caused by exploitation of the Wairakei geothermal field, New Zealand. *Geothermics 25*: 647-661.

Graham, I. J.; Cole, J. W.; Briggs, R. M.; Gamble, J. A.; Smith, I. E. M. 1995: Petrology and petrogenesis of volcanic-rocks from the Taupo Volcanic Zone - a review. *Journal of Volcanology and Geothermal Research 68*: 59-87.

Graham, I. J.; Worthington, T. J. 1988: Petrogenesis of Tauhara dacite (Taupo Volcanic Zone, New Zealand) – evidence for magma mixing between high-alumina andesite and rhyolite. *Journal of Volcanology and Geothermal Research 35*: 279-294.

Grange, L. I. 1937: Geology of the Rotorua-Taupo subdivision. *New Zealand Geological Survey bulletin 37.*

Gravley, D. M.; Wilson, C. J. N.; Rosenberg, M. D.; Leonard, G. S. 2006: The nature and age of Ohakuri Formation and Ohakuri Group rocks in surface exposures and geothermal drillhole sequences in the central Taupo Volcanic Zone, New Zealand. *New Zealand Journal of Geology and Geophysics 49*: 305-308.

Grindley, G. W. 1960: Sheet 8—Taupo. Geological map of New Zealand 1:250 000. Wellington, New Zealand. Department of Scientific and Industrial Research.

Grindley, G. W. 1965: The geology, structure, and exploitation of the Wairakei geothermal field, Taupo, New Zealand. New Zealand Geological Survey bulletin 75.

Grunewald, U.; Zimanowski, B.; Büttner, R.; Phillips, L. F.; Heide, K.; Büchel, G. 2007: MFCI experiments on the influence of NaCl-saturated water on phreatomagmatic explosions. *Journal of Volcanology and Geothermal Research 159*: 126-137.

Hadfield, J.C. 1995: A groundwater contaminant tracer study at Waitahanui, Taupo.Unpublished M.Phil. thesis, University of Waikato. 289 p.

Hadfield, J.C.; Nicole, D.A.; Rosen, M.R.; Wilson, C.J.N.; Morgenstern, U. 2001: Hydrology of Lake Taupo Catchment – Phase 1. Environment Waikato Technical Report 2001/1. 44p.

Hadfield, J.C. 2007: Groundwater Flow and Nitrogen Transport Modelling of the Northern Lake Taupo Catchment. Environment Waikato technical report 2007/39.

Head, J. W.; Wilson, L. 1989: Basaltic pyroclastic eruptions: Influence of gas-release patterns and volume fluxes on fountain structure, and the formation of cinder cones, spatter cones, rootless flows, lava ponds and lava flows. *Journal of Volcanology and Geothermal Research 37*: 261-271.

Henley, R. W.; Ellis, A. J. 1983: Geothermal systems ancient and modern: A geochemical review. *Earth-Science Reviews 19*: 1-50.

Henley, R. W.; Stewart, M. K. 1983: Chemical and isotopic changes in the hydrology of the Tauhara geothermal field due to exploitation at Wairakei. *Journal of Volcanology and Geothermal Research 15*: 285-314.

Hiess, J.; Cole, J. W.; Spinks, K. D. 2007: Influence of the crust and crustal structure on the location and composition of high-alumina basalts of the Taupo Volcanic Zone, New Zealand. *New Zealand Journal of Geology and Geophysics 50*: 327-342.

Hochstein, M. P.; Browne, P. R. L. 2000: Surface manifestations of geothermal systems with volcanic heat sources. In: Sigurdsson, H. (Ed.), Encyclopedia of Volcanoes. San Diego, Academic Press. pp. 835-855.

Hochstein, M. P.; Smith, I. E. M.; Regenauerlieb, K.; Ehara, S. 1993: Geochemistry and heat-transfer processes in Quaternary rhyolitic systems of the Taupo Volcanic Zone, New Zealand. *Tectonophysics 223*: 213-235.

Houghton, B. F.; Bonadonna, C.; Gregg, C. E.; Johnston, D. M.; Cousins, W. J.; Cole, J. W.; Del Carlo, P. 2006: Proximal tephra hazards: Recent eruption studies applied to volcanic risk in the Auckland volcanic field, New Zealand. *Journal of Volcanology and Geothermal Research 155*: 138-149.

Houghton, B. F.; Gonnermann, H. M. 2008: Basaltic explosive volcanism: Constraints from deposits and models. *Chemie der Erde 68*: 117-140.

Houghton, B. F.; Schmincke, H.-U. 1986: Mixed deposits of simultaneous Strombolian and phreatomagmatic volcanism: Rothenberg volcano, East Eifel volcanic field. *Journal of Volcanology and Geothermal Research 30*: 117-130.

Houghton, B. F.; Schmincke, H.-U. 1989: Rothenberg scoria cone, East Eifel: a complex Strombolian and phreatomagmatic volcano. *Bulletin of Volcanology 52*: 28-48.

Houghton, B. F.; Smith, R. T. 1993: Recycling of magmatic clasts during explosive eruptions: estimating the true juvenile content of phreatomagmatic volcanic deposits. *Bulletin of Volcanology 55*: 414-420.

Houghton, B. F.; Wilson, C. J. N. 1989: A vesicularity index for pyroclastic deposits. *Bulletin of Volcanology 51*: 451-462.

Houghton, B. F.; Wilson, C. J. N.; Lloyd, E. F.; Gamble, J. A.; Kokelaar, B. P. 1987: A catalogue of basalt deposits within the Central Taupo Volcanic Zone. *New Zealand Geological Survey record 18:* 95-101.

Houghton, B. F.; Wilson, C. J. N.; McWilliams, M. O.; Lanphere, M. A.; Weaver, S. D.; Briggs, R. M.; Pringle, M. S. 1995: Chronology and dynamics of a

large silicic magmatic system - central Taupo Volcanic Zone, New Zealand. *Geology 23*: 13-16.

Houghton, B. F.; Wilson, C. J. N.; Smith, I. E. M. 1999: Shallow-seated controls on styles of explosive basaltic volcanism: a case study from New Zealand. *Journal of Volcanology and Geothermal Research 91*: 97-120.

Inman, D. L. 1952: Measures of describing the size distribution of sediments. *Journal of Sedimentary Petrology 22*: 125-145.

Jurado-Chichay, Z.; Walker, G. P. L. 2001: Variability of plinian fall deposits: examples from Okataina Volcanic Centre, New Zealand. *Journal of Volcanology and Geothermal Research 111*: 239-263.

Kokelaar, B.P. 1986: Magma–water interactions in subaqueous and emergent basaltic volcanism. *Bulletin of Volcanology 48*: 275–290.

Kühn, M. 2004: Reactive Flow Modeling of Hydrothermal Systems. Berlin; New York: Springer-Verlag. 261 p.

Kurszlaukis, S.; Franz, L.; Lorenz, V. 1998: On the volcanology of the Gibeon Kimberlite Field, Namibia. *Journal of Volcanology and Geothermal Research 84*: 257-272.

Leng, M. J.; Barker, P. A. 2006: A review of the oxygen isotope composition of lacustrine diatom silica for paleoclimate reconstruction. *Earth-Science Reviews 75*: 5-27.

Lorenz, V. 1987: Phreatomagmatism and its relevance. *Chemical Geology 62*: 149-156.

Lorenz, V.; Kurszlaukis, S. 2007: Root zone processes in the phreatomagmatic pipe emplacement model and consequences for the evolution of maar-diatreme volcanoes. *Journal of Volcanology and Geothermal Research 159*: 4-32.

McDonough, W. F.; Sun, S.-S.; Ringwood, A. E.; Jagoutz, E.; Hofmann, A. W. 1992: Potassium, rubidium, and cesium in the Earth and Mooon and the evolution of the mantle of the Earth. *Geochimica et Cosmochimica Acta 56*: 1001-1012.

Mangan, M.; Miller, T.; Waythomas, C.; Trusdell, F.; Calvert, A.; Layer, P. 2009: Diverse lavas from closely spaced volcanoes drawing from a common parent: Emmons Lake Volcanic Center, Eastern Aleutian Arc. *Earth and Planetary Science Letters 287*: 363-372.

Manville, V.; Hodgson, K. A.; Nairn, I. A. 2007: A review of break-out floods from volcanogenic lakes in New Zealand *New Zealand Journal of Geology and Geophysics 50*: 131-150.

Manville, V.; Reeves, R. 2006: Acacia Heights CMP – Geology and Geomorphology. GNS Consultancy Report 2006/228. 44 p.

Manville, V.; Wilson, C. J. N. 2003: Interactions between volcanism, rifting and subsidence: implications of intracaldera palaeoshorelines at Taupo volcano, New Zealand. *Journal of the Geological Society, London 160*: 3-6.

Manville, V.; Wilson, C. J. N. 2004: The 26.5 ka Oruanui eruption, New Zealand: a review of the roles of volcanism and climate in the post-eruptive sedimentary response. *New Zealand Journal of Geology and Geophysics 47*: 525-547.

Marshall, D. C. 1970: Development of a theory of the Wairakei Geothermal Field by the <<Simplest Cases First>> technique. *Geothermics Special Issue 2*: 669-676.

Martin, R. C. 1961: Stratigraphy and structural outline of the Taupo Volcanic Zone. *New Zealand Journal of Geology and Geophysics 4*: 449-478.

Martin, U.; Németh, K. 2005: Eruptive and depositional history of a Pliocene tuff ring that developed in a fluvio-lacustrine basin: Kissomlyó volcano (western Hungary). *Journal of Volcanology and Geothermal Research 147*: 342-356.

Martin, U.; Németh, K. 2006: How Strombolian is a "Strombolian" scoria cone? Some irregularities in scoria cone architecture from the Transmexican Volcanic Belt, near Volcán Ceboruco, (Mexico) and Al Haruj (Libya). *Journal of Volcanology and Geothermal Research 155*: 104-118.

Mastin, L. G.; Christiansen, R. L.; Thornber, C.; Lowenstern, J.; Beeson, M. 2004: What makes hydromagmatic eruptions violent? Some insights from the Keanakāko'i Ash, Kīlauea Volcano, Hawai'i. *Journal of Volcanology and Geothermal Research 137*: 15-31.

Mastin, L. G.; Spieler, O.; Downey, W. S. 2009: An experimental study of hydromagmatic fragmentation through energetic, non-explosive magma-water mixing. *Journal of Volcanology and Geothermal Research 180*: 161-170.

Miyabuchi, Y.; Watanabe, K.; Egawa, Y. 2006: Bomb-rich pyroclastic flow deposit from Nakadake, Aso Volcano, southwestern Japan. *Journal of Volcanology and Geothermal Research 155*: 90-103.

Moore, J.G.; Nakamura, K.; Alcaraz, A. 1966: The 1965 eruption of Taal volcano. *Science 151*: 955-960.

Morgenstern, U. 2007: Lake Taupo Catchment Groundwater Age Distribution and Implications for Future Land-Use Impacts. Environment Waikato Technical Report 2007/49.

Morrissey, M.; Zimanowski, B.; Wohletz, K., Buettner, R. 2000: Phreatomagmatic fragmentation. In: Sigurdsson, H. (Ed.), Encyclopedia of Volcanoes. San Diego, Academic Press. pp. 431–446.

Namiki, A.; Manga, M. 2008: Transition between fragmentation and permeable outgassing of low viscosity magmas. *Journal of Volcanology and Geothermal Research 169*: 48-60.

Nelson, C. S.; G. S. Lister. 1995: Surficial bottom sediments of Lake Taupo, New Zealand - texture, composition, provenance and sedimentation rates. *New Zealand Journal of Geology and Geophysics 38*: 61-79.

Németh, K.; Cronin, S. J. 2009: Phreatomagmatic volcanic hazards where rift-systems meet the sea, a study from Ambae Island, Vanuatu. *Journal of Volcanology and Geothermal Research 180*: 246-258.

Németh, K.; Martin, U. 2006: Shallow sill and dyke complex in western Hungary as a possible feeding system of phreatomagmatic volcanoes in "soft rock" environment. *Journal of Volcanology and Geothermal Research 159*: 138-152.

Németh, K.; White, J. D. L. 2003: Reconstructing eruption processes of a Miocene monogenetic volcanic field from vent remnants: Waipiata Volcanic Field, South Island, New Zealand. *Journal of Volcanology and Geothermal Research 124*: 1-21.

Németh, K.; White, C. M. 2009: Intra-vent peperites related to the phreatomagmatic 71 Gulch Volcano, western Snake River Plain volcanic field, Idaho (USA). *Journal of Volcanology and Geothermal Research 183*: 30-41.

Ohba, T.; Kitade, Y. 2005: Subvolcanic hydrothermal systems: Implications from hydrothermal minerals in hydrovolcanic ash. *Journal of Volcanology and Geothermal Research 145*: 249-262.

Ort, M. H.; Carrasco-Núñez, G. 2009: Lateral vent migration during phreatomagmatic and magmatic eruptions at Tecuitlapa Maar, east-central Mexico. *Journal of Volcanology and Geothermal Research 181*: 67-77.

Palinkaš, L. A.; Bermanec, V.; Borojević Šoštarić, S.; Kolar-Jurkovšek, T.; Strmić Palinkaš, S.; Molnar, F.; Kniewald, G. 2008: Volcanic facies analysis of a subaqueous basalt lava-flow complex at Hruškovec, NW Croatia – Evidence of advanced rifting in the Tethyan domain. *Journal of Volcanology and Geothermal Research 178*: 644-656.

Pardo, N.; Macias, J. L.; Giordano, G.; Cianfarra, P.; Avellán, D. R.; Bellatreccia, F. 2009: The ~ 1245 yr BP Asososca maar eruption: the youngest event along the Nejapa-Miraflores volcanic fault, Western Managua, Nicaragua. *Journal of Volcanology and Geothermal Research 184*: 292-312.

Parfitt, E. A. 2004: A discussion of the mechanisms of explosive basaltic eruptions. *Journal of Volcanology and Geothermal Research 134*: 77-107.

Parfitt, E. A.; Wilson, L. 1994: The 1983-86 Pu'u 'O'o eruption of Kilauea Volcano, Hawaii: a study of dike geometry and eruption mechanisms for a long-lived eruption. *Journal of Volcanology and Geothermal Research 59*: 179-205.

Patrick, M. R.; Harris, A. J. L.; Ripepe, M.; Dehn, J.; Rothery, D. A.; Calvari, S. 2007: Strombolian explosive styles and source conditions: insights from thermal (FLIR) video. *Bulletin of Volcanology 69*: 769-784.

Petrinovic, I. A.; Colombo Piñol, F. 2006: Phreatomagmatic and phreatic eruptions in locally extensive settings of Southern Central Andes: The Tocomar Volcanic Centre (24º 10'S-66º 34'W), Argentina. *Journal of Volcanology and Geothermal Research 158*: 37-50.

Price, R. C.; Gamble, J. A.; Smith, I. E. M.; Stewart, R. B.; Eggins, S.; Wright, I. C. 2005: An integrated model for the temporal evolution of andesites and rhyolites and crustal development in New Zealand's North Island. *Journal of Volcanology and Geothermal Research 140*: 1-24.

Reid, F. 1983: Origin of the rhyolitic rocks of the Taupo Volcanic Zone, New Zealand. *Journal of Volcanology and Geothermal Research 15*: 315-338.

Riedel, C.; Ernst, G. G. J.; Riley, M. 2003: Controls on the growth and geometry of pyroclastic constructs. *Journal of Volcanology and Geothermal Research 127*: 121-152.

Riggs, N. R.; Duffield, W.A. 2008: Record of complex scoria cone eruptive activity at Red Mountain, Arizona, USA, and implications for monogenetic mafic volcanoes. *Journal of Volcanology and Geothermal Research 178*: 763-776.

Rollinson, H. 1993: Using Geochemical Data: Evaluation, Presentation, Interpretation. Harlow, Essex, England, Longman Group UK Limited. 352 p.

Rosseel, J-B.; White, J. D. L.; Houghton, B. F. 2006: Complex bombs of phreatomagmatic eruptions: Role of agglomeration and welding in vents of the 1886 Rotomahana eruption, Tarawera, New Zealand. *Journal of Geophysical Research 111*: B12205, doi:10.1029/2005JB004073.

Rowland, J. V.; Sibson, R. H. 2001: Extensional fault kinematics within the Taupo Volcanic Zone, New Zealand: soft-linked segmentation of a continental rift system. *New Zealand Journal of Geology and Geophysics 44*: 271-283.

Shelley, D. 1993: Igneous and metamorphic rocks under the microscope: classification, textures, microstructures, and mineral preferred-orientations. London, New York, Chapman & Hall. 445 p.

Sheridan, M. F.; Wohletz, K. H. 1981: Hydrovolcanic explosions: the systematic of water-pyroclast formation. *Science 212*: 1387-1389.

Sheridan, M. F.; Wohletz, K. H. 1983: Hydrovolcanism: basic considerations and review. *Journal of Volcanology and Geothermal Research 17*: 1-29.

Skilling, I. P.; White, J. D. L.; McPhie, J. 2002: Peperite: a review of magma-sediment mingling. *Journal of Volcanology and Geothermal Research 114*: 1-17.

Slejko, F. F.; Petrini, R.; Orsi, G.; Piochi, M.; Forte, C. 2004: Water speciation and Sr isotope exchange during water-melt interaction: a combined NMR-TIMS study on the Cretaio Tephra (Ischia Island, south Italy). *Journal of Volcanology and Geothermal Research 133*: 311-320.

Smith, E. G. C.; Williams, T. D.; Darby, D. J. 2007: Principal component analysis and modelling of the subsidence of the shoreline of Lake Taupo, New Zealand, 1983-1999: evidence for dewatering of a magmatic intrusion? *Journal of Geophysical Research - Solid Earth 112*: B08406, doi:10.1029/2006JB004652

Smith, R. T. 1990: The Kaiapo phreatomagmatic deposit, Taupo Volcanic Centre. Unpublished B.Sc. (Hons) project, lodged in Geology Department, University of Canterbury. 109 p.

Sohn, Y. K. 1996: Hydrovolcanic processes forming basaltic tuff rings and cones on Cheju Island, Korea. *Geological Society of America Bulletin 108*: 1199-1211.

Sohn, Y. K.; Chough, S. K. 1989: Depositional processes of the Suwolbong tuff ring, Cheju Island (Korea). *Sedimentology 36*: 837-855.

Stipp, J.J. 1968: The geochronology and petrogenesis of the Cenozoic volcanics of the North Island, New Zealand. Unpublished Ph.D. thesis, Australian National University, Canberra, Australia (unpubl.). 438 p.

Streck, M. J.; Grunder, A. L. 1995: Crystallisation and welding variations in a widespread ignimbrite sheet – the Rattlesnake Tuff, Eastern Oregon, USA. *Bulletin of Volcanology 57*: 151-169.

Streck, M. J.; Grunder, A. L. 1999: Enrichment of basalt and mixing of dacite in the rootzone of a large rhyolite chamber: inclusions and pumices from the Rattlesnake Tuff, Oregon. *Contributions to Mineralogy and Petrology 136*: 193-212.

Stroncik, N. A.; Schmincke, H-U. 2002: Palagonite – a review. *International Journal of Earth Science (Geol Rundsch) 91*: 680-697.

Sutton, A. N.; Blake, S.; Wilson, C. J. N. 1995: An outline geochemistry of rhyolite eruptives from Taupo Volcanic Center, New Zealand. *Journal of Volcanology and Geothermal Research 68*: 153-175.

Thorarinsson, S. 1964: Surtsey: The new island in the North Atlantic. New York, Viking Press. 47 p.

Tucker, D. S.; Scott, K. M. 2009: Structures and facies associated with the flow of subaerial basaltic lava into a deep freshwater lake: the Sulphur Creek lava flow, North Cascades, Washington. *Journal of Volcanology and Geothermal Research 185*: 311-322.

Valentine, G. A.; Gregg, T. K. P. 2008: Continental basaltic volcanoes – Processes and problems. *Journal of Volcanology and Geothermal Research 177*: 857-873.

Vant, B.; Smith, P. 2004: Nutrient Concentration and Water Ages in 11 Streams Flowing into Lake Taupo. Environment Waikato Technical Report 2002/18R.

Villamor, P.; Berryman, K. 2001: A late Quaternary extension rate in the Taupo Volcanic Zone, New Zealand, derived from fault slip data. *New Zealand Journal of Geology and Geophysics 44*: 243-269.

Walker, G. P. L. 1971: Grain-size characteristics of pyroclastic deposits. *Journal of Geology 79*: 696-714.

Walker, G. P. L.; Wilson, L.; Bowell, E. L. G. 1971: Explosive volcanic eruptions – I: The rate of fall of pyroclasts. *Geophysical Journal of the Royal Astronomical Society 22*: 377-383.

White, J. D. L. 1996: Impure coolants and interaction dynamics of phreatomagmatic eruptions. *Journal of Volcanology and Geothermal Research 74*: 155-170.

White, J. D. L. 2000: Subaqueous eruption-fed density currents and their deposits. *Precambrian Research 101*: 87-109.

Wilson, C. J. N. 1993: Stratigraphy, chronology, styles and dynamics of Late Quaternary eruptions from Taupo Volcano, New Zealand. *Philosophical Transactions of the Royal Society of London Series A - Mathematical Physical and Engineering Sciences 343*: 205-306.

Wilson, C. J. N.; Houghton, B. F.; McWilliams, M. O.; Lanphere, M. A.; Weaver, S. D.; Briggs, R. M. 1995: Volcanic and structural evolution of Taupo Volcanic Zone, New Zealand - a review. *Journal of Volcanology and Geothermal Research 68*: 1-28.

Wilson, C. J. N.; Smith, I. E. M. 1985: A basaltic phreatomagmatic eruption centre at Acacia Bay, Taupo Volcanic Centre. *Journal of the Royal Society of New Zealand 15:* 329-3.

Wohletz, K. H. 1983: Mechanisms of hydrovolcanic pyroclast formation: grain-size, scanning electron microscopy, and experimental studies. *Journal of Volcanology and Geothermal Research 17*: 31-63.

Wohletz, K. H. 1986: Explosive magma-water interactions: Thermodynamics, explosion mechanisms, and field studies. *Bulletin of Volcanology 48*: 245-264.

Wohletz, K. H.; McQueen, R. G. 1984: Experimental studies of hydromagmatic Volcanism. In Explosive volcanism: Inception, evolution, and hazards: Studies in geophysics. Washington, D.C., National Academy Press. p. 158–169.

Wohletz, K. H.; Zimanowski, B. 2000: Physics of phreatomagmatism-1. *Terra Nostra 6*: 515-523.

Wood, C. P.; Brathwaite, R. L.; Rosenberg, M. D. 2001: Basement structure, lithology and permeability at Kawerau and Ohaaki geothermal fields, New Zealand. *Geothermics 30*: 461-481.

Zanon, V.; Pacheco, J.; Pimentel, A. 2009: Growth and evolution of an emergent tuff cone: considerations from structural geology, geomorphology and facies analysis of São Miguel (Azores). *Journal of Volcanology and Geothermal Research 180*: 277-291.

Zimanowski, B.; Fröhlich, G.; Lorenz, V. 1991: Quantitative experiments on phreatomagmatic explosions. *Journal of Volcanology and Geothermal Research 48*: 341-358.

Appendix A

Sample Locations

Sample	Centre	NZMS260 map	Easting	Northing	Log Site	Log Height (m)	Description
W20100001	Acadia Bay	U18	2773324	6272577	ABS	0.15	Unconsolidated tephra
W20100002	Acadia Bay	U18	2773324	6272577	ABS	0.50	Unconsolidated tephra
W20100003	Acadia Bay	U18	2773324	6272577	ABS	1.00	Unconsolidated tephra
W20100004	Acadia Bay	U18	2773324	6272577	ABS	1.15	Unconsolidated tephra
W20100005	Acadia Bay	U18	2773324	6272577	ABS	1.47	Consolidated lake sediment
W20100006	Acadia Bay	U18	2773324	6272577	ABS	1.70	Unconsolidated tephra
W20100007	Acadia Bay	U18	2773324	6272577	ABS	1.90	Unconsolidated tephra
W20100008	Acadia Bay	U18	2773324	6272577	ABS	2.2	Consolidated tephra
W20100009	Acadia Bay	U18	2773324	6272577	ABS	0.23	Ignimbrite
W20100010	Acadia Bay	U18	2773324	6272577	ABS	1.15	Ignimbrite
W20100011	Acadia Bay	U18	2773324	6272577	ABS	1.15	Ignimbrite
W20100012	Acadia Bay	U18	2773324	6272577	ABS	1.15	Ignimbrite
W20100013	Acadia Bay	U18	2773324	6272577	ABS	1.15	Ignimbrite
W20100014	Acadia Bay	U18	2773335	6272594	ABSa	0.22	Consolidated lake sediment
W20100015	Acadia Bay	U18	2773335	6272594	ABSa	0.50	Unconsolidated tephra
W20100016	Acadia Bay	U18	2773304	6272566	ABSb	0.20	Unconsolidated tephra
W20100017	Acadia Bay	U18	2773304	6272566	ABSb	0.85	Unconsolidated tephra
W20100018	Acadia Bay	U18	2773304	6272566	ABSb	1.70	Unconsolidated tephra
W20100019	Acadia Bay	U18	2773998	6273109	ABN	0.12	Unconsolidated tephra
W20100020	Acadia Bay	U18	2773998	6273109	ABN	0.31	Unconsolidated tephra
W20100021	Acadia Bay	U18	2773998	6273109	ABN	0.35	Tuff
W20100022	Acadia Bay	U18	2773998	6273109	ABN	0.52	Tuff

Sample	Centre	NZMS260 map	Easting	Northing	Log Site	Log Height (m)	Description
W20100023	Kaiapo	U18	2771512	6275171	KPB	0.05	Unconsolidated lapilli
W20100024	Kaiapo	U18	2771512	6275171	KPB	0.17	Tuff
W20100025	Kaiapo	U18	2771512	6275171	KPB	0.47	Unconsolidated lapilli
W20100026	Kaiapo	U18	2771512	6275171	KPB	0.70	Tuff
W20100027	Kaiapo	U18	2771512	6275171	KPB	0.96	Unconsolidated lapilli
W20100028	Kaiapo	U18	2771512	6275171	KPB	1.45	Unconsolidated lapilli
W20100029	Kaiapo	U18	2771512	6275171	KPB	1.60	Tuff
W20100030	Kaiapo	U18	716	754	KPA	0.40	Poorly consolidated tephra
W20100031	Kaiapo	U18	716	754	KPD	0.15	Unconsolidated tephra
W20100032	Kaiapo	U18	716	754	KPD	0.36	Unconsolidated tephra
W20100033	Kaiapo	U18	716	754	KPD	1.40	Unconsolidated tephra
W20100034	Kaiapo	U18	716	754	KPD	6.80	Poorly consolidated tephra
W20100035	Kaiapo	U18	716	754	KPE	0.20	Unconsolidated tephra
W20100036	Kaiapo	U18	716	754	KPE	1.30	Poorly consolidated tephra
W20100037	Kaiapo	U18	716	754	KPE	1.90	Tuff
W20100038	Kaiapo	U18	716	754	-	-	Hard ignimbrite
W20100039	Kaiapo	U18	716	754	-	-	Consolidated tephra
W20100040	Kaiapo	U18	716	754	-	-	Poorly consolidated tephra
W20100041	Kaiapo	U18	716	754	-	-	Poorly consolidated tephra
W20100042	Kaiapo	U18	716	754	-	-	Consolidated lake sediment
W20100043	Kaiapo	U18	716	754	-	-	Poorly consolidated sediment/tephra
W20100047	Kaiapo	U18	716	754	KPB	0.70	Ignimbrite
W20100049	Kaiapo	U18	716	754	-	-	Ignimbrite

Sample	Centre	NZMS260 map	Easting	Northing	Log Site	Log Height (m)	Description
W20100050	Kinloch	T18	2762595	6278658	KL	0.02	Tuff
W20100051	Kinloch	T18	2762595	6278658	KL	0.07	Unconsolidated tephra
W20100052	Kinloch	T18	2762595	6278658	KL	0.40	Tuff
W20100053	Kinloch	T18	2762595	6278658	KL	0.87	Unconsolidated tephra
W20100054	Kinloch	T18	2762595	6278658	KL	1.20	Vesiculated tuff
W20100055	Kinloch	T18	2762595	6278658	KL	1.54	Unconsolidated tephra
W20100056	Kinloch	T18	2762595	6278658	KL	1.85	Poorly consolidated tephra
W20100057	Kinloch	T18	2762595	6278658	KL	2.30	Tuff
W20100058	Kinloch	T18	2762595	6278658	KL	2.70	Unconsolidated tephra
W20100059	Kinloch	T18	2762595	6278658	KL	3.20	Tuff
W20100060	Kinloch	T18	2762595	6278658	KL	5.60	Unconsolidated tephra
W20100061	Kinloch	T18	2762595	6278658	KL	5.60	Spherulitic rhyolite
W20100062	Kinloch	T18	2762595	6278658	KL	5.60	Spherulitic rhyolite
W20100063	Kinloch	T18	2762595	6278658	KL	5.60	Spherulitic rhyolite
W20100064	Kinloch	T18	2762595	6278658	KL	-	Perlitic rhyolite lava
W20100067	Kinloch	T18	2762595	6278658	KL	-	Unconsolidated tephra
W20100068	Kinloch	T18	2762595	6278658	KL	-	Unconsolidated tephra
W20100070	Kinloch	T18	2762595	6278658	KL	5.60	Basaltic lava ball
W20100071	Kinloch	T18	2762595	6278658	KL	-	Basaltic lava balls
W20100072	Kinloch	T18	2762912	6278630	KLb	0.12	Poorly consolidated tephra
W20100073	Kinloch	T18	2762912	6278630	KLb	0.35	Poorly consolidated tephra

Sample	Centre	NZMS260 map	Easting	Northing	Log Site	Log Height (m)	Description
W20100074	Punatekahi	U18	2773637	6278340	-	-	Lava
W20100075	Punatekahi	U18	2773637	6278340	PB	1.50	Unconsolidated scoria
W20100076	Punatekahi	U18	2773637	6278340	PB	5.00	Unconsolidated scoria
W20100077	Punatekahi	U18	2773637	6278340	PB	6.20	Unconsolidated scoria
W20100078	Punatekahi	U18	2773637	6278340	PB	-	Basalt bomb
W20100079	Punatekahi	U18	2773637	6278340	PB	-	Basalt bomb
W20100080	Punatekahi	U18	737	786	-	-	Lava
W20100081	Punatekahi	U18	737	786	-	-	Lava
W20100082	Punatekahi	U18	737	786	-	-	Welded agglutinate/lava
W20100083	Punatekahi	U18	737	786	-	-	Unconsolidated scoria
W20100084	Punatekahi	U18	737	786	-	-	Poorly consolidated tephra
W20100085	Punatekahi	U18	737	786	-	-	Lava
W20100086	Punatekahi	U18	737	786	-	-	Lava
W20100087	Punatekahi	U18	737	786	-	-	Welded agglutinate/lava
W20100088	Punatekahi	U18	737	786	-	-	Basalt bomb
W20100089	Punatekahi	U18	737	786	-	-	Welded agglutinate/lava
W20100090	Punatekahi	U18	737	786	-	-	Unconsolidated scoria
W20100091	Punatekahi	U18	737	786	PA	1.00	Welded agglutinate/lava
W20100092	Punatekahi	U18	737	786	-	-	Unconsoldated scoria
W20100093	Punatekahi	U18	737	786	-	-	Welded agglutinate/lava
W20100094	Punatekahi	U18	2773594	6278428	PA	17.80	Unconsolidated scoria
W20100095	Punatekahi	U18	2773594	6278428	PA	16.50	Unconsolidated scoria
W20100096	Punatekahi	U18	2773594	6278428	PA	14.80	Unconsolidated scoria
W20100097	Punatekahi	U18	737	786	PA	13.40	Unconsolidated scoria
W20100098	Punatekahi	U18	737	786	PA	11.00	Unconsolidated scoria
W20100099	Punatekahi	U18	737	786	PA	8.50	Unconsolidated scoria
W20100100	Punatekahi	U18	737	786	PA	5.50	Unconsolidated scoria

Sample	Centre	NZMS260 map	Easting	Northing	Log Site	Log Height (m)	Description
W20100101	Punatekahi	U18	737	786	PA	2.50	Unconsolidated scoria
W20100102	Punatekahi	U18	737	786	PAN	0.10	Unconsolidated scoria
W20100103	Punatekahi	U18	737	786	PAN	0.48	Unconsolidated scoria
W20100104	Punatekahi	U18	737	786	PAN	0.87	Unconsolidated scoria
W20100105	Punatekahi	U18	737	786	-	-	Ignimbrite
W20100107	Punatekahi	U18	737	786	-	-	Unconsolidated scoria

Appendix B

Grain Size Data

Grainsize Statistics					Sample:	W20100001					
	phi interval:	1	Cum			Cum%			Percentiles		
	mm	phi	wt (g)	wt (g)	wt%	finer	Modes			phi	mm
1	64.0000	-6	0.00	0.00	0.000	100.00%			95%	-3.55	11.732
2	32.0000	-5	0.00	0.00	0.000	100.00%			84%	-2.62	6.147
3	16.0000	-4	15.70	15.70	0.017	98.35%			75%	-2.12	4.353
4	8.0000	-3	86.60	70.90	0.075	90.87%			50%	-0.67	1.593
5	4.0000	-2	258.10	171.50	0.181	72.80%	mode at	-2.5	25%	0.64	0.644
6	2.0000	-1	408.20	150.10	0.158	56.98%			16%	1.21	0.432
7	1.0000	0	609.90	201.70	0.213	35.72%	mode at	-0.5	5%	2.07	0.238
8	0.5000	1	769.90	160.00	0.169	18.86%					
9	0.2500	2	898.40	128.50	0.135	5.31%				phi	mm
10	0.1250	3	939.20	40.80	0.043	1.01%			Inman (1952)'s stats		
11	0.0625	4	947.00	7.80	0.008	0.19%			Median diamete	-0.67	1.593
12	0.0313	5	948.80	1.80	0.002	0.00%			Graphic St. Dev	1.92	
									Folk and Ward (1957)'s stats		
		Sums	948.80	948.80	1.000				Graphic Mean (	-0.69	1.617
									Inclusive Graphi	1.81	

Grainsize Statistics					Sample:	W20100002					
	phi interval:	1	Cum			Cum%			Percentiles		
	mm	phi	wt (g)	wt (g)	wt%	finer	Modes			phi	mm
1	64.0000	-6	0.00	0.00	0.000	100.00%			95%	-3.55	11.732
2	32.0000	-5	0.00	0.00	0.000	100.00%			84%	-2.62	6.147
3	16.0000	-4	15.40	15.40	0.016	98.38%			75%	-2.12	4.353
4	8.0000	-3	104.80	89.40	0.094	88.95%			50%	-0.67	1.593
5	4.0000	-2	326.40	221.60	0.234	65.60%			25%	0.64	0.644
6	2.0000	-1	559.90	233.50	0.246	40.99%	mode at	-1.5	16%	1.21	0.432
7	1.0000	0	713.10	153.20	0.161	24.84%			5%	2.07	0.238
8	0.5000	1	832.60	119.50	0.126	12.25%					
9	0.2500	2	932.40	99.80	0.105	1.73%				phi	mm
10	0.1250	3	962.40	30.00	0.032	-1.43%			Inman (1952)'s stats		
11	0.0625	4	983.70	21.30	0.022	-3.68%			Median diamete	-0.67	1.593
12	0.0313	5	992.34	8.64	0.009	-4.59%			Graphic St. Dev	1.92	
									Folk and Ward (1957)'s stats		
		Sums	992.34	992.34	1.046				Graphic Mean (	-0.69	1.617
									Inclusive Graphi	1.81	

Grainsize Statistics					Sample:	W20100003					
	phi interval:	1	Cum			Cum%			Percentiles		
	mm	phi	wt (g)	wt (g)	wt%	finer	Modes			phi	mm
1	64.0000	-6	0.00	0.00	0.000	100.00%			95%	-3.55	11.732
2	32.0000	-5	0.00	0.00	0.000	100.00%			84%	-2.62	6.147
3	16.0000	-4	0.00	0.00	0.000	100.00%			75%	-2.12	4.353
4	8.0000	-3	7.22	7.22	0.008	99.24%	mode at	-3.5	50%	-0.67	1.593
5	4.0000	-2	14.00	6.78	0.007	98.52%			25%	0.64	0.644
6	2.0000	-1	34.68	20.68	0.022	96.34%			16%	1.21	0.432
7	1.0000	0	75.36	40.68	0.043	92.06%			5%	2.07	0.238
8	0.5000	1	443.04	367.68	0.388	53.31%					
9	0.2500	2	813.12	370.08	0.390	14.30%	mode at	1.5		phi	mm
10	0.1250	3	923.90	110.78	0.117	2.62%			Inman (1952)'s stats		
11	0.0625	4	947.58	23.68	0.025	0.13%			Median diamete	-0.67	1.593
12	0.0313	5	951.76	4.18	0.004	-0.31%			Graphic St. Dev	1.92	
									Folk and Ward (1957)'s stats		
		Sums.	951.76	951.76	1.003				Graphic Mean (	-0.69	1.617
									Inclusive Graphi	1.81	

Grainsize Statistics					Sample:	W20100004					
	phi interval:	1	Cum			Cum%			Percentiles		
	mm	phi	wt (g)	wt (g)	wt%	finer	Modes			phi	mm
1	64.0000	-6	0.00	0.00	0.000	100.00%			95%	-3.55	11.732
2	32.0000	-5	0.00	0.00	0.000	100.00%			84%	-2.62	6.147
3	16.0000	-4	146.90	146.90	0.155	84.52%	mode at	-4.5	75%	-2.12	4.353
4	8.0000	-3	227.90	81.00	0.085	75.98%			50%	-0.67	1.593
5	4.0000	-2	268.40	40.50	0.043	71.71%			25%	0.64	0.644
6	2.0000	-1	335.80	67.40	0.071	64.61%			16%	1.21	0.432
7	1.0000	0	493.20	157.40	0.166	48.02%			5%	2.07	0.238
8	0.5000	1	1070.60	577.40	0.609	-12.84%	mode at	0.5			
9	0.2500	2	1271.50	200.90	0.212	-34.01%				phi	mm
10	0.1250	3	1348.90	77.40	0.082	-42.17%			Inman (1952)'s stats		
11	0.0625	4	1366.60	17.70	0.019	-44.03%			Median diamete	-0.67	1.593
12	0.0313	5	1372.30	5.70	0.006	-44.64%			Graphic St. Dev	1.92	
									Folk and Ward (1957)'s stats		
		Sums.	1372.30	1372.30	1.446				Graphic Mean (	-0.69	1.617
									Inclusive Graphi	1.81	

ıinsize Statistics				Sample:	W20100006					
phi interval:	1	Cum			Cum%			Percentiles		
mm	phi	wt (g)	wt (g)	wt%	finer	Modes			*phi*	*mm*
64.0000	-6	0.00	0.00	0.000	100.00%			95%	-3.55	11.732
32.0000	-5	0.00	0.00	0.000	100.00%			84%	-2.62	6.147
16.0000	-4	0.00	0.00	0.000	100.00%			75%	-2.12	4.353
8.0000	-3	0.70	0.70	0.001	99.93%			50%	-0.67	1.593
4.0000	-2	27.30	26.60	0.028	97.12%			25%	0.64	0.644
2.0000	-1	188.50	161.20	0.170	80.13%			16%	1.21	0.432
1.0000	0	534.00	345.50	0.364	43.72%	mode at	-0.5	5%	2.07	0.238
0.5000	1	820.40	286.40	0.302	13.53%					
0.2500	2	935.30	114.90	0.121	1.42%				*phi*	*mm*
0.1250	3	981.50	46.20	0.049	-3.45%			Inman (1952)'s stats		
0.0625	4	998.00	16.50	0.017	-5.19%			Median diamete	-0.67	1.593
0.0313	5	1008.00	10.00	0.011	-6.24%			Graphic St. Dev	1.92	
								Folk and Ward (1957)'s stats		
	Sums.	1008.00	1008.00	1.062				Graphic Mean (	-0.69	1.617
								Inclusive Graphi	1.81	

Grainsize Statistics					Sample:	W20100007					
	phi interval:	1	Cum			Cum%			Percentiles		
	mm	phi	wt (g)	wt (g)	wt%	finer	Modes			*phi*	*mm*
1	64.0000	-6	0.00	0.00	0.000	100.00%			95%	-3.55	11.732
2	32.0000	-5	0.00	0.00	0.000	100.00%			84%	-2.62	6.147
3	16.0000	-4	0.00	0.00	0.000	100.00%			75%	-2.12	4.353
4	8.0000	-3	0.00	0.00	0.000	100.00%			50%	-0.67	1.593
5	4.0000	-2	0.10	0.10	0.000	99.99%			25%	0.64	0.644
6	2.0000	-1	1.00	0.90	0.001	99.89%			16%	1.21	0.432
7	1.0000	0	4.50	3.50	0.004	99.53%			5%	2.07	0.238
8	0.5000	1	24.10	19.60	0.021	97.46%					
9	0.2500	2	113.70	89.60	0.094	88.02%				*phi*	*mm*
10	0.1250	3	286.00	172.30	0.182	69.86%	mode at	2.5	Inman (1952)'s stats		
11	0.0625	4	338.80	52.80	0.056	64.29%			Median diamete	-0.67	1.593
12	0.0313	5	348.50	9.70	0.010	63.27%			Graphic St. Dev	1.92	
									Folk and Ward (1957)'s stats		
		Sums.	348.50	348.50	0.367				Graphic Mean (	-0.69	1.617
									Inclusive Graphi	1.81	

Grainsize Statistics					Sample:	W20100015					
	phi interval:	1	Cum			Cum%			Percentiles		
	mm	phi	wt (g)	wt (g)	wt%	finer	Modes			phi	mm
1	64.0000	-6	0.00	0.00	0.000	100.00%			95%	-3.55	11.732
2	32.0000	-5	0.00	0.00	0.000	100.00%			84%	-2.62	6.147
3	16.0000	-4	5.50	5.50	0.006	99.42%			75%	-2.12	4.353
4	8.0000	-3	19.50	14.00	0.015	97.94%			50%	-0.67	1.593
5	4.0000	-2	176.50	157.00	0.165	81.40%			25%	0.64	0.644
6	2.0000	-1	532.30	355.80	0.375	43.90%	mode at	-1.5	16%	1.21	0.432
7	1.0000	0	800.30	268.00	0.282	15.65%			5%	2.07	0.238
8	0.5000	1	935.80	135.50	0.143	1.37%					
9	0.2500	2	1004.70	68.90	0.073	-5.89%				phi	mm
10	0.1250	3	1049.60	44.90	0.047	-10.62%			Inman (1952)'s stats		
11	0.0625	4	1075.30	25.70	0.027	-13.33%			Median diamete	-0.67	1.593
12	0.0313	5	1089.60	14.30	0.015	-14.84%			Graphic St. Dev	1.92	
									Folk and Ward (1957)'s stats		
		Sums.	1089.60	1089.60	1.148				Graphic Mean (	-0.69	1.617
									Inclusive Graphi	1.81	

Grainsize Statistics					Sample:	W20100016					
	phi interval:	1	Cum			Cum%			Percentiles		
	mm	phi	wt (g)	wt (g)	wt%	finer	Modes			phi	mm
1	64.0000	-6	0.00	0.00	0.000	100.00%			95%	-3.55	11.732
2	32.0000	-5	0.00	0.00	0.000	100.00%			84%	-2.62	6.147
3	16.0000	-4	0.00	0.00	0.000	100.00%			75%	-2.12	4.353
4	8.0000	-3	0.60	0.60	0.001	99.94%			50%	-0.67	1.593
5	4.0000	-2	13.30	12.70	0.013	98.60%			25%	0.64	0.644
6	2.0000	-1	115.90	102.60	0.108	87.78%			16%	1.21	0.432
7	1.0000	0	305.00	189.10	0.199	67.85%			5%	2.07	0.238
8	0.5000	1	525.50	220.50	0.232	44.61%	mode at	0.5			
9	0.2500	2	675.00	149.50	0.158	28.86%				phi	mm
10	0.1250	3	741.10	66.10	0.070	21.89%			Inman (1952)'s stats		
11	0.0625	4	759.40	18.30	0.019	19.96%			Median diamete	-0.67	1.593
12	0.0313	5	766.60	7.20	0.008	19.20%			Graphic St. Dev	1.92	
									Folk and Ward (1957)'s stats		
		Sums.	766.60	766.60	0.808				Graphic Mean (	-0.69	1.617
									Inclusive Graphi	1.81	

Grainsize Statistics					Sample:	W20100017					
	phi interval:	1	Cum			Cum%			Percentiles		
	mm	phi	wt (g)	wt (g)	wt%	finer	Modes			*phi*	*mm*
1	64.0000	-6	0.00	0.00	0.000	100.00%			95%	-3.55	11.732
2	32.0000	-5	0.00	0.00	0.000	100.00%			84%	-2.62	6.147
3	16.0000	-4	0.00	0.00	0.000	100.00%			75%	-2.12	4.353
4	8.0000	-3	14.00	14.00	0.015	98.52%			50%	-0.67	1.593
5	4.0000	-2	124.80	110.80	0.117	86.85%			25%	0.64	0.644
6	2.0000	-1	385.50	260.70	0.275	59.37%	mode at	-1.5	16%	1.21	0.432
7	1.0000	0	634.70	249.20	0.263	33.10%			5%	2.07	0.238
8	0.5000	1	763.30	128.60	0.136	19.55%					
9	0.2500	2	827.90	64.60	0.068	12.74%				*phi*	*mm*
10	0.1250	3	858.80	30.90	0.033	9.49%			**Inman (1952)'s stats**		
11	0.0625	4	872.20	13.40	0.014	8.07%			Median diamete	-0.67	1.593
12	0.0313	5	879.60	7.40	0.008	7.29%			Graphic St. Dev	1.92	
									Folk and Ward (1957)'s stats		
		Sums	879.60	879.60	0.927				Graphic Mean (	-0.69	1.617
									Inclusive Graphi	1.81	

ıinsize Statistics				Sample:	W20100018					
phi interval:	1	Cum			Cum%			Percentiles		
mm	phi	wt (g)	wt (g)	wt%	finer	Modes			*phi*	*mm*
64.0000	-6	0.00	0.00	0.000	100.00%			95%	-3.55	11.732
32.0000	-5	0.00	0.00	0.000	100.00%			84%	-2.62	6.147
16.0000	-4	79.80	79.80	0.084	91.59%	mode at	-4.5	75%	-2.12	4.353
8.0000	-3	82.60	2.80	0.003	91.29%			50%	-0.67	1.593
4.0000	-2	98.00	15.40	0.016	89.67%			25%	0.64	0.644
2.0000	-1	133.30	35.30	0.037	85.95%			16%	1.21	0.432
1.0000	0	178.10	44.80	0.047	81.23%	mode at	-0.5	5%	2.07	0.238
0.5000	1	221.20	43.10	0.045	76.69%					
0.2500	2	244.90	23.70	0.025	74.19%				*phi*	*mm*
0.1250	3	255.70	10.80	0.011	73.05%			**Inman (1952)'s stats**		
0.0625	4	260.90	5.20	0.005	72.50%			Median diamete	-0.67	1.593
0.0313	5	263.70	2.80	0.003	72.21%			Graphic St. Dev	1.92	
								Folk and Ward (1957)'s stats		
	Sums	263.70	263.70	0.278				Graphic Mean (	-0.69	1.617
								Inclusive Graph	1.81	

Grainsize Statistics					Sample:	W20100019					
	phi interval:	1	Cum			Cum%			Percentiles		
	mm	phi	wt (g)	wt (g)	wt%	finer	Modes			phi	mm
1	64.0000	-6	0.00	0.00	0.000	100.00%			95%	-3.55	11.732
2	32.0000	-5	0.00	0.00	0.000	100.00%			84%	-2.62	6.147
3	16.0000	-4	10.38	10.38	0.011	98.91%			75%	-2.12	4.353
4	8.0000	-3	30.07	19.69	0.021	96.83%			50%	-0.67	1.593
5	4.0000	-2	127.72	97.65	0.103	86.54%			25%	0.64	0.644
6	2.0000	-1	230.62	102.90	0.108	75.69%			16%	1.21	0.432
7	1.0000	0	467.72	237.10	0.250	50.70%	mode at	-0.5	5%	2.07	0.238
8	0.5000	1	619.32	151.60	0.160	34.73%					
9	0.2500	2	897.42	278.10	0.293	5.42%	mode at	1.5		phi	mm
10	0.1250	3	1138.52	241.10	0.254	-20.00%			Inman (1952)'s stats		
11	0.0625	4	1208.12	69.60	0.073	-27.33%			Median diamete	-0.67	1.593
12	0.0313	5	1228.42	20.30	0.021	-29.47%			Graphic St. Dev	1.92	
									Folk and Ward (1957)'s stats		
		Sums.	1228.42	1228.42	1.295				Graphic Mean (	-0.69	1.617
									Inclusive Graphi	1.81	

ıinsize Statistics				Sample:	W20100020					
phi interval:	1	Cum			Cum%			Percentiles		
mm	phi	wt (g)	wt (g)	wt%	finer	Modes			phi	mm
64.0000	-6	0.00	0.00	0.000	100.00%			95%	-3.55	11.732
32.0000	-5	0.00	0.00	0.000	100.00%			84%	-2.62	6.147
16.0000	-4	0.00	0.00	0.000	100.00%			75%	-2.12	4.353
8.0000	-3	6.40	6.40	0.007	99.33%			50%	-0.67	1.593
4.0000	-2	41.00	34.60	0.036	95.68%			25%	0.64	0.644
2.0000	-1	121.10	80.10	0.084	87.24%	mode at	-1.5	16%	1.21	0.432
1.0000	0	195.70	74.60	0.079	79.37%			5%	2.07	0.238
0.5000	1	226.70	31.00	0.033	76.11%					
0.2500	2	234.20	7.50	0.008	75.32%				phi	mm
0.1250	3	237.90	3.70	0.004	74.93%			Inman (1952)'s stats		
0.0625	4	239.90	2.00	0.002	74.72%			Median diamete	-0.67	1.593
0.0313	5	240.70	0.80	0.001	74.63%			Graphic St. Dev	1.92	
								Folk and Ward (1957)'s stats		
	Sums.	240.70	240.70	0.254				Graphic Mean (	-0.69	1.617
								Inclusive Graphi	1.81	

Grainsize Statistics					Sample:	W20100023					
	phi interval:	1	Cum			Cum%			Percentiles		
	mm	phi	wt (g)	wt (g)	wt%	finer	Modes			phi	mm
1	64.0000	-6	0.00	0.00	0.000	100.00%			95%	-3.55	11.732
2	32.0000	-5	0.00	0.00	0.000	100.00%			84%	-2.62	6.147
3	16.0000	-4	741.00	741.00	0.781	21.90%	mode at	-4.5	75%	-2.12	4.353
4	8.0000	-3	1253.80	512.80	0.540	-32.15%			50%	-0.67	1.593
5	4.0000	-2	1377.50	123.70	0.130	-45.18%			25%	0.64	0.644
6	2.0000	-1	1416.70	39.20	0.041	-49.31%			16%	1.21	0.432
7	1.0000	0	1432.00	15.30	0.016	-50.93%			5%	2.07	0.238
8	0.5000	1	1442.40	10.40	0.011	-52.02%					
9	0.2500	2	1449.10	6.70	0.007	-52.73%				phi	mm
10	0.1250	3	1454.70	5.60	0.006	-53.32%			Inman (1952)'s stats		
11	0.0625	4	1459.60	4.90	0.005	-53.84%			Median diamete	-0.67	1.593
12	0.0313	5	1463.20	3.60	0.004	-54.22%			Graphic St. Dev	1.92	
									Folk and Ward (1957)'s stats		
		Sums	1463.20	1463.20	1.542				Graphic Mean (	-0.69	1.617
									Inclusive Graphi	1.81	

Grainsize Statistics					Sample:	W20100026					
	phi interval:	1	Cum			Cum%			Percentiles		
	mm	phi	wt (g)	wt (g)	wt%	finer	Modes			phi	mm
1	64.0000	-6	0.00	0.00	0.000	100.00%			95%	-3.55	11.732
2	32.0000	-5	0.00	0.00	0.000	100.00%			84%	-2.62	6.147
3	16.0000	-4	172.00	172.00	0.181	81.87%	mode at	-4.5	75%	-2.12	4.353
4	8.0000	-3	320.00	148.00	0.156	66.27%			50%	-0.67	1.593
5	4.0000	-2	570.40	250.40	0.264	39.88%			25%	0.64	0.644
6	2.0000	-1	866.80	296.40	0.312	8.64%	mode at	-1.5	16%	1.21	0.432
7	1.0000	0	1054.10	187.30	0.197	-11.10%			5%	2.07	0.238
8	0.5000	1	1197.80	143.70	0.151	-26.24%					
9	0.2500	2	1285.00	87.20	0.092	-35.43%				phi	mm
10	0.1250	3	1338.80	53.80	0.057	-41.10%			Inman (1952)'s stats		
11	0.0625	4	1374.20	35.40	0.037	-44.84%			Median diamete	-0.67	1.593
12	0.0313	5	1391.00	16.80	0.018	-46.61%			Graphic St. Dev	1.92	
									Folk and Ward (1957)'s stats		
		Sums	1391.00	1391.00	1.466				Graphic Mean (	-0.69	1.617
									Inclusive Graphi	1.81	

Grainsize Statistics					Sample:	W2010030					
	phi interval:	1	Cum			Cum%			Percentiles		
	mm	phi	wt (g)	wt (g)	wt%	finer	Modes			phi	mm
1	64.0000	-6	0.00	0.00	0.000	100.00%			95%	-3.55	11.732
2	32.0000	-5	0.00	0.00	0.000	100.00%			84%	-2.62	6.147
3	16.0000	-4	117.50	117.50	0.124	87.62%	mode at	-4.5	75%	-2.12	4.353
4	8.0000	-3	159.20	41.70	0.044	83.22%			50%	-0.67	1.593
5	4.0000	-2	205.10	45.90	0.048	78.38%			25%	0.64	0.644
6	2.0000	-1	262.90	57.80	0.061	72.29%	mode at	-1.5	16%	1.21	0.432
7	1.0000	0	306.00	43.10	0.045	67.75%			5%	2.07	0.238
8	0.5000	1	334.80	28.80	0.030	64.71%					
9	0.2500	2	351.00	16.20	0.017	63.01%				phi	mm
10	0.1250	3	361.80	10.80	0.011	61.87%			Inman (1952)'s stats		
11	0.0625	4	371.00	9.20	0.010	60.90%			Median diamete	-0.67	1.593
12	0.0313	5	378.50	7.50	0.008	60.11%			Graphic St. Dev	1.92	
									Folk and Ward (1957)'s stats		
		Sums.	378.50	378.50	0.399				Graphic Mean (	-0.69	1.617
									Inclusive Graphi	1.81	

Grainsize Statistics					Sample:	W20100031					
	phi interval:	1	Cum			Cum%			Percentiles		
	mm	phi	wt (g)	wt (g)	wt%	finer	Modes			phi	mm
1	64.0000	-6	0.00	0.00	0.000	100.00%			95%	-3.55	11.732
2	32.0000	-5	0.00	0.00	0.000	100.00%			84%	-2.62	6.147
3	16.0000	-4	2.00	2.00	0.002	99.79%			75%	-2.12	4.353
4	8.0000	-3	5.70	3.70	0.004	99.40%			50%	-0.67	1.593
5	4.0000	-2	24.10	18.40	0.019	97.46%			25%	0.64	0.644
6	2.0000	-1	127.80	103.70	0.109	86.53%			16%	1.21	0.432
7	1.0000	0	323.10	195.30	0.206	65.95%			5%	2.07	0.238
8	0.5000	1	648.20	325.10	0.343	31.68%	mode at	0.5			
9	0.2500	2	917.50	269.30	0.284	3.30%				phi	mm
10	0.1250	3	1002.10	84.60	0.089	-5.62%			Inman (1952)'s stats		
11	0.0625	4	1032.90	30.80	0.032	-8.86%			Median diamete	-0.67	1.593
12	0.0313	5	1047.70	14.80	0.016	-10.42%			Graphic St. Dev	1.92	
									Folk and Ward (1957)'s stats		
		Sums.	1047.70	1047.70	1.104				Graphic Mean (	-0.69	1.617
									Inclusive Graphi	1.81	

Grainsize Statistics					Sample:	W20100032					
	phi interval:	1	Cum			Cum%			Percentiles		
	mm	phi	wt (g)	wt (g)	wt%	finer	Modes			phi	mm
1	64.0000	-6	0.00	0.00	0.000	100.00%			95%	-3.55	11.732
2	32.0000	-5	0.00	0.00	0.000	100.00%			84%	-2.62	6.147
3	16.0000	-4	5.80	5.80	0.006	99.39%			75%	-2.12	4.353
4	8.0000	-3	25.20	19.40	0.020	97.34%			50%	-0.67	1.593
5	4.0000	-2	48.40	23.20	0.024	94.90%	mode at	-2.5	25%	0.64	0.644
6	2.0000	-1	69.20	20.80	0.022	92.71%			16%	1.21	0.432
7	1.0000	0	90.10	20.90	0.022	90.50%	mode at	-0.5	5%	2.07	0.238
8	0.5000	1	106.10	16.00	0.017	88.82%					
9	0.2500	2	122.40	16.30	0.017	87.10%	mode at	1.5		phi	mm
10	0.1250	3	133.70	11.30	0.012	85.91%			Inman (1952)'s stats		
11	0.0625	4	140.70	7.00	0.007	85.17%			Median diamete	-0.67	1.593
12	0.0313	5	145.10	4.40	0.005	84.71%			Graphic St. Dev	1.92	
									Folk and Ward (1957)'s stats		
		Sums	145.10	145.10	0.153				Graphic Mean (	-0.69	1.617
									Inclusive Graphi	1.81	

Grainsize Statistics					Sample:	W20100033					
	phi interval:	1	Cum			Cum%			Percentiles		
	mm	phi	wt (g)	wt (g)	wt%	finer	Modes			phi	mm
1	64.0000	-6	0.00	0.00	0.000	100.00%			95%	-3.55	11.732
2	32.0000	-5	0.00	0.00	0.000	100.00%			84%	-2.62	6.147
3	16.0000	-4	0.00	0.00	0.000	100.00%			75%	-2.12	4.353
4	8.0000	-3	1.30	1.30	0.001	99.86%			50%	-0.67	1.593
5	4.0000	-2	11.50	10.20	0.011	98.79%			25%	0.64	0.644
6	2.0000	-1	68.50	57.00	0.060	92.78%			16%	1.21	0.432
7	1.0000	0	161.10	92.60	0.098	83.02%			5%	2.07	0.238
8	0.5000	1	363.40	202.30	0.213	61.70%					
9	0.2500	2	660.10	296.70	0.313	30.43%	mode at	1.5		phi	mm
10	0.1250	3	775.50	115.40	0.122	18.27%			Inman (1952)'s stats		
11	0.0625	4	805.20	29.70	0.031	15.13%			Median diamete	-0.67	1.593
12	0.0313	5	816.50	11.30	0.012	13.94%			Graphic St. Dev	1.92	
									Folk and Ward (1957)'s stats		
		Sums	816.50	816.50	0.861				Graphic Mean (	-0.69	1.617
									Inclusive Graphi	1.81	

Grainsize Statistics					Sample:	W20100034					
	phi interval:	1	Cum			Cum%			Percentiles		
	mm	phi	wt (g)	wt (g)	wt%	finer	Modes			phi	mm
1	64.0000	-6	0.00	0.00	0.000	100.00%			95%	-3.55	11.732
2	32.0000	-5	0.00	0.00	0.000	100.00%			84%	-2.62	6.147
3	16.0000	-4	5.00	5.00	0.005	99.47%			75%	-2.12	4.353
4	8.0000	-3	20.00	15.00	0.016	97.89%			50%	-0.67	1.593
5	4.0000	-2	45.50	25.50	0.027	95.20%	mode at	-2.5	25%	0.64	0.644
6	2.0000	-1	64.10	18.60	0.020	93.24%			16%	1.21	0.432
7	1.0000	0	82.50	18.40	0.019	91.30%			5%	2.07	0.238
8	0.5000	1	96.60	14.10	0.015	89.82%					
9	0.2500	2	106.60	10.00	0.011	88.76%				phi	mm
10	0.1250	3	114.50	7.90	0.008	87.93%			Inman (1952)'s stats		
11	0.0625	4	119.80	5.30	0.006	87.37%			Median diamete	-0.67	1.593
12	0.0313	5	123.20	3.40	0.004	87.02%			Graphic St. Dev	1.92	
									Folk and Ward (1957)'s stats		
		Sums.	123.20	123.20	0.130				Graphic Mean (	-0.69	1.617
									Inclusive Graphi	1.81	

Grainsize Statistics					Sample:	W20100035					
	phi interval:	1	Cum			Cum%			Percentiles		
	mm	phi	wt (g)	wt (g)	wt%	finer	Modes			phi	mm
1	64.0000	-6	0.00	0.00	0.000	100.00%			95%	-3.55	11.732
2	32.0000	-5	0.00	0.00	0.000	100.00%			84%	-2.62	6.147
3	16.0000	-4	0.00	0.00	0.000	100.00%			75%	-2.12	4.353
4	8.0000	-3	9.10	9.10	0.010	99.04%			50%	-0.67	1.593
5	4.0000	-2	50.40	41.30	0.044	94.69%			25%	0.64	0.644
6	2.0000	-1	189.50	139.10	0.147	80.03%			16%	1.21	0.432
7	1.0000	0	466.00	276.50	0.291	50.89%	mode at	-0.5	5%	2.07	0.238
8	0.5000	1	705.40	239.40	0.252	25.65%					
9	0.2500	2	875.60	170.20	0.179	7.72%				phi	mm
10	0.1250	3	958.50	82.90	0.087	-1.02%			Inman (1952)'s stats		
11	0.0625	4	980.20	21.70	0.023	-3.31%			Median diamete	-0.67	1.593
12	0.0313	5	989.40	9.20	0.010	-4.28%			Graphic St. Dev	1.92	
									Folk and Ward (1957)'s stats		
		Sums.	989.40	989.40	1.043				Graphic Mean (	-0.69	1.617
									Inclusive Graphi	1.81	

Grainsize Statistics					Sample:	W20100036					
	phi interval:	1	Cum			Cum%			Percentiles		
	mm	phi	wt (g)	wt (g)	wt%	finer	Modes			phi	mm
1	64.0000	-6	0.00	0.00	0.000	100.00%			95%	-3.55	11.732
2	32.0000	-5	0.00	0.00	0.000	100.00%			84%	-2.62	6.147
3	16.0000	-4	5.60	5.60	0.006	99.41%			75%	-2.12	4.353
4	8.0000	-3	26.60	21.00	0.022	97.20%			50%	-0.67	1.593
5	4.0000	-2	63.10	36.50	0.038	93.35%			25%	0.64	0.644
6	2.0000	-1	112.80	49.70	0.052	88.11%			16%	1.21	0.432
7	1.0000	0	206.00	93.20	0.098	78.29%			5%	2.07	0.238
8	0.5000	1	309.70	103.70	0.109	67.36%					
9	0.2500	2	431.10	121.40	0.128	54.56%	mode at	1.5		phi	mm
10	0.1250	3	532.10	101.00	0.106	43.92%			Inman (1952)'s stats		
11	0.0625	4	549.80	17.70	0.019	42.05%			Median diamete	-0.67	1.593
12	0.0313	5	554.50	4.70	0.005	41.56%			Graphic St. Dev	1.92	
									Folk and Ward (1957)'s stats		
		Sums	554.50	554.50	0.584				Graphic Mean (	-0.69	1.617
									Inclusive Graphi	1.81	

Grainsize Statistics					Sample:	W20100040					
	phi interval:	1	Cum			Cum%			Percentiles		
	mm	phi	wt (g)	wt (g)	wt%	finer	Modes			phi	mm
1	64.0000	-6	0.00	0.00	0.000	100.00%			95%	-3.55	11.732
2	32.0000	-5	0.00	0.00	0.000	100.00%			84%	-2.62	6.147
3	16.0000	-4	0.00	0.00	0.000	100.00%			75%	-2.12	4.353
4	8.0000	-3	0.00	0.00	0.000	100.00%			50%	-0.67	1.593
5	4.0000	-2	0.50	0.50	0.001	99.95%			25%	0.64	0.644
6	2.0000	-1	1.80	1.30	0.001	99.81%			16%	1.21	0.432
7	1.0000	0	15.00	13.20	0.014	98.42%			5%	2.07	0.238
8	0.5000	1	45.00	30.00	0.032	95.26%	mode at	0.5			
9	0.2500	2	71.10	26.10	0.028	92.51%				phi	mm
10	0.1250	3	87.30	16.20	0.017	90.80%			Inman (1952)'s stats		
11	0.0625	4	94.10	6.80	0.007	90.08%			Median diamete	-0.67	1.593
12	0.0313	5	97.60	3.50	0.004	89.71%			Graphic St. Dev	1.92	
									Folk and Ward (1957)'s stats		
		Sums	97.60	97.60	0.103				Graphic Mean (	-0.69	1.617
									Inclusive Graphi	1.81	

Grainsize Statistics					Sample:	W20100041					
	phi interval:	1	Cum			Cum%			Percentiles		
	mm	phi	wt (g)	wt (g)	wt%	finer	Modes			phi	mm
1	64.0000	-6	0.00	0.00	0.000	100.00%			95%	-3.55	11.732
2	32.0000	-5	0.00	0.00	0.000	100.00%			84%	-2.62	6.147
3	16.0000	-4	4.30	4.30	0.005	99.55%	mode at	-4.5	75%	-2.12	4.353
4	8.0000	-3	5.40	1.10	0.001	99.43%			50%	-0.67	1.593
5	4.0000	-2	9.90	4.50	0.005	98.96%			25%	0.64	0.644
6	2.0000	-1	21.90	12.00	0.013	97.69%			16%	1.21	0.432
7	1.0000	0	43.60	21.70	0.023	95.40%			5%	2.07	0.238
8	0.5000	1	150.60	107.00	0.113	84.13%	mode at	0.5			
9	0.2500	2	216.60	66.00	0.070	77.17%				phi	mm
10	0.1250	3	255.00	38.40	0.040	73.12%			Inman (1952)'s stats		
11	0.0625	4	269.70	14.70	0.015	71.57%			Median diamete	-0.67	1.593
12	0.0313	5	275.20	5.50	0.006	70.99%			Graphic St. Dev	1.92	
									Folk and Ward (1957)'s stats		
		Sums.	275.20	275.20	0.290				Graphic Mean (	-0.69	1.617
									Inclusive Graphi	1.81	

Grainsize Statistics					Sample:	W20100051					
	phi interval:	1	Cum			Cum%			Percentiles		
	mm	phi	wt (g)	wt (g)	wt%	finer	Modes			phi	mm
1	64.0000	-6	0.00	0.00	0.000	100.00%			95%	-3.55	11.732
2	32.0000	-5	0.00	0.00	0.000	100.00%			84%	-2.62	6.147
3	16.0000	-4	0.00	0.00	0.000	100.00%			75%	-2.12	4.353
4	8.0000	-3	0.00	0.00	0.000	100.00%			50%	-0.67	1.593
5	4.0000	-2	4.70	4.70	0.005	99.50%			25%	0.64	0.644
6	2.0000	-1	83.20	78.50	0.083	91.23%			16%	1.21	0.432
7	1.0000	0	414.30	331.10	0.349	56.33%			5%	2.07	0.238
8	0.5000	1	816.90	402.60	0.424	13.90%	mode at	0.5			
9	0.2500	2	915.00	98.10	0.103	3.56%				phi	mm
10	0.1250	3	929.70	14.70	0.015	2.01%			Inman (1952)'s stats		
11	0.0625	4	936.20	6.50	0.007	1.33%			Median diamete	-0.67	1.593
12	0.0313	5	939.90	3.70	0.004	0.94%			Graphic St. Dev	1.92	
									Folk and Ward (1957)'s stats		
		Sums.	939.90	939.90	0.991				Graphic Mean (	-0.69	1.617
									Inclusive Graphi	1.81	

Grainsize Statistics					Sample:	W20100053					
	phi interval:	1	Cum			Cum%			Percentiles		
	mm	phi	wt (g)	wt (g)	wt%	finer	Modes			*phi*	*mm*
1	64.0000	-6	0.00	0.00	0.000	100.00%			95%	-3.55	11.732
2	32.0000	-5	0.00	0.00	0.000	100.00%			84%	-2.62	6.147
3	16.0000	-4	0.00	0.00	0.000	100.00%			75%	-2.12	4.353
4	8.0000	-3	5.70	5.70	0.006	99.40%			50%	-0.67	1.593
5	4.0000	-2	32.80	27.10	0.029	96.54%			25%	0.64	0.644
6	2.0000	-1	113.00	80.20	0.085	88.09%			16%	1.21	0.432
7	1.0000	0	212.30	99.30	0.105	77.62%			5%	2.07	0.238
8	0.5000	1	370.90	158.60	0.167	60.91%	mode at	0.5			
9	0.2500	2	495.20	124.30	0.131	47.81%				*phi*	*mm*
10	0.1250	3	587.20	92.00	0.097	38.11%			**Inman (1952)'s stats**		
11	0.0625	4	630.90	43.70	0.046	33.51%			Median diamete	-0.67	1.593
12	0.0313	5	651.20	20.30	0.021	31.37%			Graphic St. Dev	1.92	
									Folk and Ward (1957)'s stats		
		Sums	651.20	651.20	0.686				Graphic Mean (	-0.69	1.617
									Inclusive Graphi	1.81	

Grainsize Statistics					Sample:	W20100055					
	phi interval:	1	Cum			Cum%			Percentiles		
	mm	phi	wt (g)	wt (g)	wt%	finer	Modes			*phi*	*mm*
1	64.0000	-6	0.00	0.00	0.000	100.00%			95%	-3.55	11.732
2	32.0000	-5	0.00	0.00	0.000	100.00%			84%	-2.62	6.147
3	16.0000	-4	0.00	0.00	0.000	100.00%			75%	-2.12	4.353
4	8.0000	-3	26.50	26.50	0.028	97.21%			50%	-0.67	1.593
5	4.0000	-2	129.00	102.50	0.108	86.40%			25%	0.64	0.644
6	2.0000	-1	406.20	277.20	0.292	57.19%			16%	1.21	0.432
7	1.0000	0	773.50	367.30	0.387	18.48%	mode at	-0.5	5%	2.07	0.238
8	0.5000	1	935.90	162.40	0.171	1.36%					
9	0.2500	2	1007.90	72.00	0.076	-6.23%				*phi*	*mm*
10	0.1250	3	1048.20	40.30	0.042	-10.48%			**Inman (1952)'s stats**		
11	0.0625	4	1071.50	23.30	0.025	-12.93%			Median diamete	-0.67	1.593
12	0.0313	5	1092.40	20.90	0.022	-15.13%			Graphic St. Dev	1.92	
									Folk and Ward (1957)'s stats		
		Sums	1092.40	1092.40	1.151				Graphic Mean (	-0.69	1.617
									Inclusive Graphi	1.81	

Grainsize Statistics					Sample:	W20100057					
	phi interval:	1	Cum			Cum%			Percentiles		
	mm	phi	wt (g)	wt (g)	wt%	finer	Modes			phi	mm
1	64.0000	-6	0.00	0.00	0.000	100.00%			95%	-3.55	11.732
2	32.0000	-5	0.00	0.00	0.000	100.00%			84%	-2.62	6.147
3	16.0000	-4	19.60	19.60	0.021	97.93%			75%	-2.12	4.353
4	8.0000	-3	55.30	35.70	0.038	94.17%			50%	-0.67	1.593
5	4.0000	-2	113.20	57.90	0.061	88.07%	mode at	-2.5	25%	0.64	0.644
6	2.0000	-1	153.70	40.50	0.043	83.80%			16%	1.21	0.432
7	1.0000	0	217.00	63.30	0.067	77.13%			5%	2.07	0.238
8	0.5000	1	313.60	96.60	0.102	66.95%					
9	0.2500	2	515.30	201.70	0.213	45.69%				phi	mm
10	0.1250	3	756.40	241.10	0.254	20.28%	mode at	2.5	Inman (1952)'s stats		
11	0.0625	4	856.60	100.20	0.106	9.72%			Median diamete	-0.67	1.593
12	0.0313	5	905.30	48.70	0.051	4.58%			Graphic St. Dev	1.92	
									Folk and Ward (1957)'s stats		
		Sums.	905.30	905.30	0.954				Graphic Mean (	-0.69	1.617
									Inclusive Graphi	1.81	

Grainsize Statistics					Sample:	W20100060					
	phi interval:	1	Cum			Cum%			Percentiles		
	mm	phi	wt (g)	wt (g)	wt%	finer	Modes			phi	mm
1	64.0000	-6	0.00	0.00	0.000	100.00%			95%	-3.55	11.732
2	32.0000	-5	0.00	0.00	0.000	100.00%			84%	-2.62	6.147
3	16.0000	-4	274.30	274.30	0.289	71.09%	mode at	-4.5	75%	-2.12	4.353
4	8.0000	-3	547.80	273.50	0.288	42.26%			50%	-0.67	1.593
5	4.0000	-2	705.70	157.90	0.166	25.62%			25%	0.64	0.644
6	2.0000	-1	771.00	65.30	0.069	18.74%			16%	1.21	0.432
7	1.0000	0	816.10	45.10	0.048	13.99%			5%	2.07	0.238
8	0.5000	1	854.10	38.00	0.040	9.98%					
9	0.2500	2	886.70	32.60	0.034	6.55%				phi	mm
10	0.1250	3	914.20	27.50	0.029	3.65%			Inman (1952)'s stats		
11	0.0625	4	928.70	14.50	0.015	2.12%			Median diamete	-0.67	1.593
12	0.0313	5	934.50	5.80	0.006	1.51%			Graphic St. Dev	1.92	
									Folk and Ward (1957)'s stats		
		Sums.	934.50	934.50	0.985				Graphic Mean (	-0.69	1.617
									Inclusive Graphi	1.81	

Grainsize Statistics					Sample:	W20100072					
	phi interval:	1	Cum			Cum%			Percentiles		
	mm	phi	wt (g)	wt (g)	wt%	finer	Modes			phi	mm
1	64.0000	-6	0.00	0.00	0.000	100.00%			95%	-3.55	11.732
2	32.0000	-5	0.00	0.00	0.000	100.00%			84%	-2.62	6.147
3	16.0000	-4	0.00	0.00	0.000	100.00%			75%	-2.12	4.353
4	8.0000	-3	24.00	24.00	0.025	97.47%			50%	-0.67	1.593
5	4.0000	-2	210.10	186.10	0.196	77.86%			25%	0.64	0.644
6	2.0000	-1	679.50	469.40	0.495	28.38%	mode at	-1.5	16%	1.21	0.432
7	1.0000	0	992.40	312.90	0.330	-4.60%			5%	2.07	0.238
8	0.5000	1	1113.10	120.70	0.127	-17.32%					
9	0.2500	2	1173.40	60.30	0.064	-23.67%				phi	mm
10	0.1250	3	1214.50	41.10	0.043	-28.00%			Inman (1952)'s stats		
11	0.0625	4	1242.10	27.60	0.029	-30.91%			Median diamete	-0.67	1.593
12	0.0313	5	1247.80	5.70	0.006	-31.51%			Graphic St. Dev	1.92	
									Folk and Ward (1957)'s stats		
		Sums	1247.80	1247.80	1.315				Graphic Mean (	-0.69	1.617
									Inclusive Graphi	1.81	

Grainsize Statistics					Sample:	W20100073					
	phi interval:	1	Cum			Cum%			Percentiles		
	mm	phi	wt (g)	wt (g)	wt%	finer	Modes			phi	mm
1	64.0000	-6	0.00	0.00	0.000	100.00%			95%	-3.55	11.732
2	32.0000	-5	0.00	0.00	0.000	100.00%			84%	-2.62	6.147
3	16.0000	-4	3.60	3.60	0.004	99.62%			75%	-2.12	4.353
4	8.0000	-3	55.70	52.10	0.055	94.13%			50%	-0.67	1.593
5	4.0000	-2	136.70	81.00	0.085	85.59%			25%	0.64	0.644
6	2.0000	-1	296.70	160.00	0.169	68.73%	mode at	-1.5	16%	1.21	0.432
7	1.0000	0	435.60	138.90	0.146	54.09%			5%	2.07	0.238
8	0.5000	1	507.20	71.60	0.075	46.54%					
9	0.2500	2	559.30	52.10	0.055	41.05%				phi	mm
10	0.1250	3	609.60	50.30	0.053	35.75%			Inman (1952)'s stats		
11	0.0625	4	642.40	32.80	0.035	32.29%			Median diamete	-0.67	1.593
12	0.0313	5	663.60	21.20	0.022	30.06%			Graphic St. Dev	1.92	
									Folk and Ward (1957)'s stats		
		Sums	663.60	663.60	0.699				Graphic Mean (	-0.69	1.617
									Inclusive Graphi	1.81	

Grainsize Statistics					Sample:	W20100075					
	phi interval:	1	Cum			Cum%			Percentiles		
	mm	phi	wt (g)	wt (g)	wt%	finer	Modes			phi	mm
1	64.0000	-6	0.00	0.00	0.000	100.00%			95%	-3.55	11.732
2	32.0000	-5	0.00	0.00	0.000	100.00%			84%	-2.62	6.147
3	16.0000	-4	465.10	465.10	0.490	50.98%	mode at	-4.5	75%	-2.12	4.353
4	8.0000	-3	732.90	267.80	0.282	22.76%			50%	-0.67	1.593
5	4.0000	-2	975.90	243.00	0.256	-2.86%			25%	0.64	0.644
6	2.0000	-1	1113.15	137.25	0.145	-17.32%			16%	1.21	0.432
7	1.0000	0	1140.75	27.60	0.029	-20.23%			5%	2.07	0.238
8	0.5000	1	1145.51	4.76	0.005	-20.73%					
9	0.2500	2	1148.50	2.99	0.003	-21.05%				phi	mm
10	0.1250	3	1151.89	3.39	0.004	-21.40%	mode at	2.5	Inman (1952)'s stats		
11	0.0625	4	1154.30	2.41	0.003	-21.66%			Median diamete	-0.67	1.593
12	0.0313	5	1155.04	0.74	0.001	-21.74%			Graphic St. Dev	1.92	
									Folk and Ward (1957)'s stats		
		Sums.	1155.04	1155.04	1.217				Graphic Mean (	-0.69	1.617
									Inclusive Graphi	1.81	

Grainsize Statistics					Sample:	W20100076					
	phi interval:	1	Cum			Cum%			Percentiles		
	mm	phi	wt (g)	wt (g)	wt%	finer	Modes			phi	mm
1	64.0000	-6	0.00	0.00	0.000	100.00%			95%	-3.55	11.732
2	32.0000	-5	0.00	0.00	0.000	100.00%			84%	-2.62	6.147
3	16.0000	-4	333.00	333.00	0.351	64.90%	mode at	-4.5	75%	-2.12	4.353
4	8.0000	-3	640.70	307.70	0.324	32.47%			50%	-0.67	1.593
5	4.0000	-2	807.30	166.60	0.176	14.91%			25%	0.64	0.644
6	2.0000	-1	867.50	60.20	0.063	8.57%			16%	1.21	0.432
7	1.0000	0	901.90	34.40	0.036	4.94%			5%	2.07	0.238
8	0.5000	1	928.30	26.40	0.028	2.16%					
9	0.2500	2	948.50	20.20	0.021	0.03%				phi	mm
10	0.1250	3	959.60	11.10	0.012	-1.14%			Inman (1952)'s stats		
11	0.0625	4	963.60	4.00	0.004	-1.56%			Median diamete	-0.67	1.593
12	0.0313	5	964.40	0.80	0.001	-1.64%			Graphic St. Dev	1.92	
									Folk and Ward (1957)'s stats		
		Sums.	964.40	964.40	1.016				Graphic Mean (	-0.69	1.617
									Inclusive Graphi	1.81	

Grainsize Statistics					Sample:	W2010077					
	phi interval:	1	Cum			Cum%			Percentiles		
	mm	phi	wt (g)	wt (g)	wt%	finer	Modes			*phi*	*mm*
1	64.0000	-6	0.00	0.00	0.000	100.00%			95%	-3.55	11.732
2	32.0000	-5	0.00	0.00	0.000	100.00%			84%	-2.62	6.147
3	16.0000	-4	842.60	842.60	0.888	11.19%	mode at	-4.5	75%	-2.12	4.353
4	8.0000	-3	1080.40	237.80	0.251	-13.87%			50%	-0.67	1.593
5	4.0000	-2	1150.60	70.20	0.074	-21.27%			25%	0.64	0.644
6	2.0000	-1	1158.90	8.30	0.009	-22.14%			16%	1.21	0.432
7	1.0000	0	1162.70	3.80	0.004	-22.54%			5%	2.07	0.238
8	0.5000	1	1166.50	3.80	0.004	-22.94%					
9	0.2500	2	1171.63	5.13	0.005	-23.49%				*phi*	*mm*
10	0.1250	3	1176.89	5.26	0.006	-24.04%	mode at	2.5	**Inman (1952)'s stats**		
11	0.0625	4	1179.59	2.70	0.003	-24.32%			Median diamete	-0.67	1.593
12	0.0313	5	1180.21	0.62	0.001	-24.39%			Graphic St. Dev	1.92	
									Folk and Ward (1957)'s stats		
		Sums	1180.21	1180.21	1.244				Graphic Mean (	-0.69	1.617
									Inclusive Graphi	1.81	

Grainsize Statistics					Sample:	W20100083					
	phi interval:	1	Cum			Cum%			Percentiles		
	mm	phi	wt (g)	wt (g)	wt%	finer	Modes			*phi*	*mm*
1	64.0000	-6	0.00	0.00	0.000	100.00%			95%	-3.55	11.732
2	32.0000	-5	0.00	0.00	0.000	100.00%			84%	-2.62	6.147
3	16.0000	-4	461.56	461.56	0.486	51.35%	mode at	-4.5	75%	-2.12	4.353
4	8.0000	-3	738.82	277.26	0.292	22.13%			50%	-0.67	1.593
5	4.0000	-2	990.38	251.56	0.265	-4.38%			25%	0.64	0.644
6	2.0000	-1	1108.34	117.96	0.124	-16.81%			16%	1.21	0.432
7	1.0000	0	1169.00	60.66	0.064	-23.21%			5%	2.07	0.238
8	0.5000	1	1217.51	48.51	0.051	-28.32%					
9	0.2500	2	1257.83	40.32	0.042	-32.57%				*phi*	*mm*
10	0.1250	3	1281.31	23.48	0.025	-35.05%			**Inman (1952)'s stats**		
11	0.0625	4	1289.87	8.56	0.009	-35.95%			Median diamete	-0.67	1.593
12	0.0313	5	1292.45	2.58	0.003	-36.22%			Graphic St. Dev	1.92	
									Folk and Ward (1957)'s stats		
		Sums	1292.45	1292.45	1.362				Graphic Mean (	-0.69	1.617
									Inclusive Graphi	1.81	

Grainsize Statistics					Sample:	W20100090					
	phi interval:	1	Cum			Cum% finer			Percentiles		
	mm	phi	wt (g)	wt (g)	wt%		Modes			phi	mm
1	64.0000	-6	0.00	0.00	0.000	100.00%			95%	-3.55	11.732
2	32.0000	-5	0.00	0.00	0.000	100.00%			84%	-2.62	6.147
3	16.0000	-4	717.10	717.10	0.756	24.42%	mode at	-4.5	75%	-2.12	4.353
4	8.0000	-3	965.00	247.90	0.261	-1.71%			50%	-0.67	1.593
5	4.0000	-2	1115.60	150.60	0.159	-17.58%			25%	0.64	0.644
6	2.0000	-1	1163.50	47.90	0.050	-22.63%			16%	1.21	0.432
7	1.0000	0	1179.50	16.00	0.017	-24.31%			5%	2.07	0.238
8	0.5000	1	1189.60	10.10	0.011	-25.38%					
9	0.2500	2	1197.90	8.30	0.009	-26.25%				phi	mm
10	0.1250	3	1204.40	6.50	0.007	-26.94%			Inman (1952)'s stats		
11	0.0625	4	1208.00	3.60	0.004	-27.32%			Median diamete	-0.67	1.593
12	0.0313	5	1209.70	1.70	0.002	-27.50%			Graphic St. Dev	1.92	
									Folk and Ward (1957)'s stats		
		Sums.	1209.70	1209.70	1.275				Graphic Mean (	-0.69	1.617
									Inclusive Graphi	1.81	

Grainsize Statistics					Sample:	W20100092					
	phi interval:	1	Cum			Cum% finer			Percentiles		
	mm	phi	wt (g)	wt (g)	wt%		Modes			phi	mm
1	64.0000	-6	0.00	0.00	0.000	100.00%			95%	-3.55	11.732
2	32.0000	-5	0.00	0.00	0.000	100.00%			84%	-2.62	6.147
3	16.0000	-4	776.00	776.00	0.818	18.21%	mode at	-4.5	75%	-2.12	4.353
4	8.0000	-3	1250.00	474.00	0.500	-31.75%			50%	-0.67	1.593
5	4.0000	-2	1411.60	161.60	0.170	-48.78%			25%	0.64	0.644
6	2.0000	-1	1431.50	19.90	0.021	-50.87%			16%	1.21	0.432
7	1.0000	0	1432.10	0.60	0.001	-50.94%			5%	2.07	0.238
8	0.5000	1	1432.70	0.60	0.001	-51.00%					
9	0.2500	2	1436.20	3.50	0.004	-51.37%				phi	mm
10	0.1250	3	1446.30	10.10	0.011	-52.43%	mode at	2.5	Inman (1952)'s stats		
11	0.0625	4	1450.70	4.40	0.005	-52.90%			Median diamete	-0.67	1.593
12	0.0313	5	1451.70	1.00	0.001	-53.00%			Graphic St. Dev	1.92	
									Folk and Ward (1957)'s stats		
		Sums.	1451.70	1451.70	1.530				Graphic Mean (	-0.69	1.617
									Inclusive Graphi	1.81	

Grainsize Statistics					Sample:	W20100094					
	phi interval:	1	Cum			Cum%			Percentiles		
	mm	phi	wt (g)	wt (g)	wt%	finer	Modes			*phi*	*mm*
1	64.0000	-6	0.00	0.00	0.000	100.00%			95%	-3.55	11.732
2	32.0000	-5	0.00	0.00	0.000	100.00%			84%	-2.62	6.147
3	16.0000	-4	449.30	449.30	0.474	52.65%	mode at	-4.5	75%	-2.12	4.353
4	8.0000	-3	802.90	353.60	0.373	15.38%			50%	-0.67	1.593
5	4.0000	-2	1029.30	226.40	0.239	-8.48%			25%	0.64	0.644
6	2.0000	-1	1086.50	57.20	0.060	-14.51%			16%	1.21	0.432
7	1.0000	0	1103.80	17.30	0.018	-16.34%			5%	2.07	0.238
8	0.5000	1	1114.40	10.60	0.011	-17.45%					
9	0.2500	2	1123.20	8.80	0.009	-18.38%				*phi*	*mm*
10	0.1250	3	1131.70	8.50	0.009	-19.28%			**Inman (1952)'s stats**		
11	0.0625	4	1138.00	6.30	0.007	-19.94%			Median diamete	-0.67	1.593
12	0.0313	5	1141.30	3.30	0.003	-20.29%			Graphic St. Dev	1.92	
									Folk and Ward (1957)'s stats		
		Sums	1141.30	1141.30	1.203				Graphic Mean (	-0.69	1.617
									Inclusive Graphi	1.81	

Grainsize Statistics					Sample:	W20100095					
	phi interval:	1	Cum			Cum%			Percentiles		
	mm	phi	wt (g)	wt (g)	wt%	finer	Modes			*phi*	*mm*
1	64.0000	-6	0.00	0.00	0.000	100.00%			95%	-3.55	11.732
2	32.0000	-5	0.00	0.00	0.000	100.00%			84%	-2.62	6.147
3	16.0000	-4	112.90	112.90	0.119	88.10%			75%	-2.12	4.353
4	8.0000	-3	390.90	278.00	0.293	58.80%			50%	-0.67	1.593
5	4.0000	-2	781.60	390.70	0.412	17.62%	mode at	-2.5	25%	0.64	0.644
6	2.0000	-1	965.60	184.00	0.194	-1.77%			16%	1.21	0.432
7	1.0000	0	1023.40	57.80	0.061	-7.86%			5%	2.07	0.238
8	0.5000	1	1048.47	25.07	0.026	-10.50%					
9	0.2500	2	1063.67	15.20	0.016	-12.11%				*phi*	*mm*
10	0.1250	3	1074.66	10.99	0.012	-13.27%			**Inman (1952)'s stats**		
11	0.0625	4	1080.85	6.19	0.007	-13.92%			Median diamete	-0.67	1.593
12	0.0313	5	1083.87	3.02	0.003	-14.24%			Graphic St. Dev	1.92	
									Folk and Ward (1957)'s stats		
		Sums	1083.87	1083.87	1.142				Graphic Mean (	-0.69	1.617
									Inclusive Graphi	1.81	

Grainsize Statistics					Sample:	W20100096					
	phi interval:	1	Cum			Cum%			Percentiles		
	mm	phi	wt (g)	wt (g)	wt%	finer	Modes			phi	mm
1	64.0000	-6	0.00	0.00	0.000	100.00%			95%	-3.55	11.732
2	32.0000	-5	0.00	0.00	0.000	100.00%			84%	-2.62	6.147
3	16.0000	-4	528.40	528.40	0.557	44.31%	mode at	-4.5	75%	-2.12	4.353
4	8.0000	-3	878.90	350.50	0.369	7.37%			50%	-0.67	1.593
5	4.0000	-2	1043.80	164.90	0.174	-10.01%			25%	0.64	0.644
6	2.0000	-1	1080.90	37.10	0.039	-13.92%			16%	1.21	0.432
7	1.0000	0	1091.42	10.52	0.011	-15.03%			5%	2.07	0.238
8	0.5000	1	1096.71	5.29	0.006	-15.59%					
9	0.2500	2	1101.29	4.58	0.005	-16.07%				phi	mm
10	0.1250	3	1106.87	5.58	0.006	-16.66%	mode at	2.5	Inman (1952)'s stats		
11	0.0625	4	1111.88	5.01	0.005	-17.19%			Median diamete	-0.67	1.593
12	0.0313	5	1114.70	2.82	0.003	-17.49%			Graphic St. Dev	1.92	
									Folk and Ward (1957)'s stats		
		Sums.	1114.70	1114.70	1.175				Graphic Mean (	-0.69	1.617
									Inclusive Graphi	1.81	

ıinsize Statistics				Sample:	W20100097					
phi interval:	1	Cum			Cum%			Percentiles		
mm	phi	wt (g)	wt (g)	wt%	finer	Modes			phi	mm
64.0000	-6	0.00	0.00	0.000	100.00%			95%	-3.55	11.732
32.0000	-5	0.00	0.00	0.000	100.00%			84%	-2.62	6.147
16.0000	-4	383.50	383.50	0.404	59.58%	mode at	-4.5	75%	-2.12	4.353
8.0000	-3	698.40	314.90	0.332	26.39%			50%	-0.67	1.593
4.0000	-2	1040.90	342.50	0.361	-9.71%	mode at	-2.5	25%	0.64	0.644
2.0000	-1	1135.70	94.80	0.100	-19.70%			16%	1.21	0.432
1.0000	0	1163.30	27.60	0.029	-22.61%			5%	2.07	0.238
0.5000	1	1180.00	16.70	0.018	-24.37%					
0.2500	2	1193.80	13.80	0.015	-25.82%				phi	mm
0.1250	3	1206.10	12.30	0.013	-27.12%			Inman (1952)'s stats		
0.0625	4	1213.90	7.80	0.008	-27.94%			Median diamete	-0.67	1.593
0.0313	5	1217.70	3.80	0.004	-28.34%			Graphic St. Dev	1.92	
								Folk and Ward (1957)'s stats		
	Sums.	1217.70	1217.70	1.283				Graphic Mean (	-0.69	1.617
								Inclusive Graphi	1.81	

Grainsize Statistics					Sample:	W20100098					
	phi interval:	1	Cum			Cum%			Percentiles		
	mm	phi	wt (g)	wt (g)	wt%	finer	Modes			phi	mm
1	64.0000	-6	0.00	0.00	0.000	100.00%			95%	-3.55	11.732
2	32.0000	-5	0.00	0.00	0.000	100.00%			84%	-2.62	6.147
3	16.0000	-4	149.60	149.60	0.158	84.23%			75%	-2.12	4.353
4	8.0000	-3	447.70	298.10	0.314	52.81%			50%	-0.67	1.593
5	4.0000	-2	826.90	379.20	0.400	12.85%	mode at	-2.5	25%	0.64	0.644
6	2.0000	-1	951.10	124.20	0.131	-0.24%			16%	1.21	0.432
7	1.0000	0	988.80	37.70	0.040	-4.22%			5%	2.07	0.238
8	0.5000	1	1021.30	32.50	0.034	-7.64%					
9	0.2500	2	1037.20	15.90	0.017	-9.32%				phi	mm
10	0.1250	3	1048.70	11.50	0.012	-10.53%			Inman (1952)'s stats		
11	0.0625	4	1054.40	5.70	0.006	-11.13%			Median diamete	-0.67	1.593
12	0.0313	5	1055.70	1.30	0.001	-11.27%			Graphic St. Dev	1.92	
									Folk and Ward (1957)'s stats		
		Sums	1055.70	1055.70	1.113				Graphic Mean (	-0.69	1.617
									Inclusive Graphi	1.81	

Grainsize Statistics					Sample:	W20100099					
	phi interval:	1	Cum			Cum%			Percentiles		
	mm	phi	wt (g)	wt (g)	wt%	finer	Modes			phi	mm
1	64.0000	-6	0.00	0.00	0.000	100.00%			95%	-3.55	11.732
2	32.0000	-5	0.00	0.00	0.000	100.00%			84%	-2.62	6.147
3	16.0000	-4	713.80	713.80	0.752	24.77%	mode at	-4.5	75%	-2.12	4.353
4	8.0000	-3	993.80	280.00	0.295	-4.74%			50%	-0.67	1.593
5	4.0000	-2	1140.10	146.30	0.154	-20.16%			25%	0.64	0.644
6	2.0000	-1	1180.10	40.00	0.042	-24.38%			16%	1.21	0.432
7	1.0000	0	1189.30	9.20	0.010	-25.35%			5%	2.07	0.238
8	0.5000	1	1193.80	4.50	0.005	-25.82%					
9	0.2500	2	1198.70	4.90	0.005	-26.34%				phi	mm
10	0.1250	3	1205.10	6.40	0.007	-27.01%	mode at	2.5	Inman (1952)'s stats		
11	0.0625	4	1210.60	5.50	0.006	-27.59%			Median diamete	-0.67	1.593
12	0.0313	5	1213.30	2.70	0.003	-27.88%			Graphic St. Dev	1.92	
									Folk and Ward (1957)'s stats		
		Sums	1213.30	1213.30	1.279				Graphic Mean (	-0.69	1.617
									Inclusive Graphi	1.81	

Grainsize Statistics					Sample:	W20100100					
	phi interval:	1	Cum			Cum%			Percentiles		
	mm	phi	wt (g)	wt (g)	wt%	finer	Modes			phi	mm
1	64.0000	-6	0.00	0.00	0.000	100.00%			95%	-3.55	11.732
2	32.0000	-5	0.00	0.00	0.000	100.00%			84%	-2.62	6.147
3	16.0000	-4	116.40	116.40	0.123	87.73%			75%	-2.12	4.353
4	8.0000	-3	317.00	200.60	0.211	66.59%			50%	-0.67	1.593
5	4.0000	-2	767.80	450.80	0.475	19.08%	mode at	-2.5	25%	0.64	0.644
6	2.0000	-1	1020.10	252.30	0.266	-7.51%			16%	1.21	0.432
7	1.0000	0	1064.18	44.08	0.046	-12.16%			5%	2.07	0.238
8	0.5000	1	1079.19	15.01	0.016	-13.74%					
9	0.2500	2	1097.37	18.18	0.019	-15.66%	mode at	1.5		phi	mm
10	0.1250	3	1113.10	15.73	0.017	-17.32%			Inman (1952)'s stats		
11	0.0625	4	1120.58	7.48	0.008	-18.10%			Median diamete	-0.67	1.593
12	0.0313	5	1123.17	2.59	0.003	-18.38%			Graphic St. Dev	1.92	
									Folk and Ward (1957)'s stats		
		Sums.	1123.17	1123.17	1.184				Graphic Mean (	-0.69	1.617
									Inclusive Graphi	1.81	

Grainsize Statistics					Sample:	W20100101					
	phi interval:	1	Cum			Cum%			Percentiles		
	mm	phi	wt (g)	wt (g)	wt%	finer	Modes			phi	mm
1	64.0000	-6	0.00	0.00	0.000	100.00%			95%	-3.55	11.732
2	32.0000	-5	0.00	0.00	0.000	100.00%			84%	-2.62	6.147
3	16.0000	-4	540.40	540.40	0.570	43.04%	mode at	-4.5	75%	-2.12	4.353
4	8.0000	-3	848.00	307.60	0.324	10.62%			50%	-0.67	1.593
5	4.0000	-2	1121.80	273.80	0.289	-18.23%			25%	0.64	0.644
6	2.0000	-1	1203.00	81.20	0.086	-26.79%			16%	1.21	0.432
7	1.0000	0	1217.70	14.70	0.015	-28.34%			5%	2.07	0.238
8	0.5000	1	1228.68	10.98	0.012	-29.50%					
9	0.2500	2	1242.76	14.08	0.015	-30.98%	mode at	1.5		phi	mm
10	0.1250	3	1253.91	11.15	0.012	-32.16%			Inman (1952)'s stats		
11	0.0625	4	1260.08	6.17	0.007	-32.81%			Median diamete	-0.67	1.593
12	0.0313	5	1262.66	2.58	0.003	-33.08%			Graphic St. Dev	1.92	
									Folk and Ward (1957)'s stats		
		Sums.	1262.66	1262.66	1.331				Graphic Mean (	-0.69	1.617
									Inclusive Graphi	1.81	

Grainsize Statistics					Sample:	W20100102					
	phi interval:	1	Cum			Cum%			Percentiles		
	mm	phi	wt (g)	wt (g)	wt%	finer	Modes			phi	mm
1	64.0000	-6	0.00	0.00	0.000	100.00%			95%	-3.55	11.732
2	32.0000	-5	0.00	0.00	0.000	100.00%			84%	-2.62	6.147
3	16.0000	-4	5.21	5.21	0.005	99.45%			75%	-2.12	4.353
4	8.0000	-3	153.51	148.30	0.156	83.82%			50%	-0.67	1.593
5	4.0000	-2	495.51	342.00	0.360	47.78%	mode at	-2.5	25%	0.64	0.644
6	2.0000	-1	760.21	264.70	0.279	19.88%			16%	1.21	0.432
7	1.0000	0	884.61	124.40	0.131	6.77%			5%	2.07	0.238
8	0.5000	1	948.61	64.00	0.067	0.02%					
9	0.2500	2	985.61	37.00	0.039	-3.88%				phi	mm
10	0.1250	3	1005.61	20.00	0.021	-5.99%			Inman (1952)'s stats		
11	0.0625	4	1012.91	7.30	0.008	-6.76%			Median diamete	-0.67	1.593
12	0.0313	5	1015.61	2.70	0.003	-7.04%			Graphic St. Dev	1.92	
									Folk and Ward (1957)'s stats		
		Sums	1015.61	1015.61	1.070				Graphic Mean (	-0.69	1.617
									Inclusive Graphi	1.81	

Grainsize Statistics					Sample:	W20100103					
	phi interval:	1	Cum			Cum%			Percentiles		
	mm	phi	wt (g)	wt (g)	wt%	finer	Modes			phi	mm
1	64.0000	-6	0.00	0.00	0.000	100.00%			95%	-3.55	11.732
2	32.0000	-5	0.00	0.00	0.000	100.00%			84%	-2.62	6.147
3	16.0000	-4	190.20	190.20	0.200	79.95%			75%	-2.12	4.353
4	8.0000	-3	451.60	261.40	0.276	52.40%			50%	-0.67	1.593
5	4.0000	-2	769.70	318.10	0.335	18.88%	mode at	-2.5	25%	0.64	0.644
6	2.0000	-1	912.90	143.20	0.151	3.78%			16%	1.21	0.432
7	1.0000	0	959.20	46.30	0.049	-1.10%			5%	2.07	0.238
8	0.5000	1	985.90	26.70	0.028	-3.91%					
9	0.2500	2	1007.40	21.50	0.023	-6.18%				phi	mm
10	0.1250	3	1023.30	15.90	0.017	-7.85%			Inman (1952)'s stats		
11	0.0625	4	1032.00	8.70	0.009	-8.77%			Median diamete	-0.67	1.593
12	0.0313	5	1035.50	3.50	0.004	-9.14%			Graphic St. Dev	1.92	
									Folk and Ward (1957)'s stats		
		Sums	1035.50	1035.50	1.091				Graphic Mean (	-0.69	1.617
									Inclusive Graphi	1.81	

Grainsize Statistics					Sample:	W20100104					
	phi interval:	1	Cum			Cum%			Percentiles		
	mm	phi	wt (g)	wt (g)	wt%	finer	Modes			*phi*	*mm*
1	64.0000	-6	0.00	0.00	0.000	100.00%			95%	-3.55	11.732
2	32.0000	-5	0.00	0.00	0.000	100.00%			84%	-2.62	6.147
3	16.0000	-4	4.80	4.80	0.005	99.49%			75%	-2.12	4.353
4	8.0000	-3	63.40	58.60	0.062	93.32%			50%	-0.67	1.593
5	4.0000	-2	276.60	213.20	0.225	70.85%			25%	0.64	0.644
6	2.0000	-1	538.90	262.30	0.276	43.20%			16%	1.21	0.432
7	1.0000	0	818.10	279.20	0.294	13.78%	mode at	-0.5	5%	2.07	0.238
8	0.5000	1	954.10	136.00	0.143	-0.56%					
9	0.2500	2	991.80	37.70	0.040	-4.53%				*phi*	*mm*
10	0.1250	3	1006.40	14.60	0.015	-6.07%			Inman (1952)'s stats		
11	0.0625	4	1012.60	6.20	0.007	-6.72%			Median diamete	-0.67	1.593
12	0.0313	5	1015.10	2.50	0.003	-6.99%			Graphic St. Dev	1.92	
									Folk and Ward (1957)'s stats		
		Sums.	1015.10	1015.10	1.070				Graphic Mean (	-0.69	1.617
									Inclusive Graphi	1.81	

Appendix C

Vesicularity Data

Vadded

Run	1	2	3	4
Temp (º C)	24.6	24.6	24.6	24.6
P_A	18.625	18.621	18.616	18.615
P_B	11.471	11.467	11.464	11.463

Vadded sphere

Run	1	2	3	4	5	6	7
Temp (º C)	24.7	24.6	24.7	24.7	24.7	24.7	24.7
P_A	18.686	18.675	18.669	18.665	18.666	18.665	18.666
P_B	9.608	9.599	9.595	9.592	9.591	9.591	9.591

Vcell

Run	1	2	3
Temp (º C)	24.8	24.8	24.8
P_A	18.693	18.682	18.675
P_B	9.612	9.606	9.603
Vcell (cc)	20.779	20.7779	20.7784

Vadded=12.9514cc
Vcell=20.7784 cc

Acacia Bay (W20100004) Weight: 7.50 g

Run	1	2	3
Temp (º C)	25.4	25.4	25.4
P_A	18.677	18.669	18.663
P_B	10.912	10.907	10.904
Volume (cc)	2.5774	2.5788	2.5778
Density (g/cc)	2.9099	2.9084	2.9094

Kaiapo (W20100026) Weight: 6.75 g

Run	1	2	3	4	5	6
Temp (º C)	24.8	24.8	24.9	24.9	24.9	24.9
P_A	18.661	18.677	18.672	18.669	18.665	18.662
P_B	10.975	10.985	10.982	10.981	10.978	10.977
Volume (cc)	2.2861	2.2829	2.285	2.2816	2.2813	2.2803
Density (cc)	2.9526	2.9568	2.954	2.9585	2.9589	2.9601

Kinloch (W20100060) Weight: 7.99 g

Run	1	2	3
Temp (º C)	25	25	25
P_A	18.67	18.659	18.649
P_B	10.877	10.87	10.865
Volume (cc)	2.7006	2.7027	2.7023
Density (cc)	2.9586	2.9563	2.9567

Punatekahi B (W20100075) Weight: 9.93 g

Run	1	2	3	4	5
Temp (º C)	25.1	25.1	25.1	25.1	25.2
P_A	18.656	18.674	18.669	18.663	18.659
P_B	10.72	10.73	10.728	10.724	10.722
Volume (cc)	3.2831	3.2863	3.2808	3.2853	3.2826
Density (cc)	3.0246	3.0217	3.0267	3.0226	3.025

Punatekahi A (W20100099) Weight: 7.54 g

Run	1	2	3	4	5	6
Temp (º C)	25.2	25.2	25.2	25.2	25.2	25.2
P_A	18.674	18.665	18.661	18.659	18.656	18.678
P_B	10.93	10.925	10.921	10.921	10.919	10.933
Volume (cc)	2.4993	2.4973	2.5034	2.4992	2.5002	2.4973
Density (cc)	3.0168	3.0193	3.0119	3.0169	3.0157	3.0192

Punatekahi A North (W20100102) Weight: 7.10 g

Run	1	2	3	4	5	6	7	8	9	10
Temp (º C)	25.3	25.3	25.3	25.3	25.3	25.3	25.3	25.3	25.3	25.3
P_A	18.671	18.665	18.661	18.656	18.674	18.668	18.663	18.665	18.665	18.666
P_B	10.967	10.962	10.959	10.957	10.967	10.963	10.961	10.962	10.961	10.962
Volume (cc)	2.3431	2.3464	2.3501	2.346	2.3475	2.3507	2.3469	2.349	2.35	2.3497
Density (cc)	3.0302	3.0259	3.0212	3.0264	3.0244	3.0204	3.0253	3.0226	3.0212	3.0217

Sample	Dry weight (g)	Wet weight (g)	Ballast weight (g)	Parafilm weight (g)	Density (g/cm^3)	DRE (g/cm^3)	Vesic-ularity (%)
W20100004	6.89	1.73	0	0	1.34	2.9092	54.10
	5.76	1.59	0	0	1.38	2.9092	52.52
	5.76	1.38	0	0	1.32	2.9092	54.80
	4.43	1.06	0	0	1.31	2.9092	54.81
	10.37	2.53	0	0	1.32	2.9092	54.53
	4.71	0.70	0	0	1.17	2.9092	59.63
	5.26	1.02	0	0	1.24	2.9092	57.36
	5.81	0.97	0	0	1.20	2.9092	58.74
	10.00	4.16	0	0	1.71	2.9092	41.14
	5.23	1.27	0	0	1.32	2.9092	54.60
W2010023	5.94	1.89	0	0	1.47	2.9592	50.44
	9.57	3.76	0	0	1.65	2.9592	44.34
	9.40	4.29	0	0	1.84	2.9592	37.84
	6.46	3.19	0	0.03	1.99	2.9592	32.62
	5.25	2.00	0	0.03	1.63	2.9592	44.90
	9.68	4.65	0	0	1.92	2.9592	34.97
	5.10	2.26	0	0.03	1.81	2.9592	38.67
	4.31	1.55	0	0.03	1.58	2.9592	46.65
	7.01	3.52	0	0.03	2.03	2.9592	31.54
	4.74	2.01	0	0.03	1.76	2.9592	40.67
W20100025	5.33	1.92	0	0	1.56	2.9592	47.18
	3.49	33.10	33.28	0	0.95	2.9592	67.86
	3.88	0.64	0	0.03	1.21	2.9592	59.15
	8.66	3.10	0	0	1.56	2.9592	47.37
	4.78	2.01	0	0.03	1.74	2.9592	41.05
	10.70	3.40	0	0	1.47	2.9592	50.47
	9.89	4.13	0	0	1.72	2.9592	41.98
	5.69	2.41	0	0.03	1.75	2.9592	40.84
	3.62	1.72	0	0.03	1.94	2.9592	34.58
	1.62	0.54	0	0.03	1.54	2.9592	47.86
W20100026	8.85	2.90	0	0	1.49	2.9592	49.74
	9.77	3.56	0	0	1.57	2.9592	46.83
	7.86	2.68	0	0	1.52	2.9592	48.72
	6.83	2.29	0	0	1.50	2.9592	49.16
	7.00	2.85	0	0	1.69	2.9592	43.00
	4.74	1.67	0	0.03	1.56	2.9592	47.31
	6.35	2.35	0	0	1.59	2.9592	46.35
	6.32	2.75	0	0.03	1.79	2.9592	39.67
	7.04	2.54	0	0	1.56	2.9592	47.13
	14.48	5.50	0	0	1.61	2.9592	45.51

Sample	Dry weight (g)	Wet weight (g)	Ballast weight (g)	Parafilm weight (g)	Density (g/cm^3)	DRE (g/cm^3)	Vesic-ularity (%)
W20100027	2.27	0.90	0	0.03	1.69	2.9592	42.75
	5.17	0.73	0	0	1.16	2.9592	60.65
	4.01	1.48	0	0.03	1.60	2.9592	45.80
	3.19	1.18	0	0.03	1.61	2.9592	45.56
	7.87	2.02	0	0	1.35	2.9592	54.54
	4.79	2.24	0	0.03	1.90	2.9592	35.77
	6.57	2.69	0	0.03	1.71	2.9592	42.33
	4.49	0.60	0	0	1.15	2.9592	60.99
	9.57	3.94	0	0	1.70	2.9592	42.56
	5.52	2.41	0	0.03	1.79	2.9592	39.44
W20100028	9.06	3.04	0	0	1.50	2.9592	49.14
	4.65	1.46	0	0	1.46	2.9592	50.74
	6.89	2.53	0	0	1.58	2.9592	46.60
	6.06	2.01	0	0	1.50	2.9592	49.44
	7.57	2.95	0	0	1.64	2.9592	44.63
	10.13	3.74	0	0	1.59	2.9592	46.43
	5.20	1.74	0	0	1.50	2.9592	49.21
	9.44	2.51	0	0	1.36	2.9592	53.97
	11.47	4.78	0	0	1.71	2.9592	42.06
	11.70	5.92	0	0	2.02	2.9592	31.60
W20100060	4.72	1.91	0	0.03	1.70	2.9572	42.59
	5.67	2.88	0	0.03	2.05	2.9572	30.53
	10.14	4.6	0	0	1.83	2.9572	38.11
	7.12	3.00	0	0	1.73	2.9572	41.56
	8.30	4.05	0	0	1.95	2.9572	33.96
	6.04	2.65	0	0.03	1.80	2.9572	39.21
	19.3	9.96	0	0	2.07	2.9572	30.12
	8.26	3.98	0	0	1.93	2.9572	34.74
	4.90	2.28	0	0.03	1.89	2.9572	36.02
	5.27	2.47	0	0.03	1.90	2.9572	35.66
W20100075	6.96	44.29	45.97	0.06	0.81	3.0248	73.18
	5.10	45.30	45.97	0.06	0.89	3.0248	70.47
	6.12	0.82	0	0.06	1.17	3.0248	61.39
	8.90	45.59	45.97	0.06	0.97	3.0248	68.09
	8.69	2.66	0	0.06	1.46	3.0248	51.88
	4.31	44.54	45.97	0.06	0.76	3.0248	74.91
	4.82	45.90	45.97	0.06	1.00	3.0248	67.01
	4.74	45.38	45.97	0.06	0.90	3.0248	70.26
	8.50	1.12	0	0.06	1.16	3.0248	61.61
	5.25	44.42	45.97	0.06	0.78	3.0248	74.25

Sample	Dry weight (g)	Wet weight (g)	Ballast weight (g)	Parafilm weight (g)	Density (g/cm^3)	DRE (g/cm^3)	Vesic-ularity (%)
W20100076	6.31	45.87	45.97	0.06	0.99	3.0248	67.15
	3.82	45.3	45.97	0.06	0.86	3.0248	71.49
	8.78	2.57	0	0.06	1.43	3.0248	52.80
	3.29	0.32	0	0.03	1.12	3.0248	63.00
	13.58	6.93	0	0.06	2.06	3.0248	31.87
	4.72	0.62	0	0.06	1.17	3.0248	61.38
	4.66	1.28	0	0.03	1.39	3.0248	54.01
	5.09	45.84	45.97	0.06	0.99	3.0248	67.39
	6.90	0.23	0	0.06	1.04	3.0248	65.49
	4.95	45.31	45.97	0.06	0.89	3.0248	70.51
W20100077	6.69	2.40	0	0.06	1.58	3.0248	47.71
	7.18	0.30	0	0.06	1.05	3.0248	65.19
	2.43	0.14	0	0.03	1.08	3.0248	64.45
	10.54	3.34	0	0.06	1.48	3.0248	51.20
	5.12	1.56	0	0.06	1.46	3.0248	51.64
	4.21	0.22	0	0.06	1.07	3.0248	64.58
	4.75	0.63	0	0.06	1.17	3.0248	61.32
	2.99	0.12	0	0.03	1.05	3.0248	65.19
	5.42	0.25	0	0.06	1.06	3.0248	64.93
	3.89	0.18	0	0.06	1.07	3.0248	64.77
W20100083	9.09	1.18	0	0.06	1.16	3.0173	61.62
	11.06	1.78	0	0.06	1.20	3.0173	60.24
	8.42	3.14	0	0.06	1.61	3.0173	46.54
	7.40	2.58	0	0.06	1.55	3.0173	48.48
	9.78	3.43	0	0.06	1.55	3.0173	48.47
	3.75	1.15	0	0.03	1.46	3.0173	51.64
	4.64	0.09	0	0.06	1.03	3.0173	65.75
	5.01	0.97	0	0.06	1.26	3.0173	58.28
	3.97	0.99	0	0.03	1.35	3.0173	55.40
	4.68	0.11	0	0.06	1.04	3.0173	65.61
W20100090	5.32	0.46	0	0.06	1.11	3.0173	63.27
	4.75	0.52	0	0.06	1.14	3.0173	62.25
	4.63	45.39	46.15	0.06	0.87	3.0173	71.21
	5.51	0.19	0	0.06	1.05	3.0173	65.28
	4.17	1.45	0	0.03	1.55	3.0173	48.62
	3.32	0.49	0	0.03	1.19	3.0173	60.70
	6.45	1.92	0	0.06	1.44	3.0173	52.18
	12.31	4.87	0	0.06	1.67	3.0173	44.72
	2.88	0.14	0	0.03	1.06	3.0173	64.78
	5.94	46.13	46.15	0.06	1.01	3.0173	66.63

Sample	Dry weight (g)	Wet weight (g)	Ballast weight (g)	Parafilm weight (g)	Density (g/cm^3)	DRE (g/cm^3)	Vesic-ularity (%)
W20100092	7.12	1.45	0	0.06	1.27	3.0173	57.94
	8.64	0.55	0	0.06	1.08	3.0173	64.34
	5.08	0.32	0	0.06	1.08	3.0173	64.18
	5.75	46.09	46.15	0.06	1.00	3.0173	66.86
	6.24	1.44	0	0.06	1.32	3.0173	56.37
	4.81	1.55	0	0.03	1.49	3.0173	50.65
	2.96	0.15	0	0.03	1.06	3.0173	64.71
	4.43	0.81	0	0.06	1.24	3.0173	58.76
	7.59	0.89	0	0.06	1.14	3.0173	62.12
	4.03	45.96	46.15	0.06	0.97	3.0173	67.89
W20100094	3.15	45.85	45.97	0.06	0.98	3.0173	67.48
	5.94	1.54	0	0.06	1.37	3.0173	54.64
	11.44	3.30	0	0.06	1.42	3.0173	53.08
	6.37	1.27	0	0.06	1.26	3.0173	58.11
	3.32	45.64	45.97	0.06	0.92	3.0173	69.35
	6.86	3.41	0	0.06	2.02	3.0173	32.93
	6.35	1.72	0	0.06	1.39	3.0173	53.95
	5.10	1.56	0	0.06	1.47	3.0173	51.43
	8.43	2.02	0	0.06	1.33	3.0173	56.00
	24.86	15.01	0	0.06	2.54	3.0173	15.84
W20100095	16.23	7.29	0	0.06	1.83	3.0173	39.43
	18.46	1.68	0	0.06	1.10	3.0173	63.41
	5.42	0.40	0	0.06	1.09	3.0173	63.78
	10.38	2.53	0	0.06	1.33	3.0173	55.84
	3.81	0.22	0	0.06	1.08	3.0173	64.23
	4.09	0.58	0	0.06	1.19	3.0173	60.71
	4.87	1.40	0	0.06	1.43	3.0173	52.67
	9.17	3.06	0	0.06	1.52	3.0173	49.77
	5.44	1.38	0	0.06	1.36	3.0173	54.93
	3.93	1.36	0	0.03	1.55	3.0173	48.72
W20100096	3.88	1.00	0	0.03	1.36	3.0173	54.88
	7.05	0.48	0	0.06	1.08	3.0173	64.11
	4.51	0.70	0	0.06	1.20	3.0173	60.14
	2.09	33.22	33.28	0.03	0.99	3.0173	67.33
	9.84	2.61	0	0.06	1.37	3.0173	54.52
	5.52	0.31	0	0.06	1.07	3.0173	64.48
	3.83	46.13	45.97	0.06	1.06	3.0173	64.84
	3.82	0.94	0	0.03	1.34	3.0173	55.58
	5.15	0.70	0	0.06	1.17	3.0173	61.12
	10.63	3.86	0	0.06	1.58	3.0173	47.50

Sample	Dry weight (g)	Wet weight (g)	Ballast weight (g)	Parafilm weight (g)	Density (g/cm^3)	DRE (g/cm^3)	Vesic-ularity (%)
W20100097	11.72	5.33	0	0.06	1.85	3.0173	38.64
	11.92	4.89	0	0.06	1.71	3.0173	43.32
	6.58	1.34	0	0.06	1.27	3.0173	57.90
	4.85	1.57	0	0.03	1.49	3.0173	50.54
	8.78	3.46	0	0.06	1.67	3.0173	44.68
	3.68	0.13	0	0.06	1.05	3.0173	65.05
	6.61	1.72	0	0.06	1.37	3.0173	54.64
	4.40	1.39	0	0.06	1.49	3.0173	50.57
	6.11	0.29	0	0.06	1.06	3.0173	64.84
	6.65	1.15	0	0.06	1.22	3.0173	59.49
W20100098	7.27	3.07	0	0.06	1.76	3.0173	41.80
	3.98	33.11	33.28	0.06	0.97	3.0173	67.75
	6.79	1.32	0	0.06	1.26	3.0173	58.40
	4.37	0.08	0	0.06	1.03	3.0173	65.76
	5.92	0.90	0	0.06	1.19	3.0173	60.44
	3.63	32.66	33.28	0.06	0.87	3.0173	71.29
	6.26	1.44	0	0.06	1.32	3.0173	56.41
	12.88	4.20	0	0.06	1.49	3.0173	50.48
	10.39	2.76	0	0.06	1.37	3.0173	54.51
	3.28	0.47	0	0.03	1.18	3.0173	60.90
W20100099	5.89	1.01	0	0.06	1.22	3.0173	59.50
	7.84	2.49	0	0.06	1.48	3.0173	50.88
	6.89	0.65	0	0.06	1.11	3.0173	63.05
	4.37	0.29	0	0.06	1.09	3.0173	63.97
	6.84	0.20	0	0.06	1.04	3.0173	65.55
	7.08	1.90	0	0.06	1.38	3.0173	54.17
	4.97	1.21	0	0.06	1.34	3.0173	55.48
	4.31	0.64	0	0.06	1.19	3.0173	60.43
	3.70	0.46	0	0.03	1.15	3.0173	61.80
	7.57	1.31	0	0.06	1.22	3.0173	59.53
W20100100	7.19	1.97	0	0.06	1.39	3.0173	53.82
	10.5	3.68	0	0.06	1.55	3.0173	48.52
	3.53	1.12	0	0.03	1.48	3.0173	50.84
	4.28	0.84	0	0.06	1.27	3.0173	58.03
	3.87	1.00	0	0.03	1.36	3.0173	54.84
	5.82	1.54	0	0.06	1.38	3.0173	54.29
	3.84	1.48	0	0.03	1.65	3.0173	45.38
	5.33	2.39	0	0.06	1.85	3.0173	38.66
	3.07	32.91	33.28	0.06	0.91	3.0173	69.90
	7.45	0.63	0	0.06	1.10	3.0173	63.47

Sample	Dry weight (g)	Wet weight (g)	Ballast weight (g)	Parafilm weight (g)	Density (g/cm^3)	DRE (g/cm^3)	Vesicu-larity (%)
W20100101	9.47	2.27	0	0.06	1.33	3.0173	56.04
	11.87	4.59	0	0.06	1.64	3.0173	45.51
	4.06	0.29	0	0.03	1.09	3.0173	64.02
	6.01	1.54	0	0.06	1.36	3.0173	54.83
	5.93	1.23	0	0.06	1.28	3.0173	57.64
	4.78	33.29	33.28	0.06	1.01	3.0173	66.37
	5.28	1.97	0	0.03	1.61	3.0173	46.65
	5.12	0.97	0	0.06	1.25	3.0173	58.51
	7.09	2.46	0	0.06	1.55	3.0173	48.58
	3.75	0.18	0	0.06	1.07	3.0173	64.59
W20100102	7.45	3.12	0	0.06	1.74	3.0218	42.26
	4.98	0.85	0	0.06	1.22	3.0218	59.51
	4.08	1.02	0	0.03	1.35	3.0218	55.44
	6.67	3.43	0	0.03	2.08	3.0218	31.24
	6.29	1.62	0	0.06	1.36	3.0218	54.85
	6.41	0.96	0	0.06	1.19	3.0218	60.64
	6.59	1.32	0	0.06	1.26	3.0218	58.14
	7.99	2.20	0	0.06	1.39	3.0218	53.85
	3.09	0.58	0	0.03	1.25	3.0218	58.77
	4.45	1.11	0	0.03	1.34	3.0218	55.51
W20100103	7.56	0.63	0	0	1.09	3.0218	63.90
	2.37	32.95	33.28	0	0.88	3.0218	70.95
	4.00	33.19	33.28	0	0.98	3.0218	67.64
	5.53	0.64	0	0	1.13	3.0218	62.58
	8.51	0.96	0	0	1.13	3.0218	62.70
	5.35	33.24	33.28	0	0.99	3.0218	67.15
	5.8	2.72	0	0.03	1.90	3.0218	37.07
	9.52	4.35	0	0.03	1.85	3.0218	38.71
	5.35	1.83	0	0.03	1.53	3.0218	49.27
	3.69	0.83	0	0.03	1.30	3.0218	56.85
W20100107	4.46	0.24	0	0.06	1.07	3.0173	64.47
	4.50	0.15	0	0.06	1.05	3.0173	65.24
	3.52	0.35	0	0.03	1.12	3.0173	62.85
	4.96	1.39	0	0.06	1.41	3.0173	53.17
	5.59	1.10	0	0.06	1.26	3.0173	58.18
	4.41	0.08	0	0.06	1.03	3.0173	65.77
	7.24	1.06	0	0.06	1.18	3.0173	60.79
	3.59	0.57	0	0.03	1.20	3.0173	60.21
	8.16	2.43	0	0.06	1.44	3.0173	52.30
	4.04	1.04	0	0.06	1.37	3.0173	54.46

Appendix D

XRD Data

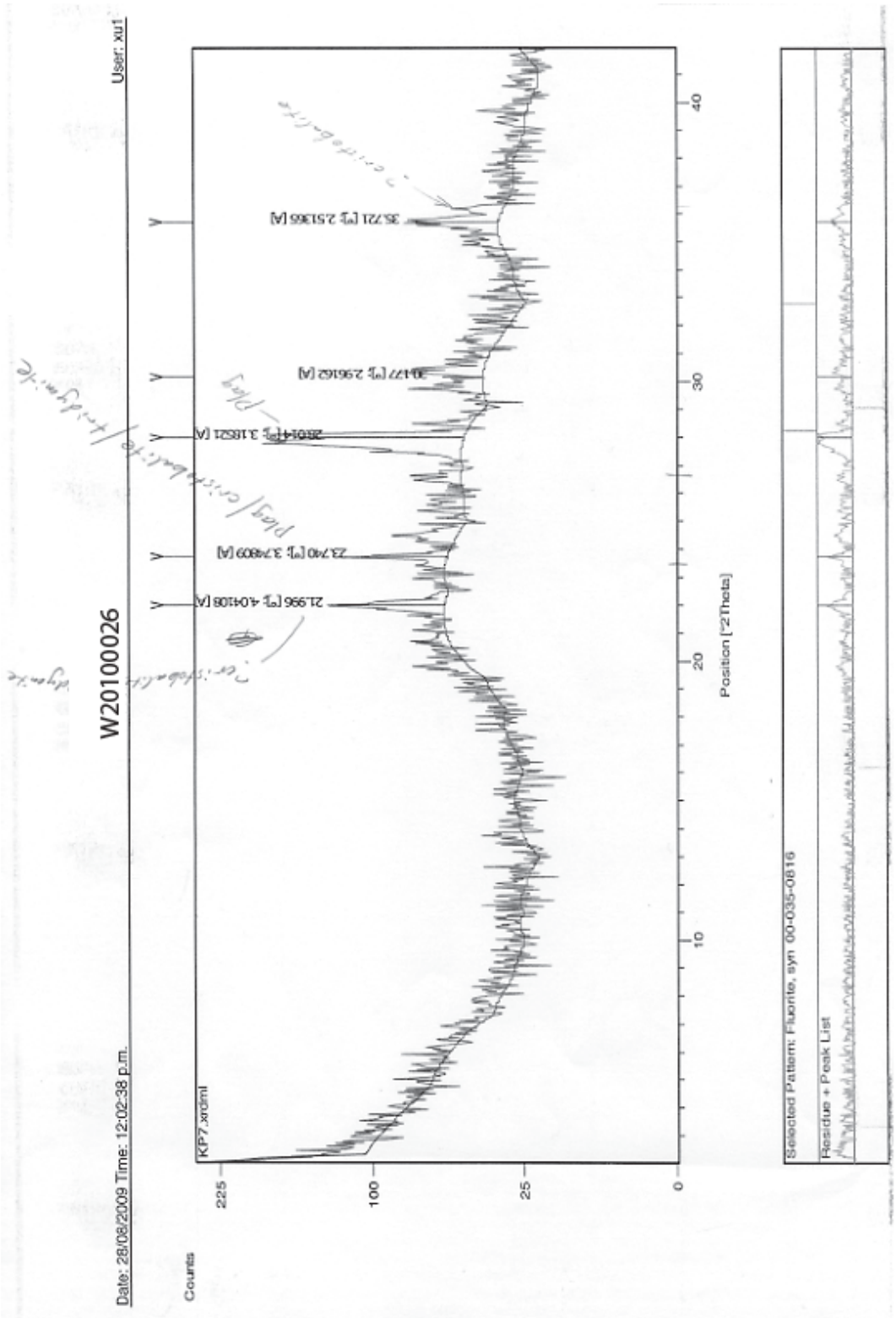
W20100026
User: xu1
Date: 28/08/2009 Time: 12:02:38 p.m.
KP7.xrdml
Counts
Position [°2Theta]
Selected Pattern: Fluorite, syn 00-035-0816
Residue + Peak List
21.996 [°] 4.04108 [A]
23.740 [°] 3.74809 [A]
28.614 [°] 3.18521 [A]
30.177 [°] 2.96162 [A]
35.721 [°] 2.51366 [A]

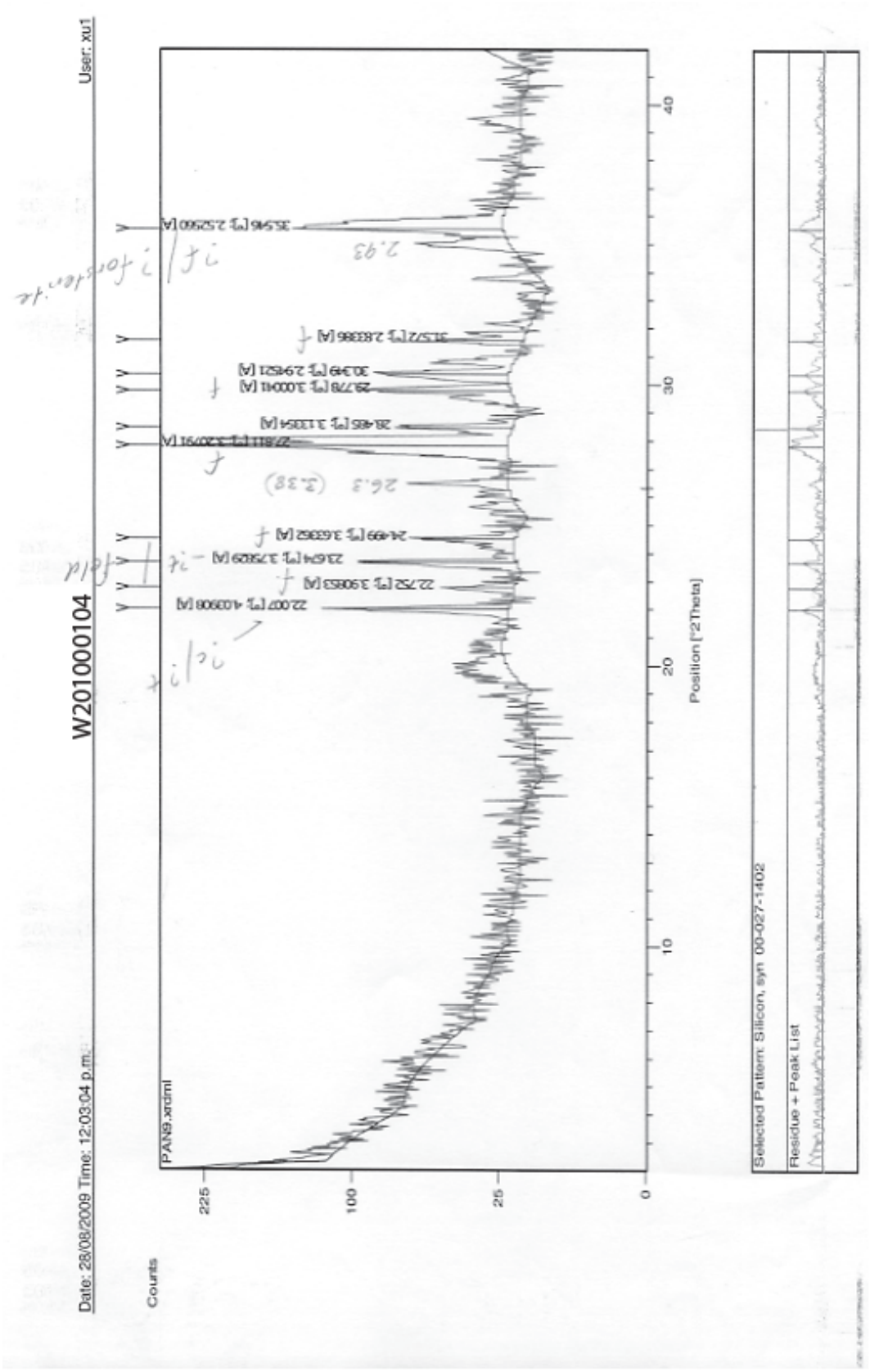
W201000104
Date: 28/08/2009 Time: 12:03:04 p.m.
User: xu1
PAN9.xrdml
Counts
225
100
25
0
10
20
30
40
Position [°2Theta]
Selected Pattern: Silicon, syn 00-027-1402
Residue + Peak List

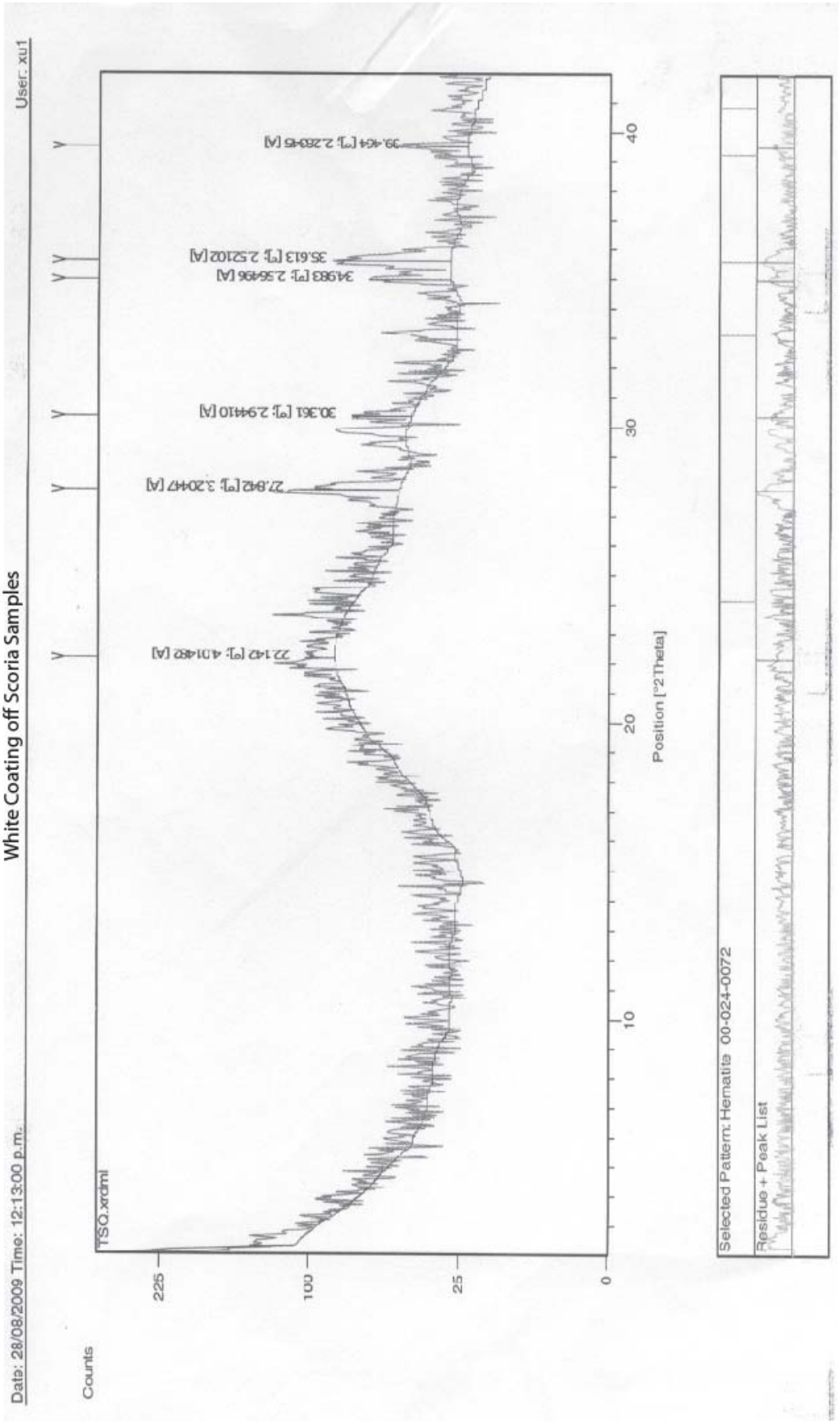
White Coating off Scoria Samples
Data: 28/08/2009 Time: 12:13:00 p.m.
User: xu1
TSO.xrdml
Counts
225
100
25
0
10
20
30
40
Position [°2Theta]
22.142 [°]; 4.01482 [Å]
27.842 [°]; 3.20447 [Å]
30.361 [°]; 2.9441 0 [Å]
34.983 [°]; 2.56496 [Å]
35.613 [°]; 2.52102 [Å]
39.464 [°]; 2.28045 [Å]
Selected Pattern: Hematita 00-024-0072
Residue + Peak List

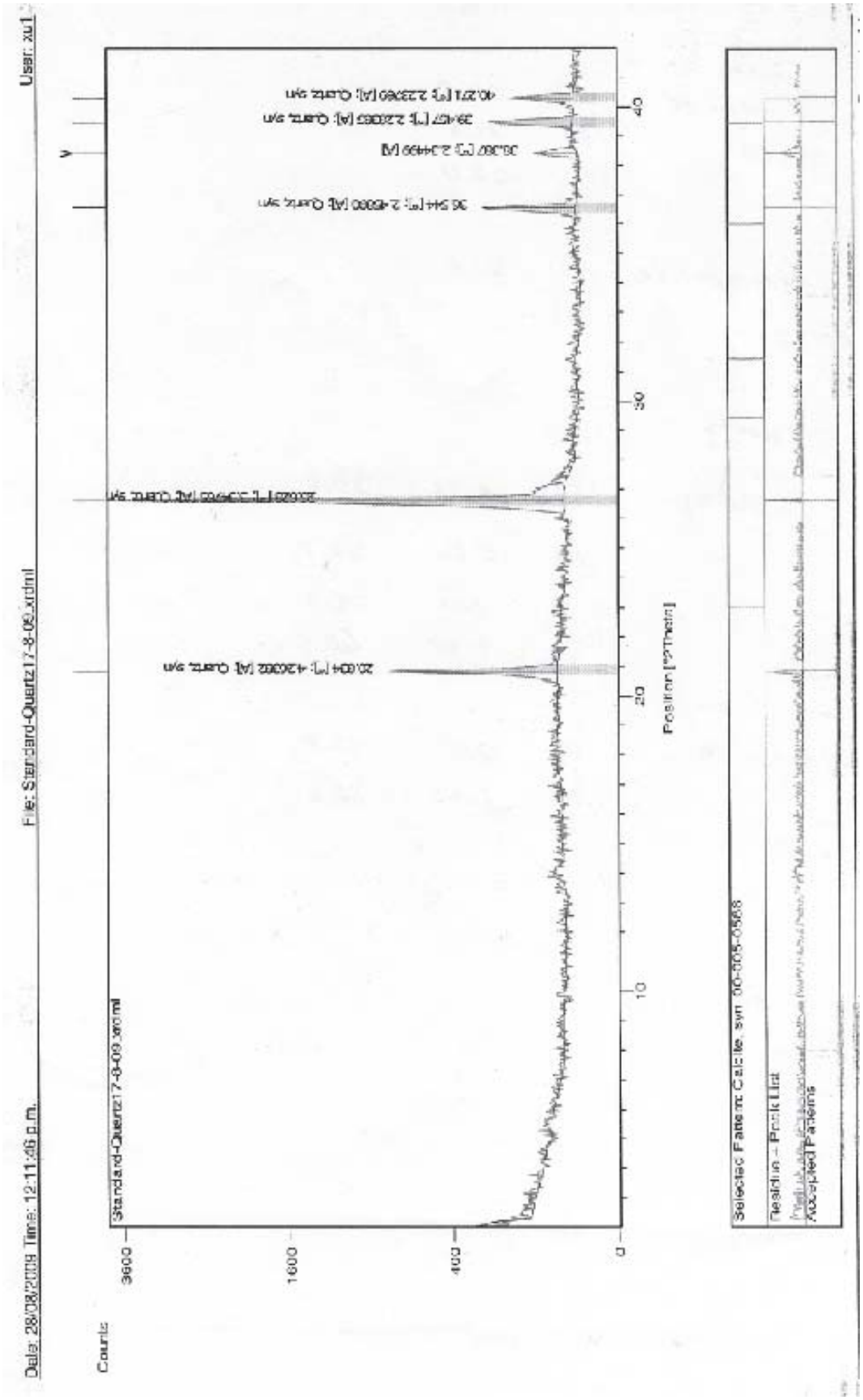
Data: 28/08/2009 Time: 12:11:46 p.m.
File: Standard-Quartz17-8-09.xrdml
User: xu1
Standard-Quartz17-8-09.xrdml
Counts
Position [°2Theta]
Selected Pattern: Calcite, syn 00-005-0586
Reading – Peak List
Accepted Peaks

Appendix E

Point Counting Data

Sample	Plag	Ol	Aug	Groundmass/ Matrix	Vesicle	Scoria	Sideromelane	Xenocryst	Ignimbrite	Rhyolite	Pumice	Other	Total
W20100003	1.3	0.3	0	-	0	31.0	35.0	13.3	0.3	6.0	2.0	10.7	99.9
W20100004	0	0	0	-	0	28.0	46.0	12.0	0.7	4.0	0.0	9.3	100
W20100005	0.3	0	0	94.4	0.7	0.3	1.3	0.3	0	0	0.3	2.3	99.9
W20100006	0	0	0	-	0	78.0	14.7	0	0.7	0.7	0.3	5.7	100.1
W20100007	13	0	0	-	0	16.7	52.7	4.6	0	3.7	0	9.3	100
W20100008	0.3	0	0	97.0	0	0.7	0	1.0	0	0.3	0	0.7	100
W20100014	1.1	0.3	0	44.9	3.5	6.2	0.6	10.6	8.2	4.1	8.5	12.0	100
W20100015	0	0	0	-	0	49.0	13.3	13.3	0.3	5	4.7	14.3	99.9
W20100016	0	0	0	-	0	26.3	31.7	18.7	1.7	3.3	0.7	17.7	100.1
W20100018	0	0.3	0	-	0	40.0	35.7	11.7	0.3	4.7	0.3	7	100
W20100019	0	0.3	0	-	0	19.7	49.0	10.0	2.7	7.3	2.3	8.7	100
W20100020	0	0	0	-	0	78.0	12.3	0.3	1.7	1.3	1.0	5.3	99.9
W20100022	1.8	0.3	0.3	49.8	3.7	13.8	4.0	12.9	1.5	3.1	0.9	7.7	99.8
W20100023	0	0	0	-	0	80.0	0	0	20.0	0	0	0	100
W20100024	0.3	0	0.6	53.2	4.8	22.8	5.8	2.9	2.2	0	3.5	3.8	99.9
W20100026	0	0	0	-	0	34.0	16.3	8.6	3.0	2.0	1.3	34.6	99.8
W20100029	0.7	0.3	0.3	57.2	2.6	18.6	10.1	4.9	0	3.3	0	2.0	100
W20100031	0	0	0	-	0	9.0	25.0	16.3	7.0	9.0	10.0	23.6	99.9
W20100033	0	0	0	-	0	2.6	9.3	41.6	3.0	2.0	9.0	32.3	99.8
W20100037	2.1	0.3	0.3	34.2	1.8	0	4.4	14.7	0.3	5.3	25.1	11.5	100
W20100039	0	0	0	38.6	1.3	1.0	9.5	6.2	0	2.6	38.9	2.0	100.1
W20100042	0	0	0	73.3	0.9	0	0.5	3.6	0	1.8	11.2	8.8	100.1
W20100042	0	0	0	62.3	1.8	0	0.5	5.5	0	5.5	2.9	21.5	100
W20100046	18.6	2.3	1.7	67.4	7.3	2.3	0	0	0	0	0	0.3	99.9
W20100050	1.3			78.3	3.9	4.2	0.3	7.1		0.3	1.6	2.9	99.9

W20100051				-		65.0	24.0	3.0		6.7	1	0.3	100
W20100052	0.3		0.3	56.0	5.2	16.9	0.9	7.7	0.9	0.9	3.1	7.7	99.9
W20100054 base	1.2			66.0	0.7	9.9	3.0	7.5		0.9	1.2	9.6	100
W20100054 top	2.2	0.3		63.8	2.5	11.6	4.4	3.1		2.5	3.4	6.3	100.1
W20100055				-		58.7	6.3	1.0	1.0	11.7	1.0	20.3	100
W20100056	0.3			45.8	8.5	24.5	3.6	4.9		6.2	4.2	2.0	100
W20100057													0
W20100059	0.7			96.3	2.0		0.3	0.3				0.3	99.9
W20100060				-		59.0	0.7	12.3	4.3	7.7	1.0	15.0	100
W20100070	3.7	0.7	0.7	84.6	10.3								100
W20100074	8.0	3.7	2.7	83.0	2.7								100.1
W20100079	3.7	1.7	1.7	89.7	1.3	2.0							100.1
W20100081	1.3	1.0		54.0	43.7								100
W20100082	7.3	1.3	2.3	65.7	23.3								99.9
W20100084	0.3					29.7	0.7	15.0	21.3	6.0	2.3	24.7	100
W20100104						98.0						2.0	100

Sample	Plag	Ol	Groundmass /Matrix	Rhyolite	Pumice	Spherulites	Other	Glass shards	Opx	Opqs	Hnbld	Qtz	Total
W20100009	7.7		57.0				3.3	31.7	0.3				100
W20100010	7.0		61.3		9.0		5	21					103.3
W20100011	6	0.7	46.3	0.7	23.3		0.7	22.3					100
W20100012	8.7		42		18.0		0.3	30.7	0.3				100
W20100013	11.7		55.3				0.3	32.3		0.3			99.9
W20100038	3.0		96.3				0.3				0.3		99.9
W20100061	16.3		11.3			54.7	1.3	14.7	0.3	1.0	0.3		99.9
W20100062	21.3		1.7			71.7	5				0.3		100
W20100063	2.7		32.7			64.3	0.3						100
W20100064	11.3		83.3				0.3		1.0	0.3	0.7	3.0	99.9